J. A. Anna Selvan

1463

Band 361

# ZnO for Thin Film Solar Cells

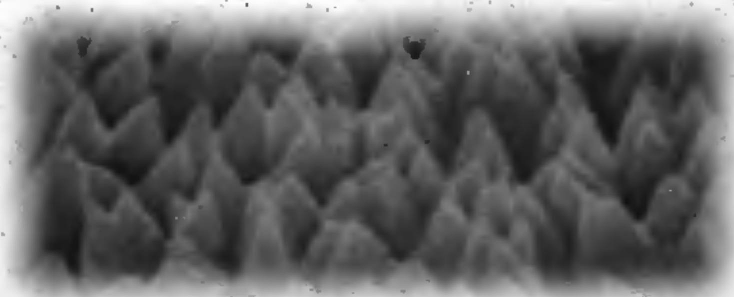

UFO Atelier für Gestaltung & Verlag

**Université de Neuchâtel**
Institut de Microtechnique
**Switzerland**

# ZnO for Thin Film Solar Cells

Thèse

Présentée à la Faculté de Sciences
pour obtenir le grade de docteur ès sciences
par

**J. A. Anna Selvan**

**UFO Dissertation Band 361**

Die Deutsche Bibliothek – CIP-Einheitsaufnahme

Anna Selvan, J. A.
ZnO for Thin Film Solar Cells / J. A. Anna Selvan. – 1. Aufl. – Allensbach : UFO, Atelier für Gestaltung und Verl., 1999
(UFO-Dissertation ; Bd. 361)
Zugl.: Neuchâtel, Univ., Diss., 1998
ISBN 3-930803-60-7

Dissertation der Universität Neuchâtel
Datum der mündlichen Prüfung: 2. Oktober 1998
Referenten: Prof. Dr. A. Shah
Dr. H. Keppner
Dr. C. Beneking
Prof. Dr. L. Zuppiroli

UFO Atelier für Gestaltung & Verlag GbR
Allensbach
Maus Druck & Medien GmbH, Konstanz
Erste Auflage 1999
Alle Rechte beim Autor
ISBN 3-930803-60-7

# IMPRIMATUR POUR LA THÈSE

**Oxyde de zinc pour des cellules solaires à couches minces**

de M. John A. Anna Selvan

---

UNIVERSITÉ DE NEUCHÂTEL

FACULTÉ DES SCIENCES

La Faculté des sciences de l'Université de Neuchâtel sur le rapport des membres du jury,

MM. A. Shah (directeur de thèse), H. Keppner, C. Beneking (Jülich) et L. Zuppiroli (EPF Lausanne)

autorise l'impression de la présente thèse.

Neuchâtel, le 2 octobre 1998

Le doyen:

F. Stoeckli

*To my Father*

# Contents

*Chapter one*

**ZNO FOR THIN FILM SOLAR CELLS: INTRODUCTION**

**1.1 Organisation of the thesis** ..... **3**

*Chapter two*

**FLAT ZNO FILMS BY SPUTTERING**

**2.1 Introduction** ..... **5**

**2.2 Experimental** ..... **5**

2.2.1 RF magnetron sputtering system ..... 5

2.2.2 RF magnetron sputtering ..... 5

2.2.3 Growth ..... 7

**2.3 Results and discussion** ..... **7**

2.3.1 Growth kinetics ..... 7

2.3.2 Optical properties ..... 10

2.3.3 Structural properties ..... 18

**2.4 Conclusions** ..... **24**

*Chapter three*

**SURFACE TEXTURED ZNO THIN FILMS**

3.1.1 Introduction ..... 26

3.1.2 Review on surface texturing for solar cells ..... 28

**3.2 Surface properties**

3.2.1 SEM analysis ..... 32

3.2.2 Results ..... 32

3.2.2.1 Water vapour series ..... 32

3.2.2.2 Power series ..... 32

3.2.2.3 Temperature series ..... 33

3.2.3 Discussion ..... 33

3.2.4 Conclusions with respect to the SEM analysis ..... 40

**3.3 Atomic Force Microscopic studies** ..... **41**

3.3.1 Introduction ..... 41

3.3.2 Experimental ..... 41

3.3.3 Results of AFM studies of ZnO thin films........................................ 42
3.3.4 Discussion........................................ 48
3.3.4.1 The water vapour series........................................ 48
3.3.4.2 Comparison of textured ZnO surface growth with the model of J. A. Thronton...... 51
3.3.4.3 Surface mobility........................................ 52
3.3.4.4 The Power series: changes in the plasma........................................ 53
3.3.4.5 Substrate temperature series........................................ 54
3.3.5 Conclusions regarding the Surface properties analysis........................................ 55

3.4 Optical properties of surface-textured ZnO films........................................ 57
3.4.1 Introduction........................................ 57
3.4.2 Experimental........................................ 57
3.4.2.1 Diffuse transmittance and diffuse reflectance........................................ 57
3.4.2.2 The Haze factor........................................ 58
3.4.2.3 Band gap determination........................................ 59
3.4.3 Results........................................ 60
3.4.3.1 The water vapour series........................................ 60
3.4.3.2 Electrical conductivity and the shape of the transmittance spectrum at the near infra red region........................................ 60
3.4.3.3 Surface morphology and the optical transmittance........................................ 61
3.4.3.4 Diffuse transmittance........................................ 61
3.4.3.5 The haze factor........................................ 61
3.4.3.6 ZnO:Al film grown only water vapour alone........................................ 62
3.4.3.7 Band gap and absorption coefficient of ZnO films grown with the atmosphere of water vapour........................................ 63
3.4.3.8 Other effects of water vapour on the optical properties of ZnO........................................ 64
3.4.3.9 Power series........................................ 65
3.4.3.10 Temperature series........................................ 67
3.4.4 Discussion........................................ 68
3.4.4.1 Free carrier absorption........................................ 70
3.4.4.2 Band gap measurements and the correction necessary in the case of surface texture. 70
3.4.4.3 *Band gap and absorption coefficient values of ZnO*........................................ 71
3.4.4.4 Colour centers........................................ 73
3.4.4.5 Excitons........................................ 74
3.4.5 Conclusions........................................ 76

**3.5 Electrical properties of surface-textured ZnO films**.................................78

3.5.1 Results and Discussion................................................................... 78

3.5.2 Conclusions ................................................................................... 80

**3.6 Structural properties of surface textured ZnO films** ..................................81

3.6.1 Results .......................................................................................... 81

3.6.2 Discussion ...................................................................................... 82

3.6.2.1 The structure of ZnO........................................................................ 82

3.6.2.2 Surface free energy density per plane.................................................. 82

3.6.2.2 Non-equilibrium growth at high partial pressure of water vapour.............. 83

3.6.2.4 Dissociation of water......................................................................... 84

3.6.2.5 The anomalous orientations along $[10\bar{1}1]$ and $[10\bar{1}3]$ directions.......................... 86

3.6.2.5.1 The cubic structure of ZnO.................................................................. 86

3.6.2.5.2 Cubic structure of ZnO during sputtering with water ............................... 86

3.6.2.5.3 Verification of cubic structure of ZnO.................................................. 86

3.6.2.5.4 Mixed cubic and hexagonal structures with Granular morphology ............. 87

3.6.2.5.5 The structure of ZnO grown with 100% water vapour.............................. 88

3.6.2.6 The Effect of RF power on the structure of ZnO: ....................................... 88

3.6.2.7 The effect of substrate temperature on the structure of ZnO ...................... 89

3.6.2.8 Explanations of growth kinetics based on surface mobility of adatoms......... 89

3.6.2.9 Columnar morphology............................................................................ 90

3.6.2.10 Granular morphology .......................................................................... 91

3.6.2.11 Grain size and interplanar distance ........................................................ 91

3.6.2.12 Mechanical properties ........................................................................... 93

3.6.2.13 Growth rate........................................................................................ 94

3.6.3 Conclusions ....................................................................................... 95

**3.7 Optical Emission Studies during surface texture growth**...........................97

3.7.1 Experimental...................................................................................... 97

3.7.2 Results and discussion ........................................................................ 97

3.7.3 Conclusions .......................................................................................101

**3.8 Surface texturing of flat ZnO** .........................................................103

3.8.1 Surface texturing of highly oriented ZnO ...............................................103

3.8.1.2 Comparison with the surface texture Growth........................................... 105

3.8.1.3 Limit for post texture etching................................................................ 108

3.8.1.4 Comparison with other texturing methods ........ 108
3.8.2 Etching by plasma ........ 108
3.8.3 Microstructure evolution of ZnO thin film ........ 111
3.8.3.1 evolution of surface roughness at the atmosphere of anisotropically reacting medium during sputtering in general ........ 113
3.8.4 Conclusions ........ 113

**3.9 Development of surface-textured ZnO/Ag/metal systems as back reflectors .. for solar cells ........ 115**

3.9.1 Experimental ........ 115
3.9.2 Results and discussion ........ 115
3.9.3 Conclusions ........ 121

**3.10 ZnO grown by Chemical Vapour Deposition (CVD) and its comparison with ZnO grown by sputtering ........ 122**

3.10.1 Introduction ........ 122
3.10.2 Experimental ........ 122
3.10.3 Results and Discussion: 1. Growth rate and electrical resistivity ........ 122
3.10.3.2 Optical properties ........ 127
3.10.3.3 Structural properties ........ 129
3.10.3.4 Surface properties and growth kinetics ........ 133
3.10.3.4.1 Variation in substrate temperature ........ 133
3.10.3.4.2 Variation in the dopants ........ 134
3.10.3.5 The surface texture growth mechanism in CVD process ........ 138
3.10.3.5.1 Ambiguities about the surface texture growth ........ 138
3.10.3.5.2 Surface texture mechanism in CVD ........ 141
3.10.3.6 Comparison between ZnO grown by sputtering and by CVD ........ 143
3.10.4 Conclusions ........ 146

***Chapter four***

**INCORPORATION OF ZNO FILM INTO SOLAR CELLS**

**4.1 Experimental ........ 148**
**4.2 Results and Discussion ........ 148**
4.2.1 Back reflectors for Microcrystalline silicon solar cells (NIP structure) ........ 148
4.2.2 Surface texture growth of ZnO on P/IN microcrystalline silicon solar cells *for the purpose of fabricating back reflectors* ........ 151
4.2.3 Use of the post textured ZnO by chemical texturing method as back reflector in NIP amorphous silicon solar cells ........ 152

4.2.4 ZnO grown by CVD ....... 153
4.2.5 ZnO as top window layer in amorphous silicon solar cells ....... 153
4.2.6 Heat mirrors with ZnO ....... 155
4.2.7 Comments on making devices with ZnO ....... 155
**4.3 Conclusions ....... 155**
***Summary and Conclusions ....... 157***
சுருக்கம் (abstract in Tamil)
**Acknowledgements**

# 1

# ZNO FOR THIN FILM SOLAR CELLS: INTRODUCTION

Transparent conducting oxides hold a great deal of technological importance. They simultaneously possess transparency in the visible region, close to that of insulators, and electrical conductivity, close to that of metals; this makes transparent conducting oxides highly attractive for many applications. A stochiometric material does not simultaneously yield high transparency and high conductivity. The way to obtain this combination of properties is to select a wide band gap oxide material and to introduce electron degeneracy. This can be done by creating a defect structure (non-stochiometry) and/or by introducing appropriate dopants. Oxides of tin, indium, cadmium and zinc are convenient materials for tuning them to be transparent conductors. Thin films of these oxides have been prepared by a number of techniques. Doped tin oxide, i.e., ATO (antimony-doped tin oxide) and FTO (fluorine-doped tin oxide), as well as indium oxide, ITO (tin doped indium oxide) films have found an important place among TCOs and some of them have attained large scale production level.

The very first report on a Transparent Conducting Oxide (TCO) has been presented by Badeker[1] in 1907 on CdO. Since then there has been a tremendous increase in technological interest in TCOs. Various deposition techniques have been developed for the fabrication of transparent conducting oxides with improved electrical and optical properties. These techniques can be broadly classified as follows: 1. Evaporation techniques 2. Sputtering techniques 3. Reactive ion plating 4. Chemical Vapour Deposition(CVD) 5. Spray pyrolisis 6. Dip technique 7. Solution growth. Among them, the growth by sputtering techniques, evaporation techniques, chemical vapour deposition and spray pyrolisis are the most widely reported. Each deposition technique with its associated parameters yields films of different properties since the electrical and optical properties of these films depend on the microstructure, stochiometry and the nature of impurities present in the films.

The development of TCOs acquires increasing importance due to their application in the fields of electronic, opto-electronic and mechanical devices. Applications of the transparent conducting oxides in the form of thin films include the following: resistors, transparent heating elements for aircraft and automobile windows, heat-reflecting mirrors for glass windows and incandescent bulbs, anti reflection coatings, selective absorber components in solar heat collectors, gas sensors, electrodes for liquid crystals, electrochromic and ferroelectric photoconductor storage and display devices, hydrogenated amorphous silicon (a-Si:H) and Cds/$Cu_2S$ solar cells, semiconductor/insulator/semiconductor (SIS) heterojunctions, protective and wear-resistant coatings for glass containers.

The present work mainly concerns the development of a particular TCO for *thin film solar cells*. However, certain results of present study are also of interest for those persons who are looking for TCOs for other applications. Solar cells are devices which convert light directly into electricity by making use of electronic properties of semiconductors. They do not involve any moving parts nor any mass flows. They can provide long term electronic out put power at low operating cost, and are virtually free of pollution. Their main limitations are their low conversion efficiency and high production cost. Present solar cell research has the main goal of improving solar cells w.r.t. these two limitations. Various photovoltaic materials with various device structures are being analysed for this purpose.

At present, thin film solar cells are considered to have many advantages over other types of solar cells and they are becoming more and more attractive as they seem to indeed be a partial solution for future energy needs. The transparent conducting oxides for thin film solar cells basically form the top electrode layer for the solar cells; they have to function as current collecting electrodes without blocking the useful sunlight to be converted into electricity. They are also used at the beck side of a thin film solar cell. When they are used in the back side they are reflecting the unused sunlight back into the device (back reflector). For thin film solar cells the use of transparent conducting oxides is mandatory. Analysis of the production cost involved in a-Si:H solar cell modules showed that at present the TCO deposition (of $SnO_2$ on glass) accounts for 42% of the total investment[2]. Clearly, the deposition of TCO has a large potential for the cost reduction of thin film solar cells.

Most commonly used transparent conducting oxides are fluorine doped tin oxide ($SnO_2$:F) and tin doped indium oxide (ITO). These TCOs enjoyed a major role in fabrication of thin film solar cells for a long time. However, it has been discovered that both of these TCOs are not resistant enough against certain deposition conditions, like exposure of hydrogen plasma and high temperatures. Both the TCOs reduce their transmittance, and also the metal atoms (In, Sn) start diffusing from the TCO into the active device part. The later effect is specifically pronounced in ITO, where In diffusion takes place even with a low temperature silane plasma. In this way the TCO for the thin film solar cells, which is supposed to be a passive layer, 'contributes' to the deterioration of cell performance. Hence, solar cell researchers started to search for a highly stable TCO. Comparison of several TCO layers showed that conducting ZnO is highly stable in comparison with the former two TCOs. Under the exposure of hydrogen plasma ZnO does not reduce the transmittance also it shows only a minimum diffusion from the ZnO layer into the active part of the solar cells when compared to ITO and $SnO_2$. The reason for the high stability of ZnO has been explained to be its high surface binding energy[3].

ZnO is cheaper than all other TCOs. In fact, the price of metallic Zn can be 12 times cheaper than that of metallic Sn[4]. Commercially available ZnO can be at least 15 times cheaper than that of tin oxide of the same purity[5]. Clearly the cost reduction of thin film solar cells depends on the choice of the TCO material. ZnO is made from highly abundant raw material and thus is well suited for use in solar cells.

ZnO is a II-VI compound semiconductor with a band gap energy of 3.3 eV. Stochiometric ZnO is an insulator. Variation from stochiometry and/or external doping makes ZnO conductive. ZnO is known to be a piezoelectric material and much work on ZnO has been done to utilise this property. Since ZnO is stable under relatively aggressive device fabrication processes (like hydrogen plasma exposure), it acts also as an diffusion barrier against atomic species from the underlying substrate like glass. Usually one needs a separate diffusion barrier layer ($SiO_2$ in the case of $SnO_2$ deposition on glass) between glass and TCO. This is not the case for ZnO. This fact further reduces the cost involved in the deposition of TCOs for thin film solar cell production when compared to the presently used $SnO_2$, for example.

With all its unique advantages ZnO has become an important TCO for thin film solar cells. Experience has showed that instead of considering a TCO material as being simply a standard, passive, conductive coating, one has to pay attention to the deposition conditions, and to the microstructure of the TCO in order to derive the best results for the solar cell. Hence, the solar cell research motivates us to study the growth conditions and the resulting microstructure as well as electro-optical properties of TCOs.

A further important aspect of TCOs in thin film solar cells is 'light trapping'. By this, one increases the amount of light, that is otherwise weakly absorbed, and couples it more effectively into the active layer of the solar cells. For this purpose, the front side of the solar cell is made rough. Due to the roughness one can firstly reduce the amount of light that escapes by primary reflection. For thin film solar cells, having surface of the TCO rough has a clear further advantage: The rough surface increases the optical path length of the light ray inside the solar cells. This increases the absorption of the otherwise weakly absorbed light. This increases the photovoltaic action (electron-hole pair generation) and hence the efficiency of the solar cells. This

will help to reduce the thickness of the solar cells, to increases the stability of solar cells (in the specific case of amorphous silicon, a-Si:H) and also to reduce the cost involved in the fabrication of solar cells. The advantages of surface texturing of ZnO is explained in section 3.1

To recapitulate, in thin film solar cells one can advantageously use ZnO as a transparent conducting oxide. The basic requirement of a TCO is its high transparency and conductivity. It is learned at present, that for thin film solar cells, as a third property one should include surface texture (roughness). Hence one requires the ZnO, apart from being conductive and transparent, to be surface textured for the purpose of light trapping. But the question is how does the surface of the ZnO grow rough? Can this type of growth be controlled? Very few studies have been done on the growth of ZnO with a rough surface. Many ambiguities still exist about the growth of surface texture of ZnO.

The aim of the present study is to analyse the growth and characteristics of ZnO so that it is used in solar cells efficiently. Hence, the task is to analyse the growth of ZnO to get *simultaneously* all the three properties, viz. electrical conductivity , optical transparency *and* surface texture. The present research is one of the first studies aiming at the analysis of surface texture growth of ZnO. In the context of solar cell technology, by the present study one obtains criteria on how to grow a rough surface of ZnO or alternatively, on how to avoid the growth of a rough surface of ZnO.

At present, sputtering and CVD are the two most successful and most commonly used methods for the growth of ZnO. Sputtering is given more importance in this work because of its advantages over other methods. Sputtering offers high control of the growth process. It is not expensive, it is usually a non-toxic method and it is well suitable for large scale production. In this work the growth of ZnO by both of sputtering as well as CVD methods are analysed and they are compared with each other.

ZnO films were grown by the method of RF magnetron sputtering using a ZnO target doped with $Al_2O_3$. The growth of flat and surface textured films and the surface, structural and opto-electronic properties have been analysed in detail. Flat and surface textured growth of ZnO films by CVD and their microstructural properties are also studied; a comparison between sputtering and CVD has been carried out in detail.

The fabrication of solar cell devices incorporated with flat ZnO films and surface textured growth of ZnO on a solar cell have been also analysed in the present study.

Studying the growth of ZnO through the microstructural properties is of great importance in order to get high over all performance from them.

## 1.1 Organisation of the thesis

The ZnO films with flat surface are analysed for their electrical, optical and structural properties and they are correlated with each other in chapter 2.

Chapter 3 treats the case of surface-textured ZnO. To make the surface of the ZnO rough, as is additionally required for thin film solar cells for the purpose of light trapping, water vapour can be additionally mixed to the sputtering gas. The growth of ZnO with such mixture of Argon and water vapour, its surface properties, the reasons for the occurrence of the surface texture growth in terms of the structural properties of the film, the resulting surface texture and the obtained electrical and optical properties are investigated in detail in sections 3.2. to 3.7. In terms of structural properties and the growth conditions one obtains insight into the growth of ZnO with flat and textured surface.

Based on these results, an alternative way to obtain all the three important properties together is investigated: Obtaining surface texture on a ZnO with an originally flat surface by post texturing is presented in section 3.8. For the use in solar cells, the surface texture growth of ZnO on silver/stainless steel is analysed in section 3.9.

ZnO growth by CVD, together with the mechanisms of surface texture growth in terms of the structural properties and the growth parameters are presented in section 3.9. These studies yield more complete information about the growth of ZnO.

The simultaneous occurrence of the optical transparency, electrical conductivity and surface texture is investigated in both the methods of CVD and sputtering

The ZnO produced by the above methods are applied in amorphous silicon and micro crystalline solar cells and the influence of the growth and micro structural properties of ZnO on the performance of solar cells is shown.

## References

[1] H. Badekar, Ann. Phys. (Leipzig), 22 (1907) 749
[2] K. S. Srinivas, 'Energy investments and prouction costs of amorphous silicon PV modules', report prepared for Swiss federal department of Energy, OFEN, 1991.
[3] S. Major, S. Kumar, M. Bhatnagar aod K. L. Chopra Appl. Phys. Lett 49 (1986) 394
[4] Metal Bulletin, January 2 1970,page 9
[5] Alfa catalogue of Finest Inorganic Research Chemicals and Metals, 1993-94

# 2

# Flat ZnO films by sputtering

## 2.1 Introduction

ZnO films with flat surface are highly useful in many fields. Except in specific individual cases where a rough surface is required (for example solar cells), ZnO films with flat surface are indeed the major requirement. In this section we will report on the ZnO with flat surfaces grown by sputtering. Various growth conditions that affect the property of ZnO films will be analysed: Electrical, optical and structural properties of ZnO film grown by RF magnetron sputtering will be presented in this chapter. Further, the ways to get high quality ZnO films will be shown.

## 2.2 Experimental

### 2.2.1 RF MAGNETRON SPUTTERING SYSTEM

For the growth of ZnO films, a RF magnetron sputtering system is constructed. It consists of a planar electrode system. Figure 1 shows the schematic diagram of the sputtering system. The target material to be sputtered (ZnO) is placed at the cathode. The substrate on which the film is to be grown is kept on the electrically grounded anode. These electrodes are housed in a chamber which is evacuated. The back side of the cathode is water-cooled. There are inlets for the sputtering gases. For the growth of flat ZnO films, as described in this chapter, we use only argon gas as sputtering gas. In subsequent chapters surface texture growth of ZnO using a mixture of Ar as well as water vapour will be explained.

The distance between the electrodes, that is the distance between the substrate and the target material can be changed by rising the anode up or down. Behind the cathode a circular magnet has been placed in order to increase the path length of an electron in the plane before it is collected or before it recombines on the electrode or wall. A plasma confining cylinder is used at the cathode. The cathode is connected with an external RF power supply. Pre-sputtering can be done by covering the substrate from film deposition by means of a shutter. For the complete documentation of the construction of the system one may refer to reference [1]. The target material is a sintered ceramic disc which contains a mixture of ZnO:$Al_2O_3$ in the ratio of 98:2 wt.%. The distance between the electrodes is 73mm, double a typically used distance for sputtering.

### 2.2.2 RF MAGNETRON SPUTTERING

The basic mechanism of sputtering is explained in this section. A sputtering system generally has a planar electrode set up similar to the one shown in figure 1. A sputtering gas (for example, Ar) is introduced into the evacuated chamber to a specified pressure. The action of electric field between the electrodes is to accelerate the electrons which in turn collide with argon atoms, breaking some of them up into argon ions and more electrons to produce the glow discharge. The charged particles thus produced are accelerated by the field, the electrons towards the anode, causing more ionisation on the way, and the ions towards the cathode, so that a current flows through the system. The glow discharge is limited by so-called shealth region that

are formed between the plasma (glow) and the electrodes, and there is a particularly strong electric field that forms in the cathode shealth.

When the ion strikes the cathode, the ion impact may set up a series of collisions between atoms of the target, possibly leading to the ejection of one of these atoms. The ejection process is known as *sputtering*. The directionality of sputtered atoms is random and some of them land on the substrate, which is on the anode, condense there, and form a thin film.

The ions may also liberate secondary electrons which are responsible for maintaining the electron supply and sustaining the glow discharge. The voltage V required to drive a current I through the system is a function of system pressure. The rate of thin film formation on the substrate will depend on the amount of sputtering at the target and thus linearly on the current. However, the amount of sputtering also depend on the sputter yield, that is on the number of target atoms or molecules ejected per incident ion. Hence it also depends on the ion energy and so on the voltage V.

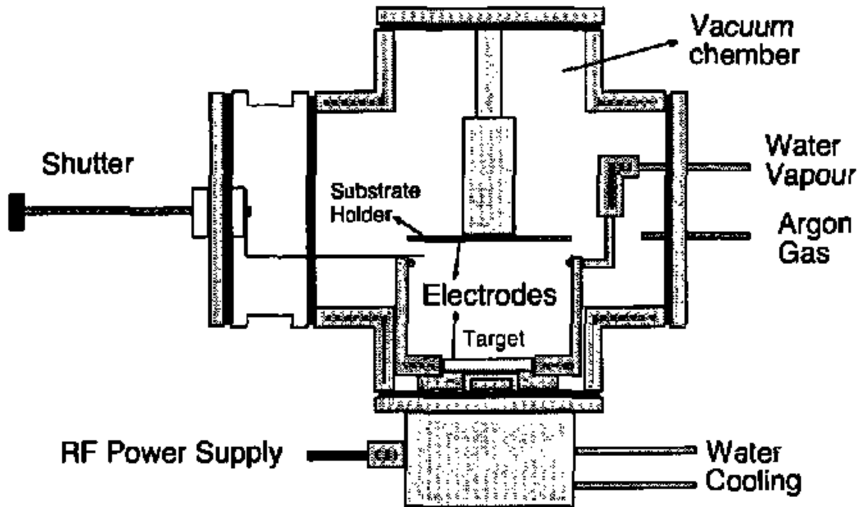


Figure 1. The schematic diagram of the RF magnetron sputtering electrode configuration constructed for the growth of ZnO films.

The above case is a typical DC sputtering situation in which the cathode is connected with a DC power supply. If the cathode is an insulating material, DC sputtering is not possible owing to the building up of positive ($Ar^+$) surface charges. However, a high-frequency alternating potential may be used to neutralise the insulator surface periodically with plasma electrons. By this technique one uses an alternating voltage power supply at RF frequencies of 13.36MHz, so that the sputtering target is alternately bombarded by ions and then electrons. Pure ZnO is an insulator. Hence DC sputtering with a pure ZnO target can be a problem. However, doped ZnO target can be used for DC sputtering. For sputtering with a metallic Zn target a mixture of Ar and O (reactive sputtering)[2] can be used. In the present case RF magnetron sputtering is used because of its additional advantages. The RF discharge makes more efficient use of the electron impact ionisation[3] so that the operating pressures could be in practise extended down to 1mtorr ($1.3 \times 10^{-3}$ m bar). Also, a possible problem of arcing can be reduced in the case of RF sputtering.

Arrangements in which the applied electric field and magnetic fields are perpendicular to each other are called magnetron sputtering systems. In a planar cathode system, such as in the present case, the magnetic field is applied parallel to the cathode to confine the primary electron

motion to the vicinity of the cathode and thus increase the ionisation efficiency and prevent the electron bombardment of the film. For this purpose a permanent magnet is placed behind the cathode. The discharge plasma is constrained near the cathode surface by trapping regions formed by endless toroid bounded by a tunnel-shaped magnetic field. Magnetron sputtering makes it possible to utilise the cathode discharge power very efficiently (up to 60%[4]) and yield higher deposition rates.

#### 2.2.3 GROWTH

For the growth of ZnO films by the RF magnetron sputtering system described above, the following procedure was utilised: Cleaned[5] substrates were placed in the substrate holder at anode. The vacuum chamber was evacuated up to $8 \times 10^{-7}$ m bar. Then sputtering gas Ar was allowed in the chamber at a specified pressure. Keeping the shutter closed, RF power was applied between the electrodes and the plasma was ignited. The plasma potential is monitored by a probe connected at the bottom of the cathode. The time the plasma potential takes to reach a constant value decides the pre sputtering time. By pre sputtering the first few atomic layers of the target are removed in order to clean it. During the time the system is open to air (to load or unload substrate) the target is liable to become contaminated by atmospheric pollution, by handling or by formation of a compound on the surface of the target. After pre sputtering the substrate is exposed to the plasma by removing the shutter. The sputtering pressure (Ar pressure), the applied RF power, the substrate temperature are the parameters that were varied to change the growth conditions. With a target diameter of 72mm and a electrode separation distance of 73mm, the growing ZnO films showed a uniform thickness values at least for $4 \times 4$ $cm^2$ area. The ZnO films grown on Corning 7059 glass substrates of size $4 \times 4$ $cm^2$ were characterised for their electrical, optical and structural properties. The thickness was measured by using a stylus profiler thickness measurement instrument manufactured by Tencor Instruments. The electrical properties were measured by using four probe as well as van der Pauw methods. The structural properties were analysed using the X-ray powder diffraction method with a Cu-$k_\alpha$ radiation source. The optical properties were analysed using a Perkin Elmer spectrometer with an integrating sphere.

## 2.3 Results and Discussion

#### 2.3.1 GROWTH KINETICS

Figure 2 shows the deposition rate of ZnO films deposited at room temperature at different RF power values. The sputtering pressure was kept at $5 \times 10^{-3}$ m bar. The distance between the electrodes is 7.3cm. As is seen, the increase in RF power linearly increases the growth rate. This increase is mainly attributed to the increase in the sputtering yield, i.e. in the number of target atoms (or molecules), ejected per incident ion, of the target. The sputtering yield S is given[3] by

$$S = \frac{3\alpha}{4\pi^2}\frac{4m_i m_t}{\left(m_i + m_t\right)^2}\frac{E}{U_0} \qquad (1)$$

where $U_0$ is the surface binding energy of the material being spottered, $m_i$ and $m_t$ are the masses of the incident ion (Ar) and of the target atom respectively, $\alpha$ is a monotonic function of $m_t/m_i$ and E is energy of incident ion. According to this equation, the yield increases linearly with E. This equation holds good for values E lower than 1 keV. At values of E, the sputtering yield becomes constant and remains unaffected by a further increase in E[6]. In the present case the sputtering yield, that is the number of atoms and molecules ejected, increases with RF power. This directly increases the growth rate since structurally there is no variation in the growth direction which may change the growth mechanism and hence affect the growth rate[7]. A maximum growth rate of 5.8Å/sec has been achieved at 200W of RF power. Since the increase is linear, an additional increase in RF can be expected to increase the growth rate further. But the limitation is the target lifetime as well as the damage on the growing surface of ZnO[8]. The target

may not withstand high energy sputtering and it may break, as it was observed in the present case, due to continuous high energy (RF power more than 200W) sputtering. *A high density target, thus, can increase the growth rate further*. Such high energy sputtering may also etch the growing surface, as will be explained in section 3.8. *Thus any requirement of obtaining a highly smooth surface also puts limitation on the increase of RF power that one may wish to undertake in order to increase the growth rate by sputtering*.

Figure 3 shows the change in the bulk resistivity of the same films as those represented in figure 2. It is seen that the increase in RF power decreases the resistivity at low RF power values. At high RF power values the resistivity seems to be saturated. A low bulk resistivity of 6.2 x $10^{-4}$ ohm. cm is achieved at RF power value of 150W. This resistivity value, obtained without substrate heating is highly useful for growing ZnO on device structures as well as on polymer substrates[9,10]. As mentioned before, the target for ZnO deposition is a sintered disc of mixture of ZnO and $Al_2O_3$ in the ratio of 98:2 wt.%. Hence the grown ZnO films are doped with Al (ZnO:Al).

A stochiometric ZnO otherwise has an empty zinc 4s-band and a filled valence 2p-band resulting in a band gap of 3.3 eV (the two valence 4s electrons of zinc transfer to the oxygen 2p-band). The reason for the conductivity of ZnO could be either intrinsic defect structure or external doping. In the defect structure, the ZnO is not in a stochiometric ratio and there is excess Zn or low amount of O. One of the two valence electrons of the Zn interstitial atom can be easily ionised and acts therefore as donor. Usually in a defect structure of ZnO an increase in O do not give rise to free holes. This means that the acceptor level corresponding to oxygen defect center is too far from the valence band[11] to be ionised at room temperature or the number of interstitial Zn is always higher than O. In the case of extrinsic doping, a III group element (Ga, In, Al) occupies the position of Zn. The excess electron from Al (as a III group element) supplies an additional electron for the process of electrical conduction [12].

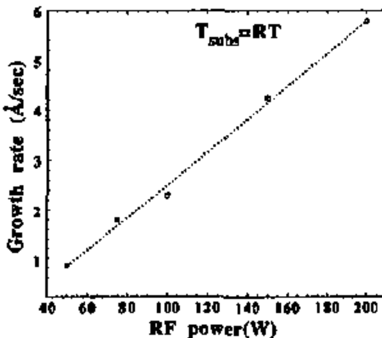


Figure 2 The growth rate of ZnO films grown at different RF power values. The sputtering pressure of Ar was 5 x$10^{-3}$ m bar.

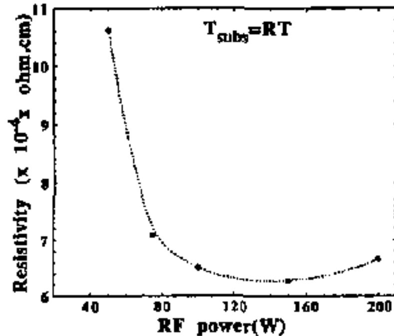


Figure 3 The resistivity of the same films of figure 2.

The increase in conductivity obtained with in an increase in RF power is due to both the increase in crystallinity as well as the increase in efficient doping. The crystallinity is seen from X-ray diffraction experiments and the change in charge carrier density is seen from optical measurements. This will be discussed later.

Figure 4 shows the variation of growth rate as a function of RF power for deposition at 175°C. The Ar pressure was 5 x $10^{-3}$ m bar. Similar to the growth at room temperature, here also the growth rate also varies linearly with RF power at increased substrate temperature. Figure 5 shows the resistivity of the same films as those represented in figure 4. At low RF power values

the bulk resistivity is lower than the resistivity values obtained at high RF power values. After 100W the resistivity seems to remain approximately the same(between 4 to 4.3 x $10^{-4}$ ohm.cm). Figure 5 can be compared with figure 3 to see the variation of resistivity in function of RF power at two different substrate temperature values. In both cases the resistivity seems to reach a constant value after RF power value of 100W. The resistivity of ZnO grown at room temperature is 6.2 x $10^{-4}$ ohm.cm whereas the resistivity of ZnO grown at a substrate temperature of 175°C is 4.1x $10^{4}$ ohm.cm. The reason for this high conductivity obtained at 175°C can be either an increase in carrier concentration or an increase in carrier mobility. The carrier mobility can be increased when the crystallinity is higher. The increase in RF power, during growth, increases the surface mobility of adatoms. On the other hand, the increase substrate temperature also increases the kinetic energy of the adatoms during growth. Increase of both of these growth parameters enhances the crystallinity and the grain size of the growing films. It is not therefore surprising that we obtain highly conducting ZnO films at increased RF power at increased substrate temperatures. The variation of resistivity with variation in RF power is small in the case of growth with substrate heating when compared to the growth without substrate heating. Note that the satisfactory conductivity values obtained without substrate heating (6.2 x $10^{-4}$ ohm.cm) indicate the possibility to obtain film that can indeed be useful for device fabrication at low substrate temperatures (for example, fabrication of thin film a-Si solar cells). With similar explanations, the variation of resistivity of ZnO films grown at low RF power values and at room temperature (in figure 3) can be readily understood. The increase in RF power can vary the resistivity from 10.8 x $10^{-4}$ ohm.cm to 6.2 x$10^{-4}$ ohm.cm (in figure 2). On the other hand, an increase in RF power at increased substrate temperature increases the resistivity from 3.2 x$10^{-4}$ ohm.cm to 4.2 x$10^{-4}$ ohm.cm. This increase can not be explained in terms of the kinetic energy of adatoms. Rather, it seems that at increased substrate temperatures, a high RF power introduces intrinsic defects in ZnO that acts as traps for charge carriers.

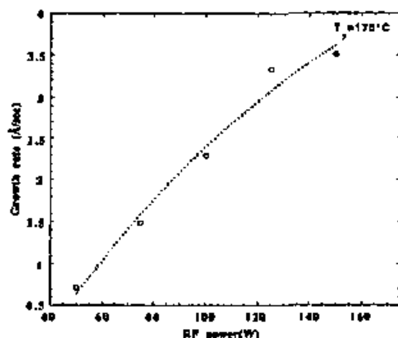


Figure 4 The growth rate of ZnO films grown at different RF power values during sputtering. The substrate temperature was 175°C. The Ar pressure was 5 x$10^{-3}$ m bar.

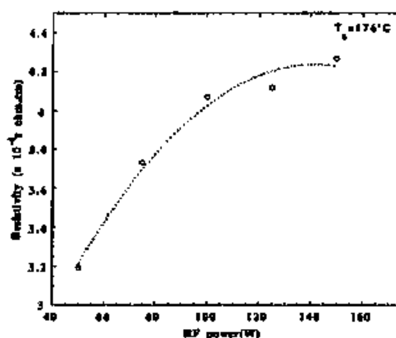


Figure 5 (right) The resistivity of the same films of figure 4

Comparison of figure 2 and figure 4 shows that the maximum deposition rate of ZnO without substrate heating is higher than the maximum deposition rate with substrate heating. This shows that even though the sputtering yield is increased at high RF power values, some of the sputtered atoms are reflected from the surface of the substrate at increased substrate temperature. This reduces the growth rate. A reduction of growth rate with increase in substrate temperature has been observed for growth of single crystalline ZnO by magnetron sputtering[13] Thus, there is an additional advantage for the growth without substrate heating in the present system.

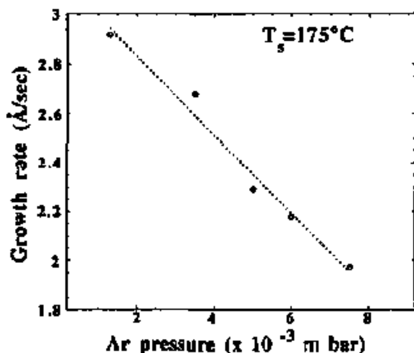


Figure 6 The growth rate of ZnO films grown at different Ar pressures during sputtering. The substrate temperature was 175°C. The RF power was 100W.

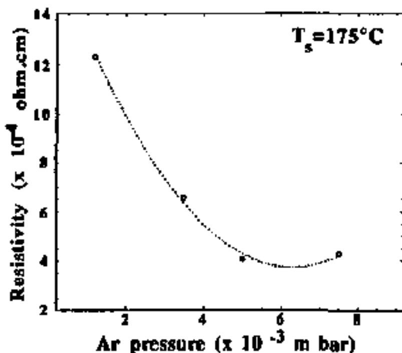


Figure 7 The resistivity of the same films of figure 6.

The variation of deposition rate as a function of sputtering pressure (of Ar) is shown in figure 6. The RF power was 100W. The substrate temperature was 175°C. As is seen, the deposition rate decreases linearly with an increase in Ar pressure. As explained in the beginning, the discharge is sustained by electrons making ionising collisions in the gas. The number of ionising collisions will increase with increasing gas density, that is, the gas pressure. On the other hand, the material sputtered from the target may collide with gas atoms on its way to the substrate. The collisions reduce the energy of the sputtered atoms. The rate of such collisions will increase with increasing pressure. As a result, the sputtered atoms will be deflected, some times back to the target. Hence the deposition rate decreases. In the present case the increase in Ar pressure increases the above mentioned collisions in the plasma and this leads to the reduction of growth rate.

The variation of resistivity of ZnO as a function of pressure of Ar is shown in figure 7. The samples are the same as those of figure 6. The resistivity decreases with an increase in Ar pressure. It appears to reach a minimum value around $5 \times 10^{-3}$ m bar. The increase in conductivity is due to increase in both the charge carrier density as well as in the crystallinity, as will be shown later. From figure 6 and figure 7 we can determine an optimum pressure of Ar for flat film growth. To obtain low resistivity of the resulting ZnO film a sputtering pressure above $5 \times 10^{-3}$ mbar is necessary. To have both high deposition rate as well as high electrical conductivity the pressure of $5 \times 10^{-3}$ m bar is optimised as suitable sputtering pressure.

Comparison between figures 7 and 5 shows that *the influence of sputtering pressure on the resisitivity is large* when compared with the influence of RF power on the resistivity. On the other hand, comparison between figures 4 and 6 shows that *the influence of RF power on the growth rate is higher* when compared with the influence of sputtering pressure on the growth rate.

### 2.3.2 Optical properties

High optical transmittance of a transparent conducting oxide along with high electrical conductivity are prime requirements for those materials. For solar cell applications, in general, the transparent conducting oxide should have a high transmittance between 400-1000 nm. In figure 8 the optical transmittance of ZnO films grown at different Ar pressures is shown. The RF power was 100W. The substrate temperature was 175°C. For all the films the transmittance is more than 80% in the visible region. The spectral dependence of transmittance of ZnO is explained also in section 3.4. Here we explain different parts of the transmittance and reflectance spectrum. At the

ultra violet wavelength region, around 375nm the band to band transition for ZnO takes place. In the near infra red(NIR) region, free carrier absorption occurs. At the low energy end of this spectral region, plasma resonance takes place in the NIR region. The band gap of intrinsic ZnO is 3.3 eV. However, with increased carrier concentration the apparent band gap value may be shifted away from the actual value. The free carrier absorption increases with increase in charge carrier concentration. The position of plasma edge (the minimum in reflectance due to plasma resonance) is also a function of charge carrier concentration. This is explained below.

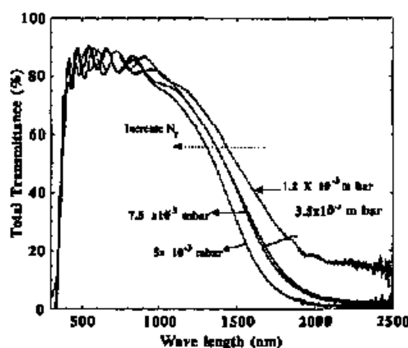


Figure 8 The transmittance spectra of ZnO films grown with different sputtering pressures of Ar. The RF power was 100W. The substrate temperature was 175°C.(see figure 7 also)

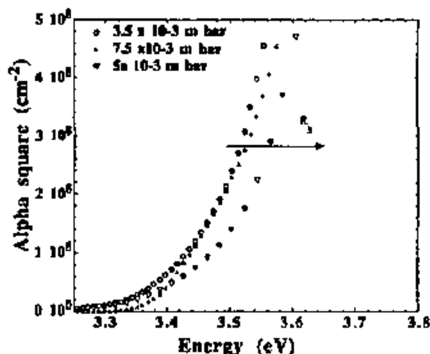


Figure 9 Variation of (absorption coefficient)² with energy. The intercept of the linear part of the curves with the energy axis gives the value of band gap. The onset of band to band transition increases with increase in free carrier absorption.

The increase in conductivity increases the free carrier absorption of ZnO films in the near infra red regions as shown in figure 8 (see also figure 7). During the process of free carrier absorption, the electrons in the conduction band are raised to higher energies by *intraband* transitions. Obviously, a stochiometric ZnO will not have this absorption. The absorbance due to free charge carriers is written as

$$\alpha = \frac{e^3 N_f \lambda^2}{\pi n (m^*)^2 c^3 \mu} \qquad (2)$$

where $N_f$ is the number of free carriers, n is the refractive index, $m^*$ is the effective mass of charge carriers and μ is the mobility[13]. It is to be noted that the free carrier absorption is a linear function of $N_f$ and is inversely proportional to the mobility of the charge carriers. Also the absorbance is a function of the square of the wavelength.

Figure 10 shows the reflectance curves of the same samples as those represented in figure 8. All the reflectance curves show a minimum in the near infra red wavelength region after which there is a maximum of reflectance. This is due to plasma resonance. The free electrons in ZnO interact with the photons electrostatistically[14], thus forming an electron 'plasma' which can be excited by light of proper photon energy to collectively perform fluid-like oscillations. This plasma possesses, just like an oscillator, a resonance frequency, which is often called a 'plasma frequency'. This explanation is well used for the analysis of the reflectance from a metal surface. The reflectivity of a metal is written as

$$R = \frac{(n-1)^2 + k^2}{(n+1)^2 + k^2} \qquad (3)$$

where n is the real part of refractive index and k is damping constant (or extinction coefficient). For the motion of a free electron which is excited to perform forced, harmonic vibrations under the influence of external alternating field, i.e., under the influence of light, the complex index of refraction may be written as

$$\hat{n}^2 = 1 - \frac{e^2 N_f}{\pi m \upsilon^2} \qquad (4)$$

where $N_f$ is the density of free electrons and m is the electron mass. Here we have two cases.

(i) At small frequencies the term $\frac{e^2 N_f}{\pi m \upsilon^2}$ in equation (4) is larger than one. Hence $\hat{n}^2$ is negative and $\hat{n}$ is imaginary. This means the real part of the complex refractive index is zero. This leads to the reflectance in equation (3) to be one. i.e. the reflectance is 100%. In figure 10 a strong reflectance due to this phenomenon, can be observed around 1500nm.

(ii) At higher frequencies the second term in equation (4) becomes smaller than one. Hence $\hat{n}^2$ is positive. The reflectivity for real values of $\hat{n}$, i.e., for k=0, is written as (from equation (3)), R= (n-1)/(n+1). That means the material is essentially transparent for these frequencies. (wavelength region below 1500nm in figure 10)

The plasma frequency is the frequency which separates the transparent and the reflective regions. By setting the second term in equation (4) equal to unity, the plasma frequency can be determined. Hence the plasma frequency is

$$\upsilon_1^2 = \frac{e^2 N_f}{\pi m} \qquad (5)$$

Experience shows that plasma oscillations already occur when $\hat{n}$ is close to zero[15]. The wavelength $\lambda_m$, at which the minimum in reflectance takes place is given by the relation, $\lambda_p$ = 1.13 $\lambda_m$, where the number of free electrons is given[16] by

$$N = \frac{4\pi^2 c^2 m^* \varepsilon_0 \varepsilon_r}{\lambda_m^2 e^2} \qquad (6)$$

Using the minimum in reflectance observed experimentally, the plasma frequency and the density of free carriers can be determined by using equation (6).

In figure 10 it is seen that the minimum in the reflectance due to plasma resonance is modified depending on the sputtering pressure. According to equations (6), the density of free carriers increases with the decrease in the value of $\lambda_m^2$. From figure 10 it is readily obtained that the density of free carriers in the resulting film changes with a change in Ar pressure during sputtering. The density of free carriers are high when the Ar pressure is 5x $10^{-3}$ m bar. Figure 9 can be compared with figure 7. The increase in conductivity of ZnO films during the change in the working pressure is mainly attributed to the increase in density of charge carriers of the resulting films.

Figure 9 shows the variation of square of absorption coefficient with energy for ZnO films grown at three different working pressures of Ar. The films are the same as those which were represented in figure 8. The intercept of the linear part of the curves (in figure 9) with the energy axis gives the value of the energy band gap. It is seen that the energy corresponding to the band to band transition changes depending on the pressure of Ar during sputtering. The band to band transition of a stochiometric ZnO (without doping) will take place at around 3.3 eV. As is seen in figure 9 there is an increase of (apparent) band gap for Al-doped ZnO. This increase is due to the density in number of charge carriers. Such an increase in the apparent band gap with increase in free carrier concentration is due to the filling up of the low energy levels in the

conduction band so that the excitation of electrons by photons of proper energy is from the valence band to the higher energy levels of the conduction band. This gives rise to the apparent shift in the band gap and this effect is known as Burnstein-Moss shift[17]. The increase in the band gap values, however are not exactly equal to those predicted by the Burnstein-Moss shift. This occurs since there are other parallel effects like apparent decrease in band gap value due to the merging of the doping levels with the conduction band at high levels of doping. As a net result there is still clear increase in apparent band gap of ZnO with an increase in carrier concentration (9 and figure 10). This means that the onset of the band to band transition is shifted towards the low wavelength side (i.e., towards high photon energies) as the density of the free carriers increases.

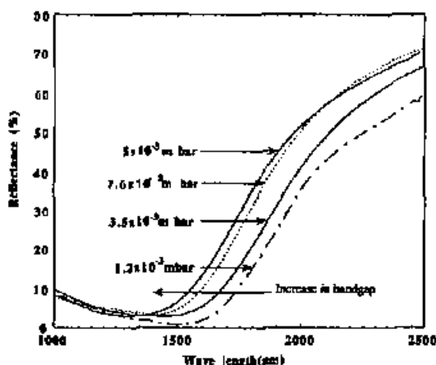

Figure 10 The Reflectance spectrum of ZnO films grown at different Ar pressures. The wavelength for minimum in the reflectance due to plasma resonance varies depending on the density of free carriers($cm^{-3}$) in the film

In figure 11, the transmittance curves of ZnO films grown at different RF power values are shown. The sputtering pressure of Ar was kept at $5 \times 10^{-3}$ mbar since this pressure was considered more suitable for the fabrication of ZnO for solar cells with high conductivity and high deposition rate. The substrate was kept at room temperature. The transmittance is around 80% in the visible region. The transmittance in the long wave length region gets decreased with an increase in RF power. The free carrier absorption in the near infra red region clearly *increases* with increase in RF power values.

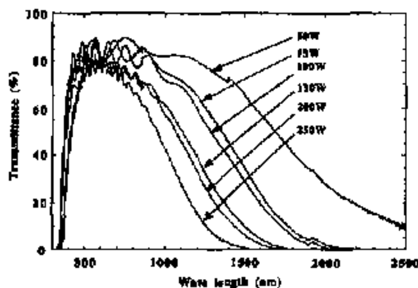

Figure 11. The transmittance spectrum of ZnO films grown at different RF power values during sputtering. The sputtering pressure was $5 \times 10^{-3}$ m bar. The free carrier absorption in the near infra red region increases with increase in RF power

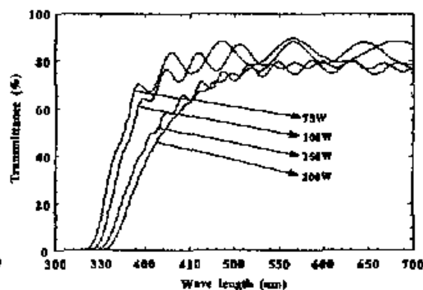

Figure 12 The same transmittance spectrum in the visible wavelength region. The onset wavelength of band to band transition decreases with increase in RF power.

Figure 12 shows the same transmittance curves as those shown in figure 11, but for the ultraviolet region. It is seen that the onset of band to band transition gets shifted towards low wavelength side as the RF power is decreased. Hence a *decrease* in RF power clearly *increases* the onset of the band to band transition. This observation is in contradiction with figure 11 in which it is shown that the absorption due to free carriers increases with increase in RF power. It is seen from equation (1) that the free carrier absorption increases with the increase in the density of charge carriers. On the other hand the band gap should, in general, increase with the increase in density of charge carriers. Our observation seems to be anomalous and need to be investigated further.

The optical band gap of undoped polycrystalline thin films are somewhat different than those reported for single crystalline films. Their actual magnitude depends on the preparation conditions. For doped polycrystalline thin films, three effects should be considered.

(i) when the effective mass varies with a variation in carrier concentration the shape of valence and conduction band can be altered

(ii) the partial filling of the conduction band leads to blocking of the lowest states and hence widening to the optically observed band gap (Burnstein-Moss effect, as observed in the previous case (of different Ar pressures))

(iii) well above the Mott critical density[18] the impurity band is broadened until it merges with the conduction band. This modifies the shape of the conduction band[19] and leads to band gap shrinkage. Effectively a *reduction in the increase of the 'apparent' band gap* will be observed.

Effectively the 'apparent' band gap is increased with increase in charge carrier density. The magnitudes may differ depending on the density of charge carriers and hence the absorption mechanism. (Here after, the term 'band gap' will designate the measured band gap value which is from a theoretical view point an 'apparent' band gap.)

From equation (2) it is seen that the free carrier absorption also increases with decrease in mobility. On the other hand one can see from equation (6) that the minimum in the reflectance due to the plasma resonance mainly depends on the density of charge carriers. Figure 13 shows the reflectance of the same films as those represented in figures 11 and 12.

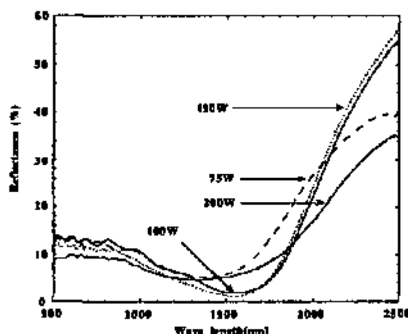

Figure 13 Reflectance spectrum of ZnO films grown with different RF power values during sputtering. The Ar pressure was 5 x $10^{-3}$m bar. There was no intentional substrate heating

As is seen the minimum in the reflectance does not vary gradually as the free carrier absorption does (as seen from the transmittance curves of the same samples). To investigate further, the density of free carriers is calculated from the minimum in the reflectance (equation 6). Such calculations have in the past been shown to yield reasonable values for ZnO[20,21,22,23]. Figure 14 shows the density of free electrons for these films at different RF power values. The charge carrier mobility, derived from the resitivity and density of free charge carriers (mobility, $\mu$=1/N*resistivity*charge of electron ) is also showed in figure 14.

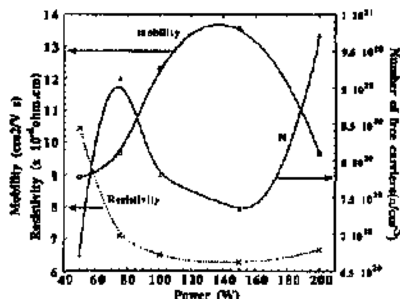


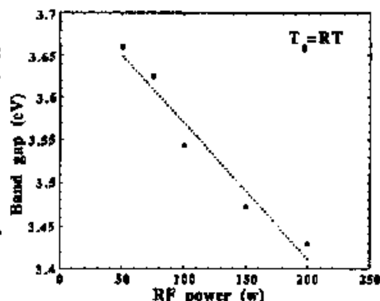


Figure 14 The density of free carriers, mobility, and the resistivity of ZnO grown at different RF power values. The sputtering pressure of Ar was 5 x $10^{-3}$m bar.

Figure 15 The band gap of the same ZnO films of figure 14. (see also figure 12).

The density of charge carriers, as is seen, does not vary in the same way as the free carrier absorption in the near infra red region varies. At RF power values of 75W, 100W and 150W the density of electrons decreases with increase in RF power values. The mobility of electrons in these films increases with increase in RF power. However, at higher RF power levels (e.g. 200W) the mobility decreases again. The variation in mobility will be discussed further in the next section. In the present case, it is noted that the free carrier absorption (shown in figure 11), however, does not follow the equation (2). The band gaps of these ZnO films were determined and figure 15 shows the resulting variation of band gap in function of RF power. (The band gap determination is explained in section 3.4. The present band gap values were calculated using the transmittance, reflectance measurements and using equation (3) and (2) of section 3.4.) As is already observed from figure 12, the band gap of ZnO in figure 15, decreases with an increase in RF power. The variation of free carrier density, shown in figure 14 can be now compared with the variation in band gap. The band gap values of the ZnO films grown at 75W, 100W and 150W increase with an increase in density of charge carriers. The Burnstein-Moss shift in the energy gap can be expressed as[24]

$$\Delta E = \frac{h^2}{8m^*_{vc}}\left(\frac{3N}{\pi}\right)^{2/3} \qquad (7)$$

where $m^*_{vc}$ is the conduction band effective mass. Figure 16 shows the shift in energy gap of ZnO grown at 75W, 100W and 150W proportional to $N^{2/3}$. This demonstrates the band gap widening effect of ZnO as already observed for other TCOs (for ATO (Al doped tin oxide) and ITO[25, 26]). *This shows that the density of free carriers and hence the band gap values can be tailored by changing the RF power*. It is already described that the doping of target is fixed (2 wt.% of $Al_2O_3$). The change in the doping concentration *in* the growing film therefore arises from a variation in the growth process.

The films grown at low RF power value of 50W as well as high RF value of 200W do not change their band gap values corresponding to the relative change in the carrier concentration. However there *is* band gap widening in these films while comparing with the intrinsic band gap value of 3.3 eV of ZnO. It seems that the band gap narrowing (BGN) effects are dominant in the case of ZnO films grown at high RF power values and they are weakly pronounced in the case of ZnO grown at low RF power values. The band gap narrowing effects are theoretically expected[27] to increase further for a polar semiconductor like ZnO due to the polar couplings (shift in the energy values due to the interaction of polar planes).

In figure 12 another important point to be noted is the reduction in the transmittance of ZnO in the wavelength region from 400nm to 500nm with increase in RF power. This reduction in transmittance corresponds to yellow color formation in the films. Hence the absorption in this wavelength region increases with an increase in RF power during sputtering. This yellow color formation is further explained in section 3.4. This absorption corresponds to formation of defects (ionised oxygen vacancies or Zn interstitial) in the material and this defect formation increases with an increase in RF power.

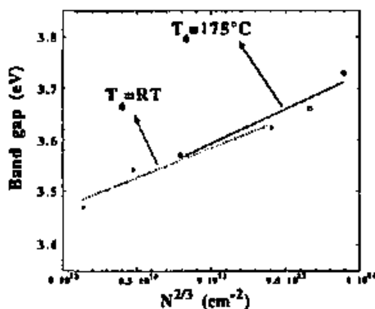


Figure 16 Variation in the band gap of ZnO with carrier concentration showing Burnstein-Moss shift.

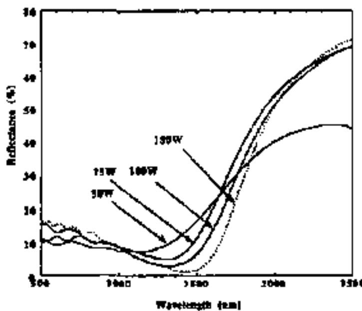

Figure 17 The reflectance of the ZnO films at the plasma resonance region . The pressure of Ar during sputtering was 5 x $10^{-3}$ mbar. The substrate temperature was 175°C.

The reflectance spectrum of ZnO films grown at 175°C with different RF power values are shown in figure 17. The density of free carriers, and the mobility are shown in figure 18. As is seen the density of charge carriers increases with a decrease in RF power. The mobility, similar to the mobility of films grown without substrate heating, increases with the increase in RF power. The difference occurs only at the low RF power values. As explained earlier, as far as the growth of ZnO film is considered, both the RF power or substrate temperature increases the kinetic energy of the adatoms during growth. Hence the growing material at low RF power (50W in figure 17) with increased substrate temperature finds a growth condition (surface mobility) somewhat similar to that of a growing material at slightly increased RF power (75W in figure 14) without increasing the substrate temperature. The band gap values of the same samples in function of RF power is shown in figure 19. In figure 16 the variation of band gap of these ZnO films is also shown in function of $N^{2/3}$. In figure 16 it is seen that in both cases of growth without substrate heating and with substrate heating(175°C), the band gap shows a linear variation with $N^{2/3}$ *explaining the band gap widening effect in ZnO.*

Figure 20 shows the density of free carriers in ZnO film and their mobility in function of Ar pressure. The films are the same as those that were represented in figures 7, 8, 9 and figure 10. At low Ar pressures the density of free carriers and the mobility vary in a similar way. This can be compared with figures 8 and 10. As the density of charge carriers and the mobility vary, for the samples grown at 1.2 x $10^{-3}$ m bar, 3.5 x $10^{-3}$ m bar and 5 x $10^{-3}$ m bar, in a similar way we can expect the free carrier absorption and the minimum in the reflectance due to plasma resonance to vary in a similar way (this means a reduction in free carrier absorption and an increase in value of $\lambda_m$ ). Figure 8 and 10 show, as expected, similar variation. Thus, by looking at the reflectance and the free carrier absorption curves one can obtain the trend of variation of mobility as well as the density of charge carriers.

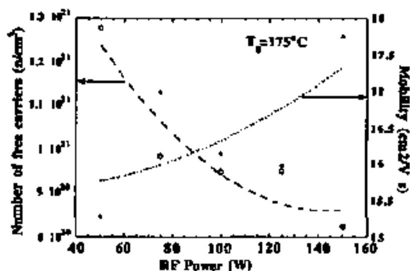


Figure 18 The density of free carriers and the mobility of ZnO films grown at different RF power values. The substrate temperature was 175°C. The pressure of Ar was 5 x 10-3 m bar.

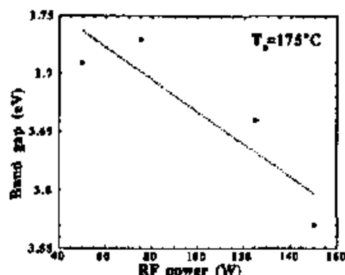


Figure 19 The band gap the ZnO films shown in figure 16 and figure 17. The band gap varies as the density of charge carriers (shown in figure 17) varies.

Figure 21 shows the value of absorption coefficient at 4 eV for ZnO films grown at $1.2 \times 10^{-3}$ m bar, $3.5 \times 10^{-3}$ m bar and $5 \times 10^{-3}$ m bar in function of the carrier concentration ($cm^{-3}$). The decrease in absorption coefficient with an increase in carrier concentration has been reported[13] to be due to the decrease in the joint density of states. Since the absorption coefficient can be expressed as

$$\alpha(h\upsilon) = A\sum P_{ij}g_{if} \qquad (8)$$

where A is a constant. The sum is over all possible transitions separated by energy hv, $P_{ij}$ is the transition probability from the initial state to the final state and $g_{if}$ is the joint density of states. When the transition probability and the electron density in the valence band are constants, the decrease in absorption coefficient occurs[13] due to the reduction of joint density of states with an increase in carrier concentration. This takes place since the increase in carrier concentration decreases the available states for transition in the conduction band (empty states). For ZnO films

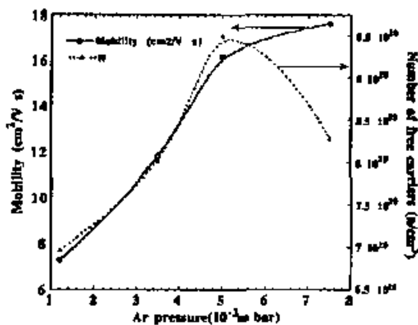


Figure 20 The density of free carriers and the mobility of ZnO films grown at different Ar pressures. The substrate temperature was 175°C. The similar variation of free carrier density and the mobility corresponds to the similar variation of free carrier absorption and the minimum reflectance due to plasma resonance (see figure 8 and 10).

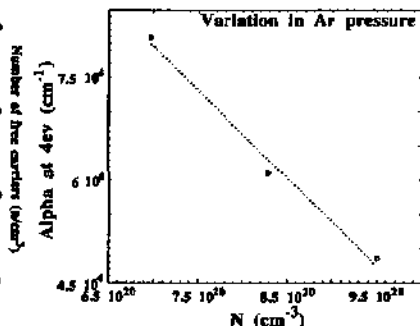


Figure 21 Variation of absorption coefficient at 4eV in function of carrier concentrations for ZnO grown at different Ar pressures.

grown with various Ar pressures, the absorption coefficient and the carrier concentration follow the above explanation. Figure 22 shows the variation of absorption coefficient at 4eV of ZnO as a function of RF power during growth. The pressure of Ar was 5 x $10^{-3}$ m bar and the growth was without substrate heating. It is clearly observed that the increase in RF power leads to decrease in the absorption coefficient. The films grown at 175°C also show a similar variation of absorption coefficient with RF power as seen in figure 22. According to equation (8), the filling up of the electrons in the conduction band should decrease the absorption coefficient at 4eV (reduction of empty states above the apparent band gap) as observed in figure 21. However for the variation in RF power, even though there is an increase in carrier density, there is no decrease in the absorption coefficient. Figure 23 shows the absorption coefficient in function of the carrier concentration for ZnO films grown at different RF power values and at two different substrate temperatures. In contrast with the series where the Ar pressure has been varied and in contrast with previous results [13], the increase in carrier concentration increases here the absorption coefficient of ZnO at 4eV. It seems that the increase in density of carriers due to change in RF power during sputtering is also due to defect formation (interstitial Zn or oxygen vacancy) that gives a free electron (see figure 12). This modifies the joint density of states as well as the transition probability in equation (8). When the increase in charge carriers are due to new defect states, the joint density of states and the transition probability increase and hence the absorption coefficient increases.

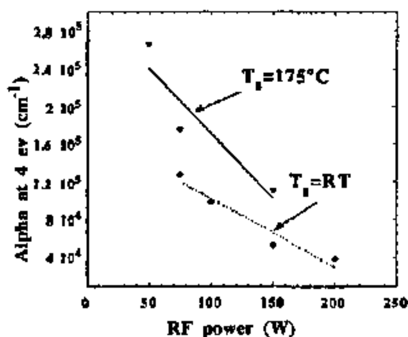


Figure 22 Variation of absorption coefficient at 4eV for ZnO in function of RF power values.

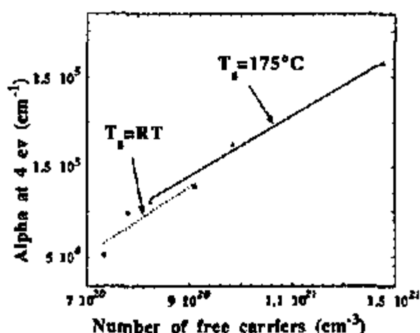


Figure 23 Variation of absorption coefficient at 4eV in function of carrier concentrations for ZnO grown at different RF power values.

### 2.3.3 STRUCTURAL PROPERTIES

The structural properties of ZnO will be discussed in this section. As this forms the base for further analysis on surface textured ZnO in the forthcoming sections, we give here an introduction to the structure of ZnO and to fiber texture growth. To start with, let us look at the X-ray powder diffraction pattern of a typical ZnO film grown by sputtering. Figure 24 shows the standard X- ray powder diffraction of ZnO powder sample[28]. The intensity distribution of diffraction of different planes can be noted. Figure 25 shows the X-ray powder diffraction pattern of ZnO grown by sputtering. The sputtering pressure of Ar was 5 x$10^{-3}$m bar. The RF power was 50W. In figure 25 it is seen that there is only diffraction due to (0002) planes. This is a typical diffraction pattern of ZnO grown by sputtering in our laboratory. The reason for such orientation is the *fiber texture* growth nature of ZnO.

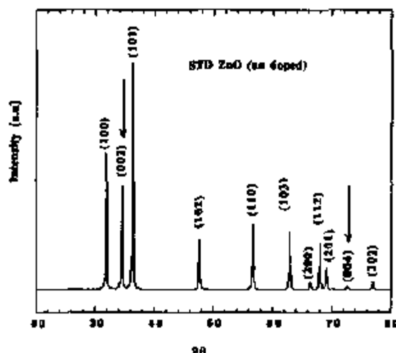


Figure 24. The X-ray powder diffraction pattern of stochiometric standard ZnO (ASTM 36-145).

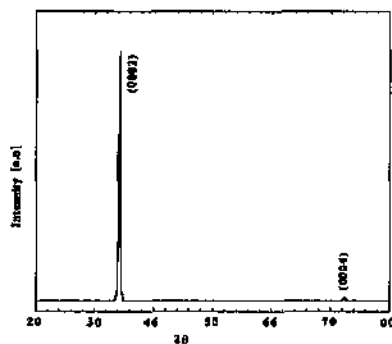


Figure 25 Typical X-ray powder diffraction pattern of ZnO grown by sputtering.

### 2.3.3.1 FIBER TEXTURE

When a crystallographic axis is aligned along some preferred direction of a crystalline aggregate, it is said to be a fiber texture. The occurrence of fiber texture has been known for a long time. Volmer and co-workers [29], in 1921 observed that the Zinc films(Zn) showed a [0001] fiber axis directed toward the evaporation source. Later workers showed that many materials develop fiber textures when evaporated onto amorphous substrates. Dixit[30], in 1933 postulated that the orientation is decided in the initial layers and it is determined by the substrate temperature, crystal structure, atomic radius and the melting point of the deposited material. His theory showed good agreement with the experimental results on Ag, Al and Zn films.

Evans and Wilman[31] described two types of orientations depending on the mobility of the depositing materials. The first one depends on the initial layer as postulated by Dixit. Here the densely populated atomic plane lies parallel to the substrate surface and this gives the fiber axis normal to the surface. In the second orientation there is no initial orientation, but a fiber axis, strongly inclined towards the evaporation source, develops at greater film thickness.

The work of Bauer[32] in 1962 still stands as a standard reference for the fiber texture growth. It gives the comprehensive general texture model. The main points of this model are: on substrates in which the interaction between the substrates and the initial nuclei is weak, the nuclei will be bounded by equilibrium crystallographic planes with one such plane preferentially parallel to the surface. This gives rise to the fiber axis normal to the surface. If the interaction is strong, different transitional and final growth orientation may develop from a randomly oriented aggregate formed either directly on the substrate or by renucleation on an oriented initial layer. The growth orientation is determined principally by the topography of the surface and the angular distribution of the depositing vapour beam.

Van der Drift [33] has given a theory for the orientational growth. It is known as principle of evolutionary selection or 'survival of the fastest' growing planes. It is based on the fastest growing planes. The initial layers may contain all possible orientations. But the plane with the higher growth rate will survive at the cost of the other planes. If two crystals meet, the less steep one ends in the flank of the steeper one: the survival of the fastest. By this theory one could predict the orientation of growing films. This theory is useful for the present study on the structural properties of ZnO.

All above mentioned work supports the general idea of a fiber texture orientation perpendicular to the substrate. ZnO generally exists in a hexagonal wurtzite structure. For ZnO the most closely packed plane or the low index plane is (0001) (the structure and the main planes

of ZnO are explained in section 3.6) This corresponds to a fiber texture orientation along [0001] direction For this orientation the c-axis of the hexagonal crystal system lies normal to the substrates. Usually, Zinc Oxide film is oriented with c-axis approximately normal to the film plane. In some cases ZnO has been grown with its c-axis parallel to the substrate. The orientation with the c axis lying in the film does not have any parallel in the reported work on CdS films[34] and has not been well understood.

N. Fujimura and co-workers [35] have recently (1993) published their work on the control of c- axis orientation for ZnO films. They have shown that by altering the gas ratio in the sputtering atmosphere one can control the orientation against the equilibrium. With that they could achieve (11$\bar{2}$0) orientation. They explain that this effect is due to a change in the tetrahedral co-ordination between Zn and O species in the vapour phase or at the target surface during sputtering.

The c-axis orientation of ZnO films are highly important for some of its applications. ZnO is a piezoelectric material with one of the largest electromechanical coupling coefficients[10] of all non-ferro electric materials and it is used for thin film ultrasonic transducers[36], surface acoustical wave(SAW) devices[37] (band-pass filters, resonators, voltage-controlled oscillators and convolvers in a frequency range of 10MHz to GHz). The ZnO thin film SAW video intermediate frequency (VIF) filters, color TV sets and VTR are now widely in production[38,39]. *For all these applications, a c-axis oriented(perpendicularly) ZnO is highly preferred[40] as the performance of the device depends on it.* To investigate the c-axis orientation of ZnO, structural analysis was carried out on a number of samples grown at different experimental conditions. The deposition parameters varied were

1. Ar pressure,
2. RF Power, and
3. Thickness.

The Ar pressure was covered for the usual sputtering range ($5 \times 10^{-2}$ m bar to $1 \times 10^{-3}$ m bar). The substrate thickness was increased up to 1500nm. The substrate temperature was increased up to 200°C. *In all these cases a fiber texture growth with the c-axis of the hexagonal crystal system perpendicular to the substrate (glass) of ZnO, similar to the one shown in figure 25 was obtained.* The growth conditions just influences the intensity of the diffracted peaks. In some cases, the glass substrates were kept inclined (around 45°C) so that the incident angle was oblique. Still the fiber texture growth was not altered. At the extreme cases of Ar pressure, thin films of ZnO show initial nucleation of other planes while keeping the (0002) plane still highly dominant. Another important point is that almost all the time polycrystalline ZnO was obtained by the sputtering growth. It is in contradiction with the common belief that the sputtering method usually lead to growth of amorphous films [41]. It is to be mentioned here that for most of the above depositions the electrode separation distance was 70mm. An usual electrode separation distance for sputtering is 40mm. The present distance increases the thermalisation of high energy sputtered particles.

As long as we do not mix other gases with Ar, the ZnO film formed by sputtering showed high fiber texture orientation. The mixing of oxygen with Ar can easily alter the orientation of ZnO by sputtering. By reactive sputtering (using mixture of Ar and $O_2$), T. Hada [42] could obtain c-axis parallel as well as c-axis perpendicular orientations of ZnO. C. R. Aita [43], more specifically reported that when the ratio of Ar to $O_2$ during sputtering is 3:1, a c-axis perpendicular orientation is obtained. N. Fujimura showed that when the same ratio is 1:3, c-axis parallel orientation can be obtained. K. Ohji et al. [44,25] have reported a need for a hemispherical electrode system for sputtering in order to get high c-axis orientation of ZnO. They used 50% oxygen in the mixture of $Ar/O_2$. According to our studies, the reason one obtains a modification of c-axis perpendicular orientation is given by the role played by the oxygen during growth. Hence, the important thing is to reduce the oxygen during sputtering rather than to vary the electrode configurations. Similarly the kinetic energy of adatoms during growth (given by the substrate temperature and the RF power) is more important than the angle of incidence for the growth of highly oriented ZnO films. From the present studies, one can realise the advantage of

using an oxide target and sputtering with Ar (than having a metallic target and to sputter with Ar/$O_2$ mixtures) for the purpose of fabricating highly c-axis oriented ZnO films.

### 2.3.3.2 Variation in Ar pressure

Figure 26 shows the X-ray powder diffraction pattern of ZnO films grown at different Ar pressures. The experimental conditions were similar to the previously explained Ar series. The RF power was 100W. The substrate temperature was 175°C. The films have comparable thickness values. The diffraction pattern has peaks due to diffraction of (0002) planes. In figure 26 the diffraction due to only (0004) (second order) is shown.

First, it is seen that the intensity increases with the increase in Ar pressure, peaks at Ar pressure of 5 x $10^{-3}$ m bar, then it decreases with further increase in Ar pressure. Figure 26 can be compared to figure 7 where the resistivity of the same samples are plotted in function of Ar pressure. The minimum resistivity of ZnO grown with Ar pressure of 5 x$10^{-3}$ m bar corresponds to the maximum in intensity of diffraction peak (0004) shown in figure 26. An increase in intensity of diffraction pattern is attributed to the increase in crystallinity of the films. Figure 27 shows the Full Width at Half Maximum of the diffraction (FWHM) peaks (shown in figure 21) in function of Ar pressure. From the FWHM, one can estimate the average grain size of the polycrystalline film that undergoes diffraction. The average grain size, as given by Scherrer's formula[30], is inversely proportional to the FWHM. As the absolute value of the grain size is difficult to estimate[45,16] we take the FWHM as a measure of the grain size. As is seen in figure 27, the average grain size of the ZnO films is maximum when the pressure of Ar is 5 x $10^{-3}$ m bar. To correlate the electrical properties with structural properties further, the density of free charge carriers(cm$^{-3}$) in the same films (from figure 20) are also shown in figure 27. It is seen that *with the increase in average grain size, the density of free electrons in the films clearly increases.* Thus, the FWHM derived from the X-ray diffraction patterns and the charge carrier density clearly correlate with each other. The mobility of the films shown in figure 20, can also be compared with the FWHM shown in figure 27. At low Ar pressures, the mobility increase with the increase in grain size. The mobility of charge carriers are affected mainly by two types of scattering. One is grain boundary scattering and the other is ionised impurity scattering. The grain boundary scattering decreases with the increase in grain size. We observe for the ZnO films grown at 1.2 x $10^{-3}$ m bar, 3.5 x $10^{-3}$ m bar and 5x $10^{-3}$ m bar that the increase in grain size increases the mobility. *This shows that , in this region the grain boundary scattering mechanism is the dominant* and that decides the mobility. In films grown at high Ar pressures, on the other hand, the mobility depends on other scattering mechanisms.

Figure 26 X-ray diffraction patterns for ZnO films grown at different Ar pressures.

Figure 27 The Full Width at Half maximum of the X-ray diffraction peaks for ZnO films grown at different Ar pressure. This can be correlated with the density of free carriers/cm$^3$ in the film.

### 2.3.3.4 VARIATION OF RF POWER

The X-ray diffraction patterns of the ZnO films grown at different RF power is shown in figure 28. The Ar pressure for the growth was $5 \times 10^{-3}$ m bar . The substrate was kept at room temperature. It is seen that the RF power increases the intensity of the diffraction peak. At high RF power values, however, the intensity decreases. It shows that the crystallinity of ZnO films decreases during the growth with high RF power values . At low RF power values an increase in RF power during sputtering increases the crystallinity. The FWHM values of the diffraction peaks (shown in figure 28) in function of RF power is shown in figure 29. It is seen that the FWHM varies with the power in the same way as the intensity of diffraction peak varied. This shows that *the average crystallite size and the crystallinity increase with an increase in RF power*. A high RF power value during sputtering reduces the crystallinity and the grain size. One can expect an increase in crystallinity and grain size with an increase in RF power during sputtering as this increases the kinetic energy of adatoms during growth. *This may not be true, however, in the case of sputtering at high RF power.*

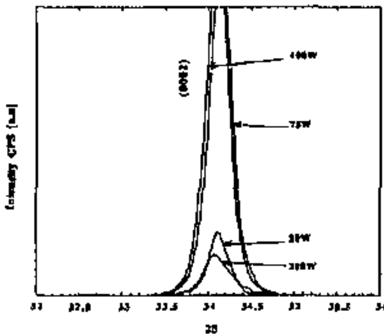

Figure 28. The X-ray diffraction pattern of ZnO films grown at different RF power values. The Ar pressure during growth was 5 x 10-3 m bar.

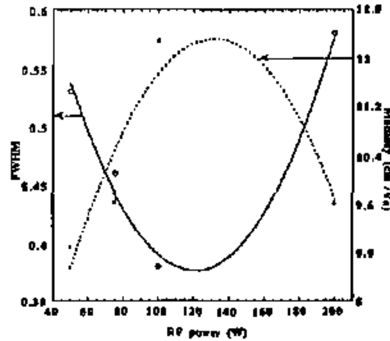

Figure 29 Variation of FWHM of the diffraction peaks shown in figure 28, in function of RF power. The increase in average crystallite size increases the mobility of charge carriers. This shows that the dominant scattering mechanism is grain boundary scattering.

In figure 29 the FWHM is also plotted together with the mobility of charge carriers. As is seen, the mobility increases as the FWHM decreases, that is, as the grain size increases. The mobility decreases when the grain size decreases. This shows that the possible scattering mechanism that affects the mobility of free charge carries is grain boundary scattering. The density of free carriers, on the other hand (shown in figure 14), can not be explained in terms of average grain size. It is observed that the density of charge carriers decrease with increase in grain size.

It is explained for the series with different Ar pressures that the free carrier density increases with an increase in the grain size. The mobility increases with an increase in grain size up to the Ar sputtering pressure of $5 \times 10^{-3}$ m bar. The pressure of Ar for the present power series is $5 \times 10^{-3}$ m bar. At high Ar pressures the variation of mobility with the average grain size may be different. It is seen from figure 29 and figure 27, that the variation in grain size with Ar pressure during sputtering mainly influences the density of charge carriers and the variation in the grain size with RF power mainly influences the mobility.

Figure 30 shows that the X-ray diffraction pattern of ZnO films grown at different RF power values during sputtering. Ar pressure was kept at $5 \times 10^{-3}$ m bar. This was done since this pressure is considered to be required for high conductivity as well as high deposition rate of ZnO

films for the application in solar cells. In contrast with the previous series, the substrate was kept at 175°C. Here also the same trend in variation of diffraction peak intensity with the RF power is observed. The low RF power increases the intensity and the high RF power reduces the intensity. Figure 31 shows the FWHM of the diffraction peaks in terms of RF power. The FWHM decreases with an increase in RF power. This shows, similar to the previous power series at room temperature, that the increase in grain size with an increase in RF power. The mobility of the charge carriers, in general, varies with grain size as the previous case. The mobility values in this present case are higher than the values obtained for the previous case as there is substrate heating plus high RF power to increase the average grain size and the crystallinity.

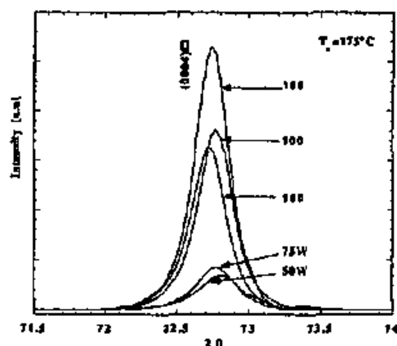


Figure 30 X-ray diffraction pattern of ZnO films grown at different RF power values during sputtering. The sputtering pressure of Ar was 5 x $10^{-3}$ m bar. The substrate temperature was 175°C.

In figure 32 the density of free carriers in function of RF power is compared with the FWHM of the peaks in the X-ray diffraction pattern (figure 30). The increase in grain size, similar to the previous case decreases the charge carrier density in the film. It seems that with increase in RF power the doping efficiency of Al in ZnO is reduced.

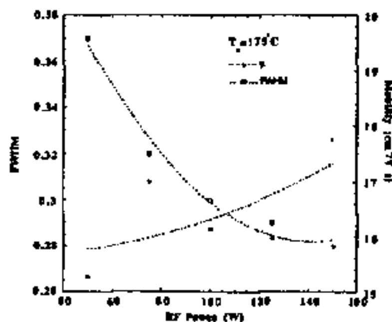


Figure 31 The FWHM of the ZnO film grown at different RF power values. The substrate temperature was 175°C. The Ar pressure was 5 x $10^{-3}$ m bar.

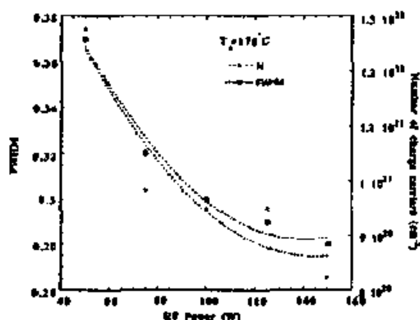


Figure 32 The FWHM of the peaks in the X-ray diffraction pattern and the density of charge carries ($cm^{-3}$) in the film.

## 2.4 Conclusions

Flat ZnO films by RF magnetron sputtering have been studied in detail in this section. The effect of sputtering pressure and of RF power on the electrical, optical and structural properties of ZnO was analysed in detail. The electro-optical properties could be well correlated with the structure of ZnO. The influence of RF power during sputtering is important for the deposition rate, for crystallinity and for charge carrier mobility of ZnO, whereas the influence of sputtering pressure of Ar is important for the conductivity and crystallinity of ZnO. It is explained how the band gap, the absorption coefficient and the structure of ZnO can be influenced by the growth conditions. These results are useful for any application of ZnO in general. These results form the base for the further optimisation of ZnO for solar cell applications. In the forthcoming chapters ZnO films with textured surface will be studied.

## References


[1] J. A. Anna Selvan and Pascal Duport, The User manual for RF sputtering unit for ZnO films,
Institute of Microtechnology internal reports, University of Neuchâtel, 1994.
[2] For example see, K. Ellmer, F. Kudella R. Mientus, R. Schieck and S. Fiechter, Thin solid films, 247 (1994) 15-23.
[3] B. Chapman , Glow Discharge Process, sputtering and plasma etching, John Wiley & sons,1980.
[4] K. L. Chopra, Thin film phenomena, New York, McGraw-Hill (1969).
[5] See for example, R. Flückiger, Annexe of Ph.D thesis, Institute of Microtechnology, University of Neuchâtel, for the cleaning procedure of glass substrates.
[6] O. Carter and J. S. Colligon, *Ion Bombardment of Solids*, Elsvier (1968).
[7] See section 3.10 for the variation of growth rate with variation in growing (crystallographic) direction.
[8] Effect of high RF power on the growing surface of ZnO is discussed in section 3.8.
[9] P. Pernet, M. Goetz and R. Felder, 'A-Si solar cells on metal and plastic substrate' in proceedings of 4th Euregional workshop on Amorphous silicon solar cells 1996.
[10] K. L. Chopra, S. Major and D. K. Pandya, Thin solid films, 102 (1983) 1-46.
[11] R. A. Smith, Semiconductors, Cambridge University Press, 1959.
[12] See also section, 3.5 on electrical properties of surface textured ZnO.
[13] K. Wasa, S. Hayakawa, Hand book of Sputter Deposition Technology, Noyes publications, 1991, p145.
[14] R. E. Hummel, Electronic properties of materials, Narosa Publishing House, 1985.
[15] Y. Qu, T. A. Gessert, K. Ramanathan, R. G. Dhere, R. Noufi and T. J. Coutts, J. Vac. Sci. Tech. A 11(4), 1993, 996.
[16] H. Kostlin, R. Jost, and W. Lems, Phys. Status, Solidi 29, 87 (1975).
[17] E. Burnstein, Phys. Rev 93, 632 (1954),
T. S. Moss. Proc. Phys. Sor. London Ser B 67, 774 (1954).
[18] N. F. Mott, *Metal-Insulator Transistors* (Barnes and Noble, New York, 1974), chap 4.
[19] M. Combescot and P. Nozieres, J. Phys. C5, 2369 (1972).
W. Kohn and L. J. Sham, Phys. Rev. 140, A1133 (1965).
P. R. Rimbey and O. D Mahan, Phys. Rev B 10, 3419 (1974).
[20] Z.-C. Jin, I. Hamberg, and C. G. Granqvist Appl. Phys. Lett. 51 (3).
[21] I. Hamberg and C. G. Granqvist, J. Appl. Phys. 60, R123 (1986).
[22] A. E. Delohoy and M. Chemy in Thin Films for Photovoltaics and Related Device Applications MRS proceddings, Volume 426, p467, 1996.
[23] J. Hu and R. G. Gorden, J. Appl. Phys 71(2) 1992, 880.
[24] H. Kölstin, R. Jost and W. Lems, Phys. Status Solidi A, 29 (1975) 87.
[25] E. Shanti, A. Banerji and K. L. Chopra, thin solid films, 88 (1982) 1615.
[26] Y. Ohhatta, F. Shinoki and S. Yoshida, Thin solid films, 59 (1979) 255.

[27] Bo E. Sernelius Phys. Rev B 36,9, 4878, 1987.
[28] ASTM card no 36145.
[29] Gross, R and M. Volmer, Z.Physik ,2 188, (1921).
[30] Dixit K.R Phil. Mag., 16, 1049 (1933).
[31] Evans, D. M., and H. Wilman, Acta Crys., 5,731 (1952).
[32] E. Bauer, Trans 9th Vac Symp.Am. Vac. Soc. (los Angeles 1962), Macmill Comp. New York, 1962, pp. 35-44.
[33] A. Van der Drift, Philips Res. Repts 22, 267-288,1967, R626.
[34] Hand book of thin film technology Edited by L. I. Maissel and R. Glang, McGraw Hill Book company, 1970.
[35] N. Fujimura, T. Nishihara, S. Goto, J. Xu and T. Ito J. Cryst. Growth 130 (1993) 269-279.
[36] Ohji, K., and Wasa, K., Proc 1981 Meeting of IEEE Japon, 5000.
[37] White .R. M Proc. IEEE 58.1238.
[38] Hays, R. M., and Harman, C. S, Porch IEEE, 64:652.
[39] Yamazaki, O., Mitsuyu, T., and Wasa, K., IEEE Trans. Sonics and Ultrason. SU-27:369
[40] Handbook of Sputter Deposition Technology by Kiyotaka Wasa and Shigeru Hayakawa, Noyes Publications, 1991.
[41] Reference [10], p6.
[42] T. Hada, Thin solid films, (1971) 135-145.
[43] C. R. Aita, A. J. Purdes, R. J. Lad and P. D. Funkenbusch J. Appl. Phys. 51 (10) 5533,1980.
[44] K. Ohji T. Tohda, K. Wasa and S. Hayakawa, J. Appl. Phys, 47(4) (1976) p.1726-1728.
[45] See section 3.6 on structural properties of surface textured ZnO.

# 3

# Surface Textured ZnO thin films

## 3.1.1 Introduction

Transparent Conducting Oxides (TCO) are essential for thin film solar cells. They are used as the top layer as well as back contact in the solar cells. When used as the top layer the TCO should have maximum transmittance, in the wavelength region between 300nm to 1000nm usually, as well as high electrical conductivity. When used as a back contact it should also serve as a good back reflector but for those wavelengths close to the absorbtion edge of the active semiconductor namely the near infra red region. Usually the back reflector is a system that consists of TCO/metal film. In both cases, the optical transmittance of the TCO should be as high as possible.

In order to increase efficiency of solar cells the amount of light entering the solar cell should be increased. By 'texturing' the surface of the TCO layer of the thin film solar cell one can increase the amount of light that is entering into the active part of the cell. 'Texturing the surface' simply means 'roughening the surface' or 'making a non smooth surface'.

It is explained in the first chaper that the TCO, in particular ZnO, can serve the purpose of windows, back reflectors and diffusion barriers for thin film solar cells. When used as the window layer, the surface textured TCO decreases the amount of reflected light. Because the primarily reflected light ray from the textured surface has a second chance of being coupled into the cell. Hence, the effective amount of light entering into the cell increases. The solar cell with a highly conducting, transparent oxide layer with the textured surface can be said to have an efficient 'window'.

On the other hand, when used as the back reflector, the unused light that reaches the back contact is reflected efficiently by a surface textured TCO/metal system. The light that is not utilised by the solar cell, thus, goes back again into the device. This increases the spectral response of solar cells in the long wavelength region (otherwise weakly absorbed region). The way of making maximum amount of light to go inside the device is known as 'light trapping'.

By having the surface of the TCO textured, one can thus increase the amount of light that is useful for photovoltaic action. This enhances the photo current and, hence, the efficiency of solar cells.

Secondly, when the light is entering through the surface textured TCO, the light ray is scattered in all directions. By this, the optical path length of the light ray inside the cell is increased. The diffused light with its with increased optical path length has a higher probability to generate electron-hole pair. This leads to enhanced photo voltaic action in the long-wavelength, low absorption region of the optical spectrum. Specifically, this increases the probability for the electron-hole pair to be generated in the i-layer of an amorphous silicon p-i-n solar cell. This is a significant advantage in having surface textured TCO; this helps to increase the efficiency further. With this, the absorption of light improves over the entire wavelength range of interest [1,2].

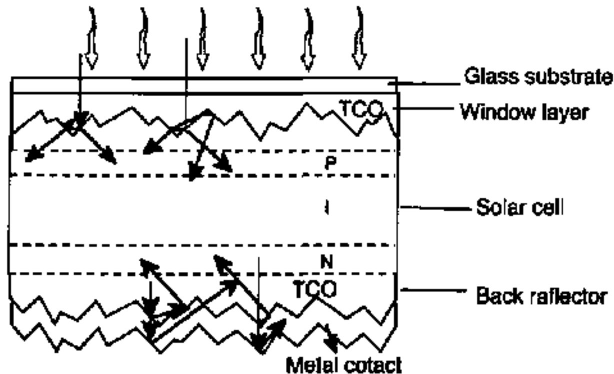


Figure 1. Light trapping in thin film solar cells. The rough surface of TCO increases the optical path length of the light inside the solar cell. This increases the amount of absorption of light which is otherwise weakly absorbed. The back reflector reflects back the unused light while increasing the optical path length of them. The figure shows the structure of PIN solar cells. Here the substrate is glass and the light enters through it. For an NIP configuration, the substrate is metal or a flexible polymer and the device structure is reversed.

The increase in the optical path length of the light inside the cell requires less amount of device material (e.g., a less thick i layer in a-Si:H or a μc-Si:H solar cell) for obtaining sufficient photovoltaic action. The reduction thickness in an a-Si:H solar cell reduces the light -induced degradation of the solar cell efficiency w. r. to its initial value (Staebler-Wronski effect)[3]. Furthermore this leads to cost reduction in fabrication of these types of solar cells, especially in the relatively thick μc-Si:H solar cells. A. Banerjee et al. [3] have reported that the use of a textured back reflector reduces the degradation of the solar cells.

To summarise, the surface texturing of the TCO is leading to

1. Increase in the amount of light for the photovoltaic action for thin active layer.

2. Increase in the optical path length of the light; increases the photo current over the entire wavelength region of interest.

3. Reduction in cell thickness; this reduces in the degradation in the efficieocy of a-Si:H cells and leads to cost reduction.

As has been explained in the introductory chapters, Zinc Oxide has been selected as a TCO mainly for the following specific reasons. ZnO is:

1. Highly stable against hydrogen plasma.

2. Highly stable against high temperature process.

3. It serves as a diffusion barrier for metal diffusion from the substrate.

4. It is less expensive

5. Inert with respect to the on growing layers

These are the *unique features of ZnO while comparing with the conventional TCOs* like tin doped indium oxide (ITO) or fluorine doped tin Oxide ($SnO_2$).

Hence it is highly desired to have surface textured Zinc Oxide thin films. The method of sputtering, as has been explained in the previous chapters is selected as a main deposition method for the following reasons:

1. Effective control over the growth

2. Suitable for large-scale applications

3. Simple and less expensive

### 3.1.2 Review on surface texturing for solar cells

Light-trapping techniques for single crystalline solar cell have been studies since quite a long time while compared with those for thin film solar cells [4]. For single crystalline silicon solar cells, the surface of the silicon is etched anisotropically to have rough surface [5]. One of the limitations of texturing the surface of the silicon itself is the trapping of all light including the unwanted infrared radiation of insufficient photon energy to create electron-hole pair. This tends to make the cells 'hotter' [5]. Texturing of TCO, in particular ZnO, will not lead to this situation as ZnO itself absorbs the near infra red light [7]. For thin film silicon solar cells, especially a-Si:H solar cells, the improvement in efficiency, in terms of the short circuit current, due to introduction of texture on the TCO surface [8] or on the back electrode [9,10,11,12,13] has been realisod since 1983.

The primary works on surface texturing of TCOs have been done with doped tin oxide films ($SnO_2$). Surface textured $SnO_2$ films have been grown by the method of spray pyrolysis[8], and by chemical vapour deposition (CVD) [14]. The commercially most successful method is the growth of fluorine doped $SnO_2$ films by using atmospheric pressure CVD[15,16] by Asahi Glass Co. Ltd. of Japan. The surface textured $SnO_2$:F films grown by this company has become a standard TCO substrate for several solar cell research groups. However, $SnO_2$ films do not show sufficient chemical stability against the action of a hydrogen plasma looking at the subsequent a-Si:H or µc-Si:H deposition. The plasma exposure of $SnO_2$ films leads to compositional changes [17]. Furthermore, higher substrate temperatures in subsequent deposition steps leads to a reduction in the optical transmission of the $SnO_2$ films. It was therefore necessary to develop a TCO which is stable w. r. to hydrogen plasma and which is optically and electrically superior to the conventional $SnO_2$ and ITO films.

In the previous chapters it has been explained that ZnO thin films show superior performance in terms of stability against hydrogen plasma and high subsequent deposition temperatures [18,19] in order to be applicable to solar cells. Therefore, it has become desirable to *have surface textured growth of ZnO films. After realising the advantage of ZnO over other TCOs* several research groups started to work on the growth of surface textured ZnO. There have been reports on surface textured ZnO films prepared by spray pyrolysis [20, 21], by metal organic chemical vapour deposition (MOCVD) [22, 23] and by magnetron sputtering [24]. It is our opinion that of all these works CVD and sputtering method reported by T.Nakada et al. have shown the most interesting results w. r. to surface textured growth of ZnO films.

It is well known that the sputtering technique is suitable for low cost and large-scale production of thin films. Even though the sputtering methods provides good control over the growth, effective methods for production of surface textured ZnO films by spottering have not yet been realised. The exception is the work in sputtering by T. Nakada et al. They used a mixture of water vapour and Ar during sputtering to obtain surface textured ZnO thin films.

The *first sputtering experiments to grow* TCOs in the *atmosphere of water vapour* was done for the growth of ITO thin films [25]. The aim was to study the effect of water vapour in the residual gas atmosphere from the view point of the mass production process. While increasing the partial pressure of water vapour Yuzu Shigesato et al. have observed roughness in the surface of the ITO films.

Tokio Nakada et al. followod the same process and used water vapour in *DC sputtering* for the growth of surface textured ZnO films. By the method of DC sputtering they achieved surface texture of ZnO films by using a mixture of Ar and water vapour. Highly conducting ZnO

films were obtained by sputtering with substrate temperature higher than 350°C and, then, by annealing the films at 400°C in vacuum for 7 hours. The corresponding haze factor obtained was 18%.

For surface textured ZnO transparent electrodes deposition on the top of the active layers of a-Si:H and $CuInSe_2$ solar cells, however, the film deposition must be carried at temperatures below 250°C, in order to avoid interdiffusion of metal ions between the underlying thin-film layers. Hence, the method of Tokio Nakada et al. could not be used for the deposition of ZnO on the active layers of such solar cells

In this work we have mainly concentrated on the surface textured growth of ZnO by *RF magnetron sputtering*. In contrast with previously reported methods, our aim is to have surface textured growth of ZnO thin films at low temperatures (temperatures below 200°C) so that the method can be very well used in the thin film solar cell technology: We thereby have studied study in detail the corresponding growth process and mechanisms.

As the potential of surface texturing is most important for the field of solar cells, there is an increasing necessity to grow surface textured TCO thin films. There are lot of theoretical models about the effect of having textured TCO [26] in solar cells. In practice very few attempts have been made to understand the growth procedure of 'surface texturing'. The importance was given in optimising the growth conditions for surface textured growth. But the basic questions are: How can one obtain sufficient surface texturing during growth? What growth mechanism causes surface texturing of any thin film, and in particular, of ZnO? Is it possible to tailor the surface properties of the thin films of ZnO? These are the very basic questions we tried to answer in this work on surface textured growth.

In order to carry out this, we constructed a RF magnetron sputtering system for the growth of surface textured ZnO thin films. The details of the system are explained in the previous chapter. By using the mixture of water vapour and Ar during sputtering we have successfully grown surface textured ZnO:Al films.

The target material for the sputtering is a sintered ceramic disc with the composition of ZnO:$Al_2O_3$ in the stochiometric ratio of 98:2 wt.%. The addition of 2% aluminium is due to the necessity of doping ZnO. This is an optimised composition and has been used by many research groups. The diameter of the target is 72mm. The distance between the target and the substrate has been kept at 70mm.

Highly textured and electrically conducting ZnO thin films were obtained at the following 'standard' experimental conditions: the total sputtering pressure was $3.5 \times 10^{-2}$ m bar, the partial pressure of water vapour was kept at $2 \times 10^{-4}$ mbar. The RF power was 200W. The substrate temperature was 150°C.

During the experiments, the growth conditions were changed and the resulting properties were analysed. The partial pressure of water vapour during growth in addition to Ar, the RF power and the substrate temperature were the main parameters that were varied. Three series of ZnO thin films were grown by varying these parameters and departing from the standard values.

In a first series the partial pressure of water vapour is varied. We refer here to the water vapour that is mixed with the Ar gas. This series of ZnO films was deposited at a fixed value of RF power and substrate temperature. The partial pressure of Ar was kept constant so as to obtain a corresponding total working pressure that was also constant. This series is called 'water vapour series'.

In a second series, we vary the RF power while keeping the partial pressure of water vapour and the substrate temperature constant. This series is called 'the power series'.

In a third series we vary the substrate temperature while keeping the partial pressure of water vapour and the RF power constant. This series is called 'the temperature series'.

All these ZnO films were characterised w. r. to their surface, optical, structural and electrical properties. The surface properties were analysed using a Scanning Electron Microscope

(SEM) and a Atomic Force Microscope (AFM). The optical properties were analysed using a spectrophotometer that has an integrating sphere. The structural properties were analysed using the X-ray powder diffraction method with Cu-$k_\alpha$ radiation. The electrical properties were analysed using the four probe method and Van der Poe method.

In this chapter, the growth of surface textured ZnO thin films and their resulting properties are studied in detail. In the analysis of surface properties, it will be shown that the ZnO thin films manifest two distinct surface morphologies. Furthermore the AFM analysis reveals a clear distinction between these two type of morphologies. The optical properties reveal the effect of water vapour on the *optical transmittance*, the *optical reflection* and on the *'haze factor'* of *ZnO* thin films. In the same section a method that can be used to achieve low temperature surface texturing of ZnO thin films has been explained. In the analysis of structural properties the effect of water vapour on the structure of ZnO thin films has been studied. It has been found that the water vapour should be dissociated to obtain a surface texture growth.

Non equilibrium growth of ZnO, as an effect of adding water vapour during sputtering, has been demonstrated. The structural transition of ZnO from the hexagonal wurtzite structure to the cubic structure has been shown. The reasons that lead one to obtain two different surface morphologies as well as the connection between the surface properties and the structure have been explained.

The connections between haze factor, RMS roughness, excess area (i.e. excess surface area over the geometrical area) and the grain size of these films have been shown.

Thanks to the mastering of the effects control related to surface morphology and to other film properties, surface textured ZnO films with a conductivity of 14 x$10^{-4}$ ohm.cm and a haze factor of 50% have been obtained. The performance of solar cell using surface textured ZnO thin films has been demonstrated.

NOTE

There is confusion of terms in the literature. Usually a TCO with rough surface is called 'textured TCO'. However, the usual meaning of the word 'texture' in crystallography is a preferred orientation which is in reality a bulk property of material. Hence there results a confusion when explaining the real preferential orientation of the TCO and its surface roughness at the same time. To avoid this we use the term 'surface texture'.

### References

[1] H. Lida, T. Mushuku, A. ITO and Y. Hayashi, IEEE Electron device ED-34 (1987), 271.
[2] H.Sakai, Y. Ichika, Maruyama, T. Yoshida, M. Kamiyama and Y. Uchida No.SPC 85-87 *of semiconductor power conversion research meeting*, Tokyo.
[3] A. Banerjee, K. Hoffman, X. Xu, J. Yang, and S. Guha, first WCPEC, Dec 5-9, 1994, Hawai.
[4] S. R. Chitre, 13th IEEE photovoltaic Specialists Conference, Washington, D. C., 1978, pp 943-947.
[5] M. A. Green, Solar cells, National Library of Australia, University of New South Wales, 1982, p165
[6] See for example, J. A. Anna Selvan, 'Development of Back Surface field Silicon Solar Cells', M. Tech thesis, Indian Institute of Technology, 1992 and references there in.
[7] See the optical properties of conducting ZnO in chapter 2 or in section 3.4.
[8] H. Lida, N.Shiba, T. Mishuku, H. Karasawa, A. Ito, M. Yamanaka and Y. Hayashi; IEEE Electron Device Lett. EDL-4 (1983).
[9] V. L. Dalal, IEEE Electron Devices ED-27 (1980) 662.
[10] W. Chubatji, M. Shur, K. Ng and A. Madan, Proc. 14th IEEE potovoltaic conference, San Diego, 1980 (IEEE; NY, 1980).
[11] W. Den Boer and R. M. van Strijp, Proc 4th commision of the EC Conf. on PV solar

energy, Stesa, May 10-14, 1982 (Riedel, Dordrecht, 1982).
[12] H.Deckman, C. Wronski, H. Witzke and E. Yablonovitch, Proc.16th PV specialist' Conf., San Diego, Sept 27-30.
[13] K.Fujimoto, Okamoto and Y. Hamakawa Sol. Cells 11 (1984).
[14] M. Mizuhashi, Y. Gotoh and K. Adachi Jap. J. Appl. Phys. 27. No. 11, 1988, 2053.
[15] K. Sato, Y. Gotoh, Y. Hayashi, K. Adachi and H. Nishimura, Technical Digest PVSEV 5, Kyoto Japan, 1032.
[16] M. Komakine, H. H. Nishimura, Y. Gotoh, K. Adachi and K. Kondo, Mat. Ress. Symp. Proc. Vol.192.
[17] K. Sato, A. Adachi and M. Mizuhashi, Reports Res. Lab. Asahi Glass Co., Ltd., 37, 13 (1983).
[18] S. Major, S.Kumar, M. Bhatnagar and K. L. Chopra Appl. Phys. Lett. 49 (1986) 394.
[19] T. Minami, H. Nanto and S. Takada: Jpn. J. Appl. Phys.23 (1984) L280.
[20] S. Major and K.L. Chopra, sol Energy Material 17, 319 (1988).
[21] C. Lee, K. Lim, J. Song, Sol Energy Mat. and Sol. Cells 43 (1969) 37.
[22] A. Yamada, W.W. Wenas, M. Yosshino, M. Konagai and K. Takahashi Jpn. J. Appl phys. 30, L1152 (1991).
[23] J. Hu and R. G. Gorden J. Appl. phys. 71, 880 (1992).
[24] T. Nakada, Y. Ohkubo and S. Takada Jpn. J. Appl. Phy, 30 No. 12A, Dec 1991, 3344.
[25] Yuzu Shigesato, Yasuo Haya shi, Akio Masui and Takeshi Haranou, Jap. J.App.Phy 30, no.4 1991. p 814-819.
[26] See for example, G.Tao, J. W. Metselaar Sol. Energy mat. and Sol. Cells 34 (1994) 359-366.
Also J. Furlan, S. Amon, P. Popovic, F. Smole First WCPEC, Hawai, 1994, p.658.

# 3.2 Surface properties

There are three important properties we require from ZnO thin films. They are;

1. High electrical conductivity to make ohmic contact layers.

2. High optical transmission to allow maximum amount of useful light inside the solar cells

3. Textured surface for the purpose of light trapping.

Among these three properties the third property is a recent requirement and it is yet to be developed. In order to study the surface texture growth of ZnO thin films, the study of the surface properties is essential. In this section, the variation in surface morphology of ZnO thin films that occurs at different experimental conditions is explained in detail.

## 3.2.1 SEM analysis

For the analysis of surface properties, Scanning Electron Microscope (SEM) and Atomic force microscope studies (AFM) were done. In the present section SEM studies on ZnO:Al films are discussed. The SEM studies were executed using an electron microscope of Cambridge Instruments co. (Type 250, M-K-3). The apparent viewing angle is around 45°. Those ZnO films that were highly conducting rendered good quality image of the surface. For those samples that had high resistivity it was, due to the low value of the electron current, difficult to make a good image of the surface. In order to get clear images, the surface of all the films under study in this section were coated with very thin gold film. The deposition of the gold film was done by sputtering.

## 3.2.2 Results

### 3.2.2.1 Water vapour series

Figure. 1 shows the Scanning Electron Microscope (SEM) photographs of the surface of ZnO films that were grown at different partial pressures of water vapour in the mixture of $H_2O$:Ar. The RF power was kept constant at 200W and the substrate temperature was kept constant at 200°C. The total sputtering pressure was $3.5 \times 10^{-2}$ mbar. At first sight one can observe the following points: The ZnO film that is grown with 100% Ar shows a flat surface (figure 1.a). The increase in partial pressure of water vapour increases the surface roughness of the ZnO films. A closer look at these surfaces clearly demonstrates two different surface morphologies. We classify these surface morphologies into two types: Type I and Type II. The sample that is grown at nearly 100% water vapour shows again an almost flat surface (figure 1.f).

At low partial pressure of water vapour the surface morphology has well formed faceted angular grains (figures 1.b and 1.c). We will call this surface morphology 'columnar morphology'. As the partial pressure of water vapour increases, the surface morphology changes completely to a new appearance. Here, the faceted angular grains have completely disappeared and the surface has more rounded grains (figures 1.d and 1.e). We will call this surface morphology 'granular morphology'.

A closer observation of columnar surface morphology reveals that the surface consists of grains with *hexagonally shaped pits*.

### 3.2.2.2 Power series

Keeping the partial pressure of water vapour and the substrate temperature to the fixed values of $2.5 \times 10^{-4}$ mbar and 200°C, respectively, the RF power values were varied. Figure 2

shows the surface morphologies of ZnO films at different RF power values. The transition from Type I to Type II of ZnO:Al films can now be perceived, as we change the RF power for sputtering from 100W to 200W. At low RF power values, the ZnO films show the surface morphology of Type I (columnar morphology). At high RF power values, the ZnO films show surface morphology of Type II (granular morphology).

3.2.2.3 TEMPERATURE SERIES

Keeping the RF power and the partial pressure of water vapour at the values of 200W and $2.5 \times 10^{-4}$ mbar, respectively, the substrate temperatures were varied. Figure 3 shows the surface morphology of the samples prepared at different substrate temperatures. Here also, it is seen that when we change the substrate temperature from lower values to higher values, the surface morphology changes at around 200°C from Type I (figure 3.a and 3.b) to Type II (figure 3.c).

### 3.2.3 Discussion

Sputtering with Ar gas alone results in a flat surface of the ZnO:Al film. Water vapour, as an additional effort to make surface texture growth, is mixed with Ar during sputtering. The water vapour series shows that with an increase in water vapour, the surface roughness increases. But when sputtering is carried out with water vapour alone, the films have again nearly a smooth surface. The surface texture growth takes place in between these two extreme cases, i.e., in between 100% Ar and 100% water vapour growth conditions. This means: surface texture growth takes place only by having a *mixture* of Ar and water vapour during sputtering.

Surface texturing growth of ZnO by DC sputtering has been done by T. Nakada et al [1, 4]. The SEM pictures of the surfaces of our ZnO films can be compared only with their SEM pictures as there was no other sputtering method, by the time, for ZnO reported in the literature using water vapour. Following these two works [1,4,2], recently O. Kluth et al.[3] have reported the growth of ZnO using mixture of Ar and water vapour during RF magnetron sputtering. With their high resolution SEM photographs they showed the existence of columnar and granular morphologies with increase in partial pressure of water vapour.

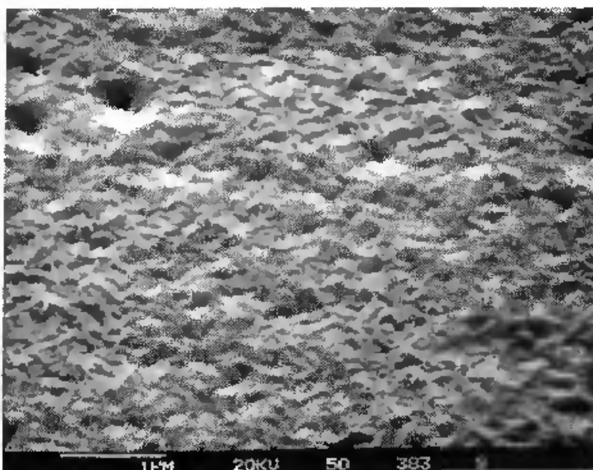


Figure 1.a. SEM image showing the surface morphology of ZnO film grown with 100% Ar gas during sputtering. The total working pressure was $3.5 \times 10^{-2}$ mbar. The RF power was 200W. The substrate temperature was 200°C. The film shows an almost flat surface.

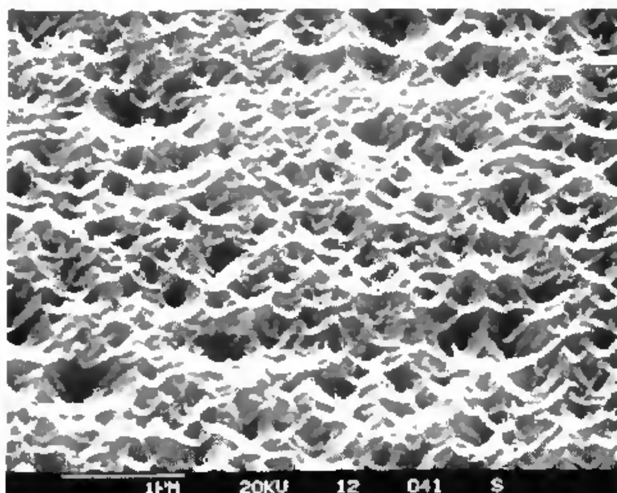


Figure 1.b. SEM image showing the surface morphology of a ZnO film grown with a mixture of Ar and water vapour during sputtering. The partial pressure of water vapour was 2 x $10^{-3}$ mbar The total working pressure was 3.5 x $10^{-2}$ mbar. The RF power was 200W. The substrate temperature, Tsubst, was 200°C. The SEM image shows that the surface morphology contains regularly faceted grains. This type of surface morphology will be called 'Type I' (columnar morphology).

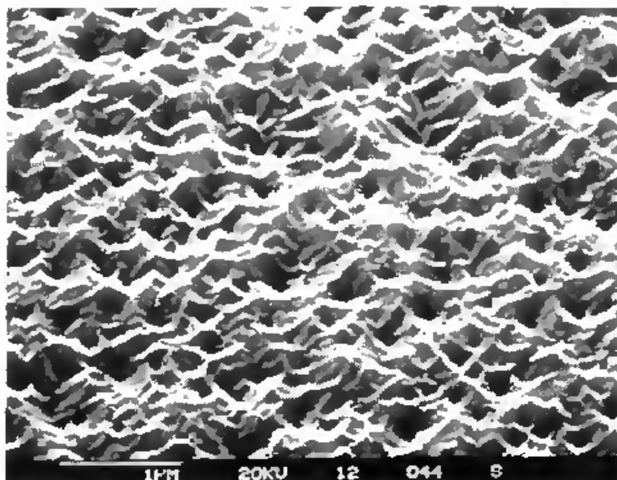


Figure 1.c. SEM image showing surface morphology of a ZnO film grown with a mixture of Ar and water vapour during sputtering. The partial pressure of water vapour was 1.5 x $10^{-4}$ mbar. RF power = 200W. Tsubst 200°C. The SEM image shows that the surface morphology contains regularly faceted grains. This type of surface morphology will be called 'Type I' (columnar morphology).

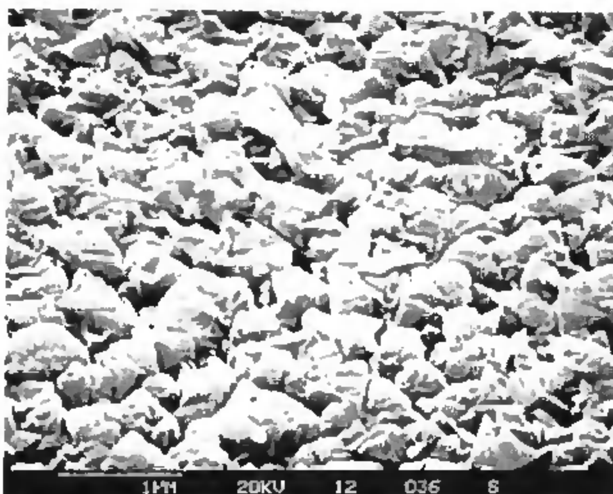


Figure 1.d. SEM image showing surface morphology of a ZnO film grown with a mixture of Ar and water vapour during sputtering. The partial pressure of water vapour was $2.5 \times 10^{-4}$ mbar. RF power = 200W, Tsubst = 200°C. The SEM image shows that the surface morphology contains more rounded grains. This type of surface morphology will be called 'Type II'( granular morphology).

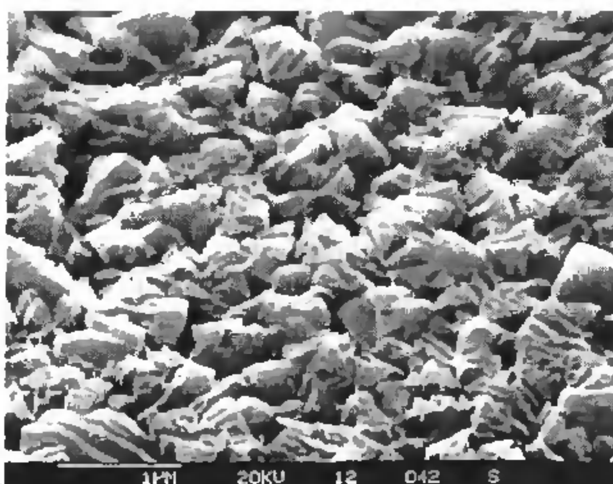


Figure 1.e. SEM image showing surface morphology of a ZnO film grown with a mixture of Ar and water vapour during sputtering. The partial pressure of water vapour was $3.5 \times 10^{-4}$ mbar. RF power = 200W. Tsubst = 200°C. This type of surface morphology will be called 'Type II' (granular morphology).

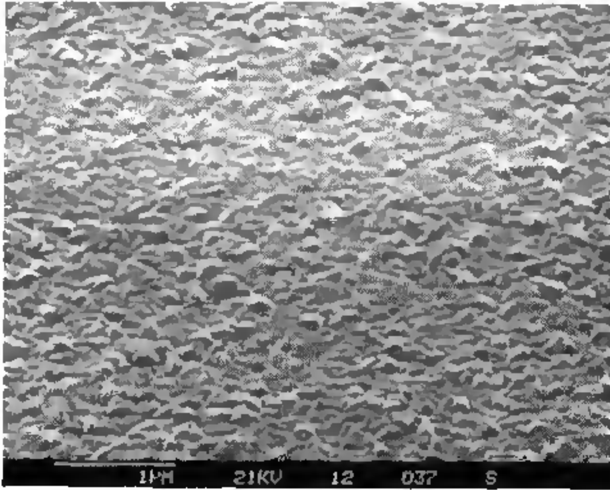


Figure 1.f. SEM image showing surface morphology of ZnO film grown with 100% water vapour during sputtering. The total pressure was 3.5 x $10^{-3}$ mbar. There is no Ar mixed with the water vapour. The RF power was 200W. The substrate temperature was 200°C. The film shows an almost flat surface

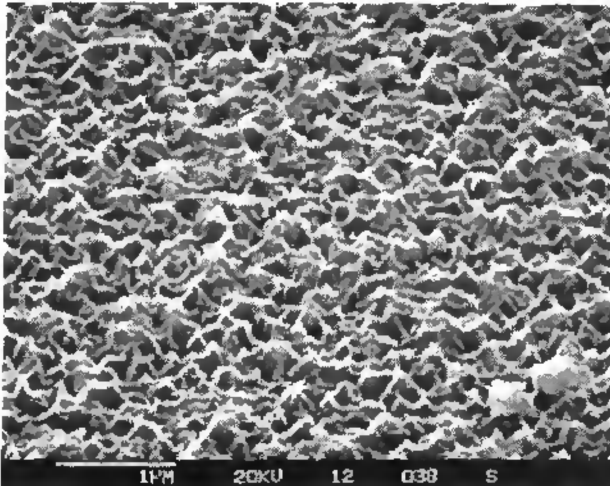


Figure 2.a. SEM image showing the surface morphology of a ZnO film grown with RF power = 100W. The partial pressure of water was 2.5x $10^{-4}$ mbar. The total pressure was 3.5x $10^{-3}$ mbar. The substrate temperature, Tsubst was 200°C. The SEM image shows a surface morphology with regularly shaped grains. This type of surface morphology belongs to the surface morphology of 'Type I' (columnar morphology).

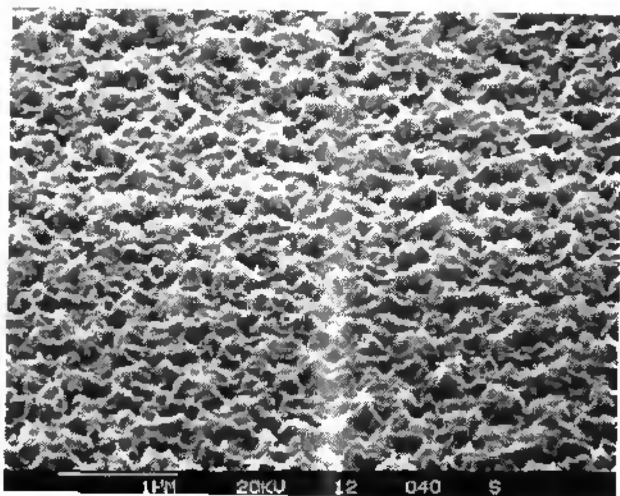


Figure 2.b. SEM image showing the surface morphology of a ZnO film grown with RF power = 150W. The partial pressure of water, was 2.5 x $10^{-4}$ mbar. The total pressure was 3.5x $10^{-3}$ mbar. The substrate temperature, Tsubst was 200°C. This type of *film belongs to surface morphology of 'Type I' (columnar morphology).*

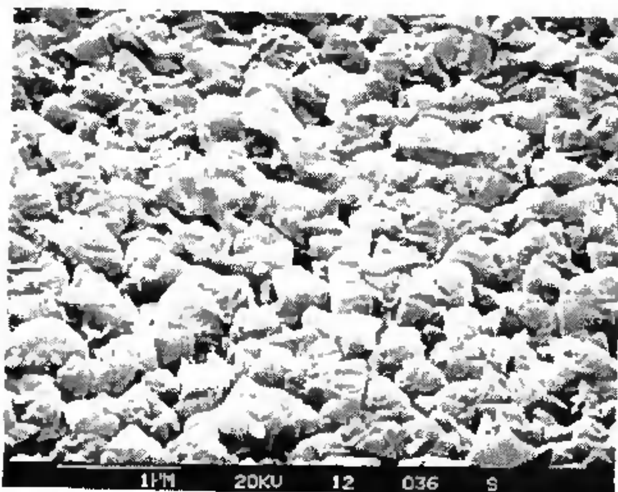


Figure 2.c. SEM image showing the surface morphology of a ZnO film grown with RF power = 200W. The partial pressure of water was 2.5x $10^{-4}$ mbar. The total pressure was 3.5x $10^{-3}$ mbar. The substrate temperature, Tsubst was 200°C. When the power is increased from 150 W to 200W, the columnar surface morphology ('Type I') changes to granular morphology ('Type II').

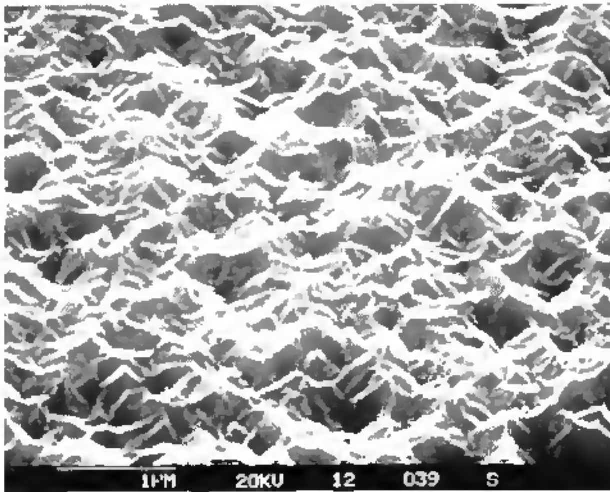


Figure 3.a. SEM image showing the surface morphology of a ZnO film grown with substrate temperature = 100°C. The partial pressure of water was 2.5x $10^{-4}$ mbar. The total pressure was 3.5x $10^{-2}$ mbar. The RF power was 200W. The film has a morphology with regularly shaped grains. This type of film belongs to surface morphology of 'Type I' (columnar morphology)

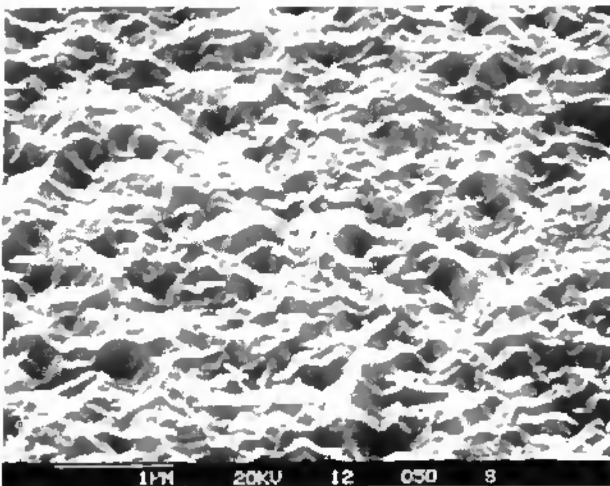


Figure 3.b. SEM image showing the surface morphology of a ZnO film grown with substrate temperature = 150 °C. The partial pressure of water was 2.5x $10^{-4}$ mbar. The total pressure was 3.5x $10^{-2}$ mbar. The RF power was 200W. This type of film belongs to surface morphology of 'Type I' (columnar morphology)

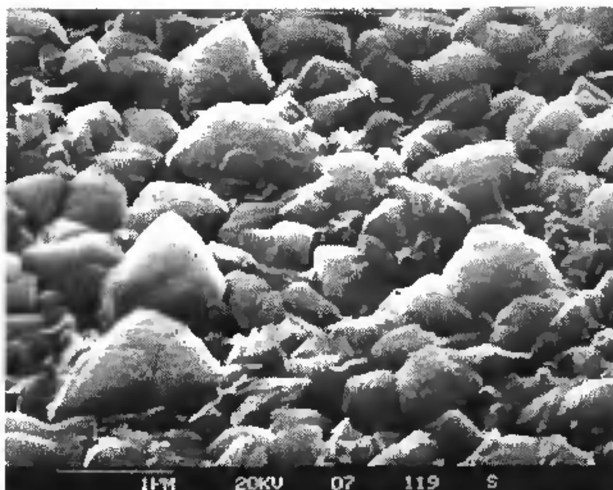


Figure 3.c SEM image showing the surface morphology of a ZnO film grown with substrate temperature = 200 °C. The partial pressure of water was 2.5x $10^{-4}$ mbar. The total pressure was 3.5x $10^{-2}$ mbar. The RF power was 200W. The increase in substrate temperature changes the columnar surface morphology('Type I') to granular morphology ('Type II')

Our above results are partially in contradiction with the work of T. Nakada et al.: In their case the increase in water vapour *always* resulted in rough surfaces. The ZnO samples grown with 100% water vapour (in dc sputtering) were also reported by T. Nakada et al. to show a rough surface. In our case these conditions lead to flat surfaces. In our experience (with RF magnetron sputtering), to obtain surface texture of ZnO at low substrate temperature (below 200°C ) one has to *mix* water vapour with Ar gas.

The reason why Ar should be *mixed* with water vapour can be explained as follows. By adding the Ar with water vapour, the water vapour is dissociated in the plasma. The dissociated species, and not directly the $H_2O$ molecule, is responsible for the surface texture growth of ZnO. It is mainly the OH molecules that are dissociated from water vapour in the plasma that play an important role in the surface texture growth of ZnO.

A diagnostic analysis[1,4] of water vapour in Ar plasma has revealed that such water vapour consists of molecules or ions including H, OH, $H_2O$, $H_2O^+$, $O_2$, $O_2^+$, and $O_3$. Sputtering with Oxygen alone or sputtering with hydrogen alone did not lead to surface texture growth of ZnO[1,4]. It was speculated[1,4] that the OH species may be responsible for the surface textured growth. Our observation with the SEM analysis exactly fits this hypothesis.

Our explanations about dissociation of water vapour will be analysed further in the section on structural properties. There, it will be shown that the water vapour is dissociated by the Ar gas. Hence, adding Ar to water vapour for sputtering means dissociating the water vapour. Therefore, it is necessary to dissociate water vapour to obtain textured surface. The haze factor which is a measure of surface roughness has always been observed by us to increases with the *degree of water vapour dissociation*.

In the surface-textured ZnO films, clearly, two different surface morphologies are observed. They have been called type I and type II morphologies. Based on the shape of the grain, and their appearance, we call them also '*columnar morphology*' and '*granular morphology*' *respectively*. ZnO thin films with columnar morphology have columnar growth along the preferred orientation. In the section on structural properties it will be shown that these

films have an orientation along the c-axis of their hexagonal wurtzite structure. On the other hand, the ZnO films with granular morphology have rounded grains. Furthermore, they do not have a preferred orientational growth.

The columnar and granular morphologies stand as a major classification of surface of the ZnO films by RF sputtering. These two morphologies will be analysed further in the following sections. The transition from one type to the other happens with the structural transition of ZnO crystals in the polycrystalline film. In the following sections a corresponding transition from the usual hexagonal wurtzite structure of ZnO to the cubic structure will be demonstrated. Thus the resultant ZnO films with columnar morphology (figure 1.d and 1.e) have mixed hexagonal wurtzite and cubic grains.

The increase in RF power during growth can strongly influence the surface morphology. A change in RF power also causes a change from columnar to granular morphology. Similarly, on increase in substrate temperature can also cause the transition from columnar to granular morphology.

Basically, the RF power and substrate temperatures can change the surface mobility during the growth. Higher surface mobilities will result in uniformly textured surfaces (this is further explained in the following sections). However, the increase in RF power result in rounded granular morphology rather than a uniform faceted morphology. This is due to the change in the plasma conditions as well as the change in the growth environment on the substrate, at increased RF power levels, and with increased substrate temperatures. The dissociation of water vapour, that results in granular morphology is enhanced further with an increase in RF power. It is also seen that an increase in substrate temperature leads to a granular morphology. Hence the change into granular morphology from columnar morphology in the cases of our power series and our substrate temperature series is mainly attributed to the combined action of the species present in the plasma as well as on the substrate

In all these series the columnar morphology exhibits hexagonal pits on the surface. This is further explained in the section on structural properties.

### 3.2.4 Conclusions with respect to the SEM analysis

Our SEM analysis has shown the effect of water vapour, RF power and substrate temperature on the surface morphology of ZnO:Al thin films. Water vapour, when it is added to Ar during sputtering, leads to surface texture growth of ZnO. The roughness of the surface increases with the addition of water vapour. It has been observed, in our present work on magnetron sputtering, that the water vapour should be mixed with Ar in order to obtain surface texture in ZnO. Two distinct surface morphologies, namely columnar morphology ('Type I') and granular morphology ('Type II') were identified. The columnar morphology exhibits hexagonal pits on the surface. A variation in RF power and/or in substrate temperature can change the surface morphology from columnar to granular. The surfaces of the ZnO have been analysed further to gain more insights into the growth process, in the following section.

### References

[1] T.Nakada, Yukinobu Ohkubo and Akio Kunioka, Japanese Journal of Applied Physics.,30, no 12A (1991), 3344-3348
[2] J. A. Anna Selvan, H. Keppner, A. Shah in Thin Films for Photovoltaics and Related Device Applications, Proceedings of MRS spring meeting 1996, Vol. 426 P.497
[3] O. Kluth, C. Beneking, B. Rech, W. Appenzeller, H. Wagner, R. Waser and S. Hoffmann,. Technical Digest of the international PVSEC-9 Miyazaki, Japan, Nov., 1996, 357
[4] Tokio Nakada, Yukinobu Ohkubo and Akio Kunioka, IEEE PVSEC 1991, 1389

# 3.3 Atomic Force Microscopic studies

## 3.3.1 Introduction

Since the invention of the Atomic Force Microscope (AFM) in 1986 [1], it has rapidly developed into a very useful technique for studying materials in the nanoscale regime. The use of the phenomenon of electron tunnelling for the imaging of a conducting surface on atomic scale was implemented only in 1982, when the first scanning tunnelling microscope (STM) was built by Binnig et al [2]. In 1986 O. Binning and H. Rohrer were awarded the Nobel prize for the design of the STM. For both metallic and semiconducting surfaces, STM has now become a powerful analysing tool. The most important feature of the STM is the real-space visualisation of surfaces on atomic scale.

The central part of the STM is a sharp tip either mounted on a spring or incorporated into a spring(integrated tip), which is used as a probe, called cantilever, to sense the tip/sample interaction forces. What is converted into image in STM is either the spatial variation of tunnelling current or the spatial variation of the tip height. The tunnelling current decreases exponentially with increasing tip-sample distance. Thus, at any given location of the tip over the sample surface, the electron transfer involves only one atom, or only a few atoms, those at the apex of the tip and on the surface closest to the apex. This gives rise to the local character of STM measurements, which makes it possible to visualise surface structures with sub-Angstrom resolution and to detect various atomic-scale defects that are inaccessible by diffraction and spectroscopy techniques[3]. In addition, STM is used to examine adsorbate structures and dynamic phenomena on surface (example, diffusion and chemical reactions)

Since tunnelling current is employed in STM, the application of this method is mostly limited to metals and semiconductors. To enable the detection of atomic-scale features of insulating surfaces, the Atomic Force Microscope(AFM) was invented as a variance of the STM. In the AFM, it is now the repulsive force between the tip (located at the end of the cantilever) and the sample that is measured, on the basis of the deflection of a cantilever. In this contact-mode AFM, the spatial variation of the tip- sample repulsive force or that of the tip height is converted into an image. Because the repulsive force is universal, AFM is applicable to conducting as well as to insulating materials. Therefore, for the study of surface properties of ZnO thin films, where the conductivity varies from sample to sample, AFM was an appropriate method. In general, AFM enables one to detect surface morphology, nanoscale structures and molecular- and atomic scale lattices.

So far, STM and AFM are the most advanced scanning probe methods and the only ones providing atomic- resolution images. AFM has found much broader application than STM and is currently the dominant scanning probe technique[3].

With the Scanning Electron Microscope (SEM), one can 'see' the surface of metallic and semiconducting materials. It can be directly linked to the fundamental properties of materials (for example; grain size, facets, structural properties, etc.). But at nanoscale resolution SEM can not be used as a surface analysing technique. In this sense SEM on one hand and AFM, in addition to the STM, on the other hand, have their unique places and can not be replaced by the other method. Hence in addition to the SEM analysis of our surface textured ZnO films, we conducted AFM studies in order to learn more about surface our textured ZnO surfaces. In this section the results and discussion of these AFM studies are presented.

## 3.3.2 Experiment

The Atomic Force Microscope studies, in this work were carriad out for ZnO thin films using an AFM instrument known as the Atomic Scale Tribometer (AST) [4,5], manufactured by the CSEM company. This instrument allows the samples to be imaged and measured with both

the vertical and lateral deflection of the cantilever. For all the measurements, contact mode AFM imaging was carried out. For this work mainly the vertical signal (topography) was recorded for roughness analysis. The lateral signal was measured for samples with columnar morphology . The cantilever deflections were measured using a laser beam and a position- sensitive photo detector (PSPD) set up. The tip of the cantilever has been fabricated with a thin film of silicon nitride. The tip is pyramidal in shape and it is a few nanometers in size. All the measurements were done at atmospheric pressures. The samples were not coated with gold film as it was the case for our SEM analysis, since a conducting surface is not a necessary requirement for AFM studies. The projected area for the analysis was 5µm x 5µm.

To quantify the surface roughness we generally used as a measure the parameter of excess area over the geometrically projected area. However, we also used the RMS roughness to describe the surfaces further as a second parameter. As the first parameter is the standard one [14], it is important to explain the relationship between the two values.

The excess area over the geometrical area

The excess area over the geometrical area is the arithmetic mean roughness, $R_a$, which is simply the average deviation of the profile from the reference mean line. It is described by the following equation, where L is the assessment length, y the peak height and x the peak spacing:

$$R_a = \frac{1}{L}\int_0^L |y(x)|dx \qquad (1)$$

RMS roughness

The root mean square roughness, $R_{rms}$ is the standard deviation of the distribution of the surface heights, and is defined by the following equation which also describes its relation to $R_a$

$$R_{rms} = \sqrt{\frac{1}{L}\int_0^L y^2(x)dx} \qquad (2)$$

The RMS roughness is calculated by summing up the squared deviation of each image point with respect to an average height value of the surface and by dividing this value by the number of data points (256x 256). Finally the square root is taken. The $R_{rms}$ value is the only roughness parameter with basic significance and it is fundamental in describing surface roughness by statistical methods.

We take both the RMS roughness as well as the excess area into account for the study of our surface textured ZnO films.

### 3.3.3 Results of AFM studies of ZnO thin films.

WATER VAPOUR SERIES

The ZnO samples grown in the water vapour series were analysed with AFM. Figures 4.a and 4.b show the AFM image of the ZnO films grown at low and high partial pressures of water vapour, respectively. The images are the result of a three dimensional scan. It is observed that similar images as those that we obtained by SEM is reproduced by AFM. The columnar and granular surface morphologies, at low and high partial pressures of water vapour, respectively, are clearly depicted by the AFM images. In the water vapour series, one AFM image from each morphology is shown in figure 4. Figure 4.a shows the columnar morphology of ZnO films grown with 2 x$10^{-5}$ mbar pressure of water vapour during sputtering. Regularly faceted grains are clearly visible from the image. Figure 4.b shows the granular morphology of ZnO films grown

with 3.5 x $10^{-5}$ mbar pressure of water vapour during sputtering. This morphology is very different from columnar morphology and we observe the rounded grain boundaries.

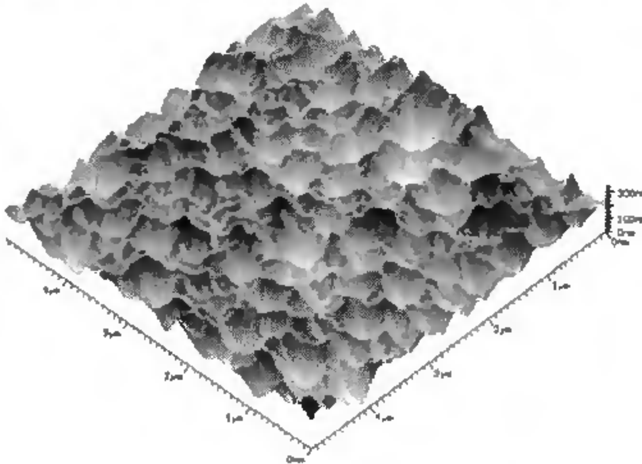

Figure 4.a An AFM image showing the columnar surface morphology of a ZnO film grown with a mixture of Ar and water vapour during sputtering (water vapour series). The partial pressure of water vapour, $P_{H2O}$, was 2x $10^{-5}$ mbar. The total pressure was 3.5 x $10^{-2}$ mbar. The substrate temperature was 200°C. The RF power was 200W. The AFM image shows that the surface morphology contains regularly faceted grains It is seen that the maximum height of the surface peak is around 350nm.

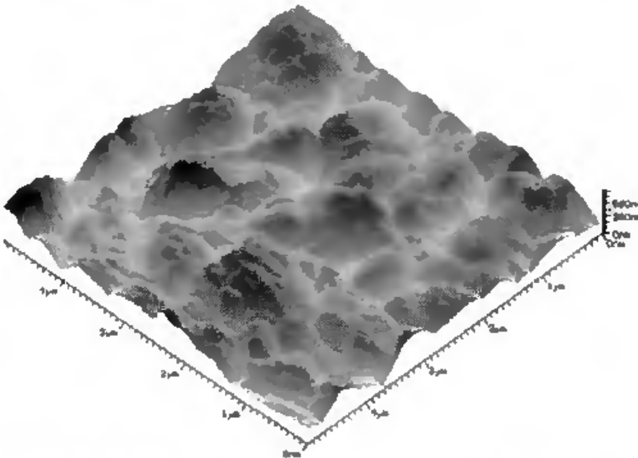

Figure 4.b AFM image showing the granular surface morphology of a ZnO film grown with a mixture of Ar and water vapour during sputtering (water vapour series). The partial pressure of water vapour, $P_{H2O}$, was 3.5x $10^{-4}$ mbar. The total pressure was 3.5 x $10^{-2}$ mbar. The substrate temperature was 200°C. The RF power was 200W. The substrate temperature, $T_{subs}$, was 200°C. The AFM image shows that the surface morphology contains rounded grains. The maximum height of the surface peak is around 730nm.

The excess area over the geometrical area and the RMS roughness are both calculated using the formulas mentioned in section 3.3.2. Figure 5.a shows the excess area of the surface textured ZnO films grown in the water vapour series in function of the partial pressure of water vapour during sputtering. As is seen, the excess area increases with the increase in partial pressure of water vapour during sputtering. It can be seen that the increase is almost linear.

*Figure 5b shows the variation of* the RMS *roughness of* the *surface-textured ZnO films* grown in the water vapour series in function of the partial pressure of water vapour during sputtering. The figure clearly shows two different regimes for the variation of RMS roughness. The two regimes correspond to the columnar and granular morphologies. In the columnar morphology region, the RMS roughness increases with the increase in the partial pressure of water vapour. Similarly in the granular morphology region the RMS roughness also increases with increase in the partial pressure of water vapour. However, in between these two regions, when the transition from columnar to granular morphology takes place, the RMS roughness remains the same.

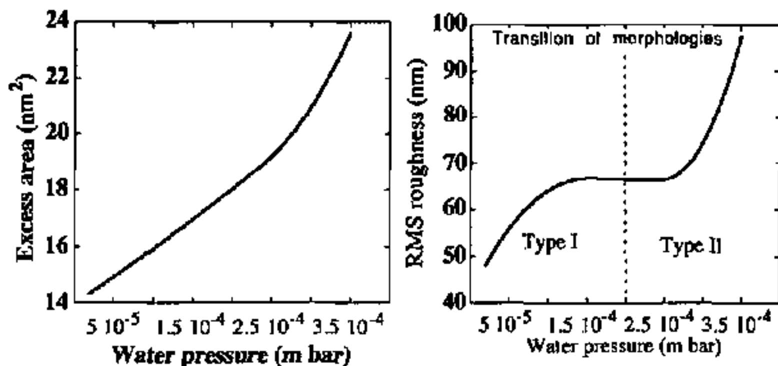


Figure 5.a The variation of excess area over the geometrical area of the ZnO thin films in function of partial pressure of water vapour during sputtering. The substrate temperature was 200°C. The RF power was 200W. The total pressure of the mixture of Ar and water vapour is $5 \times 10^{-2}$mbar. The two regions of surface morphologies, the regions of columnar(type I) and the granular(type II) morphologies are shown in the figure. The surface roughness increases continuously. There is no smooth surface during the transition from type I to type II.

Figure 5.b. Variation of RMS roughness of surface-textured ZnO films. These are the same surfaces as shown in figure 5.a. During the transition of surface morphologies, the RMS roughness does not change. This shows that there is a continuous transition w.r.t. RMS roughness between granular morphology and columnar morphology

Figure 6 shows the cross-section of the surface of the ZnO films at different partial pressures of water vapour. The columnar morphology(type I) and the granular morphology(type II) are clearly manifested in the figure. The transition from one surface morphology to the other is also shown in the figure. This figure helps us to visualise clearly the shape of the surface peaks that results due to surface texturing. Also, the effect of the addition of partial pressure of water vapour on the shape of the surface peaks can be seen.

As explained in subsection 3.3.2, images of the surface of ZnO film using lateral variations of the tip are also scanned. This is called the FFM image (frictional force microscopy image) [6,7]. This was done to investigate the surface features further. Figure 7 shows the Frictional Force Microscopy image of a columnar morphology ZnO film with columnar

morphology. The figure clearly manifests the hexagons on the surface that were also mentioned in the SEM analysis. Different grains and grain boundaries with pits of hexagons can be seen from the figure.

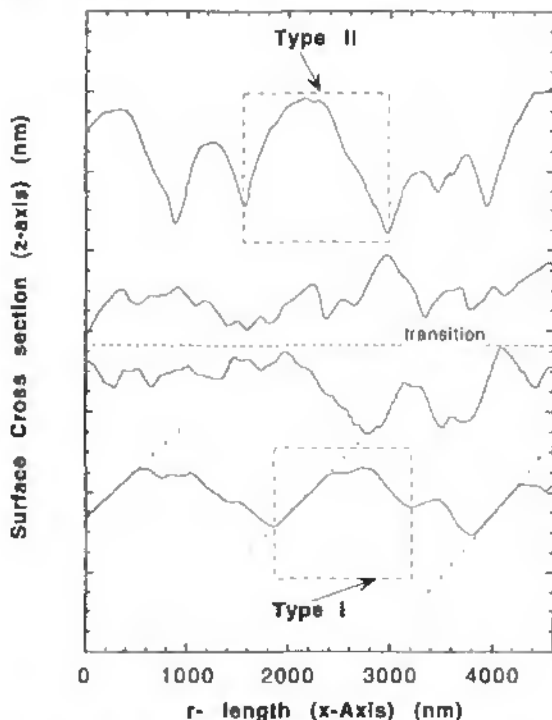


Figure 6. The cross-section of the of the textured surfaces of the ZnO thin films at different partial pressures of water vapour. The picture clearly demonstrates the shapes underlying the columnar (type I) and the granular (type II) morphologies. The transition from one type to the other is shown. The columnar morphology has *a constant inclination angle* with the substrate. This is due to the facets that occurs with the preferred orientation growth of ZnO thin films along the (0001) axis of its hexagonal crystal structure.

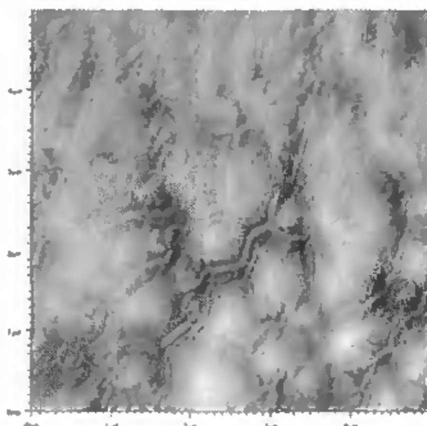

Figure 7 A typical frictional force microscopy image of a ZnO surface columnar morphology. For the growth of this film shown above the partial pressure of water vapour, $P_{H_2O}$, was $2x\ 10^{-4}$ mbar. The total pressure was $3.5\ x\ 10^{-3}$ mbar. The substrate temperature was 200°C It shows that columnar morphology consists of hexagonal pits. Each line on the surface can be derived as a part of hexagon. The surface roughness in the case of columnar morphology occurs due to these surface hexagons. The hexagons are due to the crystallographic orientation of ZnO films. In the figure the grain boundaries can be noted. A grain has more than one hexagonal pit. The pits are due to the combined action of growth as well as etching.

POWER SERIES

Figure 8.a, 8.b and 8.c show the AFM image of the samples grown in the power series. The partial pressure of water vapour was kept at 2.5 x $10^{-4}$ mbar. The total pressure of sputtering was 5 x 10 $^{-2}$ mbar. The substrate temperature was 200°C. These are the same experimental conditions as those that were mentioned in the beginning of the chapter. Here also the change in surface morphology from columnar to granular morphology is shown. The maximum height of the surface peaks is increased from 290nm to 540nm in the columnar morphology and when the surface morphology changes to granular morphology the maximum height of the surface peak is around 540nm.

Figure 9 shows the excess area over the geometrical area and the RMS roughness of the ZnO films grown in the power series. As is seen, in the columnar morphology region, the RMS roughness and the excess area both increase with the increase in RF power and they both decrease in the granular morphology region with the increase in the RF power.

SUBSTRATE TEMPERATURE SERIES

Figures 10.a, 10.b and 10.c show the AFM image of the samples grown in the temperature series. The partial pressure of water vapour was kept at 2.5x $10^{-4}$ mbar. The total pressure of sputtering was 5x $10^{-2}$ mbar. The RF power was 200 W. These are the same experimental conditions that were mentioned in the beginning of the chapter. Here also the change in surface morphology from columnar to granular morphology is shown. With the increase in substrate temperature from 100°C to 150°C, the maximum height of the surface peaks decreases from 720nm to 640nm in the region of columnar morphology and when the surface morphology changes to granular morphology the maximum height of the surface peak is around 540nm.

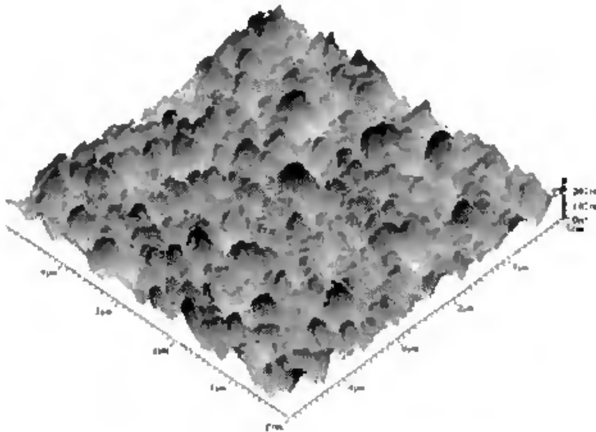

Figure 8.a AFM image showing the surface morphology of a ZnO film grown at a power of 100W. The partial pressure of water vapour, $P_{H2O}$, was 2.5x $10^{-4}$ mbar. The total pressure was 3.5 x 10 $^{-2}$ mbar. The substrate temperature, $T_{sub}$, was 200°C. The AFM image shows that the surface morphology contains regularly faceted grains. This feature belongs typically to surface with columnar morphology. The maximum height of the surface peak is around 290nm.

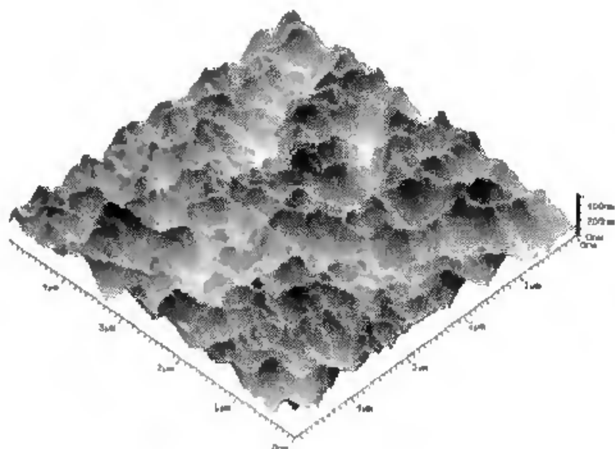

Figure 8.b. AFM image showing the surface morphology of a ZnO film grown at RF power of 150W. The partial pressure of water vapour, $P_{H2O}$, was 2.5x $10^{-4}$ mbar. The total pressure was 3.5 x $10^{-3}$ mbar. The substrate temperature, $T_{sub}$, was 200°C. The surface has columnar morphology. The maximum height of the surface peak is increased (w.r.t to the previous figure) here to 540nm. The increase in RF power from 100W to 150W is the main reason for increase in surface peak height.

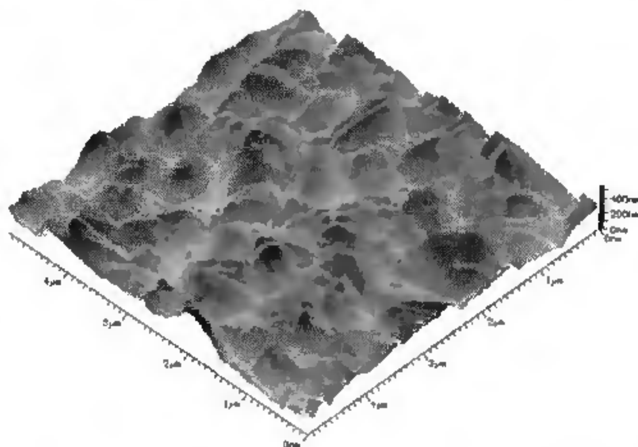

Figure 8.c AFM image showing the surface morphology of a ZnO film grown at RF power of 200W. Other parameters are the same as mentioned in figure 8.a and 8.b. The surface has granular morphology. The increase in RF power has changed the surface morphology from columnar to granular morphology. The maximum height of the surface peak has further increased to 550nm w.r.t. the previous figure.

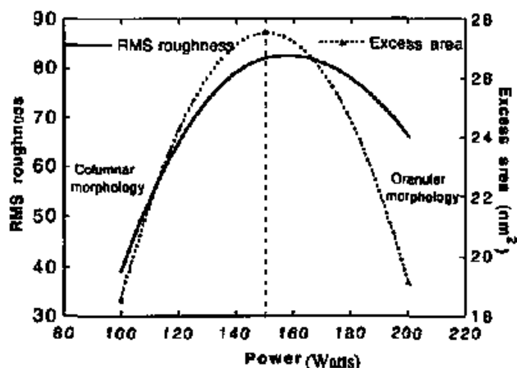


Figure 9. The variation of excess area and of RMS roughness for surface-textured ZnO thin films in function of RF power during sputtering. The region of columnar and of granular morphology are shown. The increase in RF power increases the height of the surface peak in the region of columnar morphology. Hence, the RMS roughness and the excess area increases with an increase in RF power in region of columnar morphology. In the region of granular morphology the density of surface peaks is lower than the density of surface peaks in the columnar morphology. This *occurs due to the change in the plasma* conditions with the increase in the RF power.

Figures 10.a and 10.b also exhibits another interesting and important feature. Let us compare those two AFM for the case of columnar morphology with the other images, also for the case of columnar morphology in the power series (figure 10.a and 10.b). There is a notable difference in the images for the case of columnar morphology in the power series and for the case of columnar morphology in the temperature series. The images for the case of columnar morphology in the power series show regularly faceted grains. *The images for the case ofcolumnar morphology in the temperature series has some regions of granular morphology* . In figure 10.a, the AFM image of the ZnO film grown at 100°C, the regions of granular morphology is marked. In figure 10.b these regions are still present but their amount is decreased in comparison to figure 10.a. Now, a close look at the SEM picture of the ZnO film grown at 100°C (figure 3.a) will reveal local region of granular morphology superimposed on the general case of columnar morphology.(also see also figure 19 insection 3.4)

Figure 11 shows the excess area over the geometrical area and the RMS roughness of the ZnO films grown in the substrate temperature series. Here in the temperature series, the RMS roughness and the excess area vary differently with the variation of substrate temperature. In both the columnar morphology region as well as in the granular morphology region, the excess area decreases with an increase in substrate temperature. The RMS roughness, on the other hand, with an increase in the substrate temperature, increases in the columnar morphology region and decreases in the granular morphology region.

## 3.3.4 Discussion

### 3.3.4.1 The water vapour series

First, the AFM has reproduced the same morphologies that we obtained using SEM. The surface morphology of the ZnO films at different experimental conditions are very well visualised in the 3 dimensional scan images.

STM analysis of ZnO has already been done by several other research groups. In general, the respective papers mainly concentrated on the interfaces between doped ZnO and liquids [8] and on the studies of the electronic structure of large band gap materials like ZnO [9, 10]. The AFM images of ZnO were shown in some reports on ZnO [11, 12]. However, the analysis of the surface morphology of rough ZnO films using AFM has so far (to the best our knowledge), not been reported in the literature. AFM has been just used to show the surface roughness of the films. Among the available work on surface-textured ZnO only in this work, to our knowledge, has AFM been used to analyse the surface texture of ZnO films.

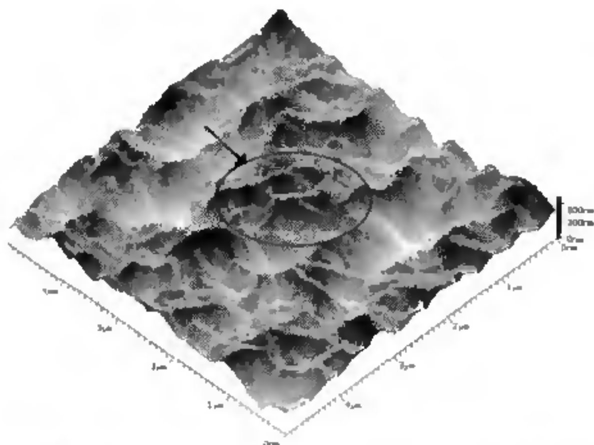

Figure 10.a AFM image showing the surface morphology of a ZnO film grown with the substrate temperature of 100°C. The partial pressure of water vapour, $P_{H2O}$, was 2.5x $10^{-4}$ mbar. The total pressure was 3.5 x $10^{-2}$ mbar. The RF power was 200W. The AFM image shows that a surface with columnar morphology can contain individual grains with granular morphology. The maximum height of the surface peak is around 730nm. The basic columnar morphology is due to an increased surface mobility because of the increase in RF power. The granular grains are due to the reduced substrate temperature.

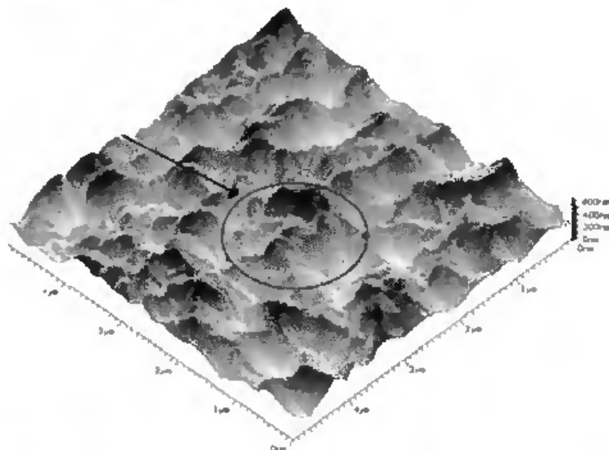

Figure 10.b AFM image showing the surface morphology of a ZnO film grown with the substrate temperature of 150°C. The partial pressure of water vapour, $P_{H2O}$, was 2.5x $10^{-4}$ mbar. The total pressure was 3.5 x $10^{-2}$ mbar. The RF power was 200W. This AFM image shows again that a surface with columnar surface morphology can contain grains of granular morphology. The amount of granular grains seems to decrease with increase in substrate temperature. The maximum height of the surface peak is around 640nm.

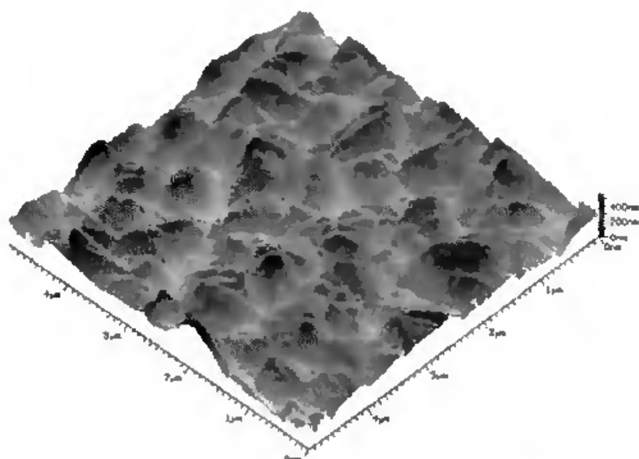

Figure 10.c AFM image showing the surface morphology of a ZnO film grown with the substrate temperature of 200°C. Other parameters are the same as mentioned in figure 10.a and 10.b. The surface has granular morphology. The maximum height of the surface peak is around 640nm.

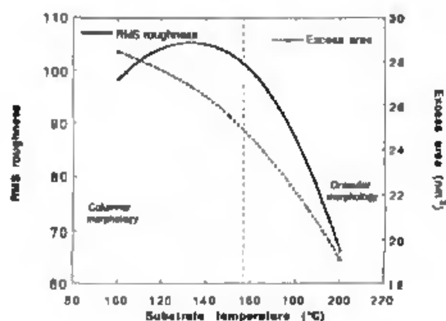


Figure 11. The variation of excess area and the RMS roughness of surface textured ZnO thin films in function of substrate temperature during growth. The columnar and the granular morphology regions are shown. In the columnar morphology the decrease in substrate temperature lead to the formation of grains of granular morphology *over the columnar morphology*. This increases the excess area. In the columnar morphology, the RMS roughness decrease with decrease in substrate temperature due to less number of columnar peaks. In the granular region, both RMS roughness and the excess area decreases with increase in substrate temperature due to decrease in the number of peaks in the rounded grains

Figure 6 clearly depicts the columnar and granular morphologies. We observe that the columnar morphology has regularly faceted grains. The surface peaks consists of straight lines. *It is demonstrated that the straight lines form a constant angle with the substrate*. On the other hand, the granular morphology shows rounded grains. In figure 5.a the variation of excess area with an increase in partial pressure of water vapour is shown. This demonstrates the corresponding increase in the total area of the surface of ZnO. On the other hand, figure 5.b shows the RMS roughness which clearly displays two distinct regions, i.e., for columnar and for granular morphologies. This explains the dependence of the RMS roughness values on the shape of the surface peaks. From the definitions of the excess area and of the RMS roughness, the difference between the two parameters can be understood. The RMS roughness mainly depends on the amplitude of the peaks in the surface whereas the excess area just describes the area. From figure 8b it is seen that during the transition the RMS roughness remains the same. It means that the density of surface peaks in the 'beginning' of the type of granular morphology is the same as the density of surface peaks in the 'end' of the region of columnar morphology. The density of

surface peaks in the region of columnar morphology is defined by the hexagons which are the main feature of columnar surface morphology. Hence, *the granular morphology is, infact based on the columnar morphology*. This means that the granular morphology is formed based on the surface variations in the columnar morphology. The transition from columnar to granular morphology is gradual. There is no intermediate change in the surface roughness and *the granular morphology starts as a slight modification from the columnar morphology*. Figure 5.a shows that the surface roughness increases almost linearly with the addition of partial pressure of water vapour. The effect of water vapour on the shape of the surface peak is explained in figure 13.

In the frictional force microscope (FFM) image (figure 7), the columnar morphology of ZnO films is shown. In this image the hexagonal pits can clearly be seen. A closer look at the image will reveal that almost *every line in the image can be derived as a part of a hexagon*. Another point to note is that the surface grain is not simply a single hexagon. A grain can have more than one hexagon. This is noted here because many times it is mentioned in literature that the surface roughness is equivalent to the density of 'grains on the surface'. However, this is not the case; the surface roughness is related to the density of hexagons on the surface and not to the density of grains The reason for the hexagonal shape is due to the orientation of the growing film. The dissociated water vapour in the plasma leads to a growth that is combined with etching. This is discussed further in the section of structural properties.

In the cross-section of two morphologies shown in figure 6, the columnar morphologies exhibited a constant inclination angle with the substrate. This constant angle arises from the crystallographic facets of ZnO. Here, the facets are associated with the minimum energy planes of ZnO. This will be shown in the section on structural analysis.

#### 3.3.4.2 Comparison of textured ZnO surface growth with the model of J. A. Thronton

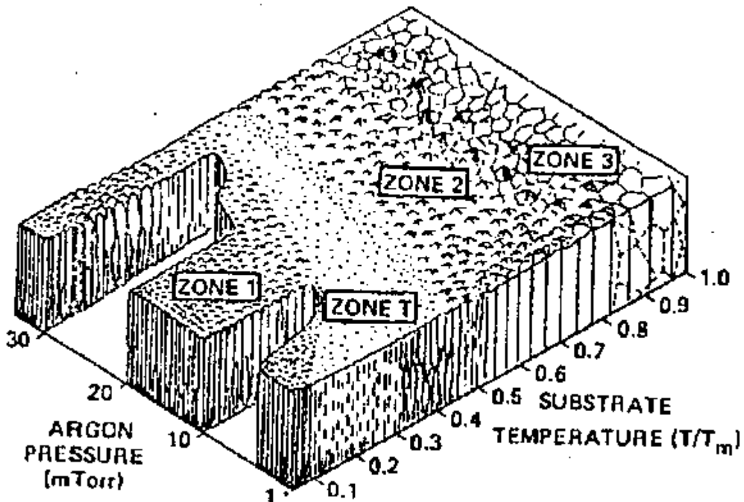


Figure 12. J. A. Thronton's 'standard' growth model generally used to explain the evolution of the surface morphologies. Zone 1 is a low surface mobility regime. Zone 2 is a high surface mobility regime. When the surface mobility changes the surface morphology undergoes a transition region, Zone T, in which the film has a flat surface.

A 'standard' growth model generally usable in the case of sputtering with Ar for the surface of a thin film is explained by J. A. Thronton[13]. Figure 12 shows the surface morphology of thin films at different experimental conditions during sputtering. It is

demonstrated in the figure that the surface roughness occurs due to the increase in substrate temperature and an increase in Ar pressure. There are four regions shown in the picture; Zone 1, Zone 2, Zone 3 and Zone T. The Zone 1 and Zone 2 show two different types of surface roughness. Zone 1 contains more rounded grains whereas Zone 2 contains regularly faceted grains. Zone T is the transition region from Zone 1 to Zone 2: The film shows a smooth surface in this region. An increase in substrate temperature leads to the crystallographic facets (Zone 2) and recrystallization (Zone 3) of the thin film. This model will be discussed further in later sections. Here, we see that during the change in surface morphology the film comes to a region of the smooth surface morphology (ZoneT).

During the growth of surface-textured ZnO thin films we come across two different morphologies namely columnar and granular morphology. To understand the surface texture growth of ZnO, we compare our observations with Thronton's growth model. We notice the following points.

1. Our regions of columnar morphology seems to correspond with Thronton's Zone 2. But the substrate temperature regime is not close to the value (0.5 $T/T_m$) as given by J. A. Thronton.

2. Our region of granular morphology resembles Thronton's Zone 1. But the regions are not the same as in Thronton's model.

3. Taking the surface morphology in to account (see below), there is no smooth transition Zone T during the transition of the two surface morphologies which one would expect according to Thronton's model (as mentioned above).

The main difference between the well known Thronton's model and the present case is the use of ***a mixture of Ar and water vapour instead of only Ar gas as in Thronton's model.***

3.3.4.3 SURFACE MOBILITY

We introduce here an important mechanism that occurs during the growth; we give much consideration to this mechanism in our efforts to explain the growth of surface-textured thin films; this is the mechanism of *surface mobility*. Surface mobility designates the movement of atoms or molecules during the growth process of the thin films. The atoms can move inside the grains and even on the surface of the substrate during growth. Obviously the surface mobility depends on the kinetic energy of the adatoms (the incoming atoms) during growth. This depends on the growth parameters. During sputtering, the RF power, the substrate temperature and the working pressure are the main parameters which can affect the surface mobility.

How does the surface mobility affect the surface roughness? When the adatoms have *very poor surface mobility*, they just stick on the site where they intercept the substrate. Further addition of adatoms make statistical fluctuations in the thickness, which, in other words, we call 'surface roughness'. When the adatoms have *sufficient* kinetic energy they can move around and give rise to a smooth surface, since the system requires a smooth surface to minimise the surface energy. Hence the surface always has in fact an inherent tendency to obtain a smooth or 'flat' surface during growth, but it needs an input of kinetic energy to reach this state. The high input of kinetic energy (i.e., high enough surface mobility) is necessary but not a sufficient condition, as we will just see. Indeed smooth surface should result for intermediate values of surface mobility.

In fact, when there is *very high surface mobility*, the adatoms try and can find minimum - energy atomic sites in the grains. This results in the growth of particular crystal planes. Note that this can again lead to 'surface roughness'; regularly-faceted surface morphology may indeed result during this process.

We see uniformly-faceted grains in the columnar morphology of ZnO films. Hence, it seems that these belong to the high surface mobility regime as described above. The corresponding RF power of 200W and substrate temperature of 200°C (for figure 4.a) assures an increased kinetic energy of the adatoms.

On the other hand, the granular morphology probably correspond to a low surface mobility regime. The increase in water pressure could decrease the surface mobility during growth. Now, the curve showing the variation of RMS roughness with partial pressure of water vapour indicates that there is no intermediate smooth surface region. It also shows that the granular morphology is based on the columnar morphology.

Note, therefore, that the excess area of the surface of ZnO film grown with water vapour alone is 3.9 $nm^2$, a value which is very close to that for flat films. This value again confirms the requirement of mixture of Ar and water vapour to grow surface textured Zn thin films.

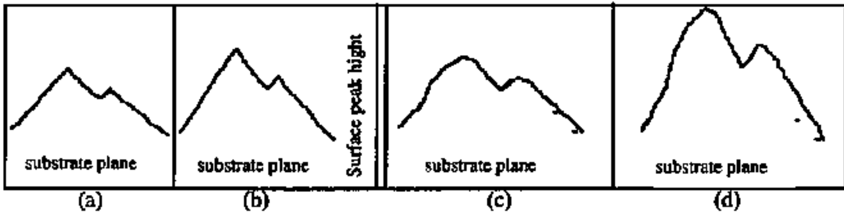


Figure 13 Schematic diagram showing the effect of water vapour on the shape of the surface peaks. The amount of water vapour increases from 13(a) to 13(d). The 13(a) and 13(b) correspond to columnar morphology and 13(c) and 13(d) correspond to the granular morphology. In the columnar morphology, the increase in water vapour increases the height of the surface peaks. Figure 13(a) and 13(b) show an increase in RMS roughness and an increase in the excess area with the increase in the amount of water vapour. During the transition granular morphology is formed over the columnar morphology configuration. Just at the beginning of transition, this increases the excess area and the RMS roughness does not change. A further increase in the amount of water vapour increases the height of the surface peaks by producing more granular grains. This is shown in 13(c) and 13(d)

#### 3.3.4.4 The Power series: changes in the plasma

In the power series, the cases with columnar morphology show (figure 8.a and 8.b) that they are in the high surface mobility regime. In figure 8.c further increase in RF power from 150W to 200W leads to the granular morphology. An increase in RF power will certainly not decrease the kinetic energy of the adatoms. Hence, it seems that the increase in RF power makes changes in the plasma that may be the cause of granular morphology. The change in the plasma, mainly the dissociation of water vapour, may change the surface mobility. In this case, it is certainly the change in the plasma that leads to the transition from columnar to granular morphology.

Hence, for the granular morphology regime in the power series, the RF power alone can not explain the growth. Later it will be shown that there is a change in the plasma associated with the change in the morphology. Also it will be shown that there is a change in the structure of ZnO during this transition from columnar to granular morphology.

The variation in RMS roughness and in excess area as a function of RF power is shown in figure 9. Both RMS roughness and the excess area increase with the RF power in the columnar morphology region. And both decrease in the granular morphology region. Based on the knowledge of the shapes associated with columnar and granular morphologies (figure 8.a, 8.b and 8.c) and also based on the definitions of RMS roughness and excess area, we can now point out the changes in the shape of the surface peaks with RF power.

The increase in RMS roughness means that there is a higher standard deviation of the surface peaks from the reference line (in two dimensions). The excess area, is thereby, just increased in length. Hence in the columnar morphology region of the power series, as is seen in the figures, we have more surface peaks than in the granular morphology region. The higher density of peaks lead to an increase in the excess area. The increase in RMS roughness within the

same columnar morphology region is due to an increase in the peak height, as seen in the figures 8.a and 8.b when the RF power is changed from 100W to 150W. This is explained in figure 14.

Mainly, the increase in RF power increases the peak height. This is due to the collision of high-energy ions and molecules during sputtering on the growing surface. In the section on structural properties, it will be shown that there is an etching process that is associated with the growth of surface-textured ZnO films in the columnar morphology region. Here, we see that the increase in RF power increases the etching process. The increase in the height of the surface peaks increases with the etching.

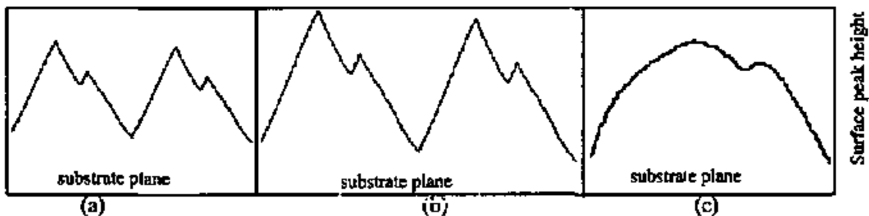


Figure 14. Schematic diagram showing the effect of RF power on the shape of the surface peaks. The RF power increases from 14(a) to 14(c). The 14(a) and 14(b) illustrates a case of columnar morphology and 14(c) illustrates a case of granular morphology. The increase in RF power increases the height of the surface peaks. *As the angle of inclination is constant since it is defined by the crystallographic facets of ZnO, the increase in peak height is always associated with an increase in the size of hexagon.* Figure 8.a and 8.b demonstrates an increase in the size of the surface peaks associated with an increase in their height. Figure 14(a) and 14(b) illustrate the increase in RMS roughness and the increase in excess area with the increase in RF power. In 14(c) we schematically show that the case with granular morphology has less RMS roughness and less excess area when compared with the cases of columnar morphology as illustrated schematically in figures 14(a) and 14(b).

#### 3.3.4.5 Substrate temperature series

The variation in RMS roughness and in excess area as a function of substrate temperature is shown in figure 11. The RMS roughness increases with substrate temperature within the region of columnar morphology and it decreases with in the region of granular morphology. The excess area is higher for low substrate temperatures and it decreases with an increase in substrate temperature. The surface morphologies found in the substrate temperature series are different from those found in the power series. As mentioned in section 3.3.3, there are regions of columnar grains with the ZnO sample grown at relatively low temperatures (figure 10.a and 10.b). It is also noted in figure 10.a and 10.b that the peak height is higher for 100°C and it has here a relatively higher fraction of granular regions.

This behaviour of RMS roughness and excess area as a function of substrate temperature is explained in figure 15:

An increase in substrate temperature increases the surface mobility. A reduction in substrate temperature leads to a reduction in the surface mobility and the film 'tries' now to grow with a granular morphology. But with an increased RF power of 200W, the surface always obtain columnar morphology. However, the reduction in substrate temperature can indeed form grains with granular morphology. (Figure 19 in section 3.4, shows SEM image of surface of ZnO with mixed granular and columnar morphologies. *The ZnO film was grown without substrate heating* and the RF power during growth was 200W. The increase in the granular grains in the surface when compared with the surface of ZnO in a similar growth condition but at high substrate temperature (figure 3 in section on SEM analysis, section 3.2) is in accordance with the above explanation )

The evolution of surface morphology with the substrate temperature leads to a very interesting conclusion of some practical importance. The RMS roughness of the sample with

columnar morphology grown at 100°C is still as high as the RMS roughness value obtained with high partial pressure of water vapour. In the section on electrical properties (section 3.5), it will be shown that the increase in partial pressure of water vapour increases the electrical resistivity of the ZnO films. On the other hand, the reduction in water pressure reduces the surface roughness. Hence with this low temperature process, we increase the surface roughness without any lose in electrical conductivity. The main point of practical importance is that by this we achieve low temperature surface texture growth of ZnO thin films. The high RF power used gives rise to high surface mobility: This fact allows us to correspondingly reduce the substrate temperature.

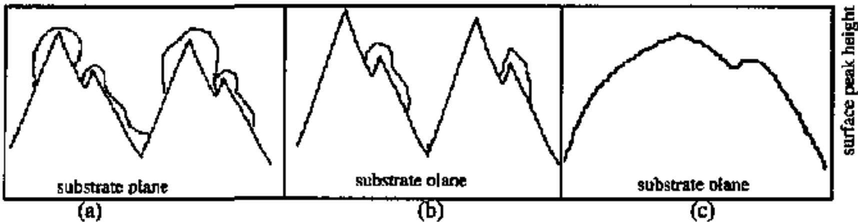


Figure 15. Schematic diagram regarding the effect of substrate temperature on the shape of the surface peaks. The substrate temperature increases from 15(a) to 15(c).The 15(a) and 15(b) show columnar morphology and 15(c) shows granular morphology. Fig 15(a) and 15(b) also show granular morphological grains on the columnar morphology. A decrease in substrate temperature decreases the surface mobility of the adatoms. The surface mobility of adatoms thanks to an increase in RF power lead to the columnar growth. However, there still exist individual grains of granular morphology when one reduces the substrate temperature. This increases excess area. This is shown schematically in figure 15(a). However, there is now relatively lower density of surface peaks and this causes a reduction in RMS roughness. An increase in substrate temperature reduces the amount of granular grains. This reduces the excess area. This is shown in figure 15(b). Granular morphology together with a relatively low surface peak height leads to both low RMS roughness value and low excess areas. This is schematically shown in figure 15(c)

## 3.3.5 Conclusions regarding the Surface properties analysis

The study of surface texture growth of thin films has become an important requirement, both to produce films that are suited to solar cell application as well as for the basic understanding of the evolution of the surface morphologies. Surfaces of ZnO thin films that were grown by RF magnetron sputtering were studied in detail in this section. The effect of various growth parameters on the surface morphologies were investigated. AFM and SEM analysis were done on the surfaces of ZnO thin films. The role of water vapour , RF power, substrate temperature were studied. The following conclusions are made:

There are two different surface morphologies obtained depending on the partial pressure of water vapour during RF magnetron sputtering. We call them 'columnar' and 'granular' morphologies. The increase in partial pressure of water vapour increases the roughness of the ZnO thin film. But water vapour should be mixed with Ar to provoke efficient surface-textured growth. It has been noted that the water should be dissociated to obtain surface-textured growth. By the AFM analysis the surface morphologies were quantified using the values of RMS roughness and excess area. This allows one to study the growth process as well as to quantify, with two parameters, the shape of the surface grains.

A comparison with the 'standard' growth model of J. A. Thronton showed that the columnar and granular morphologies are associated with high surface mobility and low surface mobility regimes, respectively. But AFM analysis has proven that the granular morphology

region is, in fact, not a genuine transition from columnar morphology, but it is just based on the columnar morphology.

Cases with columnar morphology exhibit hexagonal pits which are due to the crystallographic orientation of the growing ZnO films.

RF power and substrate temperature also change the surface morphologies. Basically, these two parameters change the surface mobility of adatoms. The RF power increases the height of the surface peaks. It is observed that the RF power changes the plasma conditions; depending on these conditions the surface of the film can form either granular or columnar morphologies.

The substrate temperature mainly changes the surface mobility. The reduction in substrate temperature leads to grains of granular morphology on the columnar morphology. In this case, the low-temperature surface texture growth has been achieved; the reasons for achieving this are explained.

Different growth process were illustrated thanks to the AFM images. The cross-section of the columnar morphology displays a constant inclination angle with respect to the substrate; this is due to crystallographic faceting. The FFM images of columnar morphologies showed that the surface peaks can be devided into many hexagonal pits.

The important mechanism to be considered during surface texture growth is the surface mobility of adatoms during growth. In these sections it is shown how the surface mobility can be modified by changing the partial pressure of water vapour, RF power and substrate temperature. By using these parameters, one can modify the surface texture of ZnO during growth.

These results give us, as main outcome, insight into the mechanism of surface textured growth. Based on these results, we will now study further these surface-textured ZnO thin films with respect to the properties that are relevant for thin film solar cell applications.

## References


[1] G.Binning, C.F. Quate, and C. Gerber, Phys. Rev. Lett. 56. 930 (1986).
[2] G.Binning, H.Rohrer, Ch. Gerber, E. Webel, Phys. Rev. Lett. 1982, 49, 57.
[3] Sergei. N. Magonov et al. VCH-Weinheim publishers 1996.
[4] Atomic Scale Tribometer (AST) manufactured by Centre Suisse d' Electronique et de Microtechnique (CSEM).
[5] Nidermann. P, Burger. J, Binggeli. M, Christoph.R, Hintermann. H, and Marti. O, A scanning force and friction microscope: proceedings of the NATO ARW on 'The ultimate limits of fabrication and measurements', Cambridge, April 1994.
[6] Martin Binggeli, Ph.D thesis on 'Nanotribology at the Solid- Liquid Interface, CSEM, University of Neuchâtel, Switzerland.
[7] M. Binggeli, R. Christoph and H.E . Hintermann, surface and Coating technology 62 (1993) 523-528.
[8] Kingo Itaya and Eisuke Tomita, Surface Science 219 1989) L515-L520.
[9] Dawn A. Bonnell and David R. Clarke J. Am. Cerm. Soc., 71 [8] 629-37 (1989).
[10] Gregory S. Rohrer and Dawn A. Bonnel Surface Science Letters 247 (1991) L195-L200 and the references there in.
[11] Grehory J. Exarhos, Shiv K. Sharma, Thin solid films 270 (1995) 27-32.
[12] Vesa Lujala, Jarmo Skarp, Markku Tammenmaa, Tuoma Suntola and Jeike Wallinga private communication (preprint).
[13] J. A. Thronton, J. Vac. Sci.Tech, 11 (1974), 666
J. A. Thronton, Ann. Rev. Mater.Sci, 7 :239 (1977)
[14] Handbook of Thin film Technology, Edited by Leon I Maissel and Reinhard Glang, McGraw Hill co. P 6-13 to 6-17 and 8-41 to 8-42.

# 3.4 Optical properties of surface-textured ZnO films

## 3.4.1 Introduction

The most important characteristic features of transparent conducting oxides are their optical and electrical properties. The usefulness of surface texturing of the TCO is immediately seen in the optical context w.r.t. solar cell applications; surface texturing increases the effective optical absorption of the solar cells by introducing light scattering. The surface texturing of ZnO films that can be used in the solar cells as window layer has an importance mainly in the wavelength region of 300 to 600 nm. On the other hand, the surface textured ZnO films that can be used in solar cells as back reflector should have a high transmission in the wavelength region of 600 to 1100 nm. The higher wavelength limit depends on the device. For example, a microcrystalline silicon cell can use the light up to 1100nm and an amorphous silicon cell can use the light up to 950 nm. In this section the optical properties of surface-textured ZnO films will be presented. The effect of surface texturing on the optical properties will be shown. The effect of adding water vapour, RF power and the substrate temperature during sputtering, on the optical properties will be studied in detail.

## 3.4.2 Experimental

The optical properties of the ZnO films were studied using a UV/VIS/NIR spectrometer (Lambda 900) with an integrating sphere manufactured by Perkin Elmer co. Two radiation sources, a deuterium lamp (DL), and a halogen lamp (HL), cover the working wavelength range (UV/VIS/NIR) of the spectrometer. The radiation passing alternately through the sample and reference beams is reflected by the optics of the detector assembly onto the appropriate detector. A photomultiplier (PM) is used in the UV/VIS range while a lead sulphide (Pbs) detector is used in the near infrared range.

With the integrating sphere we can analyse the surface texture of the thin films. The schematic diagram of the integrating sphere is shown in figure 1. The entrance port of the reference beam (A), entrance port of the sample beam (E), specular (direct) exit port for transmittance (B), and specular (direct) exit port for the reflectance (C) are shown in the figure. A special feature of this sphere is that the collimated beam can be allowed to escape out of the sphere through a port and thus only the scattered (diffused) radiation is recorded. This possibility to distinguish between the scattered and collimated (direct) radiation is necessary to characterise optically the surface texture of ZnO thin films. Various methods of measurements used here are explained below.

#### 3.4.2.1 Diffuse transmittance and diffuse reflectance

The surface roughness is optically characterised by a number called haze factor. To explain this term, one should mention the meaning of diffuse transmittance and diffuse reflectance. When a light beam falls on a surface, transmittance, reflectance and absorption take place. At the same time, the amount of light that is transmitted, reflected or absorbed is highly modified by the morphology of the surface. A rough surface always scatter the light in all possible directions depending on the surface morphology. A measure of the transmitted or reflected light in all directions other than the direction of transmitted or reflected light ray (normal to the surface of the film) can be a measure of the surface roughness. The sum of all the light that is transmitted except the directly transmitted light is called diffuse transmittance. A similar sum for the reflected light is called diffuse reflectance. The diffuse transmittance, $T_d$, the diffuse reflectance $R_d$, the direct transmittance $T_{direct}$ and the total transmittance $T_{total}$ are shown figure 2[1].

3.4.2.2 THE HAZE FACTOR

The haze factor H(hν) is defined as the ratio of diffuse transmittance to the total transmittance.

$$H = \frac{T_{total} - T_{direct}}{T_{total}}$$

$$H = \frac{T_{diffused}}{T_{total}} \qquad (1)$$

The haze factor is spectrally dependant. Generally, the haze factor is mentioned at the wavelength of 550nm. The effectiveness of the scattering by textured TCOs are measured by this number.

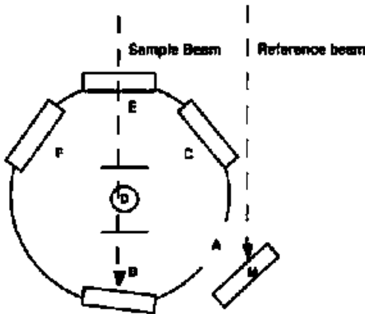


Figure 1. Schematic diagram (top view) of the integrating sphere. In the figure A is entrance port of the reference beam, E is entrance port of the sample beam, B is specular (direct) exit port for transmittance and C is specular (direct) exit port for the reflectance. Also in figure M is mirror and D is detector.

Figure 3 and figure 4 explain the measurement of total transmittance, diffused transmittance, total reflectance, diffused reflectance[2]. For the measurement of total transmittance the sample is placed at the port E and the ports B, C, and F are closed with the white windows made up of the same material like the sphere. For the measurement of only diffuse transmittance the direct transmittance is allowed to escape from the measurement by opening the window B. G is a light trap that collects all the light that come to it . Similarly for the measurement of total reflectance, the ports B and C are closed and the sample is placed at the port B. Note, the port B is kept tilted with a small angle of around 7° to make the primarily reflected light to travel to the port C and not to the same port where the incident light is arriving. For the measurement of only diffuse reflected light the window C is kept open so that the direct reflectance from the sample escapes, through G, out from the measurement. With these measurements we can clearly quantify the direct, diffuse and the total radiation reflected or transmitted from the thin film samples.

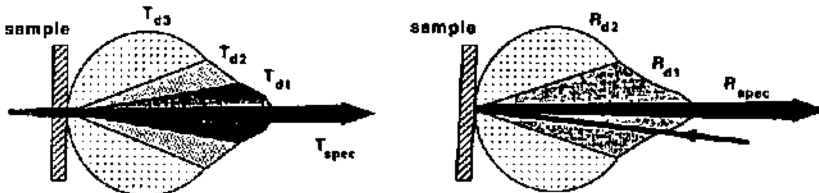


Figure 2. Schematic representation of angular distribution of reflected and transmitted radiation. Diffuse transmittance $T_d$, specular transmittance $T_{spec}$, diffuse reflectance $R_d$, specular reflectance $R_{spec}$ are shown in the figure.

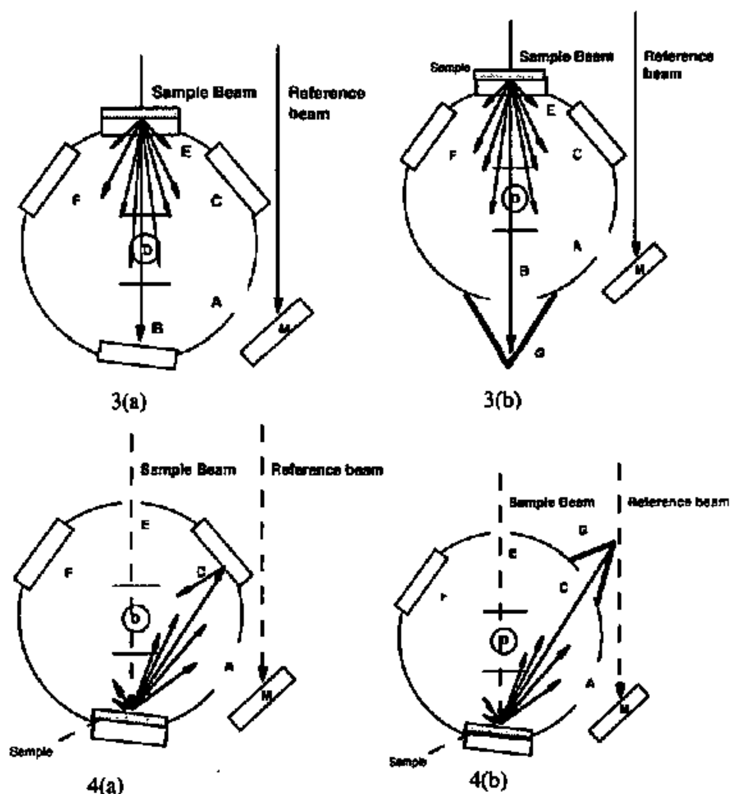


Figure 3 and 4 Total and specular measurements using integrating sphere: 3(a) total transmittance, 3(b) diffuse transmittance, 4(a) total reflectance, 4(b) diffuse reflectance. G is a light trap.

### 3.4.2.3 BAND GAP DETERMINATION

Band gap is an important individual parameter. Determination of band gap is necessary to monitor the changes in the material properties during the growth of surface-textured ZnO thin films. The band edge of ZnO thin films are calculated using the theory developed for optical transitions in semiconductors[3] and in insulators[4, 5]. The absorption coefficient ($\alpha$) of ZnO is a parabolic function of the incident energy and the optical band gap. For direct allowed band to band transitions,

$$\alpha(h\upsilon) = A^*(h\upsilon - E_g)^{1/2} \qquad (2)$$

where A* is a constant of the material that depends on refractive index and effective mass. Using this equation the band gap can be derived by plotting $\alpha^2$ as the function of incident photon energy and extrapolating the linear part of the curve to intercept the energy axis. The intercept gives the value of Band gap [6,3]. The absorption coefficient is derived from the equation,

$$T(\lambda) = [(1 - R(\lambda)]^2 \cdot \exp(-\alpha d) \qquad (3)$$

where d is the thickness of the film, T(λ) is the measured transmittance and R(λ) is the measured reflectance of film on a non absorbing substrate.

## 3.4.3 Results

### 3.4.3.1 The water vapour series

The optical properties were measured for the samples of water vapour series. Figure 5 shows the total transmittance of the ZnO:Al films that were grown with different partial pressures

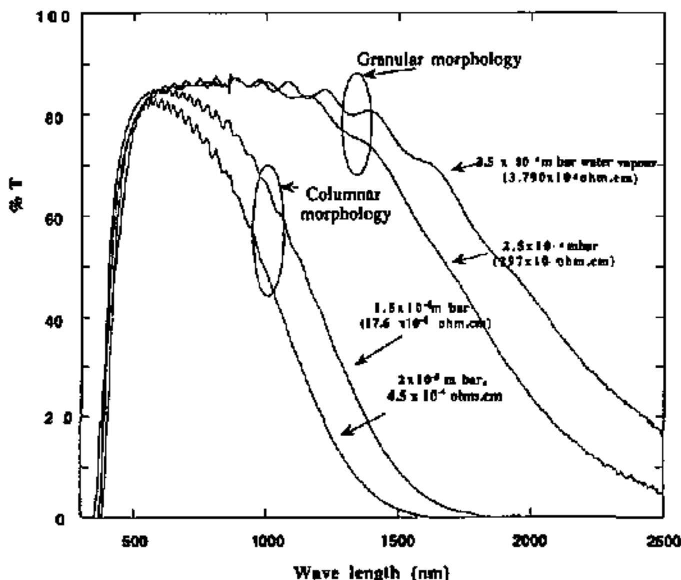


Figure 5. Total transmittance of ZnO films grown at different partial pressures of water vapour during sputtering. The total working pressure was 5 x $10^{-3}$ mbar. The RF power was 200W. The substrate temperature was 200°C. As the partial pressure of water vapour increases the film shows more rough surface. The resistivity of the films increases with increase in water pressure. The free carrier absorption (at the near infra red region) varies depending on the resistivity (the number of charge carriers) of the films.

of water vapour during sputtering. The substrate temperature was kept at 200°C. The RF power was 200W. As the partial pressure of water vapour is increased, the roughness of the surface of the ZnO films gets increased. This is can be seen from the picture. When the surface of the film is flat, the transmittance displays an interference pattern. The interference pattern decreases with the increase in roughness of the surface of the ZnO films.

### 3.4.3.2 Electrical conductivity and the shape of the transmittance spectrum at the near infra red redion

From figure 5 it is also noted that the transmittance in the near infra red region gets modified depending on the partial pressure of water vapour. The ZnO film grown with high partial pressure of water vapour shows transmittance in the wavelength region that is more than 1500 nm. As the partial pressure of water vapour during growth decreases the films show more

absorption in the near infrared region and the films have increase in electrical conductivity. This absorption is mainly due to the free charge carriers in the film and will be discussed later.

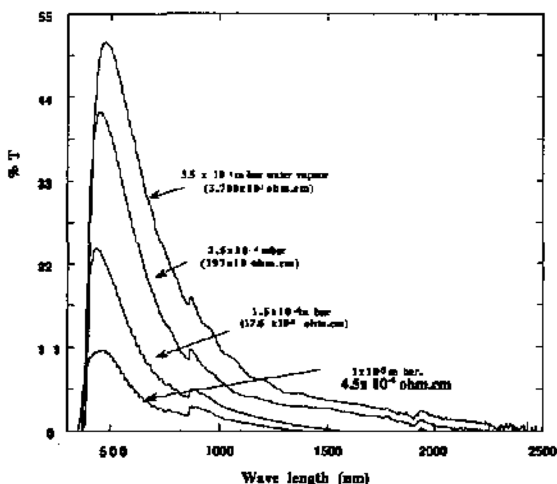


Figure 6 Diffuse transmittance of the same samples in figure 5. The increase in partial pressure of water vapour increases the diffuse transmittance

3.4.3.3 Surface morphology and the optical transmittance

In the SEM analysis it has been seen that the ZnO films exhibit mainly two classes of surface morphologies depending on the partial pressures of water vapour during growth. The columnar and granular morphologies show clearly different behaviours in the transmittance spectrum. The size of the grain, shape of the grains, number and mobility of charge carriers; all these factors can affect the shape of the transmittance curve in the near infra red region. The granular morphology has a salient transmittance in the near infra red region.

3.4.3.4 Diffuse transmittance

The diffuse transmittance is measured by integrating all the light that is transmitted by ZnO:Al films in all directions and then by subtracting the direct transmittance from the earlier one. Figure 6 show the diffuse transmittance of the ZnO:Al films grown with different partial pressures of water vapour during sputtering. With the increase in the partial pressure of water vapour the diffuse transmittance increases.

For each set of experimental parameters, the surface roughness and hence the diffuse transmittance was observed to increase with the increase in film thickness. After certain thickness, of around 1500nm, the diffuse transmittance reaches a constant value and then it gets saturated.

3.4.3.5 Variation of the haze factor

The haze factor is calculated for these films using equation (1). Figure 7 shows the variation of haze factor with the partial pressure of water vapour. The haze factor is calculated at 550nm. The classification of the surface morphologies also made in the diagram. The maximum value of 48% is obtained at the partial pressure of $3.5 \times 10^{-4}$ mbar. The corresponding surface has granular surface morphology.

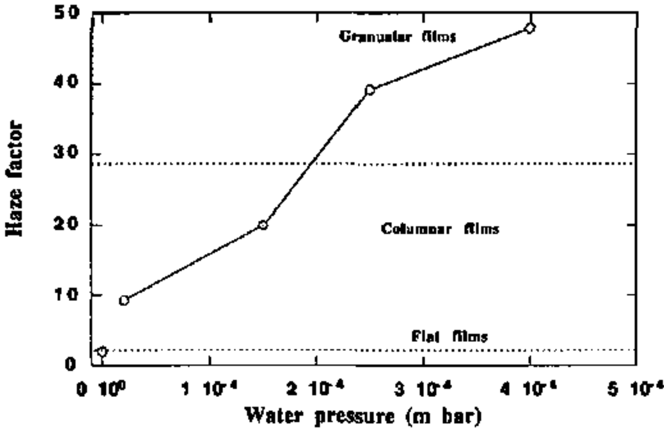


Figure 7. Haze factor values of the samples grown at different partial pressures of water vapour during sputtering (see fig 6). The flat film, columnar and granular regimes are shown in the figure.

### 3.4.3.6 ZnO:Al FILM GROWN ONLY WITH WATER VAPOUR DURING SPUTTERING

The ZnO film grown with water vapour alone has total transmittance and diffuse transmittance as shown in the figure 8. The transmittance measurement is done with a background correction for glass substrate. The interference patterns shows the smoothness of the film. The high transmittance at the near infra red is due to the poor electrical conductivity of the film. The diffuse transmittance is very low and it resembles the diffuse transmittance of the flat films grown with only Ar gas. This shows, as mentioned in the earlier section, that water vapour needs to be mixed with Ar gas to have surface textured growth.

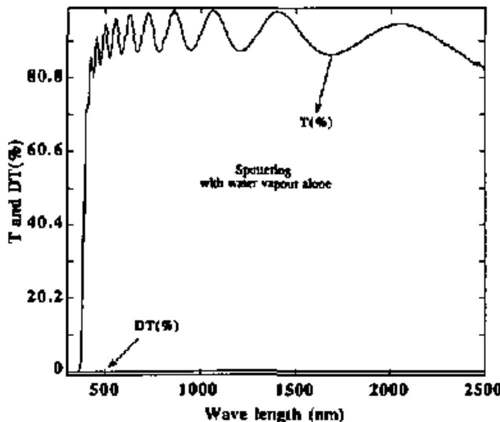


Figure 8 Total and diffuse transmittance of the films grown by using water vapour alone for sputtering. Without addition of Ar gas there is no surface texture growth and the film shows flat surface. This is seen from the diffuse transmittance. The high transmittance at the near infra red region shows the films are electrically highly resistive (due to very low number of charge carriers).

### 3.4.3.7 Band gap and absorption coefficient of ZnO films grown with the atmosphere of water vapour

The absorption coefficient($\alpha$) is derived from the optically measured transmittance and reflectance values as well as the thickness values using the equation (3). The band gap is derived by plotting the $\alpha^2$ versus photon energy, E(hv) and by using equation (2). Figure 9 shows the $\alpha^2$ versus E(hv) curve for the samples grown at different partial pressures of water vapour. The absorption coefficients were calculated using the specular transmittance and specular reflectance as well as total transmittance and total reflectance. The variation of $\alpha^2$(specular) and the $\alpha^2$(total) are shown in the figure 9. We see that *the linear part of the $\alpha^2$(specular) and the $\alpha^2$(total) give different intercepts at the x-axis thereby giving different apparent band gap values. Associated with this, there is a shift in the apparent (i.e. measured) band gap values when the surface of the thin film is rough.* The difference between band gap determined using 'specular' data and the band gap determined using 'total' data increases as the surface roughness increases. This is explained further and the correction necessary for the measurement of band gap of ZnO with rough surface will be demonstrated in the discussion part.

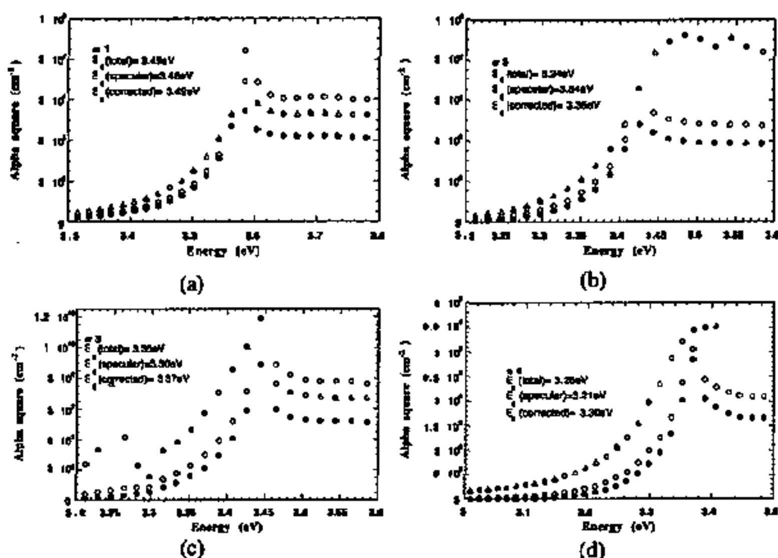


Figure 9 Square of absorption coefficient as a function of photon energy for ZnO films grown at different partial pressures of water vapour (see table I and Table II): Δ- values obtained with specular measurements, O-values obtained with total measurements (also see figure 3 and 4) and •-corrected values (see the discussion). The roughness in surface leads to an apparent shift in the band gap measurements. Also the band gap obtained using the total measurements does not give the correct value.

The intercepts of the linear portion of the $\alpha^2$ versus the photon energy curve the band gap of ZnO. The band gap of intrinsic single crystal ZnO is 3.32eV. The band gap of flat ZnO (grown with only Ar) is higher than that of intrinsic ZnO. The band gap of the ZnO film grown at low partial pressure of water vapour shows also higher band gap than the intrinsic ZnO. Further increase in water vapour during growth shows a 'reduction' of this 'increased' band gap. It is noted that the values of band gaps are higher for the samples with high electrical conductivity

(grown at low partial pressure of water vapour). As the water pressure increases the band gap comes to a value around 3.3 eV.

Figure 10 shows the $\alpha^2$ versus E(hv) curves for ZnO films grown with only Ar and only water vapour during sputtering. Both of the films have flat surfaces. We observe the increase in band gap values for the conductive ZnO film grown with only Ar. The band gap value of ZnO film grown with only water vapour is close to the intrinsic band gap value of ZnO.

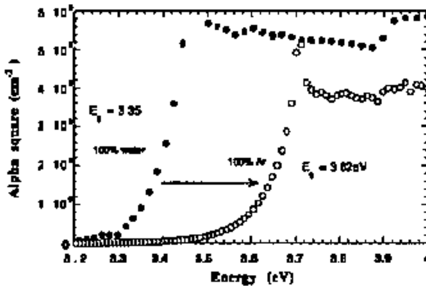


Figure 10 Square of the absorption coefficient as a function of photon energy for the ZnO films grown at 100% water vapour and at 100% Ar (see table III). The ZnO film grown with only Ar has shown an increase in the band gap value whereas the sample grown with only water vapour has a band gap value similar to that of intrinsic ZnO. The shift is due to high carrier concentration in the first case.

### 3.4.3.8 Other effects of water vapour on the optical properties of ZnO

The effects of water vapour on the optical properties of ZnO films apart from the effect of surface roughness, are equally important. By this, one can also analyse the changes in the material properties due to the growth of surface textured ZnO by addition of water vapour during sputtering. Also, in general cases of flat film growth, this is helpful to study the effect of background water vapour [7] on the properties of ZnO films.

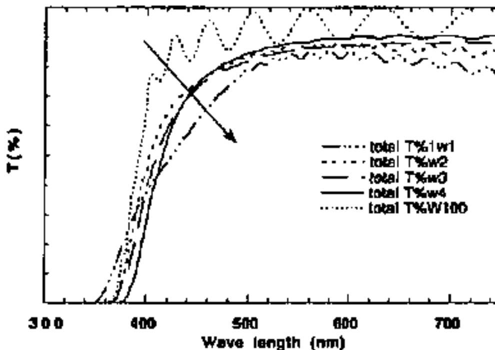


Figure 11. Total transmittance spectra of the ZnO films grown at different partial pressures of water vapour.(see figure 5) At 400-500nm there is reduction in transmittance while comparing with the transmittance spectra of the sample grown with only water vapour. The distinct reduction in transmittance in this wave length region is due to the formation of yellow color centers in the films. The resistance to yellow color formation is high in the case of the films grown with only water vapour. The addition of Ar with water vapour lead to the formation of yellow color centres

Comparison between the transmittance spectrum of ZnO films grown at different partial pressures of water vapour with the transmittance spectrum of film grown by using only water vapour (flat surface) is shown in figure 11. It shows that there is an absorption at around 400 to 500nm. Generally, except the sample grown with very low water vapour, this absorption increases with increase in partial pressure of water vapour. This corresponds to the development of a yellow coloration in the films. This will be discussed further. The sample grown with only water vapour shows a good transmittance at this wave length region. Therefore, we take this transmittance spectrum to compare all other samples.

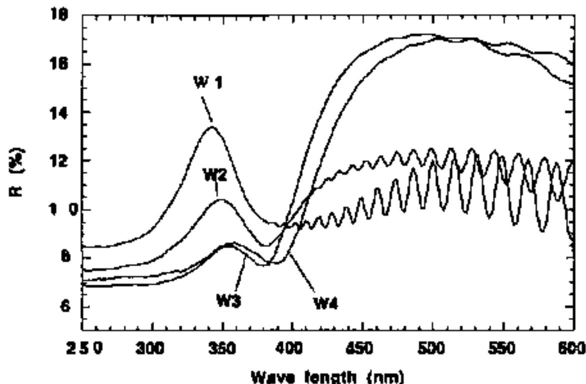


Figure 12. Reflectance spectra of the ZnO films grown at different partial pressures of water vapour (same samples shown in figure 5; see table I and table II for the experimental parameters).The peak in the UV regions are due to excitons[8] . The exciton peaks are highly pronounced only in the diffuse reflectances.

Figure 12 shows the reflectance of the ZnO films grown at different partial pressures of water vapour. At the shorter wavelength region where we have strong absorption, the reflectance shows clearly distinctive peaks. These peaks are reported to be due to excitons and they are explained later. It is observed that the absorption is pronounced in diffuse reflectance measurements

3.4.3.9 Power series

Figure 13 shows the diffuse transmittance of ZnO:Al films grown at different RF power values. The substrate temperature was kept at 200°C. The partial pressure of water vapour was kept at 2.5 x $10^{-4}$ m bar. The increase in RF power makes the surface morphological change from columnar morphology to granular morphology. The ZnO:Al films grown with 100W and 150W belong to columnar surface morphology and the film grown with 200W belong to granular morphology. The diffused transmittance increases with increase in RF power during the growth. The strong influence of RF power on the surface texture growth can be seen from the picture.

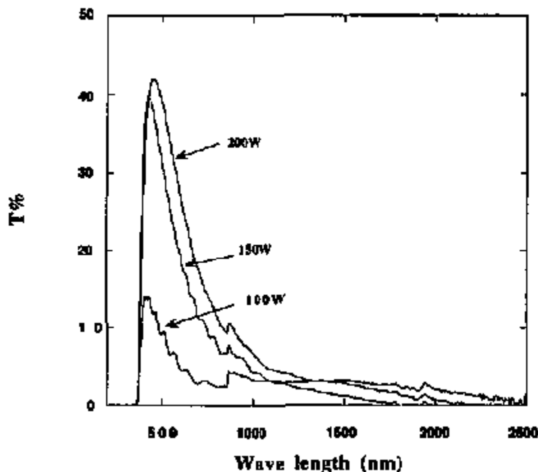


Figure 13 Diffuse transmittance of the ZnO films grown at different RF power values. The partial pressure of water vapour is 2.5 x $10^{-4}$ m bar. The substrate temperature was 200°C. The total working pressure was 5 x $10^{-2}$ m bar. The increase in RF power increases the diffuse transmittance and hence the haze factor. The samples grown at 100W and 150W have columnar surface morphology whereas the sample grown at 200W has granular surface morphology

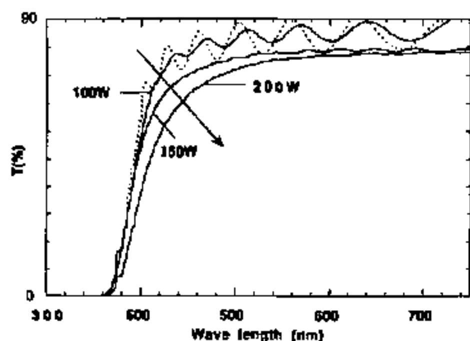


Figure 14. Total transmittance spectra of the ZnO films grown at different RF power values during sputtering (see figure 13). At 400-500nm there is reduction in transmittance of the sample grown at 200W while comparing with the transmittance spectra (dotted curve) of the sample grown with only water vapour. The distinct reduction in transmittance in this wave length region is due to the formation of yellow color centers in the films. The resistance to yellow color formation is high in the case of the films grown with low RF power values. The sample grown at 100W shows almost no yellow color formation.

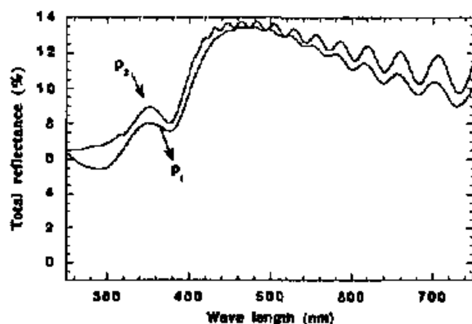


Figure 14.b Total reflectance at the ultraviolet region for the samples grown at different RF power values. See table (IV).

The comparison of the transmittance of these ZnO samples with the transmittance of ZnO grown at 100% water vapour do not show a notable difference in the absorption at 400-500 nm. Figure 14 shows the transmittance of the samples grown with different RF powers. We observe that *reduction in RF power lead to reduction in yellow colour formation in ZnO films*. Figure 14.b shows the reflectance of the same samples shown in figure 14. Similar to figure 12, here also the absorption due to excitons is observed.

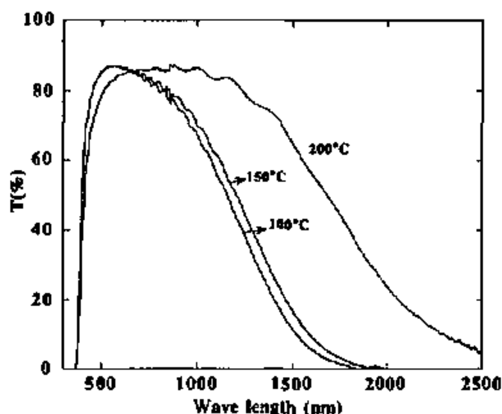


Figure 15. Total transmittance of ZnO films grown at different substrate temperature values during sputtering. The partial pressure of water vapour was $2.5 \times 10^{-4}$ mbar. The total working pressure was $5 \times 10^{-2}$ mbar. The RF power was 200W. As the substrate temperature decreases the films show mixed columnar and granular morphologies. The resistivity of the films increases with increase in substrate temperature. The free carrier absorption (at the near infra red region) varies depending on the resistivity (the number of charge carriers) of the films.

### 3.4.3.10 TEMPERATURE SERIES

The total transmittance of the films grown at different substrate temperatures are shown in figure 15. The RF power was 200W. The partial pressure of water vapour was $2.5 \times 10^{-4}$ m bar. It is observed that at an increased RF power of 200W, the change in substrate temperature makes a change in near infra red absorption region.

Figure 16 shows the diffuse transmittance of the same samples. From these figures it is seen that the substrate temperature modifies the surface morphology. The increase in substrate temperature from 100°C to 150°C increases the diffuse transmittance. These films have the columnar surface morphologies. The sample grown with 200°C substrate temperature belong to granular surface morphology. Hence the structure of the film grown at 200°C is also different from the other samples. The diffuse transmittance can not be directly compared because of this reason. The interesting result from this curve is that *the diffuse transmittance of columnar morphology could be more than the diffuse transmittance of granular morphology*. Also by this it is seen that one could achieve high diffuse transmittance hence the high haze factor at low temperatures. This is an important requirement for thin film solar cells. Especially for a-Si:H and micro crystalline silicon solar cells the film growth process should be always under 200°C to prevent the diffusion of metal atoms.

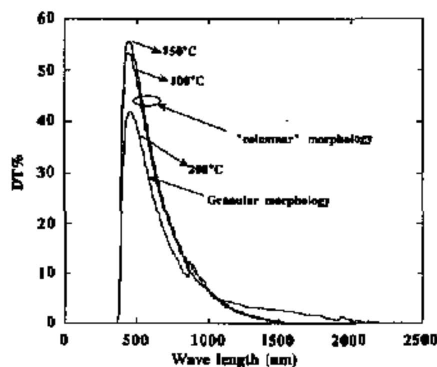


Figure 16 Diffuse transmittance of the ZnO films grown at different substrate temperature values. The partial pressure of water vapour is $2.5 \times 10^{-4}$ m bar. The substrate temperature was 200°C. The total working pressure was 5 x 10-2 m bar. *The decrease in substrate temperature increases the diffuse transmittance*. The samples grown 200°C show granular morphology whereas the samples grown at 150°C and 100°C have *shown mixed columnar and granular morphologies*.

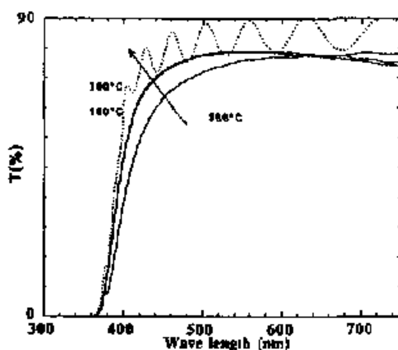


Figure 17. Transmittance spectra of the ZnO films grown at different substrate temperature values (see figure 15). At 400-500nm there is reduction in transmittance of the sample grown at 200°C while comparing with the transmittance spectra (dotted curve) of the sample grown with only water vapour. The resistance to yellow color formation is high in the case of the films grown with low substrate temperature values. The sample grown at 100°C and 150°C show no yellow color formation. Comparing figure 11 and 14 we observe that *the reduction in kinetic energy during growth reduces the yellow color centre formation.*

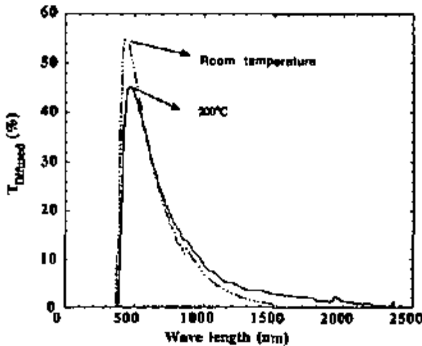


Figure 18. Achieving high diffuse transmittance at low temperatures. Diffuse transmittance of the sample grown at *room temperature* with partial pressure of water vapour at 3.5 x $10^{-4}$ m bar. It is compared with the sample grown at 200°C at relatively reduced water pressure of 2.5 x $10^{-4}$ m bar (solid line). The RF power was 200W and the total pressure was 5 x $10^{-2}$ m bar. The surface morphology of the sample grown at room temperature shows mixed columnar and granular morphologies. The increased value of RF power helps to reduce the substrate temperature. With reduced substrate temperature increase in water vapour lead to higher surface texturing (see figure 19 also).

## 3.4.4 Discussion.

The addition of water vapour with Ar gas increases the diffuse transmittance and hence the haze factor. Sputtering with water vapour alone does not make surface texture. The Ar gas mixed with water vapour during sputtering dissociates the water vapour into mainly hydrogen and OH group molecules and ions. This dissociation is necessary to make surface texturing of ZnO films. During the growth with only water vapour, of course there is dissociation of water vapour. But the degree of dissociation is very less while comparing with the dissociation that takes place when the water vapour is mixed with Ar gas.

The change in the RF power as well as the substrate temperature mainly changes the *surface mobility* of the adatoms during growth. The surface mobility of adatoms plays one of the key roles in making the surface texture growth and this is discussed in other sections. The increase in surface mobility enhances the surface texturing in the case of columnar morphology. At a high RF power of 200W it is easy to achieve the maximum haze values corresponding to the respective partial pressure of water vapour. Any increase in substrate temperature, as seen in the transmittance curves for 100°C and 150°C (in temperature series), does not show big change in transmittance like the change with increase in the RF power (fig 13 and 16). (Similarly at an elevated substrate temperature, a low RF power can still result in high diffuse transmittance, hence the high haze factor). By this important conclusion we achieved the low temperature surface texturing of ZnO thin films with high RF power values. This low temperature process of surface textured growth of ZnO is highly useful for a-Si and microcrystalline silicon solar cell technologies [9].

At an increased RF power, the increase in partial pressure of water vapour helps to reduce the substrate temperature to room temperature and still obtain surface texture growth. This *increases the haze factor more than what is obtained by the film grown at 200°C grown at the* same partial pressure of water vapour. The electrical resistivity of such film is 14.1x $10^{-4}$ Ω.cm. This describes the way to achieve surface texture growth at low temperatures. Figure 18 shows the diffuse transmittance of ZnO:Al films at increased partial pressure of water 3.5 x$10^{-4}$ mbar at substrate temperature as low as room temperature. It has an increased haze value that is more than 50%. The surface morphology of ZnO:Al film at this experimental growth condition is shown in figure 19. A closer look at the surface morphology reveals that the *it contains both columnar and granular morphologies*.

The ZnO films grown at low substrate temperature are superior in haze factor as well as electrical conductivity values than previously reported surface textured ZnO films [10].

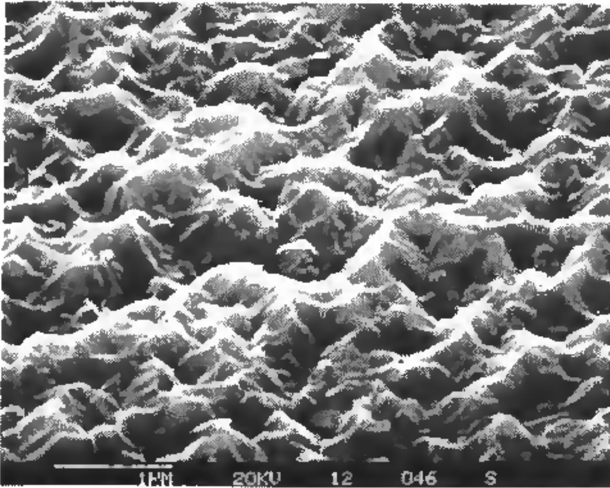


Figure 19. Scanning electron microscope photograph of the sample grown at room temperature (see figure 18). The RF power value was 200W. The partial pressure of water vapour was 3.5 x 10 $^{-4}$ m bar. The total pressure was 5x10-2 m bar. Figure shows mixed columnar and granular morphologies.

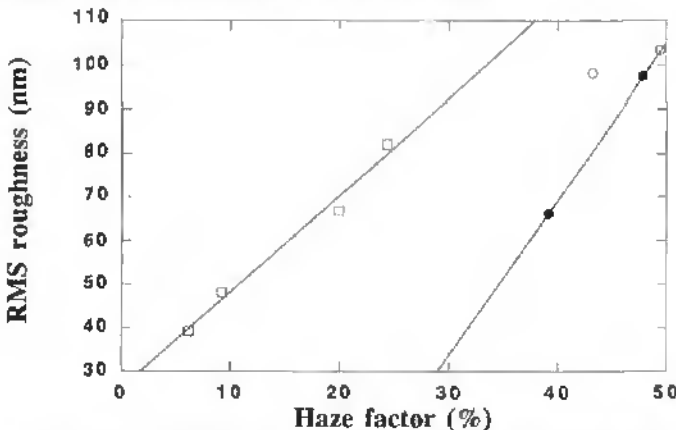


Figure 20. Root Mean Square roughness values measured using atomic force microscopy as the function of optically measured haze factor (at 550nm) values using spectrometer; 1. Square-samples with columnar morphology, 2.●-samples with granular surface morphology and 3.O-samples with mixed columnar and granular morphologies. The samples with columnar surface morphologies have a linear relationship of RMS roughness with the haze factor. Similarly the samples with granular morphology have another slope. Also this figure shows that RMS roughness can be directly connected with diffuse radiation.

In figure 20 the RMS roughness of all the samples with columnar, granular and mixed surface morphologies in function of haze factor is shown. The haze factor is an optically measured property that has a link with surface roughness. On the other hand, RMS roughness is a roughness measurement that is done *on* the surface of the thin films (see the section on AFM studies). It is interesting to see the connection between these two parameters. In figure the samples with columnar morphology, samples with granular morphology and the sample with

mixed granular and columnar morphologies are shown. As is seen for the columnar morphology, the RMS roughness measurement has a linear relationship with the haze factor. Similarly the granular samples have another slope. The convincing thing is that the haze factor increases linearly with the increase in RMS roughness value and thus it can be connected with RMS roughness values. On the other hand, the excess area measurement does not give a coherent relation with the haze factor. This shows that, as discussed earlier, the RMS roughness measurement is more useful parameter than the excess area over the geometrically projected area.

#### 3.4.4.1 Free carrier absorption

In the transmittance spectra there is an absorption in the near infra red region in the case of ZnO films with high electrical conductivity (figure 5 and figure 15). This absorption is due to the free charge carriers in the film. In the near infra red region the frequency of the incident radiation is insufficiently high to cause band to band transition or formation of excitons and absorption is due to transition between the states in a single energy band (intra band transition)[11]. Clearly, for a completely filled band, no such transitions are possible. For the conduction band, the absorption will be proportional to the number of free electrons. Generally, the absorption due to free carriers is directly proportional to the square of the wavelength and is inversely proportional to the mobility. The free carrier absorption is already explained in chapter 2 (see equation 2 in chapter 2). For ZnO films, the absorption at the near infra red region is a measure of number of charge carriers in the films. More is the absorption towards low wavelength side more is the number of charge carriers. Hence by looking at the optical transmittance spectra one may say if the film is conductive or not. Clearly the conductivity measurements show that the conductivity increases with decrease in partial pressure of water vapour during sputtering. (as seen in figure 5)

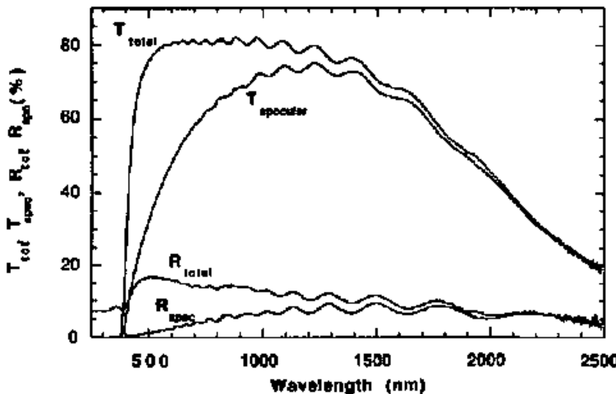


Figure 21. The total and specular transmittance and reflectance spectra of surface-textured ZnO film (sample W4 in table II). This explains that the specular transmittance and reflectance measurements 'see' the diffuse light as 'absorbed' light. This lead to a shift in absorption coefficient *also in* the band gap measurement values.

#### 3.4.4.2 Band gap measurements and the correction necessary in the case of surface texture

In the band gap measurement (figure 9 and table I, II, IV and V), it is seen that the specular transmittance and specular reflectance measurements show an apparent shift in the band gap of ZnO films. This is clear when we look at the transmittance and the reflectance spectrum for total and specular measurements (figure 21). In specular measurements, the light which is diffused in all other direction than the direction normal to the film, will be seen as the light 'absorbed' by the film. Hence the absorption coefficient derived using specular-measurements always lead to higher values of absorption coefficients. On the other hand, in the total-measurements all the light that is transmitted and reflected by the film is collected by the detector. Hence it should give the correct value of absorption coefficient. However, there is the light that escapes through the edge of the glass substrate by the wave guide action. Hence the absorption coefficient derived using total-measurements will also be slightly higher than the original values.

Hence when the film has a rough surface, both the specular and total- measurements may lead to wrong values of the band gap. To derive more correct value we need to apply a correction. In a general transmittance formula, the contribution of scattering can be written as

$$I_{transmitted}^{spec} = I_0 e^{-(\alpha+\alpha_{sc})d}$$

where $(\alpha+\alpha_{sc})$ is the total attenuation where $\alpha$ is the true optical absorption of the film and $\alpha_{sc}$ is the scattering coefficient. For strong scattering and strong absorption, we can calculate the optical scattering coefficient. The absorption coefficient $\alpha_{sc}$, is calculated using the following relation [12].

$$\frac{T_{scat}}{T_{spec}} = C_\theta\left[\exp(+\alpha_{sc}d) - 1\right] \qquad (4)$$

Where $T_{scat}$ is the diffuse transmittance (only scattered transmittance) and $T_{spec}$ is the direct transmittance (only specular transmittance). $C_\theta$ describes the space of the cone of the total reflectance angle $\theta_c$. The $C_\theta$ is given by $C_\theta = (1-\cos\theta_c)$. The light ray reaching the substrate with an angle above $\theta_c$ will perform a waveguide action. The value of $\theta_c$ depends on the refractive indices of the substrate and the ZnO film. For doped ZnO film we take the value of n to be 2 (at 4 eV)[13] . The absorption coefficient derived from these measurements is the absorption due to the scattering and this also take the light which goes through the edges of the glass into account. Now the true absorption coefficient can be written by the following relation.

$$\alpha = \alpha(spec) - \alpha(scat) \qquad (5)$$

Because what is measured in specular measurement ('apparent') is the real absorption plus the contribution from the scattering. From the corrected absorption coefficient $\alpha(h\nu)$, the band gap can now be determined. In figure 9, the third curve (closed circles-●) shows the corrected values of $\alpha^2$ in function of incident energy and the band gap at different partial pressures of water vapour. It is seen that the corrected values are very close to the total-measurement values. This means that the light that escapes by the internal reflectance is weak due to comparable value of refractive index of ZnO with the substrate. As the partial pressure of water vapour increases the surface roughness, and hence the haze factor increases. The correction is necessary for the samples with high haze factors; flat films do not need this correction.

The value of band gap of the ZnO films with columnar morphologies is listed in table I.

*Table I. Band gap and the absorption coefficient values of ZnO films with columnar surface morphology grown at different partial pressures of water vapour. $W_1=1.5 \times 10^{-5}$ m bar, $W_2=1 \times 10^{-4}$ m bar. The RF power was 200W and the substrate temperature was 200°C.*

| Sample | $E_g$ from specular measurements (eV) | $E_g$ from total measurements (eV) | $E_g$ corrected values (eV) | Corrected absorption coefficient $\alpha$ at 4 eV($cm^{-1}$) | Haze factor (%) |
|---|---|---|---|---|---|
| W1 | 3.46 | 3.49 | 3.49 | 23104 | 9 |
| W2 | 3.34 | 3.34 | 3.35 | 20044 | 20 |

### 3.4.4.3 Band gap and absorption coefficient values of ZnO

The value of band gap of intrinsic single crystalline ZnO is 3.32eV at room temperature[14, 15]. However this value varies from 3.29eV to 3.32eV in the literature. It is seen from the table that the sample W1 has a band gap of 3.49eV. This is well above the band gap of intrinsic ZnO and

this is explained as follows. In the section on electrical properties we will see that the resistivity of the ZnO films increase with the increase in partial pressure of water vapour. The resistivity is decided by the number of charge carriers as well as the mobility of the charge carriers. The amount of charge carriers in the ZnO can be immediately seen in the transmittance and the reflectance spectrum. As the number of charge carriers increases the wavelength at which the plasma resonance takes place moves towards the shorter wavelength side. From the transmittance curves of the samples shown in figure 5, it is seen that the sample W1 has more number of charge carriers. When the number of charge carriers are very high, this lead to filling up of the lowest levels of conduction band. When the lower levels of conduction band are occupied, the excited electrons from the valence band occupies higher energy levels than the bottom of the conduction band. Hence the threshold for the band to band transition shifts to higher energy. The apparent shift in band gap due to heavy doping has been explained by Burnstein[16] and Moss[17]. It is known as Burnstein-Moss effect (see chapter 2). However the magnitude of the shift can be less than the values according to the Burnstein Moss effect due to the merging of the impurity band (e.g. Al donor state) into the conduction band, thereby shrinking the band gap[18,19]. We see that the samples with increased number of charge carriers showing increase in band gap, hence Burnstein-Moss effect dominates here.

*Table II Band gap and the absorption coefficient values of ZnO films with granular surface morphology grown at different partial pressures of water vapour. $W_3$=2.5 x$10^{-4}$ m bar, $W_4$=3.5 x$10^{-4}$ m bar. The RF power was 200W and the substrate temperature was 200°C.*

| Sample | $E_g$ from specular measurements | $E_g$ from total measurements | $E_g$ corrected values | Corrected absorption coefficient $\alpha$ at 4 eV | Haze factor (%) |
|---|---|---|---|---|---|
| W3 | 3.30 | 3.35 | 3.37 | 80522 | 39 |
| W4 | 3.21 | 3.28 | 3.30 | 41816 | 48 |

The band gap values for the samples grown with granular surface morphology are shown in table II. As the surface roughness increases, the difference between the band gap values measured using specular and total measurements as well as the correction values increase. The values of the band gap for the samples with granular morphologies are slightly different from the values corresponding to the sample with columnar surface morphology. The sample W3 is relatively less resistive when compared with sample W4. However it is more resistive than the sample W2. The corresponding free carrier absorption (figure 5) indicates W3 has relatively less number of charge carriers. Hence the band gap value is expected to be less than the value corresponding to W2. But the values are very close to each other. Hence we can not consider the samples with columnar and granular morphology in a similar manner. In fact the samples with columnar morphology show higher crystallinity with larger grain sizes (shown in the section of structural properties) where as the granular morphology samples show low crytallinity with small grain sizes. Redfield [20, 21, 22] has shown that the electric fields of charged defects (point, line and planar defects) in a solid broaden its fundamental optical absorption edge. Recently [15], it has been proposed that the effective band gap can be reduced when the grain sizes are small ( between 30-80nm) and the number of charge carriers are lower. Also it has been explained that on an amorphous (glass) substrate, the thermal mismatch strains lead to increase in the band gap. Hence the effective band gap of films on glass substrate is further influenced by the interplay between the periodic potential in the grain boundaries, which decreases the band gap, and the thermal mismatch strains which increases the band gap.

The absorption coefficients measured at 4 eV are shown in Table I as well as table II. The comparison between these two tables show that the water vapour increases the absorption coefficient when there is transition in surface morphologies. The absorption coefficient can be written as [23]

$$\alpha(h\nu) = A\sum_{i,f} P_{if} g_{if} \qquad (6)$$

where A is a constant. The sum is over all possible transitions between states separated by energy hv, $P_{if}$ is the transition probability from the initial state to the final state, and $g_{if}$ is the joint density of states. According to this equation, when there is a morphological transition (also structural transitions), we assume that the joint density of states and/or the transition probably increase resulting in increase in an absorption coefficient.

Figure 10 shows the $\alpha^2$ versus energy curve for the samples grown with 100% water vapour and 100% Ar. Both the films show flat surfaces with haze factors less than 2%. Table III lists the main parameters. The band gap of the film grown with Ar alone as a sputtering gas has higher value. The band gap of the films grown with only water vapour has band gap close to that of the intrinsic ZnO. The sample grown with Ar has a good electrical conductivity (resistivity, $\rho$=4.9x $10^{-4}$ $\Omega$.cm). The density of charge carriers are higher, as seen from the transmittance curve. Hence the increase in band gap can be attributed to the Burnstein -Moss effect. The sample grown with 100% water vapour has a high resisitivity with very low number of charge carriers. Therefore we have a band gap that is closer to that of intrinsic ZnO.

The absorption coefficient is higher in the case of sample grown with only water vapour. Generally the samples grown at high partial pressure of water vapour (granular morphology) show small grain size with multiple orientations during growth. This increases the number of states available and thus the joint density of states resulting in the observed increased absorption coefficient. Y. Qu et al.[13] explained the increase in absorption coefficient of same quality ZnO films with different thickness values only in terms of the increase in states available in conduction band due to reduced number of charge carriers. However we can not directly attribute the increase in absorption coefficient to the number of charge carriers, as the material properties like grain size, the growth orientations, defects (point, line and planar defects) vary due to the increase in water vapour during growth which may result in the change in transition probability in equation (6).The band gap values, absorption coefficient and haze factor values of the samples grown at different RF power values and substrate temperatures are listed in table III and table IV.

*Table III. Comparison between optical properties of the samples grown with 100% Ar (at a pressure of 2x $10^{-2}$ m bar) and with 100% water vapour (at a pressure of 2x $10^{-2}$ m bar). The substrate temperature is 200°C and the RF power is 200W. The working pressure, RF power and substrate temperature are the same as that of the water vapour series.*

| sample | $E_g$ (measured) Total | absorption coefficient at 4 eV ($cm^{-1}$) | Haze factor |
|---|---|---|---|
| W100 | 3.35 | 76590 | >2% |
| A100 | 3.62 | 63045 | >2% |

3.4.4.4 Colour centers

Figure 11 shows the transmittance of the films grown at different partial pressures of water vapour. For comparison the transmittance of the sample grown with only water is also shown. A closer look (eliminating the effect due to the shift in band edge) reveals that there is a reduction in the transmittance at around 400nm for the samples grown with water vapour. This corresponds to yellow coloration in the films.

H.Rafla-Yuan et al.[24] have done reflectance studies on aluminium doped ZnO powders. They observed yellow coloration in their samples. This was displayed in reduction in reflectance at around 400nm explaining an absorption. They also observed that the resistance against this yellow coloration increases with increase in Al doping.

J. C. Simpson et al[25], based on DLTS studies of the deep levels in ZnO, suggested that the yellow coloration might be related to the charge transfer of an electron from the valence band to a deep donor like level located a few tenths of an eV below the conduction band edge. This might be related to either an interstitial zinc atom, a singly ionised oxygen vacancy[27] ($F^+$ center) or a cluster forming a donor like species[25] .

W. E. Veshe et al[28] observed a 410nm optical absorption band in ZnO crystals. This absorption wavelength corresponds to a 3.0. eV optical excitation. This was accompanied by a change in the crystal color from clear to pale yellow.

There are two species of intrinsic defects reported in the ZnO literature[29, 30,31] , Zinc interstitials $Zn_i$, and oxygen vacancies, $V_o$. These species may act as electron donors or traps through the following reactions

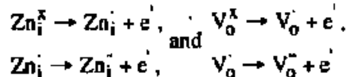

$$Zn_i^x \rightarrow Zn_i^{\cdot} + e', \quad V_O^x \rightarrow V_O^{\cdot} + e'$$
$$Zn_i^{\cdot} \rightarrow Zn_i^{\cdot\cdot} + e', \quad \text{and} \quad V_O^{\cdot} \rightarrow V_O^{\cdot\cdot} + e'$$

where $Zn_i^{\cdot}$ and $Zn_i^{\cdot\cdot}$ are first and second ionisation of interstitial zinc, and $V_O^{\cdot}$ and $V_O^{\cdot\cdot}$ are first and second ionisation of oxygen vacancies. In the literature, the value of the trap level varies for ionised zinc interstitial and ionised oxygen vacancies. A good estimate of this deep donor like level is 0.24 eV below the conduction band[24]. As the band gap of ZnO, as determined for our films is 3.35eV, the difference $E_g$-$E_t$=3.11eV which is approximately the energy where the decrease in transmittance occurs. The optical excitation may, therefore correspond to the charge-transfer reaction [25] as follows.

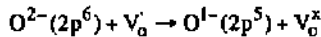

$$O^{2-}(2p^6) + V_O^{\cdot} \rightarrow O^{1-}(2p^5) + V_O^x$$

The optical absorption process leaves behind a hole and the ionised oxygen vacancy ($F^+$ centre) goes to a defect associated with a neutral oxygen vacancy or cluster. H. Raffla et al. have observed that upon pressure grinding, ZnO powder with low Al has yellow color formation.

In figure 14 it is seen that the reduction in RF power reduces the yellow color formation in ZnO films. Similarly the reduction in substrate temperature reduces the yellow color center formation (figure 17). Basically, the increase in RF power increases the kinetic energy of impinging ions and adatoms during the growth. Similarly, the increase in substrate temperature increases the kinetic energy of the mobile adatoms. We observe that increased values of RF power and substrate temperature lead to yellow color center formation. This is the same effect we observe with water vapour series.

The ZnO film grown with only water vapour shows high resistivity against yellow color centre formation. During the growth with only water vapour the dissociation of water vapour is very poor and the plasma is very weak. In other words, the plasma is very 'soft' (the ion energy in the plasma is low). By the addition of Ar with water vapour, the water vapour is highly dissociated and this lead to yellow color formation in addition with surface texture growth.

This is an important conclusion for growing ZnO films for solar cell applications where no loss in transmittance in the 400-500nm is preferred.

3.4.4.5 Excitons

Figure 12 shows the reflectance spectra of the samples grown at different partial pressures of water vapour. At the near band edge region, we have pronounced peaks. Similar absorption peaks are observed for the samples of power series and the substrate temperature series (figure 14.b and 23). The reflectance peaks at this energy values are reported to be due to excitons. Frenkel[32] postulated that a photon may excite an electron so that it remains in the vicinity of its nucleus, thus forming an electron-hole pair, called an *exciton* . Electrons and holes are bound by electrostatic forces and revolve around their mutual centre of mass. The electrons may hope through the crystal and change their respective partner. One depicts[3] the excitons by introducing 'excitonic levels' in the forbidden gap. R. L. Henghold et al.[8] have studied the ultra violet

reflectivity spectra of ZnO single crystals at *room temperature*. Around 3.3eV they have identified the peaks in the reflectance spectra. R. Klucker et al.[33] have also obtained the pronounced peak at 3.3 eV at room temperature and they explained these peaks to be due to excitons. The exciton spectra of ZnO crystals were first investigated systematically by Thomas et al.[34]. Afterwards there are several reports[35,36,37] about the exciton peaks at the fundamental absorption edge of ZnO. W. Y. Liang et al.[37] have shown the positions of the excitons to be at 366nm, 361nm, 360nm, 357nm and 356 nm for single crystalline ZnO at low temperature. For our polycrystalline samples at room temperature we have broadened peak like that of R. L. Henghold et al and R. Klucker et al from 345nm to 365nm due to all these excitonic states.

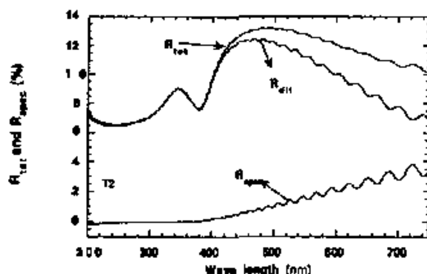


Figure 22 Total specular and diffuse reflectance of sample grown at 150°C (see table V). It is shown as an example that the exciton absorption is observed only through the diffuse reflectance and hence through the total reflectance. Similarly for all the samples the absorption at the ultraviolet region is highly pronounced in the diffuse reflectance.

*Table IV Band gap and the absorption coefficient values of ZnO films grown at different RF power values. The partial pressure of water vapour was 2.5 x $10^{-4}$ bar. The RF power values are p1= 100W, p2= 150W . The substrate temperature was 200°C.*

| Sample | $E_g$ from specular measurements | $E_g$ from total measurements | $E_g$ corrected values | Corrected absorption coefficient α at 4 eV($cm^{-1}$) | Haze factor (%) |
|---|---|---|---|---|---|
| p1 | 3.376 | 3.38 | 3.38 | 32593 | 6 |
| p2 | 3.34 | 3.363 | 3.367 | 28517 | 24 |

It is worth to be noted that theses peaks are pronounced *only* in the diffuse reflectance and hence in total reflectance and not in specular reflectance.(figure 22) It is usually observed that the absorbed energy is dissipated mainly by diffuse radiation[39] .

*Table V Band gap and the absorption coefficient values of ZnO films with columnar surface morphology grown at different substrate temperature values. Partial pressure of water vapour was 2.5 x$10^{-4}$ m bar. The RF power was 200W and the substrate temperature values are $T_1$ = 100°C, $T_2$ =150°C.*

| Sample | $E_g$ from specular measurements | $E_g$ from total measurements | $E_g$ corrected values | Corrected absorption coefficient α at 4 eV($cm^{-1}$) | Haze factor (%) |
|---|---|---|---|---|---|
| t1 | 3.316 | 3.362 | 3.382 | 33157 | 43 |
| t2 | 3.297 | 3.350 | 3.364 | 23139 | 49 |

### 3.4.5 Conclusions

The optical properties of surface textured ZnO:Al films were analysed in this section. The effect of deposition conditions on the optical properties were studied. The addition of water vapour during sputtering along with Ar gas increases the diffuse transmittance of ZnO films. Both the change in RF power as well as substrate temperature increases the kinetic energy for the film growth. At increased RF power values low substrate temperature can give high haze values. This lead to the achievement of surface texture growth with high haze values. The effect of surface roughness on the band gap value measurement has been studied. The band gap measurement using the specular-measurement lead to incorrect values. Similarly the band gap value measured using total-measurements has also shown slightly deviated values. Correction for the light lost due to wave guide action is applied and the true band gap values were obtained. The difference between the band gap value obtained using specular and total measurements as well as the correction values increases with increase in the surface roughness. The values of band gap of ZnO are explained using existing theories. The value of absorption coefficient is found to increase with increase in water vapour. The absorption due to excitons are found in the surface textured ZnO films. The formation of yellow color centers were found in the samples grown using water vapour. The yellow color centre formation is found to decrease with reduction in RF power as well as in substrate temperature. It clearly shows that a 'soft' growth leads to ZnO films with less yellow color centers. This, again, is an advantage of growing ZnO films at low substrate temperature. The optically measured haze factor values are compared with RMS roughness values measured using AFM. The ZnO films grown at low substrate temperature show high haze values with good electrical properties. They can be used for low temperature thin film, especially a-Si and μ-c-Si, solar cells fabrication.

The study on the optical absorption at the near infra red region, shift of the band edge in the UV region and transmittance loss due to color centers, are highly important for the growth of ZnO films for any application as transparent conductors, especially in thin film solar cells.

## References


[1] A.Roos, Sol Energy Mat. and Solar cells 30 (1993) 77-94

[2] In this work, also in the works about characterisation of surface textured TCOs the terms diffused transmittance or diffused reflectance mention the diffused radiation without the primarily transmitted or reflected radiation. This is mentioned because the reflectivity of the metals are measured by diffused reflectance which is, according to the definition of terms here, 'total reflectance'

[3] R. A. Smith *Semiconductors* Cambridge University Press 1978,p72-76, 331-334, 316

[4] D. L. Dexter, Proceedings of Atlantic city photoconductivity conference (Wiley, New york, 1954), pp. 155-183.

[5] J. E. Bardeen, F. J. Blatt, and L. H. Hall, Proceedings of Atlantic city photoconductivity conference (Wiley, New York, 1954), pp. 146-153.

[6] Ref.[3] p.312-313

[7] The aim of a previous work to study the effects of water vapour during growth on ITO films was to study the effect of background water vapour during large scale manufacturing of those films.

[8] R. L. Henghold and R. J. Almassy, Physical review B 1, 12. 1970, p.4784-4791

[9] J. A. Anna Selvan, H. Keppner and A. Shah in 'Thin Films for Photovoltaic and Related Device Applications' edited by David Ginley, Anthony Catalano, Hans W. Shock, Chris Eberspacher, Terry M. Peterson, Takahiro Wada, MRS symposium proceddings, Volume 426, p 997.

[10]T. Nakada, Y. Ohkubo and A. Kunoko IEEE photovoltaic specialists conference 1991

[11]Rolf. E. Hummel, 'Electronic properties of Materials', Narosa publishing house, 1994, p.207 and ref[3], page 295-300

[12]Nathalie Beck, privat communication.
[13]Y. Qu, T. A. Gessert, K. Ramanathan, R. G. Dhere, R. Noufi and T. J. Coutts J. Vac. Sci and Technology A 11(4), Jul/Aug 1993, p 999
[14]Current topics in material science, V.7 Edited by Kaldis, North- Holland publishing company 1981
[15]V. Srikant and D. R. Clarke, J. Appl. Phys. 81 (9), 1997 p6357
[16]E. Burnstein Phys. Rev. 93, 632 (1954)
[17]T. S. Moss, Proc R. Phys. Soc. London Ser. B 67, 775 (1954)
[18]A.P. Ruth, J.B. Webb, and D. F. Williams, Phys. Rev B 25, 7836 (1982)
[19]V. L. Blonch- Bruevich, in semiconductors and semi metals, edited by R. K. Williardson (Academic, New York, 1966), Vol.1, p.101.
[20]D. Redfield, Phys. Rev. 140, A2059 (1963)
[21]D. Redfield, Phys. Rev. 130, 914 (1963)
[22]D. Redfield, Phys. Rev. 130, 916 (1963)and ref [15]
[23]O. Madelung, in Introduction to solid state theory,,(Springer, Berlin, 1978), pp.266-269. Also ref. [13]
[24]H. Raffla- Yuan and J. F. Cordaro J. Appl. Phys. 69 (2), 15, p.959
[25]J. C. Simpson and J. F Cordaro, J. Appl. Phys. 63, 1781 (1988)(repeated)
[26]F. A. Kroger, the chemistry of Imperfect crystals (Wiley-Interscience, New York, 1964)
[27]J. C. Simpson and J. F Cordaro, J. Appl. Phys. 63, 1781 (1988)(repeat)
[28]W. E. Veshe, W. A. Sibley, F. J. Keller, and Y. Chen, Phy. Rev. 167 828 (1968)
[29]A. Rohatgi, S. K. Pang, T. K. Gupta and W. D. Straub J. Appl. Phys. 63, 5375 (1988)
[30]A. Nityama, H. Sakaki, and T. Ikoma, Jpn. J. Appl. Phys. 19 L743 (1988)
[31]M. A. Alim, M. A. Seitz, and R. W. Hirthe, J. Appl. Phys. 63 2337 (1988) Also ref. [27]
[32]J. Frenkel, Phys. Rev (1931) 37, 17 1276
[33]R. Klucker, H. Nelkowski, Y. S. Park, M. Skibowski and T. S. Wagner, Phys. Stat. Solidi (b) 45 (1971)265.
[34]D. G. Thomas, J. Phys. Chem. Solids 15 (1960) 86
[35]K. Hummer, Phys. Stat. Solidi. (b) 56 (1973) 249.
[36]Y. S. Park, C. W. Litton, T. C. Collins and D. C. Renolds, Phys. Rev. 143 (1966) 512. Also ref. [34]
[37]W. Y. Liang and A. D. Yoffe, Phys. Rev Lett. 20 (1968) 59.
[39]Ref. [11] p.187
[40]M. D. Sturge , Phys. Rev. 127, 768 (1962)
[41]G. Yu, G. Wang, H. Ishikava, M. Umeno, T. Soga, T. Egawa, J. Watanabe
[42]T. Jimbo, Appl. Phys. Lett. 70 (24), 16, 1997.

## 3.5 Electrical properties of surface-textured ZnO films

Partially discussed in the previous section, the electrical properties of the surface textured ZnO will be further discussed in this section. The ZnO films with surface texture can not be used as such for solar cell applications when the conductivity is very poor. The resisitivity of the ZnO film that lead to ohmic contact should be less than 20 x $10^{-4}$ $\Omega$.cm. A resistivity of 4 x $10^{-4}$ $\Omega$.cm for the flat ZnO has been optimised by using Ar (chapter 1). However, the resistivity changes considerably when there is an addition of water vapour during sputtering.

*For the present studies, the sheet resistance was measured using four probe [13] and* Van der Pauw methods [14]. The thickness was measured using a stylus thickness measurement sytem manufatured by Tencor Instruments.

### 3.5.1 Results and Discussion

The resistivity of the ZnO films deposited at different partial pressures of water vapour are shown in figure 1. As is seen the resistivity increases with the addition of water vapour. This is expected, as there is water vapour in the plasma more oxygen is incorporated in the films. It was seen in the previous section on optical properties that the haze factor (surface texture) also increases with addition of water vapour. For solar cell applications, high electrical conductivity as well as high value of the haze factor and of the optical transmittance are necessary. The films with low conductivity values corresponding to samples W3 and W4 (see table I) can not be used in the solar cells without any further treatment.

The Zn has two valence 4s electrons which transfer to the oxygen 2p band. ZnO, if strictly stochiometric, has thus a filled valence 2p-band and an empty zinc 4s-band employing a gap energy of 3.3 eV. Stochiometric ZnO is therefore an insulator or a wide band-gap semiconductor. But when there is zinc in the interstitial position the valence electron of these Zn atoms are easily ionised (0.05 eV) and acts therefore as a donor. Nonstochiometric ZnO is an n-type semiconductor [15]. By introducing Al atoms, which have three valence electrons, (or other III group elements like B, Ga, In) in the Zn positions the conductivity is increased very much and they can be used for ohmic contacts. The number of electrons in the film has a direct impact on the absorption at the near infra red region (see chapter 1). The electron density in the film can be obtained from the plasma frequency [1] due to free carriers in the film [1, 5]. One considers thereby the free electrons in the semiconductor, i.e., in the ZnO to be governed by the same way as the electrons in an actual plasma. The charge carrier density is given by the relation [2, 3, 4]:

$$n = \frac{\varepsilon_0 \varepsilon_\infty m^* \omega_m^2}{e^2} \qquad \text{where } \lambda_m = \frac{2\pi c}{\omega_m}.$$

where $\varepsilon_\infty$ is the high frequency dielectric constant whose value is taken to be 4.5 [4] and $m^*$ is the effective mass and is taken to be $0.35m_e$. From the reflectance spectra $\lambda_m$, the wavelength at which the minimum in reflectance due to plasma resonance occurs, values are taken. The plasma wavelength can be obtained by using the relation $\lambda_p=1.13\lambda_m$ [4]. Table 1 shows the number of charge carriers at different experimental conditions. As the partial pressure of water vapour increases (W1, W2, W3) the number of charge carriers decreases. This is due to the incorporation of oxygen in the films [10]. As mentioned, the number of charge carriers for conduction can increase by mainly two ways; 1) increase in interstitial Zn (deviation from stochiometry) or deficiency in oxygen (deviation from stochiometry) and 2) effective doping. The deficiency in oxygen can be reduced if there is more oxygen in the film. The oxygen also occupies the grain boundaries [10]. These factors reduce the conductivity of the films considerably.

The mobility of the ZnO films (obtained using the values of conductivity and charge carrier density) can be affected by scattering mechanisms such as ionised impurity scattering and grain boundary scattering. Muller [7] as well as Noguchi and Sakata [8] interpreted their mobility data for sputtered and evaporated $In_2O_3$ films respectively in terms of scattering by ionised imperfections. For sprayed $SnO_2$ films Imai [11] concluded that the ionised impurity scattering is the dominant scattering mechanism. However, all these conclusions are questionable [5] as the computed and experimental values do not agree well. Shanthi et al. [5] have calculated the contribution due to ionised impurity scattering and optical lattice scattering and have found that the contribution of these two electron scattering mechanisms is very small. Further, the computed value of mobility due to ionised impurity scattering using the Brooks- Herring formula [6] is much higher than the measured values. Hence, the grain boundary scattering mechanism is considered to be dominant [12].

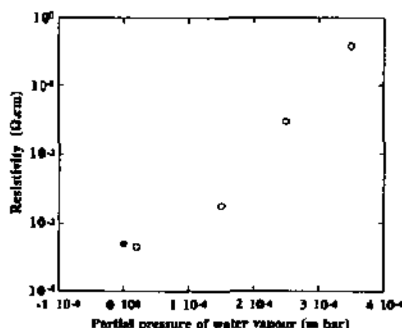


Figure 1. The variation of electrical conductivity of surface textured ZnO films in function of partial pressure of water vapour. The black circle is for flat ZnO grown without water vapour.

*Table 1 Electrical properties of surface texture ZnO films at different experimental conditions. The general conditions are; the working pressure is $2.5 \times 10^{-2}$ m bar. Ar 100 is grown without water vapour. From $W_1$ to $W_4$ the partial pressure of water vapour increases. The partial pressures of water vapour are; $W_1 = 1.5x\ 10^{-5}$m bar, $W_2 = 1.5x\ 10^{-4}$m bar, $W_3 = 2.5x\ 10^{-5}$ m bar and $W_4 = 4 \times 10^{-5}$ m bar. The RF power is 200W and the substrate temperature is 200°C. The film $P_2$ is grown at reduced RF power of 150W and $T_2$ is grown at reduced substrate temperature of 150°C. For $P_2$ and $T_2$ the partial pressure of water vapour is $1.5x\ 10^{-4}$ mbar.*

| Sample | Plasma wavelength (nm) | number of free electrons ($x10^{20}/cm^3$) | Resistivity ($x10^{-4}$ Ω.cm) | Mobility ($cm^2/V.s$) |
|---|---|---|---|---|
| Ar100 | 1923 | 4.7 | 4.94 | 26.6 |
| W1 | 1534 | 7.5 | 4.5 | 18.6 |
| W2 | 2074 | 4.1 | 17.6 | 8.7 |
| W3 | 2448 | 2.9 | 297 | .7 |
| W4 | high(above 2500) | low | 379 | low |
| P2 | 2110 | 3.9 | 19.4 | 8.2 |
| T2 | 1990 | 4.4 | 14.6 | 9.6 |

Obviously, it is preferred to have larger grain size to reduce the grain boundary scattering of electrons. The grain size decreases considerably when the partial pressure of water vapour is increased from the conditions corresponding to sample W2 to sample W3 (transition from columnar to granular morphology). Samples W1, W2 have a larger grain size than W3 and W4.

We take the partial pressure of water vapour corresponding to the film W3 and then we change the other deposition parameters like RF power and substrate temperature. As it is seen the conductivity of the samples grown at low substrate temperature (T2) and low RF power (P2) is high enough to be used in the device. The samples P2 and T2 grow with columnar morphology. The main difference between W3 and P2 or T2 are the kinetic energy for the film formation. We have studied that when there is *less amount of water dissociation* we have columnar growth. The columnar morphology of the samples grown at low RF power, and substrate temperature values suggests that the reduction in RF power or substrate temperature is mainly reducing the *dissociation of water in the plasma*. The reduced dissociation leads to enhanced columnar growth with high surface texture. This is seen in the high haze factor values of the samples grown with low RF power and substrate temperature values. The increase in number of charge carriers in these films shows the effective doping of Al atoms in the columnar structure. The corresponding grain sizes are very high while comparing with the samples grown at high RF power and high (200°C) substrate temperature values (at the same partial pressure of water vapour). Hence we contribute the increase in conductivity to the effective doping and increased grain size. The value of the as grown-resistivity is the lowest achieved so far for ZnO films grown in water plasma [9]. By this one can grow device quality ZnO films with surface texture as well as high electrical conductivity.

It should be noted that the reduction of substrate temperature or substrate temperature *with in the columnar morphology*, however, does reduce the grain size and growth rate following the usual growth mechanisms (see chapter 1).

### 3.5.2 Conclusions

The electrical properties of surface textured ZnO at different experimental conditions were discussed in this section. The addition of water vapour which increases the haze factor also increases the resisitivity. It is found that the effective doping, increase in grain size that lead to high electrical conductivity can be achieved by reducing the kinetic energy of the *species in the water plasma* during growth and thus by bringing them from granular morphology to the columnar morphology.

## References

[1] R. E. Hummel, Electronic properties of materials, Narosa Publishers, 1994. Also see chapter 1 of this thesis.
[2] Z. C. Jin, I. Hamberg and G. Granqvist Appl. Phys. Lett 51 (3), 1987,p 149.
[3] A. E. Delahoy and M. Cherny in Thinfilms for pholtovolataic and related Device Applications,edited by David ginley, Anthony Catalona Hans W. Shock, Chris Eberspacher, Terry M. Peterson and Takahiro Wada, MRS proceedings volume 426, p. 467-478.
[4] Y. Qu, T. A. Gessert, K. Ramanathan, R. G. Dhere, R. Noufi and T. J Coutts. J. Vac Sci. Technol. A 11(4). 1993, 996 -100.
[5] E. Shanthi, V. Dutta, A. Banerjee and K. L. Chopra J. Appl. phys., 51 (1980) 6243.
[6] H. Brooks, phys. Rev. 83 (1951) 879.
[7] H. K. Muller, Phys. Status solidi, 27 (1968), 723.
[8] S. Noguchi and H. Sakata, J. Phys. D, 13, (1980), 1129.
[9] T. Nakada, Y. Ohkubo and A.Kunioka, J. J. Appl. Phys, 30, 12A, 1991, pp 3344-3348.
[10]T. Nakada, Y. Ohkubo and A. Kunioka, proceedings of IEEE PVSEC, 1991, p1381.
[11]I. Imai, J. Phys.Soc.Jpn 15, (1960), 937.
[12]K. L.Chopra, S. Major and D. K. Pandya, Thin solid films, 102, (1983) 1-46.
[13]F. M. Smith, The Bell system technical journal, May 1958, p 711-718.
[14]L. J. Van der Pauw, Philips Research Reports, vol 13, no 1 feb 1950.
[15]Current Topics in Materials Science, edited by E. Kaldis, North-Holland, Vol. 7, pp 143-482.

# 3.6 Structural properties of surface textured ZnO films

In this section the structural properties of surface textured ZnO will be analysed in detail. The connection between the surface morphology and the structural properties, the effect of water vapour on the structural properties of ZnO will be studied and the main reasons to get columnar and granular morphology will be examined. These studies give more insights about the surface texture growth of ZnO and also of thin films in general.

X-ray powder diffraction was done on the ZnO thin films grown at different experimental conditions. The diffraction experiment was carried out using SCINTAG XDS 2000 instrument. Cu-$K_{\alpha}$ radiation with the wavelength 1.5406Å was used for this structural analysis by powder diffraction method. The interplanar distance, 'd', and the lattice parameter 'c', are calculated from the diffraction angles. The grain size is calculated by using the value of full width at half maximum of diffraction peaks. Mechanical properties were studied using a Nano Hardness Tester manufactured by CSEM instruments.

## 3.6.1 Results

The X-ray diffraction patterns (2θ versus intensity patterns) of the ZnO films grown at different partial pressures of water vapour are shown in figure 1(a), (b), (c) and (d). The total pressure for the deposition of these films was 5x $10^{-2}$ m bar. The RF power was 200W. The substrate temperature was 200°C. It is explained in the first chapter that the flat ZnO films has 'fiber texture growth' along [0002] orientation. This is the c-axis of the hexagonal crystal system and it is perpendicular to the substrate.

As is seen in figure 1(a) and (b) the ZnO grown with low partial pressure of water vapour show fiber texture growth. (The peak at 2θ = 72° is the second order diffraction of (0002) planes). As the partial pressure of water vapour is increased further, the fiber texture growth gets modified and there are additional orientations. The ZnO film grown at 2.5 x $10^{-4}$ mbar of waterpressure (figure 1(c)) has dominant [10$\bar{1}$3] orientation along with [0002] orientation.

Further at 4 x $10^{-4}$ mbar (figure 1(d)), the ZnO film has a dominant orientation of (10$\bar{1}$1) planes. The relative intensity of the diffraction peaks corresponding to (10$\bar{1}$1) is 100%. There are peaks corresponding to (10$\bar{1}$0), (10$\bar{1}$2), (11$\bar{2}$0) and (11$\bar{2}$2) planes other than the (0002) plane. Clearly, the addition of water vapour during growth has an impact on the orientation of ZnO films. The fiber texture growth gets modified into multiple orientations.

The comparison of the X-ray diffraction patterns with SEM and AFM pictures reveals that the *fiber texture ZnO thin films that were grown at low partial pressures of water vapour have columnar surface morphology*. (See SEM photo graphs in section 2.1). The ZnO films grown at *high partial pressure of water vapour have the granular morphology and they have multiple orientations* mainly along [11$\bar{2}$0], [10$\bar{1}$0] and [10$\bar{1}$1] directions.

The diffraction pattern for the ZnO films grown with only water vapour is shown in figure 2. The ZnO thin films grown at 100% water vapour (no Argon) have shown predominant orientation along [10$\bar{1}$0] direction. There are diffraction peaks for (11$\bar{2}$0) and (10$\bar{1}$0) planes. It is to be noted that there is no diffraction peak for (0002) plane.

The diffraction pattern of the samples grown at different RF power values are shown in figure 6. As is seen there is diffraction only due to (0002) planes. These films have columnar surface morphology (see SEM figures 2.b and 2.c in section 3.2). The diffraction pattern of the samples grown at different substrate temperature values are shown in figure 7. As is seen there is diffraction only due to (0002) planes. The corresponding surface morphologies of these films *basically* have columnar morphology (see SEM figures 3.a and 3.b in section 3.2). Within the

columnar morphology, an increase in RF power or an increase in substrate temperature increases the intensity of the diffraction peaks and the grain size.

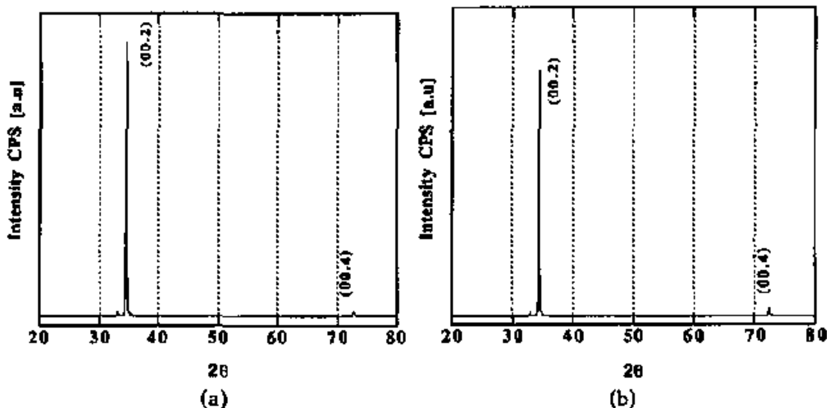


Figure 1 (a) and (b). The X-ray diffraction patterns for ZnO films grown at low partial pressures of water vapour. The partial pressures of the water vapour during growth were (a). $1.5 \times 10^{-5}$ m bar, (b) $1.5 \times 10^{-4}$ m bar, the total sputtering pressure was $2.5 \times 10^{-2}$ m bar, the RF power was 200 W, the substrate temperature was 200°C. The films exhibit fiber texture growth along the c-axis of the hexagonal wurtzite structure. The surfaces of these films are typical of films with columnar morphology.

The diffraction at $2\theta = 36°$ (peak for (0002) planes) for the samples at different partial pressure of water vapour including 100% water vapour shows that as the pressure increases the intensity for (0002) planes gets reduced and at 100% water vapour there is no diffraction from (0002) planes. The fiber texture orientation is completely modified with addition of water vapour during growth.

## 3.6.2 Discussion

### 3.6.2.1 The structure of ZnO

Basically ZnO has hexagonal wurtzite structure. The structure of ZnO is shown in figure 3. The positions of Zn and O are marked in the figure. The Zn and O are bonded by $sp^3$ hybridisation. The hybridisation occurs along the c-axis of the hexagonal crystal system. That means the Zn and O atoms are stacked with ABABA... sequence along the c-axis [21]. Here A and B are Zn and O respectively or vice versa. This makes the c-direction of the hexagonal crystal system close packed direction.

### 3.6.2.2 Surface free energy density per plane

There are some basic questions arising from the study: 1. Why does the fiber texture growth correspond to columnar surface morphology? 2. What is the meaning of granular morphology? 3. How were the other orientations selected? 4. How are the surface and structural properties connected? These questions lead to more insights of surface texture growth of ZnO films. Also these questions lead to the general explanations for the evolution of rough thin films.

To investigate further the structural properties, the surface free energy per plane for ZnO structure is considered. Zn has 2 valence electrons, i.e., 2 bonds per atom. The oxygen has 6 valence electrons. They have tetrahedral co-ordination with typical $sp^3$ covalent bonding along [0001] direction. The number of bonds varies in each crystallographic directions. Depending on the number of atoms in each plane, the density of surface energy per plane varies. The atoms in a

crystal always prefer to occupy a place of minimum energy. The calculation of surface energy density per plane for ZnO shows the planes with minimum surface energy. Figure 4.b shows three important planes of ZnO. They are (0001), $(11\bar{2}0)$ and $(10\bar{1}0)$ planes. These are the three minimum surface energy planes of ZnO. The (0001) plane has the lowest density of surface energy and it is followed by $(11\bar{2}0)$ and $(10\bar{1}0)$ respectively.

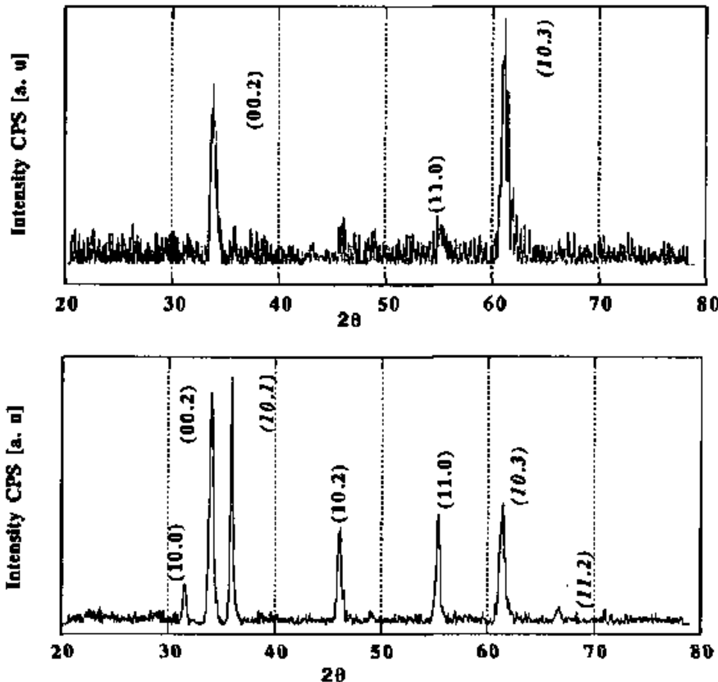


Figure 1 (c) (top) and (d) (bottom). The X-ray diffraction pattern for the ZnO films grown at high partial pressures of the water vapour. The partial pressures of the water vapour during growth were (c). $2.5 \times 10^{-5}$ m bar, (d) $4 \times 10^{-4}$ mbar, the total sputtering pressure was $2.5 \times 10^{-2}$ m bar, the RF power was 200 W, the substrate temperature was 200°C. During growth at high partial pressure of water vapour, the fiber texture was modified and there are peaks due to non equilibrium growth (see text). Figure 1(d) shows anomalous peaks due to $(10\bar{1}1)$, $(10\bar{1}3)$ and $(11\bar{2}2)$ planes.

During growth the adatoms always try to occupy the minimum energy lattice points. This means during growth of ZnO film *the adatoms will prefer to occupy the* (0001) *planes*. If the growth is disturbed *the second most energetically favoured plane is the* $(11\bar{2}0)$ plane *and the third plane is* $(10\bar{1}0)$. Hence if the adatoms have enough kinetic energy during the growth they always result in orientation along [0001] direction. We call this 'equilibrium growth of ZnO'. Figures 1(a) and 1(b) belong to the equilibrium growth of ZnO.

### 3.6.2.2 NON-EQUILIBRIUM GROWTH AT HIGH PARTIAL PRESSURE OF WATER VAPOUR

When the ZnO film can not grow along the [0001] direction, it prefers to grow along $[11\bar{2}0]$ or $[10\bar{1}0]$ directions. We call this 'non-equilibrium growth of ZnO'. The term 'non equilibrium' is due to the fact that the atoms could not select the minimum energy direction during growth. Such a non-equilibrium growth depends on the oxygen in the plasma, the RF power,

and the substrate temperature [2]. The ZnO films grown in non-equilibrium conditions show different behaviours w.r.t microscopic as well as macroscopic properties.

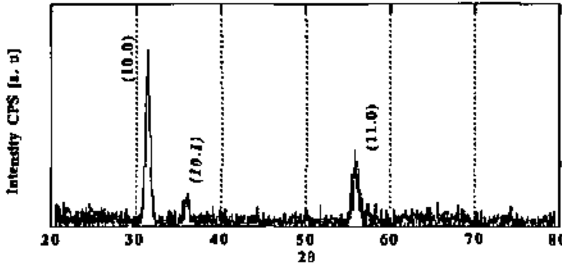


Figure 2. X-ray diffraction pattern for ZnO film grown with 100% water vapour. There is no diffraction for (00.2) planes. The (11.0) and (10.0) are the second and third minimum energy planes and the growth of these planes are due to the non equilibrium growth of ZnO due to increased oxygen in plasma during growth.

Figure 5 shows only the diffraction due to $(11\bar{2}0)$ plane at different partial pressures of water vapour. As the partial pressure of water vapour increases the intensity of this peak increases. This shows that the increase in partial pressure of water vapour enhances the non equilibrium growth [20] of ZnO along the second energetically favoured direction $[11\bar{2}0]$.

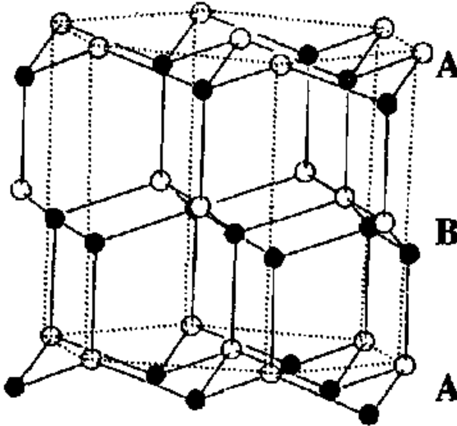


*Figure 3. The wurtzite structure of ZnO. The* position of Zn and O atoms are shown.(black and white spheres respectively or vice versa). The hexagonal unit cell is shown by dotted line. Zn and O are bonded by $sp^3$ hibridization along the c-axis as shown in the figure

3.6.2.4 Dissociation of water

The work of C. R. Aita et al. [1] and the work of N. Fujirama et al. [2] on *reactive* sputtering of *intrinsic* ZnO helps one to understand more about the $(11\bar{2}0)$ orientation of *intrinsic ZnO*. C. R. Aita has changed the ratio of oxygen to Ar during the reactive sputtering. When the ratio of pressures of oxygen to Ar is 1:3 he got highly pronounced preferred orientations along the $[000\bar{1}]$ direction. N. Fujimura showed that when the ratio of oxygen to Ar is 3:1 he could get the orientation of $(11\bar{2}0)$ planes. He explained that the growth along $[11\bar{2}0]$ direction changes with the variation in oxygen pressure by the change in*formation of tetrahedral bonding with Zn and O atoms in the vapour state as well as on the substrate.*

This means that the equilibrium growth is highly disturbed by the addition of oxygen. During the addition of water vapour, the oxygen is not added intentionally. But there is the growth of $(11\bar{2}0)$ and $(10\bar{1}0)$ planes that occurs mainly due to the oxygen during sputtering. This growth of $(11\bar{2}0)$ and $(10\bar{1}0)$ planes increases with the partial pressure of water vapour. Obviously this oxygen comes from water. During sputtering the water is dissociated in to ions

and molecules. Hence we have atoms, molecules and ions of O, H, OH, $H_2$, $O_2$ during the growth. The OH group that results from this dissociation plays an important role in the surface modifications and the oxygen atoms leads to the growth of $(11\bar{2}0)$ and $(10\bar{1}0)$ planes[2]. According to N. Fujimura, if the plasma has Zn and O atoms are tetrahedrally bonded *in plasma* before they make the growth, a [0001] orientation will result and if the Zn and O do not have bonding before they make the growth, a $[11\bar{2}0]$ orientation will result. The latter is highly probable when there is more oxygen in the plasma.

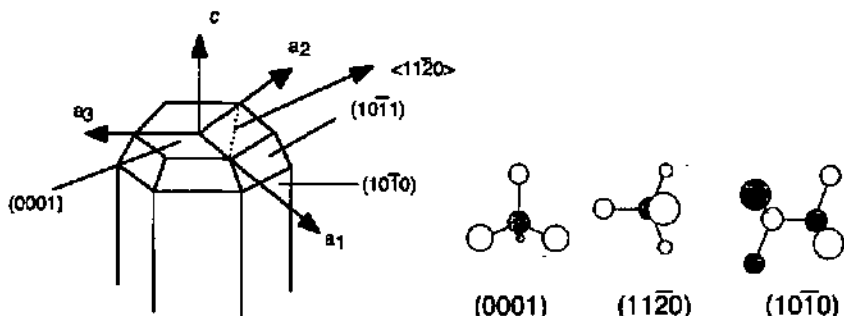


Figure 4(a) (left) and 4(b) (right). Main planes and their atomic arrangements of ZnO with hexagonal wurtzite structure. The black sphere corresponds to Zn atoms and the white spheres correspond to O atoms (see also the previous figure). The calculation of energy per plane based on the number of bonds in each plane shows that (0001) is the plane with the minimum surface energy density followed by $(11\bar{2}0)$ and $(10\bar{1}0)$ planes. In equilibirium growth conditions ZnO grows along [0001] directions

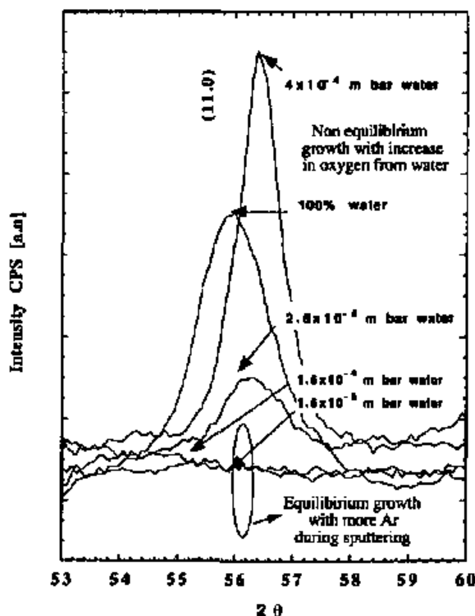


Figure 5. X-ray diffraction due to $(11\bar{2}0)$ planes of ZnO grown at different partial pressures of water vapour. The RF power was 200W. Substrate temperature was 200°C. Total sputtering pressure was 2.5 $\times 10^{-2}$ mbar. The increase in partial pressure of water vapour enhances the growth of these planes leading to non equilibrium growth of ZnO. The films grown at high partial pressure of water vapour have granular morphology. The films grown at low partial pressure of water vapour do not have $[11\bar{2}0]$ orientations and they have columnar surface morphology.

The bond strength of the diatomic molecule of H-O is 428 kJ mol⁻¹[19]. When the partial pressure of water vapour is low in the plasma, the energy spent in the plasma to dissociate the water is reduced while comparing with the energy spent in dissociating the water at high partial pressure. At low partial pressure of water vapour, there may be Zn-O bonds formed in the plasma since there is low amount of oxygen in the plasma. According to N. Fujimura [2], when there is low or no Zn-O bond formation in the plasma (during reactive sputtering) the growth will be along $[11\bar{2}0]$ direction. At low partial pressure of water vapour, there is no growth along $[11\bar{2}0]$ direction. This is, therefore due to the presence of bonding between Zn and O in the plasma. At high partial pressure of water vapour, the amount of oxygen in the plasma is high and hence there could be dissociated bondings between Zn and O atoms in the plasma. This results in orientation of the growing films along $[11\bar{2}0]$ direction. The oxygen atoms come from dissociated water molecules as well as from the target. Note that due to reduced amount of Ar, at high partial pressure of water vapour, the species in the plasma have reduced kinetic energy.

### 3.6.2.5 THE ANOMALOUS ORIENTATIONS ALONG $[10\bar{1}1]$ AND $[10\bar{1}3]$ DIRECTIONS

The origin of the peaks corresponding to the $(11\bar{2}0)$ and $(10\bar{1}0)$ planes can be successfully explained as described above. But the diffraction pattern of ZnO films grown at high partial pressure of water vapour do have other peaks like $(10\bar{1}1)$ and $(10\bar{1}3)$. In fact, the ZnO film grown at 3.5 $\times 10^{-3}$ mbar shows a diffraction peak for $(10\bar{1}1)$ relative intensity of 100%. Also the diffraction peak for $(10\bar{1}3)$ is more dominant than the non equilibrium $(11\bar{2}0)$ peak. The diffraction along $[10\bar{1}1]$ is not expected according to the calculation of surface energy density per plane [2] as explained above and the evolutionary selection theory. The preferred orientation along $[10\bar{1}1]$ is reported to be anomalous for ZnO film grown by ECR sputtering [3]. This is investigated further in the following section.

#### 3.6.2.5.1 THE CUBIC STRUCTURE OF ZnO

ZnO generally exists in hexagonal wurtzite structure. But there have been reports about cubic structure of ZnO. In 1969, cubic structure of ZnO was reported by Radczewski and R. F. Schicht[8]. In 1976, J. Nowak explained a transition of hexagonal ZnO to cubic ZnO [4] as well as double hexagonal close packing structure. Particles found in ZnO smoke (prepared by burning Zn metal) consists of four needle crystals united at a common juncture (fourlings). Fuller [5] found that the legs of the fourlings, elongated along the c-axis, are united by a twinning of $\{11\bar{2}2\}$ planes. Strunz and Meldau [6] postulated that the center of the fourfold tetrahedral twins of ZnO crystal should consist of the cubic ZnO. M. Shiojiri and C. Kaito [7] experimentally confirmed this. Hence, the existence cubic ZnO at the centre of the fourlings was confirmed. There are a few reports about the metastable cubic phase of ZnO. The ASTM card for ZnO has the information about cubic ZnO. But the interplanar distances, 'd' values, are referred from Radczewski work (1969) itself as there is not many reports about cubic ZnO.

#### 3.6.2.5.2 CUBIC STRUCTURE OF ZnO DURING SPUTTERING WITH WATER

The 'd' values corresponding to the diffraction pattern peaks of the ZnO films grown at high partial pressures of water vapour were compared to the 'd' values of hexagonal ZnO as well as cubic ZnO. In table I the comparison the 'd' values observed with the 'd' of the standard ZnO of hexagonal wurtzite structure and the 'd' values of cubic structure planes reported by Radczewski and R. F. Schicht [8] is given. It is seen that the 'd' values corresponding to $(10\bar{1}1)$, $(10\bar{1}3)$ and $(11\bar{2}2)$ planes are more closer to the values corresponding to the cubic structure of ZnO [18].

#### 3.6.2.5.3 VERIFICATION OF CUBIC STRUCTURE OF ZnO

The ratio of the reciprocal of the interplanar distance 'd' values of selected planes of a crystal system is an universal constant. The ratios of reciprocals of 'd' values of different planes have been calculated. The following ratio was calculated for those planes corresponding to cubic structure (from table I) and the planes corresponding to hexagonal structure (only for planes with l=0).

$$\frac{g_1}{g_2} = \frac{1/d_1}{1/d_2} \qquad (1)$$

The values were then compared with the constant values for hexagonal and cubic structures taken from crystallographic handbook [22].

The ratio, given in equation (1), for the planes $(11\bar{2}0)$ planes and $(10\bar{1}0)$ demonstrates that they belong to the hexagonal crystal. On the other hand, the ratio of (012) and (312) planes (for hexagonal they are $(10\bar{1}1)$ and $(10\bar{1}3)$ planes) corresponds to the simple cubic structure. Table II summarises the values for hexagonal as well as cubic structures. We conclude that there is a structural transition from hexagonal to cubic structure at high partial pressure of water vapour during sputtering. The main evidences are,

1. The fiber texture nature of ZnO: At high partial pressures of water vapour the sputtering at high power does not yield a fiber texture growth of ZnO. The diffraction peaks for the planes $(10\bar{1}1)$ and (1013) do not correspond to the minimum energy planes.

2. The 'd' value of ZnO: The 'd' value for the peaks correspond to the cubic structure of ZnO.

3. The $g_1/g_2$ value: This value is a universal constant for certain planes for the crystal systems. The values for the planes (103) and (112) correspond to the cubic structure.

Even though the $[10\bar{1}1]$ orientation is explained to be anomalous orientation [2,3,10], E. Bauer [9] gave explanations for peculiar textures in films of hexagonal crystal system in terms of the twin with the [0001]oriented crystals. However, the evolutionary selection theory strongly disagrees with the previous one.

*Table I Comparison of d values of ZnO grown at high partial pressure of water vapour with standard Hexagonal and Cubic structures*

| Planes for hexagonal structure | Corresponding planes for cubic structure [8] | d value observed | d value for Hexagonal STD from ASTM values | d value for Cubic STD (form reference 1) |
|---|---|---|---|---|
| (100) | | 2.833 | 2.814 | |
| (002) | | 2.633 | 2.603 | |
| (101) | (012) | 2.495 | 2.4759 | 2.50 |
| (102) | | 1.925 | 1.9111 | |
| (110) | | 1.630 | 1.6247 | |
| (103) | (312) | 1.486 | 1.4771 | 1.48 |
| (112) | (410) | 1.3820 | 1.3782 | 1.37 |

#### 3.6.2.5.4 Mixed cubic and hexagonal structures with Granular morphology

As is seen with high partial pressures of water vapour during growth, there are diffraction peaks for hexagonal structure as well as for cubic structure of ZnO films. These films have granular surface morphology. The films have grains of hexagonal ZnO as well as grains of cubic ZnO.

To summarise, the effect of water vapour on the structure of ZnO is mainly the following.

1. The non equilibrium growth of ZnO films that lead to other orientations than the fiber texture orientation.

2. There is a structural change from hexagonal to cubic structure so that the resulting films have mixed hexagonal as well as cubic grains.

*Table 11 Comparison of values of ratios of inverse of inter planar distances for cubic and hexagonal structures. The constant values for cubic and hexagonal structures are taken from hand book of crystallography.*

| $d_1/d_2$ values of | crystallo-graphic planes for equation (1) | values obtained from present study | constant from the crystallo-graphic table | corresponding value for the STD hexagonal structure of ZnO | corresponding value for Cubic structure from the Ref. 8 |
|---|---|---|---|---|---|
| Hexagonal | $d_{(200)}/d_{(110)}$ | 0.869 | 0.866 (Hex) | 0.866 | |
| Cubic(SC) | $d_{(012)}/d_{(312)}$ | 1.679 | 1.673 (Cubic) | | 1.6891 |
| Cubic(BCC) | $d_{(420)}/d_{(312)}$ | 0.839 | 0.837 (Cubic) | | 0.845 |

3.6.2.5.5 THE STRUCTURE OF ZNO GROWN WITH 100% WATER VAPOUR.

The ZnO films grown with 100% water vapour shows peaks corresponding to $(11\bar{2}0)$ and $(10\bar{1}0)$ planes. The peak for $(10\bar{1}0)$ plane is present with 100% relative intensity. The plane $(10\bar{1}0)$ is the plane with third lowest energy density plane for ZnO. The plane $(11\bar{2}0)$ is the second lowest energy plane. The film belongs to hexagonal structure and it is a demonstration for the non-equilibrium growth of ZnO.

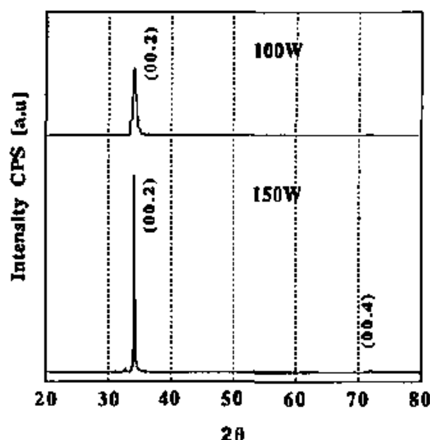


Figure 6. X-ray diffraction pattern of ZnO films grown at different RF power values. The partial pressure of water vapour was $2.5 \times 10^{-4}$ m bar. The substrate temperature was 200°C. The total working pressure was $2.5 \times 10^{-2}$ mbar. With these experimental conditions, at low RF power values (up to 150W) the ZnO grows with columnar morphology. It has fiber texture orientation as shown above. Further increase in RF power changes the morphology to granular morphology and the fiber texture orientation is modified as shown in figure 1(c). Those films show smaller grain size. Here, with in the columnar morphology the increase in RF power increases the grain size and growth rate following the usual growth mechanisms (refer chapter 2).

### 3.6.2.6 The Effect of RF power on the structure of ZnO:

It has been shown that the films with columnar surface morphologies that were grown at low partial pressure of water vapour have single orientation that corresponds to (0002) planes (fiber texture). On the other hand the granular morphology films show mixed hexagonal and cubic structures. The RF power also has resulted in columnar as well as granular morphologies. The X-ray diffraction pattern of ZnO samples with columnar morphology grown at different RF power values can be expected to have fiber texture orientation. Figure 6 shows the X-ray diffraction pattern of ZnO films grown at low RF power values. The partial pressure of water vapour was kept constant at 2.5 x 10 -4 mbar. The substrate temperature was kept at 200°C. As expected they show fiber texture growth at low RF power. At high RF power there is diffraction corresponding to $(10\bar{1}3)$ planes.

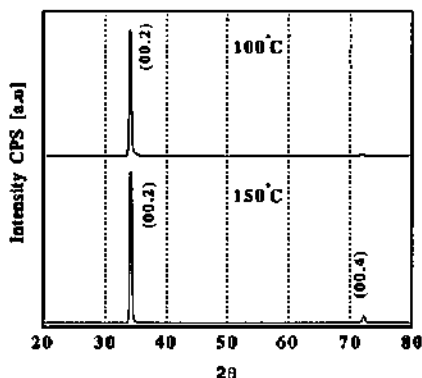


Figure 7. X-ray diffraction patterns of ZnO films grown at different substrate temperature values. The partial pressure of water vapour was 2.5x $10^{-4}$ mbar. The RF power was 200W. The total working pressure was 2.5 x$10^{-2}$ mbar. With these experimental conditions at substrate temperature values the ZnO grows with columnar morphology. They grow with fiber texture orientation as shown in this figure. Further increase in substrate temperature changes the morphology to granular morphology and the fiber texture orientation is modified as shown in figure 1(c). Those films show smaller grain size. Here, with in the columnar morphology the increase in substrate temperature increases the grain size following the usual growth mechanisms.

### 3.6.2.7 The effect of substrate temperature on the structure of ZnO

The substrate temperature mainly increases the surface mobility of adatoms and they lead to better crystallinity. At a RF power of 200W and at a fixed partial pressures of water vapour, the change in substrate temperature results in ZnO films that have the diffraction pattern as shown in figure 7. At low substrate temperatures the films have columnar surface morphology and the films have fiber texture growth along the c-axis. Further increase in substrate temperature lead to mixed orientations similar to the orientations obtained at increased RF power values in the power series.

### 3.6.2.8 Explanations of growth kinetics based on surface mobility of adatoms

The evolution of surface morphology in terms of surface mobility has been explained in section on atomic force microscopic studies (section 3.3). According to evolutionary selection theory of Van der Drift [10], the fastest growing plane will be the preferred orientation of a polycrystalline film. The fastest growing plane suppresses the growth of other planes. As is seen for ZnO, the fastest growing plane is (0001). This growth is supported when there is high surface mobility of adatoms. That is when the adatoms have the freedom to select the growing plane. When the surface mobility of adatoms is not enough to make selection for the minimum energy plane there will be multiple orientations.

As is seen the increase in water vapour during growth reduces the fiber texture growth. Further increase in water vapour gives rise to multiple orientations. *This explains that the adatoms have lost enough surface mobility to cause orientation of the fastest growing (0001) plane and this leads to multiple orientations*. Hence the addition of water vapour reduces the surface mobility of adatoms.

As the amount of high energetic Ar ions that reaches the target surface is reduced by the addition of water vapour (since the water pressure is increased with a constant total pressure),

The kinetic energy of Ar ions is lost in dissociating water molecules in the plasma. This reduces the kinetic energy of the adatoms sputtered from the target.

Thus, we can see that *the surface mobility of adatoms is higher during the growth of films with columnar morphology and is lower during the growth of films with granular* morphology . The columnar morphology has hexagons on the surface by the action of etching by energetic species (OH group molecules and ions). During the growth of granular morphology, the adatoms stick to the sites where they intercept the substrate, as they do not have enough surface mobility to form a flat surface.

The increase in RF power also gives rise to a change from columnar to granular morphology. How does the increase in RF power reduce the surface mobility? It is seen in the surface property analysis (section 3.2 and 3.3) that during the transition in surface morphology the change must be *in the plasma* as well as on the substrate. Now we can see that the increase in water pressure reduces the surface mobility. The increase in water vapour increases the dissociation of water vapour in the plasma. At a constant water pressure *the increase in RF power increases the dissociation of water vapour* . This leads to an increased scattering of adatoms in the plasma. As a result, when they reach the substrate they would have lost the kinetic energy so that the selection of minimum energy lattice sites of the film is not possible. Hence we have multiple orientations as well as granular morphology. Similarly with an increase in substrate temperature the dissociation of water vapour near the substrate is increased and this leads to evolution of granular morphology.

### 3.6.2.9 Columnar morphology

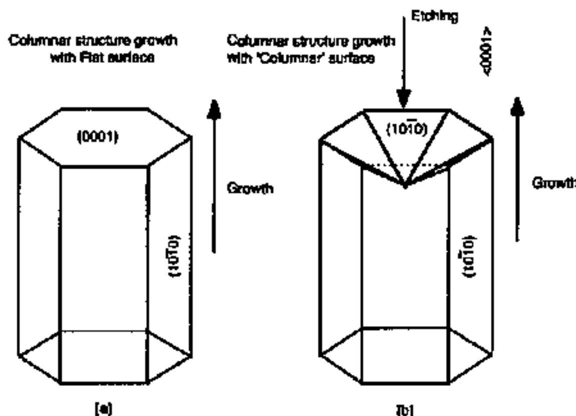


Figure 8. Unit cell of ZnO in columnar structure: [a] shows the unit cell of flat ZnO (grown with Ar alone). [b] is the unit cell of ZnO grown at low partial pressure of water vapour. The surface morphology is referred as 'columnar surface morphology'. The columnar surface morphology is the result of combined action of growth and etching along [0001] direction.

From the SEM analysis it is seen that the columnar morphology shows hexagons on the surface. Here, by the structural analysis it is seen that *all the columnar morphology films have fiber texture growth*. This growth is along the c-axis of the wurtzite structure of the hexagonal system. Hence, the hexagonal unit cells are standing normal with respect to the glass substrate. The water vapour during growth (the OH group) reacts with this surface and reveals the hexagons on the surface. G. Mattman et al. [23] have speculated, based on their IR studies on ZnO, that the OH groups are reactive on the basal planes of ZnO and that they are inert to other crystallographic directions. In the case of columnar surface morphology we observe that the

surface consists of hexagonal *pits*. This pits are due to etching on (0001) planes of ZnO and probably caused by the OH group that is dissociated from water vapour. This shows that *the growth is the combination of growth as well as etching*. Figure 8 shows the flat and textured surface with columnar *structure* [24]. It has been already seen that the AFM cross section picture consists of surface peaks with constant slopes (see figure 6 in section on AFM studies). Now it is understood that the constant angles are due to crystallographic facets as shown in figure 8.

### 3.6.2.10 Granular morphology

It is noted in the diffraction pattern of the samples of water vapour series that the [0002] orientation always exists in all the films. For the columnar morphology the [0002] orientation is the only orientation and the growth is explained to be accompanied by etching along the basal planes ((0001) planes). Hence as long as there are grains of [0002] orientation there could be surface roughness. On the other hand the surface mobility is reduced during growth with high partial pressures of water vapour. Hence the adatoms stick in the places where they are intercepting the substrate. As the surface has roughness due to the etching, this leads to surface peaks which hides certain sites of substrate from the exposure to the coming adatoms. Also the adatoms do not have sufficient kinetic energy to move on the substrate to make the surface of the film flat (to minimise the surface energy). This leads to surface roughness of granular morphology. This is the reason why the transition from columnar to granular surface morphology does not have a flat transition region. Due to this, it is observed in AFM analysis that the granular morphology is based on columnar morphology.

### 3.6.2.11 Grain size and interplanar distance

The (0002) diffraction peak can be used to estimate the crystallite size of the grains with[0002] orientation. The calculated values using the formula,

grain size = 0.94 .λ/B cosθ

where B if the full width at half maximum (FWHM) and θ is the diffraction angle, gives the values of grain size much lower than the one that is observed during SEM and AFM analysis. Similar observation has been made by Hu and Gorden for surface textured ZnO films by CVD. They observed that the grain size of the surface textured ZnO calculated was *much lower* than that of the values determined by scanning electron microscopy. The $CuK_\alpha$ radiation contains two lines of wavelength 1.54056 Å and 1.54439 Å with an intensity ratio 2:1 [11]. This will give two diffraction peaks separated by $\Delta 2\theta = 0.08°$ with an intensity ratio of 2:1. When the grain sizes are small this will appear as one peak [11]. Another factor that influences the broadening of the diffraction peak is the instrumental broadening and that can be determined by using a single crystal wafer diffraction peak. As these corrections are not made, in the present study, we can not get the true grain size values. However, the FWHM gives an indication of the

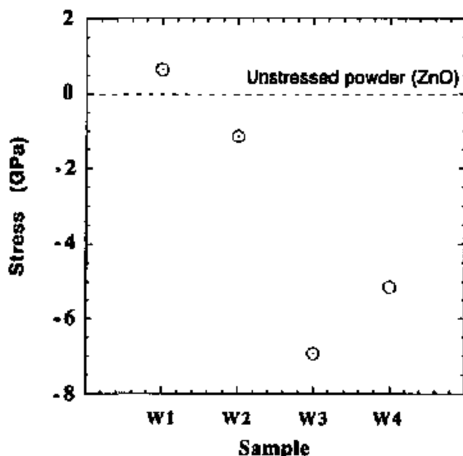


Figure 9. Intrinsic stress in ZnO films grown at different partial pressures of water vapour (see table IV). The negative sign shows that the film is in a state of elongation. The ZnO films grown at high partial pressures of water vapour have higher intrinsic stress in the film

grain size. *We see from the table IV that the grain size is relatively lower for ZnO with granular* morphology.

The interplanar distance, 'd' values are calculated from the diffraction angle and the X-ray wavelength by using Bragg's equation. The lattice constant 'c' of ZnO is the twice of the inter planar distance d of the basal planes (0002). Table III shows the lattice parameter, 'c' values of the ZnO films grown at different partial pressures of water vapour. The value for the standard ZnO is also shown in the figure. As is seen the 'c' values increase with increase in partial pressure of water vapour. The lattice constant can be used to evaluate average uniform strain, $e_{zz}$ in the lattice along the c axis[12] using the formula,

$$e_{zz} = \frac{c_0 - c}{c_0} \tag{2}$$

Where $c_0$ is the strain free lattice parameter measured from ZnO powder sample. The biaxial film stress is related to the measured c-axis strain by the modules of elasticity [13]

$$\sigma = [(2C_{13} - (C_{11} + C_{12}(C_{33}/C_{13})]e_{zz} \tag{3}$$

where $C_{ij}$ are elastic stiffness constants for ZnO. The compressive biaxial stress can be calculated by using the following values for $C_{ij}$ [14], $C_{11}$= 209.7 GPa, $C_{12}$= 121.1 GPa, $C_{33}$= 210.9 GPa, $C_{13}$= 105.1 GPa. The stress in the ZnO films grown at different partial pressures of water vapour is shown in figure 9. The negative stress indicates that the lattice constant c is elongated as compared to unstressed powder and therefore ***the films are in a state of elongation.*** It is seen that the stress in the films with columnar morphology is lower in comparison with the stress in the films with granular morphology. Table IV and table V show various parameters obtained for ZnO grown at different RF power values as well as different substrate temperature values. It is seen that the increase in RF power as well as increase in substrate temperature reduces the intrinsic stress in the material (within the columnar morphology). The stress in sputtered ZnO, in general cases, is reported to be mainly due to interstitial oxygen [15].

The stress in the sputtered ZnO film in the as grown condition is reported [15] to be tensile along the c-axis. Annealing of ZnO films [15,16] leads to strain relaxation. Both the groups [15, 16] reported that the increase in annealing temperature lead to reduction of tensile stress along c-axis. In other words, the increase in annealing temperature increases the activation energy and this lead to strain relaxation. Further increase (after 673K in ref. [16] and 773 K in ref. [15]) in temperature had lead to compressive stress along c direction due to the difference in thermal expansion of the film and substrates. In the present case, the as grown films show very low compressive stress that is closer to powder samples. The increase in water vapour leads to the development of intrinsic tensile stress. This indicates that the increase in water vapour reduces the kinetic energy of adatoms during growth and this leads to intrinsic stress in the film. This is in agreement with the annealing studies.

*Table III Structural properties of ZnO grown at different partial pressures of water vapour(the same samples shown in figure 1 (a) to (d)).*

| Sample | 2θ for (002) plane diffraction | Lattice constant 'c' (Å) | Stress (GPa) | Full Width at half maximum (°) | Morphology |
|---|---|---|---|---|---|
| W1 | 34.472 | 5.1993 | 0.63741 | 0.16600 | Columnar |
| W2 | 34.333 | 5.2197 | -1.1395 | 0.16000 | Columnar |
| W3 | 33.889 | 5.2861 | -6.9250 | 0.44120 | Granular |
| W4 | 34.025 | 5.2656 | -5.1368 | 0.39000 | Granular |
| STD powder ZnO(ASTM) | 34.43 | 5.2060 | 0 | -- | |

*Table IV Structural properties of ZnO grown at different RF power values*

| RF power | 2θ for (002) plane diffraction | Lattice constant 'c' (Å) | Stress (GPa) | Growth rate (Å/Sec) | Morphology |
|---|---|---|---|---|---|
| 100 | 34.00 | 5.2693 | -5.4641 | 1.5139 | Columnar |
| 150 | 34.166 | 5.2445 | -3.2998 | 2.6250 | Columnar |
| 200 | 33.889 | 5.2861 | -6.9250 | 1.0694 | Granular |

The density of the films can be calculated by using the following expression: density D = M/NV, where M is the total mass of unit cell of ZnO, N the Avogadro constant, V the volume of the unit cell of ZnO. As the value of the lattice parameter 'c' is known, the lattice parameter 'a' can be taken from standard powder samples (The error due to this is very small, ≈0.002g/cm$^3$) [16]. Hence, the density is inversely proportional to the value of the lattice parameter 'c'. As the value of 'c' (see table III) increases with addition of water vapour, the samples W2, W3, W4 show *reduction in film density due to the addition of water vapour during growth*. This is in accordance with our explanations in terms of surface mobility of adatoms during growth. This is a confirmation that the growth with high partial pressures of water vapour takes place with less surface mobility. Because the growth with less kinetic energy of adatoms will result in porus material with less density. This is also in accordance with the J. A. Throntons model of evolution of microstructure of thin films in which the films grown with less surface diffusion will have tapered crystals separated by open, voided boundaries (see section 3.3 on AFM studies ).

*Table V Structural properties of ZnO grown at different substrate temperature values*

| Substrate temperature (°C) | 2θ for (002) plane diffraction | Lattice constant 'c' (Å) | Stress (GPa) | Growth rate (Å/Sec) | Morphology |
|---|---|---|---|---|---|
| 100 | 34.083 | 5.2568 | -4.3754 | 4.3819 | Columnar |
| 150 | 34.222 | 5.2361 | -2.5718 | 3.9236 | Columnar |
| 200 | 33.889 | 5.2861 | -6.9250 | 1.0694 | Granular |

### 3.6.2.12 Mechanical properties

To investigate the mechanical properties of ZnO films we made experiments to study the elastic constants of surface textured ZnO. The measurements were done using Nano Hardness Tester manufactured by CSEM instruments. For each sample the measurements were done on many places of the film and the mean value was taken. Figure 10 shows the hardness and young's modulus of ZnO films grown at different partial pressures of water vapour. The values *in the figure can be taken only qualitatively as the instrument was not calibrated.* The bulk value of elastic constant is influenced by the change in lattice parameter. According to Zhenxing et al. [17] the bulk elastic constant along the c-axis is inversely proportional to the fourth power of the change in lattice parameter. Hence the elastic constants shown in figure 10 can be correlated with the intrinsic stress in the film (shown in figure 9). Furthermore when the columns are not perfectly aligned, the elastic constant vary. From the figure 10, it is noted that the films with columnar morphology grown at low partial pressure of water vapour show high hardness and young's modulus values compared with the values of the films grown at high partial pressure of water vapour. That is; mechanically the ZnO with columnar morphology is superior than the ZnO with granular morphology. This is in accordance with the variation of density of these films derived from X-ray measurements.

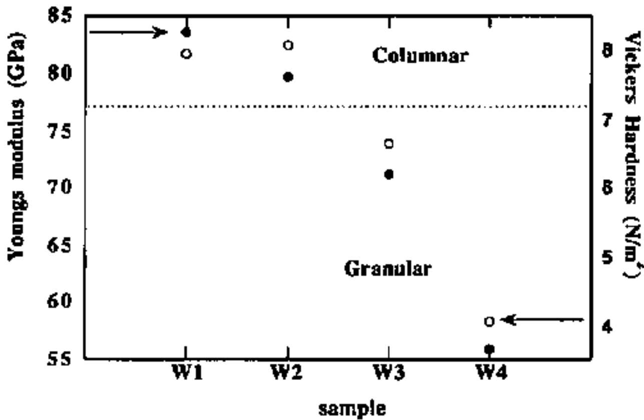


Figure 10. Mechanical properties of ZnO grown at different partial pressure of water vapour. Qualitatively, the hardness as well as young's modulus values of ZnO decreases due to the addition of water vapour during growth. This is in accordance with the stress measurements using X-ray diffraction data (figure 9). The films with granular morphology have low hardness and density values.

### 3.6.2.13 Growth rate

The growth rate of ZnO films grown at different experimental conditions are shown in figure 11. Ar 100 is the ZnO film grown without water vapour addition. W100 is the ZnO film grown without addition of Ar. For other samples the partial pressure of water vapour are; $w_1$=1.5 x $10^{-5}$ mbar, $w_2$=1.5 x $10^{-4}$ mbar, $w_3$=2.5 x $10^{-5}$ mbar and $w_4$=4 x$10^{-4}$ mbar. The total sputtering pressure was 2.5 x $10^{-2}$ m bar. The RF power was 200W and the substrate temperature was 200°C. The growth rate makes a clear distinction between columnar and granular morphologies. The growth rate has reduced from an average value of 4,5Å/sec for columnar films, to an average value of 2Å/sec. The reduction in growth rate can be due to the reduction of amount of Zn, O or ZnO species sputtered from the target due to the reduction in the kinetic energy of the ions during sputtering. Considerable part of the energy of Ar ions is spent in dissociating water vapour. This decreases the number of atoms and molecules sputtered from the target per ion (the sputter yield). This reduction of growth rate with an increase in partial pressure of water vapour is in accordance with the sub section on 'explanations with surface mobility' (3.6.2.8).

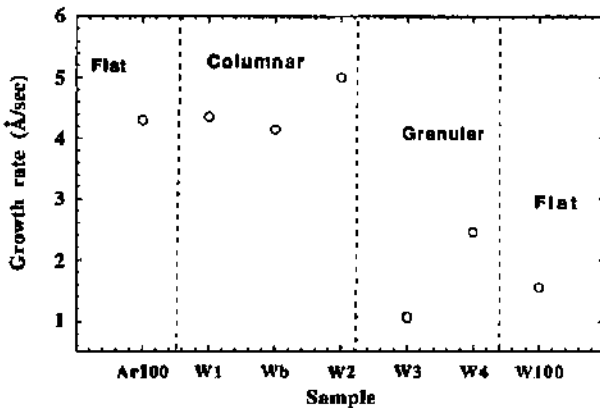


Figure 11 Growth rate of ZnO films grown at different partial pressures of water. (See table). W100 is the ZnO film grown with water vapour alone. The corresponding surface morphologies are also noted. The high growth rate of ZnO films at low partial pressure of water vapour reduces to low values at high partial pressures of water vapour. *The energy of ions for sputtering is highly reduced due to the addition of water vapour and this reduces the sputter yield.*

### 3.6.3 Conclusions

The structural properties of surface textured ZnO thin films are analysed in this section. It is found that the ZnO films grow with fiber texture orientation at low partial pressures of water vapour. The orientation gets highly modified at high partial pressures of water vapour. An anomalous orientation and the presence of cubic ZnO are explained. The growth at high partial pressure of water vapour gives rise to mixed cubic and hexagonal grains. The connection between the surface texture and structure is established. The columnar morphology and the surface hexagons correspond to the fiber texture growth. The mixed orientations correspond to granular morphology. When the amount of water vapour in the plasma is more the films grow with low surface mobility. The reasons to get different surface morphologies are explained in terms of surface mobility of adatoms during growth. The values of grain size, the inter planar distance, intrinsic stress in the films and the mechanical properties show that the high quality ZnO with surface texture has columnar morphology.

### References


[1] C. R. Aita, A. J. Purdes, R. J. Lad and P. D. Funkenbusch J. Appl. Phys. 51 (10), 1980, p. 5533.

[2] N. Fujimura, T. Nishihara, S. Goto, J. Xu and T. Ito J. Cryst. Growth 130 (1993) 269-279.

[3] Morito Matsuoka and Ken'ichi Ono, Appl. Phys. Lett. 53 (15), 10 October 1988.

[4] J. Nowak Kristall und Technik, 11, 9, 1976, 947-953.

[5] M. L. Fuller, J. Appl. Phys. (15) 1944, 164.

[6] H. Strunz and R. Meldau, Heidelb. Beitr.M in. Petr. 2 (1950) 216.

[7] M. Shiojiri and C. Kaito J. Crys. Growth 52 (1981) 173-177.

[8] O.E. Radczewski und R. F. Schicht Naturwissenschaften, 1969, p.514.

[9] E. Bauer, Trans. 9th Vac Symp. Am. Vac. Soc. (Los Angeles 1962), Macmill Comp. New York, 1962, pp. 35-44.

[10] A. van der DRIFT, Philips Res. Repts. 22, 1967, 267-288.

[11] D. R. Lide, Handbook of Chemistry and Physics, 71st Ed, (CRC, Boca Raton, FL, 1991) and
J. Hu, and Roy. G. Gorden J. Appl. Phys. 72 (11), 1, 1992, p5381.

[12] S. Maniv, W. D. Westwood, and E. Colombini, J.Vac. Sci. Technol. 20, 162 (1982).

[13] A. D. Sathe and E. S. Kim, The 7th International Conference on Solid State Sensors and Actuators , 1993 also
S. Maniv., W. D. Westwoed and E. Colombini, J. Vac. Sci. Technol. 17, 808 (1980) also
M. K. Puchert, P. Y. Timbrell, and R. N. Lamb, J. Vac. Sci. Technol. A 14 (4), 1996, 2220. See also reference [15].

[14] Numerical data and Functional relationships in Science and Technology, edited by K. H. Hellwege and A. M. Hellwege (Springer, Berlin, 1946). Vol. 2. p.58.

[15] C. J. Gowlak, and C. P. Aita, J.Vac sci. and Technol. A.1, 415, (1983) also
W.Hirshwald, P.Bonasewicz, L. M. Grade, D. Hofmann, S. Krebs, R. Littbarski, G. Neumann, M. Grunze, D. Kolb, and H. J. Schulz, Current topics in Materials science, edited by E. Kaldis, (North- Holland, Amsterdam, 1981), Vol 7.

[16] Vinay Gupta and Abhai Mansingh, 80 (2), 15, 1996, 1063.

[17] O. Zhenxing, Z. Xiaozhong, Z. Mingzhou, W. Xizhong, and L. Yujin, IEEE trans. Sonic and ultrason. SU-32, 630 (1985).

[18] J. A. Anna Selvan, H. Keppner, A. Shah in Thin Films for Photovoltaics and Related Device Applications, proceedings of MRS spring meeting, San Francisco 1996, Vol. 426 P.497.

[19] CRC Hand book of Chemistry and physics, CRC press, 59th edition, edited by R. C Weast, 1978-79 pages F215-246.

[20] J. A. Anna Selvan, H. Keppner, U.Kroll, J. Cuperus, T. Adatte, N. Randall and A. Shah in

'Polycrystalline Thin Films-Structure, Texture and their applications' ,Material Reasearch Society, spring 97 to be published.
[21] W. A. Deer, R. A. Howie and J. Zussman, An introduction to the rock forming minerals, Longman group limited, London sixth impression 1972.
[22] A. G. Jackson, Handbook of crystallography for electron microscopists and others, springer- verlog edition, ISBN 0387 973990.
[23] G. Mattman, H. R. Oswald and F. Schweizer Helvetica Chemica Acta 55, (1972), p.1249.
[24] J. A. Anna Selvan, H. Keppner, U. Kroll, J. Cuperus, T. Adatte, C. Ketterer and A. Shah. Helvetica Physica Acta 70 S9-S10

# 3.7 Optical Emission Studies during surface texture growth

Control and analysis of the growth by the sputtering (glow discharge) is possible by optical emission studies. By these studies one observes the emission lines of the excited species in the plasma. This allows one to get direct information about the growth of films. It is the target of this present study to correlate the appearance of the emission lines with macroscopical properties of ZnO. To analyse the surface texture growth of ZnO further, in this section, we present the plasma emission studies during the growth of surface textured ZnO using water vapour during sputtering.

## 3.7.1 Experimental

Figure 1 shows the schematic diagram of the experimental set up for the measurement of the plasma emission spectrum during the deposition of surface textured ZnO using water vapour and Ar mixtures. During the sputter growth of ZnO, the emitted light from the plasma is collected by a convex lens and focused on slit of a monochromator equipped with a photo detector at the exit. Using this set up emission spectrum for plasma is obtained in a X-Y recorder.

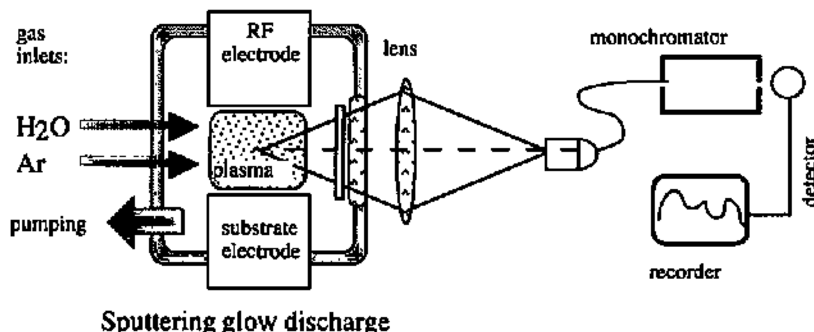


Figure 1. Experimental set up for measuring the plasma emission spectrum.

## 3.7.2 Results and Discussion

Figure 3(a) shows the emission spectra of the plasma during growth of ZnO film. The Ar pressure was $7.5 \times 10^{-3}$ m bar. The RF power was 200W. The substrate was kept at room temperature. With only Ar, under these experimental conditions, the ZnO film shows a smooth surface. In figure 3 the emission lines are identified as noted in the figure. With only Ar in the plasma, there are emission lines of Ar and Zn. These lines are due to electronic transitions of the atomic and molecular states of Ar and ZnO. The argon atom can make several atomic transitions as shown in figure 2. The transitions corresponding to the emission lines at wavelengths 416nm, 602nm, 696nm and 707nm can be seen from the figure. The intensity of Ar[416] is dominant in this spectrum. For Zn there are emission lines at 635nm and 481nm [1]. Water vapour is added in the plasma as a second step. The total pressure was kept constant at $5 \times 10^{-2}$ m bar for the whole series using mixture of Ar and water vapour. The RF power and substrate temperature are the same as mentioned before. Figure 3(b) to 3(h) show the emission spectrum of plasma with different partial pressures of water vapour. For figure 3(b) the partial pressure of water vapour was $2 \times 10^{-5}$ m bar. This small addition of water vapour increases the intensity of Zn emission lines both at 635nm and 481nm wavelengths. This means the slight addition of water vapour

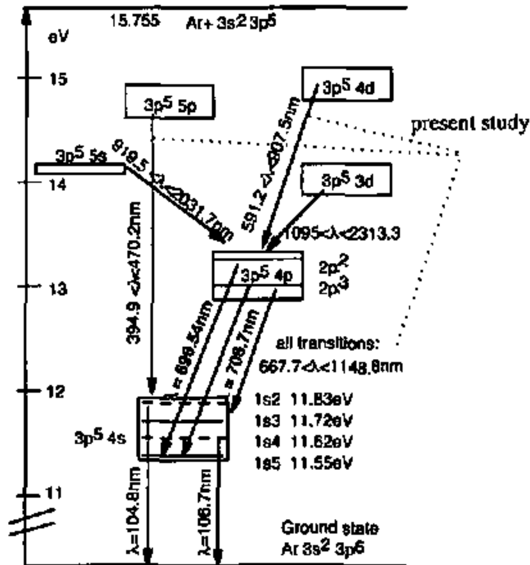


Figure 2. The schematic energy level diagram of the argon atom (after [2] and [3]). The possible transitions in energy states of Ar atom are shown. The transitions corresponding to the emission lines observed in the present study are noted.

increases the amount of atomic Zn in the plasma. Hence the deposition rate of ZnO with slight addition of water vapour can be expected to be more. In figure 11 of the section on structural properties (section 3.6), it is shown that the slight addition of water vapour does not decrease the deposition rate. The deposition rates of ZnO films grown with slight addition of water vapour are found to be equal or slightly more than the case for ZnO film growth with only Ar. With low partial pressures of water vapour, we get columnar surface morphology and the films grow with columnar structures.

With increasing partial pressure of water vapour the surface morphology turns to be granular. As is seen the increase in water vapour reduces the relative intensity (relative to Ar emission lines) of Zn emission lines. At the partial pressure of $1.5 \times 10^{-4}$ m bar the intensity of Zn and Ar emission lines are almost the same. Further increase in partial pressure of water vapour decreases the intensity of Zn emission lines. It is to be noted that at around this partial pressure values (around 1.5 x 10-4 m bar), the transition between columnar to granular morphology takes place. It is mentioned that as the total pressure is constant, an increase in partial pressure of water vapour means decrease in the partial pressure of Ar. This means that the increased addition of water vapour decreases the atomic Zn in the plasma (figure 4). First, the growth rate of ZnO may be reduced. As the amount of water vapour increases, the sputtering yield S, number of target atoms (or molecules) ejected per incident ion, decreases. Since the sputtering yield is directly proportional to the product of the masses of the colliding atoms, Ar, with relatively high atomic mass number, is more efficient in removing an atom or molecule by collision from the ZnO target. Hence increase in water vapour reduces the amount of Zn ejected from the target. Due to this, the growth rate of ZnO grown at high partial pressure of water vapour is expected to be low. Again we look at the variation of deposition rate of ZnO shown at different partial pressures of water vapour in figure 11 of section on structural properties (section 3.6). It is seen that the deposition rate of ZnO is considerably reduced at high partial pressures of water vapour. This is well in accordance with the emission spectra of the plasma.

Figure 3(b) shows the emission spectrum of plasma with almost water vapour alone. It is seen that the plasma, at room temperature, is mainly due to the slight addition of Ar. At high temperatures the plasma can sustain without Ar. The emission lines corresponding to O at 304nm, OH, H at 434 nm and O at 777 nm [1] could not be identified here due to the absorption of the emission lines by the window material of the chamber, due to dominant Ar emission lines at 400-470nm and due to dominant Ar emission lines in the infra red regions respectively. However, an emission line of $H_2O^+$ at 659nm is identified. At very high partial pressure of water vapour this line has considerable relative intensity and this decreases with decrease in partial

pressure of water vapour. The emission line of water vapour at 659nm is shown by down arrows in the figure 3 .

The decrease of the amount of water molecule in the plasma with decrease in partial pressure of water vapour can be attributed to the total reduction of water vapour in the plasma as well as increase in the dissociation of water vapour. The increase in dissociation of water vapour (for a given partial pressure of water vapour) at low partial pressure of water vapour in the plasma is due to the increase in energetic Ar ions. In the surface as well as structural property analysis (sections 3.2, 3.3 and 3.6) it was shown that the hexagonal pits on the surface of ZnO grown with low partial pressure of water vapour is mainly due to the etching action of dissociated OH molecules from water vapour. This is in agreement with the present diagnostic study of plasma at low partial pressure of water vapour.

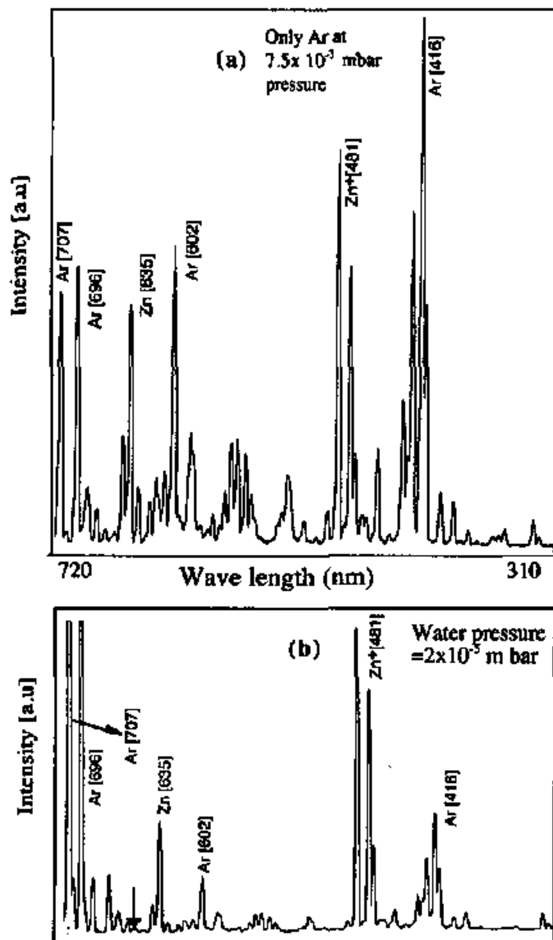

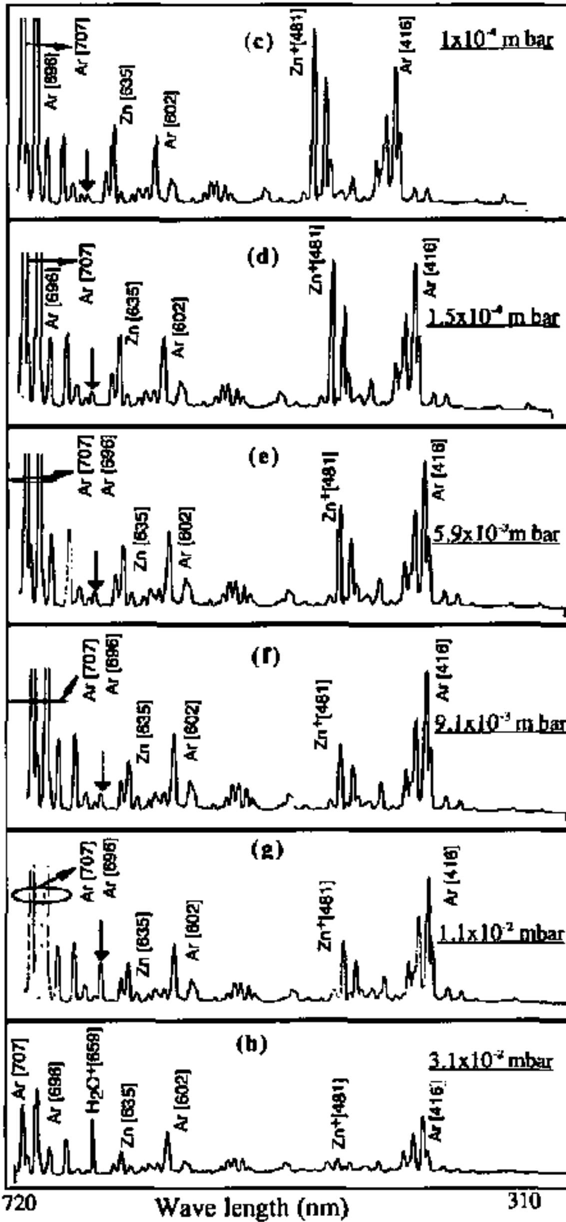


Figure 3 The emission spectra during sputtering with mixture of Ar and water vapour;
(a) pure Ar at a pressure of 7.5 x $10^{-3}$ m bar
and (b) to (h) increase in partial pressures of water vapour in the mixture of Ar and water vapour during surface texture growth of ZnO. The partial pressures of water vapour are as follows;
(b) 2 x $10^{-5}$ m bar,
(c) 1 x $10^{-4}$ m bar,
(d) 1.5 x $10^{-4}$ mbar,
*(e) 5.9 x $10^{-3}$ mbar,*
(f) 9.1 x $10^{-3}$ mbar,
(g) 1.1x $10^{-2}$ mbar and
(h) 3.1x $10^{-2}$ mbar.
The substrate was kept at room temperature and the RF power was 200W. The total pressure was 5 x $10^{-2}$ m bar. Only in case (h) the total pressure is 3.1 x$10^{-2}$ mbar and almost all the gas in the growth atmosphere is water vapour. The down-arrow shows emission line of water vapour

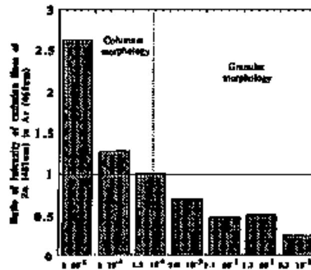


Figure 4. The ratio of intensities of emission tines of Zn at 481nm to emission lines of Ar at 416nm in function of partial pressure of water vapour. The corresponding regions of surface morphologies of ZnO are also noted.

It was mentioned that the sputtering yield S is more when the target atoms or molecules are collided with Ar ions. The continuous decrease in the amount of Zn in the plasma as well as Ar also suggests that the kinetic energy of the adatoms during growth continuously decreases with the addition of water vapour (high partial pressure regime). The sputtering yield at low ion energies is proportional to

$$S \propto \frac{4 m_i m_t}{(m_i + m_t)^2} \frac{E}{U_0} \qquad (1)$$

where $m_i$, $m_t$ are the masses of the incident ion and target atom respectively. $U_0$ is the surface binding energy of the material being sputtered and E is ion energy. According to this expression the amount of sputtered atoms increases with the increase in the ion energy. Hence the decrease in the amount of sputtered atoms shows the decrease in the ion energy. The kinetic energy of the neutral atoms ejected from the target depends on the energy of the incident ions. Hence the kinetic energy of the adatoms decreases with the decrease in the incident ion energy. *This ultimately decreases the surface mobility of adatoms during growth*. It was explained in previous sections that reduction in surface mobility correspond to the growth with granular surface morphology. In agreement with that the growth at high partial pressures of water vapour has granular surface morphology.

Plasma diagnostic analysis with different RF power values were also done. With a fixed partial pressure of water vapour at 2 x$10^{-4}$ m bar and with all other parameters the same, it was seen that the increase in RF power, the amount of Zn[635] and $Zn^+$[481] increases. This is accordant with the above explanations that the increase in amount of sputtered atoms implies the increase of ion energy.

On the other hand, it is seen that the amount of Zn is high when the partial pressures of water vapour in plasma is low. According to the equation (1), this shows the increase in ion energy at low partial pressures of water vapour. This, in turn, suggests an increased surface mobility of adatoms during growth. This is in agreement with our previous studies. It was shown in previous chapters that at low partial pressures the ZnO films have columnar surface morphology and this correspond to high surface mobility of adatoms during growth.

### 3.7.3 Conclusions

The plasma diagnostic analysis during surface texture growth of ZnO has given more insight about the surface texture growth of ZnO by sputtering. The two different regimes of columnar and granular growth can be identified by the emission spectra during growth. The deposition rate, surface morphological transitions and the growth mechanisms derived from the present study are in accordance with the studies described in the previous sections.

## References

[1] T. Nakada, Y. Ohkubo and A. Kunoko IEEE photovoltaic specialists conference 1991
[2] C. M. Ferreira and J. Loureiro J. Appl. Phys, 57(1), 1985
[3] H. Keppner, P. Torres, J. Meier, R. Platz, D. Fischer, U. Kroll, N. Beck, S. Dubail, J. A. Anna Selvan, N. Pellaton Vaucher, M. Goerlitzer, Y. Ziegler, R. Tscharner, Ch. Hof, M. Goetz, P. Pernet, N. Wyrsch, J. Vuille, J. Cuperus, A. Shah, J. Pohl, Proceedings of the MRS Symp., Fall Meeting, December 1996, Boston, 1997, Vol. 452, pp. 865-874.

# 3.8 Surface texturing of flat ZnO

## 3.8.1 Surface texturing of highly oriented ZnO

After studying the properties and growth mechanisms of surface textured ZnO, now we can analyse other methods to obtain surface texture of ZnO. For example, surface texturing of flat ZnO films grown in a 'standard manner', i.e. for example by sputtering using only Ar without the addition of water vapour; such a method will be highly useful due to its simplicity. In this section we will show the considerations to obtain surface texture of ZnO. With those considerations we will demonstrate the surface texture of ZnO obtained on the flat ZnO.

Let us recapitulate very shortly some general facts obtained for surface textured ZnO. There are two types of surface morphologies: columnar and granular morphologies. For the columnar morphology the ZnO grows with its hexagonal columns of grains perpendicular to the substrate (hence the name). For granular morphology there are grains with multiple orientations including the one with perpendicular columns. The columnar morphology results when there is high surface mobility during growth. The granular surface morphology is associated with low surface mobility during growth. The ZnO film with columnar surface morphology is superior in mechanical, and micro structural properties when compared with the ZnO with granular surface morphology. For use in device the surface textured ZnO with columnar morphology is more suitable one. The ways to arrive at columnar morphology were described in previous sections.

By sputtering it is seen that the flat ZnO grown with only Ar has fiber texture growth, that is, it displays hexagonal columns perpendicular to the substrate. *In mast of the cases*, the sputtering with only Ar lead to fiber texture growth. It is shown in the chapter on flat ZnO, (chapter 2) independent of the substrate temperature, RF power Ar pressure and position of the substrate, sputtering lead to the fiber texture growth of ZnO. This is a unique feature of ZnO grown by sputtering. This mainly happens due to the fact that the adatoms during sputtering (with Ar) have enough energy for the equilibrium growth and also there is no other disturbance for Zn and O bonding (that may happen by addition of oxygen)[1] *in plasma*. We want to use this fact for surface texturing of flat ZnO.

In the structural property analysis of surface textured ZnO, it was revealed that the growth with the mixture of water vapour and Ar is the combination of growth as well as *etching* along [0001] direction.

Hence if we etch a flat ZnO grown with fiber texture orientation it should reveal its hexagonal pits on the surface. The etching will be different from the usual etching of polycrystalline films as the ZnO has only one orientation and it will lead to surface nearly *similar to an anisotropically etched single crystal surface.*

With these considerations we made chemical etching of flat ZnO grown with orientation along[0001] direction. We used diluted $HNO_3$, diluted HCl as etchants to etch the flat ZnO. The SEM photograph of the surface morphology of a etched film is shown in figure 1. As expected the flat ZnO reveals the hexagonal pits on the surface. They are uniformly spread as if it is a surface of single crystalline wafer. Figure 2 shows the SEM photograph of the hexagon on the surface. This shows that the ZnO has [0001] as the growing direction. Anisotropic etching results due to the differences in the etch rates in different crystallographic planes. Here, etching along [0001] direction is faster than other crystallographic directions. Figure 3 shows the cross section of the surface hexagons. It shows the constant inclination angle of the surface peaks. This is the same as the surface facets obtained during surface texture growth (see AFM studies). It reveals along the intercepting crystallographic plane $(10\bar{1}1)$ as shown in figure 8 of previous section on structural properties (section 3.6).

The total transmittance and diffuse transmittance of the ZnO before the etching is shown in figure 2. The film was deposited at a pressure of $2 \times 10^{-2}$ m bar. The substrate was kept at

room temperature. The total and diffuse transmittance of the same films after chemical etching is shown in figure 3. We have seen that the surface textured ZnO shows superior diffuse transmission as well as total transmission. The diffuse transmission and hence the haze factor can be varied by changing the concentration of etchants or the duration of etching. The value of haze factor at 550nm for the post textured ZnO shown in figure 4(b) is 80.3% (means 80.3% of the incident light is diffused). The haze factor of the same films before post texturing (shown in figure 4(a)) is 1.6%. The increase is substantial. The comparison of the diffuse transmission with other surface textured TCOs by other methods shows the superiority of post textured ZnO.

The sheet resistance of the film before etching was 3.5 Ω per square. After etching, the surface textured films shows a resistance of 6 Ω per square. Thus the film remains highly conductive after the etching. The increase in sheet resistance is mainly due to the reduction in thickness of the etched films. The bulk resistivity remains almost the same. At high concentration of etchants or at high duration of etching time, the bulk resistivity slightly vary. However this value, still could be controlled to be less than $10 \times 10^{-4}$ Ω.cm. This value is very well suitable for obtaining ohmic contacts of ZnO.

Hence the post textured ZnO has superior electrical and optical properties. The post etching of fiber texture oriented ZnO thus becomes an highly useful way to obtain surface textured ZnO[2].

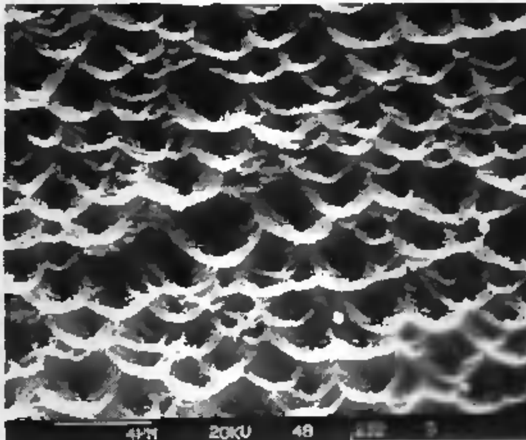


Figure 1 SEM photograph of surface morphology of ZnO film post textured using highly diluted $HNO_3$ The ZnO was grown at 200W at room temperature by using only Ar during sputtering. The total working pressure was $5 \times 10^{-3}$ m bar. The uniform surface morphology shows the fiber texture orientation of ZnO.

We observe two important facts

1. ZnO has fiber texture growth during sputtering. By this, *the polycrystalline film has only one orientation*. This is similar to a single crystalline wafer. The single crystalline wafers can very well be surface textured by etching. Today it is one of the efficient ways to make surface texturing for single crystalline solar cells[3,4]. However this can not be used for polycrystalline films due to the multiple orientation of them[5]. Here by the fiber texture growth it is possible to have texturing by etching so that the resulting surface morphology has uniform patterns representing the crystallographic fiber texture direction (one of the crystallographic axes).

2. The growth by sputtering: for fiber texture growth of ZnO it is efficient than any other available methods. Hence it gives an easy way to obtain highly efficient surface texturing. Further, mechanical properties of sputtered ZnO is superior than ZnO grown by other methods.

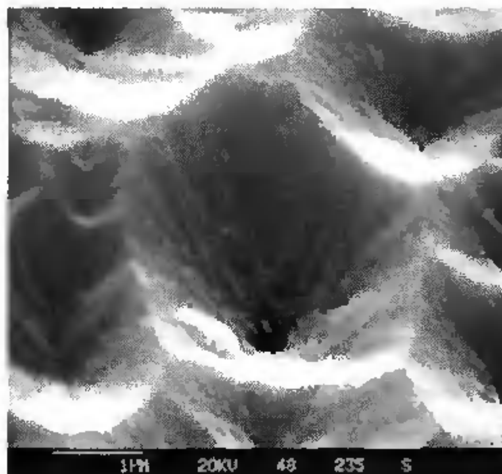


Figure 2 SEM photograph of surface hexagon of post textured ZnO film The ZnO was grown at 200W at room temperature by using Ar alone during sputtering. The total working pressure was $5 \times 10^{-3}$ mbar. The surface hexagons show that the orientation of ZnO is along c-axis of the hexagonal crystal system.

Figure 3(a) (left) The cross section of the surface hexagons of the post textured ZnO. The constant inclination angle of the surface peaks are the same as the angle for facets obtained during growth. This can be compared with the AFM cross section of ZnO with columnar surface morphology shown in section of 3.3 (figure 6) as well as figure 8 in the section on structural properties (section 3.6). Figure 3(b)(right) shows the cross section of the film etched very strongly. The material is etched until the substrate. The material just follows the crystallographic plane (0001) to be etched. Other part of the material remains unaffected. This shows the superior mechanical strength (resistivity to etchants and chemical stabilty) of ZnO grown by sputtering.

### 3.8.1.2 Comparison with the surface texture Growth:

During the external efforts to make surface texture growth like adding water, there is a reduction in electrical conductivity. The addition of water vapour has chances to increase the stress in the film, reduce the density and thus lead to poor mechanical properties (granular films).

However, it is explained in previous sections how to grow high quality surface textured ZnO. By growth, there is a need to go to higher thickness values to obtain the maximum surface roughness. By the post etching one can grow high quality films with good electrical properties and than can make the post etching. The resitivity does not change by the post etching. The haze factor can be easily controlled by changing the dilution of the etchants or by changing the etching time. Hence this gives good control over the haze factor. Therefore it is simple, efficient and meaningful way of surface texturing[6]. This method has high potential to be a standard process to make surface texturing.

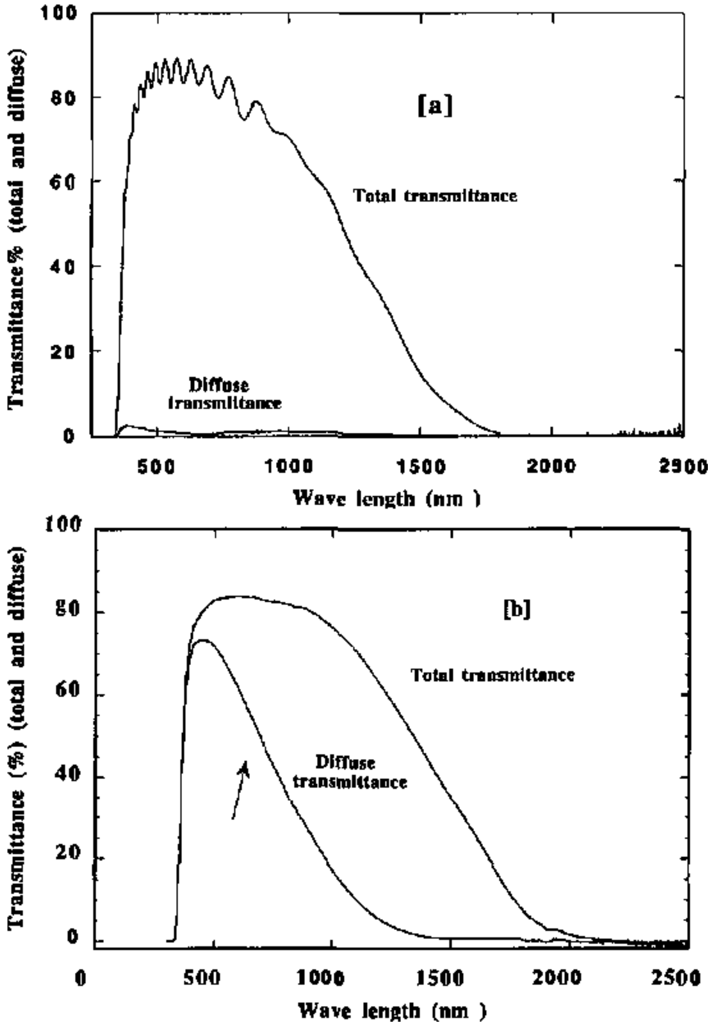


Figure 4(a) and 4(b). Total and diffuse transmittance of ZnO film before and after post chemical texturing. The increase in diffuse transmission is substantial.

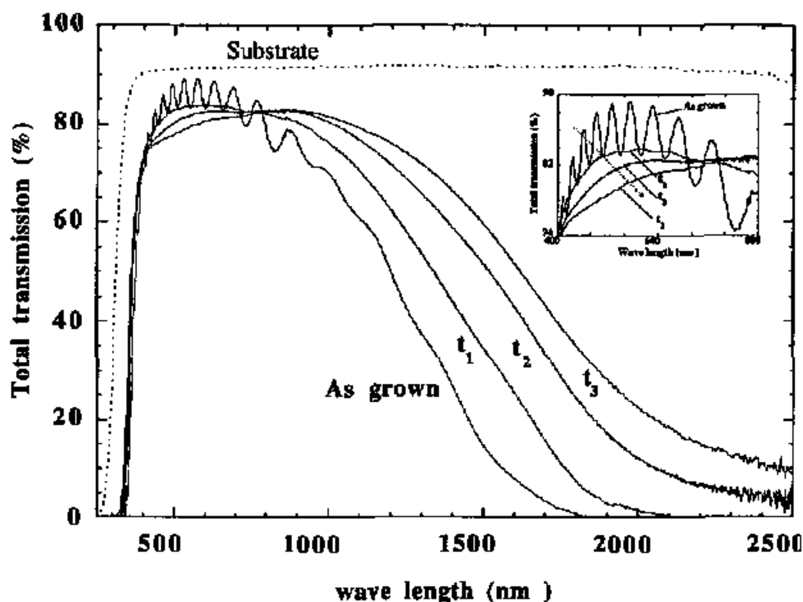


Figure 5(a). The total transmittance of ZnO at long duration of etching. The total transmittance of ZnO film after etching for different duration. $t_1<t_2<t_3$. As the duration of etching increases the thickness of the film is reduced. Hence the absorption due to free carriers shifts towards the long wave length side due to the reduction in number of charge carriers. This, in turn, reduces the sheet resistance.

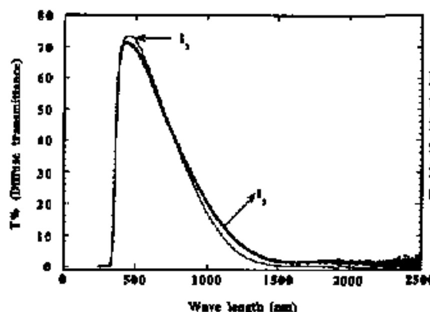


Figure 5.(b). The diffuse transmittance of ZnO film post textured at two different duration of etching time (same films shown in figure 5(a)). The reduction in diffuse transmittance due to the colour centres and the small increase in transmittance due to the change in the film thickness can be noted

As long as the post textured ZnO forms the substrate for the solar cells (on glass as window layers for PIN and as back reflectors on metallic substrates for NIP solar cells), the post texturing is highly useful way. On the other hand this method has practical problems to be used *on the device* ( ex. window layer for NIP structures, back reflectors for PIN solar cells). In this case a surface texture *growth* method is the only practical way.

However the disadvantage of post texturing is that there could be residual chemicals on the surface of the ZnO (same as on the surface of crystalline wafers). This could be overcome by the following ways.

1. Cleaning it efficiently. 2. Depositing another flat ZnO layer (this will just cover the surface while keeping the surface morphology unaffected).

#### 3.8.1.3 LIMIT FOR POST TEXTURE ETCHING

The maximum haze by etch texturing can be easily obtained without loss in transmittance. Once the maximum is reached, further etching does not increase the haze factor but slightly reduces the total transmittance (and hence the diffuse transmission) by the absorption at low wavelength region. For example, in figure 5(a), the curve $t_1$ is for the maximum haze obtained by etch texturing for the same ZnO film shown in figure 4(b). After this, further increase in duration of etching ($t_2$, $t_3$) does not increase the diffuse transmission. The total transmission shows that there is an increase in the total transmission at the long wavelength side. This is due to the reduced charge carriers in the film. The reduction in charge carriers is mainly due to the reduction in thickness of the film. On the other hand the total transmittance at low wavelength region (around 400-600nm) shows a reduction at increased duration of etching time. The absorption at this wavelength region is analysed in the section on optical properties of surface textured ZnO. The absorption corresponds to yellow colour formation in the film. The color centres are formed due to the formation of ionised oxygen vacancies ($F^+$ centre). Probably these point defects are formed only on the surface. For the use as surface textured ZnO, such a long duration is obviously not needed.

#### 3.8.1.4 COMPARISON WITH OTHER TEXTURING METHODS

For texturing polycrystalline films (or wafers) several attempts have been made. There are; laser scribing[7], plasma etching of patterns defined by using photolithography [8], and mechanical grooving[9]. Laser texturing is slow, expensive and incompatible with thin substrates. Mechanical grooving also appear to be incompatible with thin substrates[3]. Comparing with other methods wet chemical isotopic etching is reported to be a potentially low cost method of texture etching polycrystalline films[3]. For the chemical etching of polycrystalline films two methods can be applied.

1. Crystallographic anisotropic etching (efficient for single crystalline wafers).
2. Photolithographically nucleated wet chemical etching.

The first method can not be used for polycrystalline films due to their multiple orientations. Therefore the second method is followed usually.

In the present case due to the fiber texture orientation of ZnO films, we can use the first method. Thus it is further low cost method of surface texturing.

### 3.8.2 Etching by plasma

In the post chemical etching we have etched the material to reveal the surface hexagons. As is understood for sputtered ZnO, it is important to etch the surface of the [0001] oriented ZnO to have high quality surface textured ZnO. In this section we will analyse the other methods to bring the same effect. Even though the chemical etch texturing is a low cost highly efficient technique, a texturing method in the vacuum chamber can be useful for the on line fabrications. For example, an etching method using plasma can be useful for the on line fabrication of thin film solar cells.

During the growth of flat ZnO we change the RF power to see their effect on the surface of the flat ZnO. We have grown ZnO using only Ar at different values of RF power. The substrate temperature was 200°C. The total working pressure was $5 \times 10^{-3}$ m bar. The RF power was varied to different values from 75 W to 250W. Figure 6(a) to 6(c) show the SEM photograph of the surface morphology of ZnO films grown at different RF powers. As is seen the surface roughness increases with an increase in RF power values. The surface shows uniformly distributed hexagonal pits. The size of hexagons increases with increase in RF power. The surface roughness obtained with high RF power during growth (with only Ar), however, is

not sufficient to have increased diffuse transmission and haze factor. But this gives an indication that the RF power can be used for the purpose of post texturing.

(a)75W

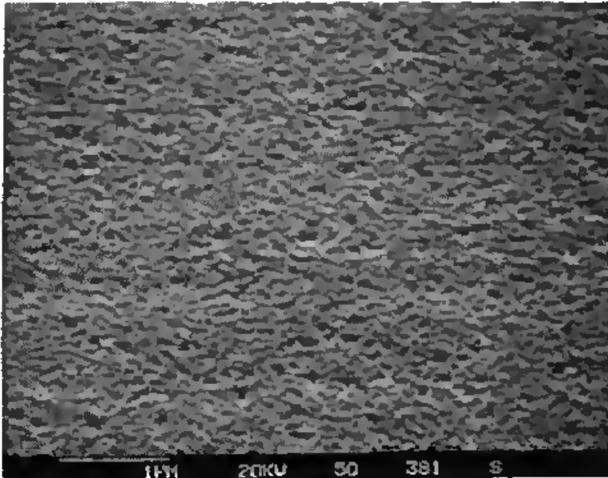


(b)100W

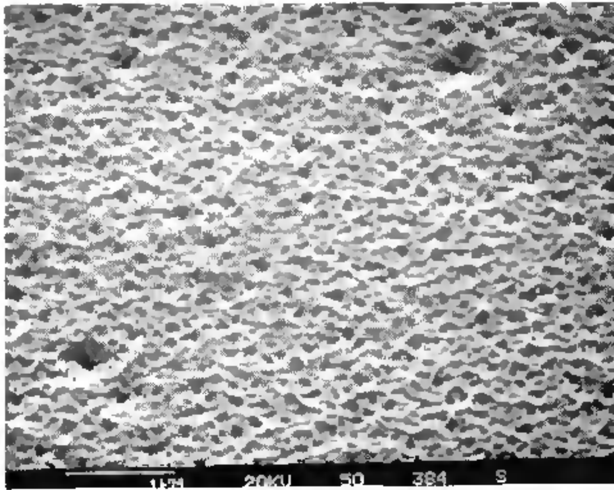


(c) 250W

Figure 6(a), (b) and (c).The SEM photograph of the surface of ZnO films grown by sputtering at different RF power values. All other deposition parameters were kept constant. The films were grown by using only Ar during sputtering. The working pressure was 5x $10^{-3}$ m bar. The substrate temperature was 200°C. The increase in RF power increases the *etching* of the growing film. The surface consists of hexagons. The morphology is uniform due to the fiber texture orientation of growing ZnO films. This suggests that the plasma power can be used to obtain surface texture by post treatments.

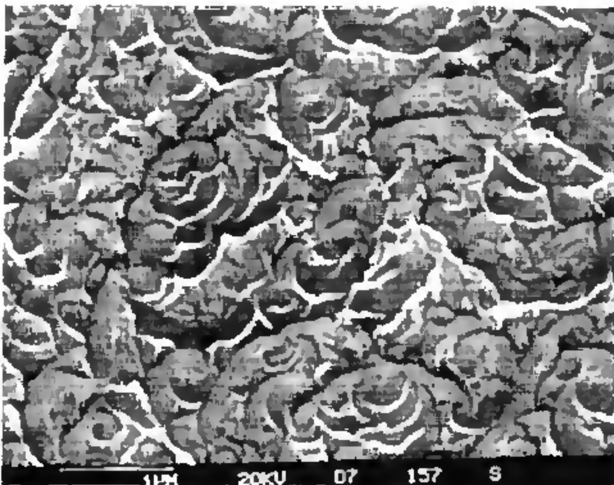


Figure 7. SEM photograph of the surface of the ZnO film *etched by Ar plasma*. The material was grown using mixture of Ar and water vapour. The plasma power was 200W. The Ar plasma did not make, in this case anisotropic etching. The surface roughness is not sufficient to increase the diffuse transmittance considerably.

A post plasma etching can increase the surface texturing efficiently, as there is only etching rather than etching along with growth. We made some preliminary experiments on the post plasma etching. Milky ZnO surface was obtained during the etching of flat ZnO by using Ar, oxygen mixtures. Still this is not as efficient as the growth using water vapour or post chemical texturing.

During growth with water vapour, when the total working pressure was low, in other words, when the ratio of water vapour to Ar in the plasma is high it gives rise to flat surface morphology. (similar to that of '100% water vapour during growth') Such a flat film shows poor crystallinity. The plasma etching of these film using only Ar do not show surface hexagons but a surface morphology shown in figure 7.

We observed that during surface textured growth using water vapour the OH group is highly responsible for the growth of surface textured ZnO (see the structural properties). During the addition of water vapour the OH group comes from the dissociated water vapour. Hence *a plasma etching using water vapour rather than Argon or oxygen could give an efficient surface texturing*. This can be examined by the future investigators.

### 3.8.3 Microstructure evolution of ZnO thin film

Up to now, we have studiad the growth mechanisms of ZnO films under different experimental conditions. Basad on this we proposed some methods to texture the surface of sputtered ZnO. Using all these information together we introduce our model of evolution of surface morphology and microstructure. This model describes the surface and microstructure evolution of ZnO which is grown by sputtering in an atmosphere where the species in the plasma react with the film.

Figure 8 shows the schematic diagram of the evolution of surface morphology of ZnO in the atmosphere of water vapour. In one axis the amount of water vapour during sputtering is increased from $W_1$ to $W_{100}$ keeping the total pressure the same. As the total working pressure is fixed this means the increase of water vapour to Ar ratio in plasma. It is important to note that the total pressure is below $2.5 \times 10^{-2}$ m bar. Because at increased Ar pressure, with out any additional efforts the growth would be of low surface mobility. In the other scale, the RF power increases from $P_1$ to $P_4$.

There are different zones indicated in the figure 8. They are explained as follows.

Zone 1: In this zone the RF power is low. There is no water vapour in the plasma. The film has a smooth or flat surface morphology. The film grows with its c-axis perpendicular to the substrate. The adatoms in this region have enough surface mobility to form flat surface so that the surface free energy of the film is reduced. It is a columnar growth with flat surface.

From zone 1, any addition water vapour does not increase the surface roughness. The deposition rate is highly reduced. The film shows poor crystallinity. The orientation of the films changes from fiber texture to multiple orientations. At high partial pressures of water vapour, the film has low density and high intrinsic stress.

Zone 2: At an increased RF power a small addition of water vapour reveals the surface hexagons by the etching action of dissociated water species. In this region the adatoms have high surface mobility. without any water vapour in the plasma the film will try to have a smooth surface. However, even when there is no water vapour there will be an etching due to the Ar ions (figure 6(c)). Hence the surface is textured to a small extent. However this is small while comparing with zone 2. When there is etching due to dissociated water, it is no more physical etching as is the case when there is only Ar. With the addition of water vapour there is reactive etching and the growth is combined with etching. The growth is columnar along the c-axis of the hexagonal system. The film has rough surface with hexagonal pits on it. The surface morphology is called 'columnar morphology'. There is not a considerable change in the deposition rate due to the addition of water vapour. The film has good mechanical properties. Further addition of water

vapour increases surface roughness due to the increased action of etching by dissociated species of water vapour.

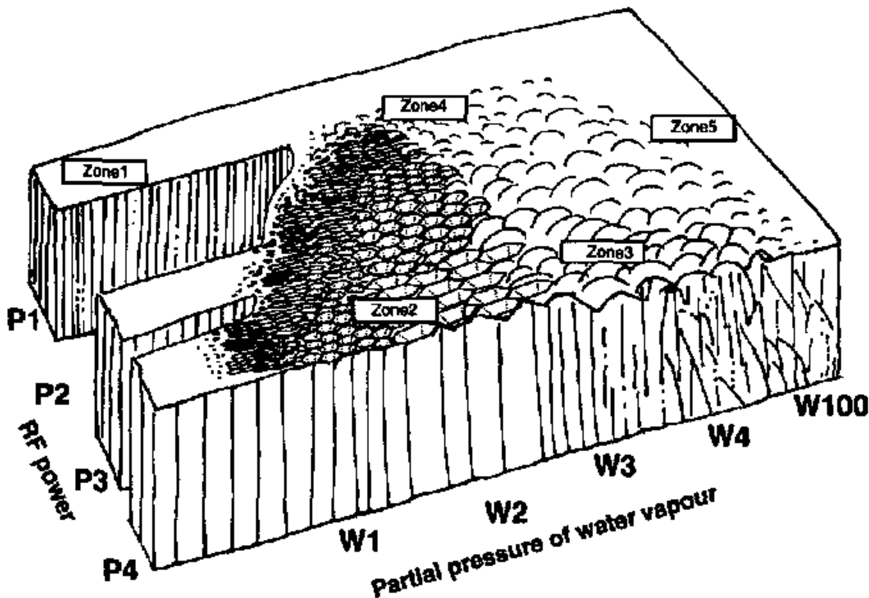


Figure 8. Evolution of surface morphology and microstructure of ZnO by sputtering.

W100 is the ZnO film grown without addition of Ar. (The partial pressure of water vapour, in the mixture of Ar and water vapour increase from $W_1$ to$W_4$; $W_1$=1.5 x $10^{-5}$ mbar, $w_2$=1.5 x $10^{-4}$ mbar, $w_3$=2.5 x $10^{-5}$ mbar and $w_4$=4 x$10^{-4}$ mbar. The total sputtering pressure was 2.5 x $10^{-2}$ m bar. The substrate temperature was 200°C)

<u>*Zone 3*</u> : From Zone 2 increase of water vapour at increased power lead to a transition of surface morphology. At high partial pressure of water vapour, not all the water vapour is dissociated. Most of the power is lost in dissociating the water vapour. The growth takes place with low surface mobility. The action of etching by dissociated water simultaneously takes place along the polar planes of ZnO. On the other hand, the adatoms at the substrate do not have enough surface mobility. Hence the adatoms just stick at sites of the substrate where they intercept. At this zone the films have a surface morphology called 'granular morphology'. The films may not have the minimum energy planes corresponding to the growing direction. The films have multiple orientations. At high partial pressures of water vapour the film has high intrinsic stress in the film and low density. The growth rate reduces considerably.

As is explained, the granular morphology results due to the etching and low surface mobility growth. At low partial pressures of water vapour in the plasma during growth (Zone 2) there is etching but the surface mobility is relatively high. As the action of reactive etching continues in both the morphologies, the transition is continuous. That means *there is no smooth transitional zone when the surface mobility changes from high to low values*. In usual conditions, according to the standard zone model of J. A. Thronton[10] (see section 3.3), the change in surface mobility will give rise to a transition zone in which the film has smooth surface.

<u>*Zone 4:*</u> In the atmosphere of water vapour, any reduction in RF power reduces the surface roughness. This is due to the reduction of dissociation of water vapour. Of course the surface mobility during growth also reduces with the reduction in the RF power. Hence at low

power values the granular and columnar morphologies mix together and the surface has a granular morphology. However this surface roughness is small. The orientation of the film follows the same trend as the growth at the high power values. It changes from c-axis oriented columns to mixed orientations as the partial pressure of water vapour during growth increases.

*Zone 5:* This zone describes the growth at extremely high partial pressures or 100% of water vapour during sputtering. The film has smooth surface. The growth takes with low surface mobility. Obviously very few amount of water vapour is dissociated. The growth is due to the ions that are dissociated from water vapour as there is no Ar or very few Ar in the plasma. But the etching is highly reduced. Hence the adatoms could make a smooth surface.

At very high partial pressures of water vapour, the reduction in RF power increases the range of the flat zone as shown in the diagram. Because the reduction of power further reduces the dissociation of water vapour. As we can expect, the growth rate is considerably low in this region. The film has multiple orientations. The mechanical properties of the films are inferior to the films with columnar morphology.

From zone 1 an increase in RF power increases the *grain size*. The films at zone 1 as well as the following flat regions (only with Argon) have flat surface with device quality microstructural properties. The ZnO films in these region beve fiber texture growth and they can be easily post textured. ***This gives a great controll over the optical scattering properties of the films.*** That is, the size of the grains and surface hexagons can be easily tailored during the growth and depending on the size, the wave length dependence of diffuse transmittance or reflectance can be changed.

#### 3.8.3.1 EVOLUTION OF SURFACE ROUGHNESS AT THE ATMOSPHERE OF ANISOTROPICALLY REACTING MEDIUM DURING SPUTTERING IN GENERAL

Even though the model we described is particularly for ZnO by sputtering based on our experimental results, some general trends can be followed for the growth of all thin films by the method of sputtering in similar condition. The similar conditions are as follows; the process is not physical vapour deposition. As we introduce water vapour in the present case, the process becomes reactive sputtering. The dissociated water species, namely *OH group reacts anisotropically* with the growing film. ***When the dissociated species react on the growing film, this model can be followed and explanations for the evolution of microstructure can be given in terms of surface mobility.***

Also it should be noted that when the total working pressure is too high there will be reduction of surface mobility and this will lead to the growth of surface with morphology similar to granular morphology, even at the absence of reactive species in the plasma. In the above model the total working pressure is sufficient to make smooth surface.

## 3.8.4 Conclusions

In this section the surface texturing mechanisms have been analysed in detail. A simple, highly efficient technique has evolved as a result for the fabrication of surface texture of ZnO films grown by sputtering. By chemically etching the fiber texture oriented ZnO grown by sputtering, we have highly pronounced surface texturing without much loss in electrical properties. This gives a good freedom for the growth of ZnO films that can be post surface textured. Other ways of surface texturing have been analysed. Anisotropic plasma etching has been suggested. Based on the experimental results, a model for the evolution of surface morphology and the microstructure has been presented. These results are important for the efficient fabrication of surface textured ZnO films for thin film solar cells.

## References


[1] N. Fujimura, T. Nishihara, S. Goto, J. Xu and T. Ito J. Cryst. Growth 130 (1993) 269-279.
[2] J. A. Anna Selvan , Progress Report III, IMT internal reports dated 23rd december. 1995.
[3] S. R. Chitre, 13th IEEE photovoltaic specialists conference, Washington, D. C., 1978,pp943-947.
[4] For example, J. A. Anna Selvan, Development of Back Surface Field Silicon Solar Cells, M.Tech thesis, 1993, Indian Institute of Technology, Madras.
[5] M. J. Stocks, A. J. Carr, A.W Blakers, Sol. Energy materials and Sol. Cells 40, (1996) 33-42.
[6] *Claus Beneking, Anto Löffl, Stephan Wieder, Bernd Rech, Oliver Kluth, Wolfgang Appenzeller Forschungszentrum , IFKA, Julich and J A. Anna Selvan, H. Keppner Institute of Microtechnique, University of Neuchâtel, Patent number PT 1.1453.*
[7] S. Narayanan, S. R. Wenham and M. A. Green, 4th Photovoltaic Solar Energy Conf., Sydney, January 1989, p111.
[8] U. Kaiser, M. Kaiser and R. Schindler, Proc. 10th EC photovoltaic Solar Energy Conf. (Kluwer, Lisbon, 1991) pp. 480-483.
[9] G. Willeke, H. Nussbaumer, H. Bender and E. Baucher, Proc. 11th EC photovoltaic Solar Energy Conf. (Kluwer, Montreux, 1992) pp.480-483.
[10] J. A. Thronton, J. Vac. Sci.Tech, 11 (1974), 666.
J. A. Thronton, Ann. Rev. Mater.Sci, 7 :239 (1977).

# 3.9 Development of surface-textured ZnO/Ag/metal systems as back reflectors for solar cells

Surface texturing of ZnO plays an important role in thin film solar cells. Surface-textured ZnO can be advantageous in many ways for thin film solar cells, as was explained in section 3.1. Surface-textured ZnO can be used in the cell either as a front contact (window) or as a back contact (back reflector). In P/I/N solar cell structures, a glass/TCO system will be used as substrate. In the inverted structure, i.e., in N/I/P solar cell structures, a substrate other than a glass substrate, for example, a metal or a flexible polymer, can be used. In the present case, we study surface texture growth of ZnO on stainless steel covered by a silver film. The surface-textured ZnO/Ag/ stainless steel system will be analysed in this section for its future incorporation in N/I/P solar cells as described in chapter 4.

## 3.9.1 Experiment

Clean stainless steel sheets of of size 4cm x 4cm were used as substrates. The thickness of the stainless steel substrate was 250μm. For silver deposition, RF sputtering method was used with a silver target. The electrode separation was 4 cm. The silver deposition was done without any substrate heating. The RF power was 40W. The sputtering pressure was $5 \times 10^{-3}$ m bar. The thickness of the silver deposited for all the samples in this study was kept constant at 3200 Å. When the thickness of the silver on stainless substrate was further increased, the change on the reflection was, infact, observed to be negligible.

Surface-textured ZnO was deposited on stainless steel substrates where silver had been previously deposited. Surface texture growth of ZnO was the same as explained in previous sections. The only difference is that the substrate is changed from glass to Ag/stainless steel. Three different series of depositions were carried out. They are the water vapour series, the RF power series and the substrate temperature series. A fourth series was done to change the thickness of ZnO. It was difficult to measure the thickness of ZnO on the stainless steel substrate. Hence, the deposition was carried out for different durations until we obtained a 'saturated' i.e. maximum value of surface roughness of ZnO. For this, a number of depositions were done at different experimental conditions and at different thickness values.

## 3.9.2 Results and discussion

Figure 1 shows the total reflection from the stainless steel substrate alone, silver-coated stainless steel substrate and finally from surface-textured ZnO on Ag/stainless steel with two different haze values. As we see from the figure, the reflection from the stainless steel is lower than other reflections. Optically, we need to reflect more light back in to the device. It is seen that stainless steel alone is not very efficient to serve this purpose. This is indeed the reason why silver is coated on the stainless steel. Due to the interference patterns in the curves, the reflectance curves given in this chapter are smoothened in order to distinguish one with the other.

The reflection of silver below 3.8 eV can be explained in terms of free carrier absorption [1]. After 3.8 eV interband transitions need to be considered. The reflection values of metals are connected with their electrical resistivities. Silver has one of the lowest resistivities. The value is $1.59 \times 10^{-6}$Ω.cm. According to the classical Hagen -Rubens relation the reflectivity is given by,

$$R = 1 - 2\sqrt{\frac{v}{\sigma_0}}$$

where v is the frequency and $\sigma_0$ is the dark conductivity. When the dark conductivity very high the second term is very small and the reflection of silver is a maximum. In figure 1 we see the maximum reflection of silver. The resistivity of stainless steel is 72 $\times10^{-6}$ $\Omega$.cm. Reflection studies on thermal evaporated Ag, Al and Cr were also done. As expected silver has a better reflection than these metals (figure 2). The reflection of aluminum is reduced around 8% in the visible region (at 600nm). Gold has a good reflection at higher wavelength, but significant absorption starts around 500nm. Chromium has only 48% of reflection in the visible region (around 600nm). All these metals other than silver have contribution to absorption from their solid state atomic structure. Due to this reason silver should be used as it qualifies as one of the best back reflectors for thin film solar cells.

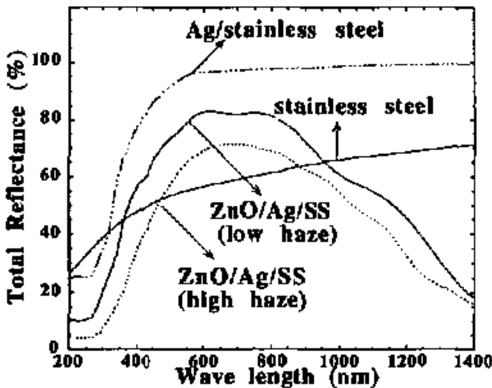


Figure 1. Total reflectance of stainless steel, Ag/stainless steel and ZnO/Ag/stainless steel with ZnO having high and low haze values. The total reflectance of strongly surface-textured ZnO (high haze)/Ag/ stainless steel is lower than *the total reflectance of the same system* with ZnO of less pronounced surface texture (low haze).

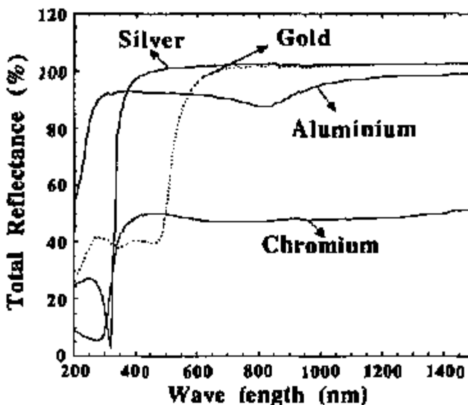


Figure 2. The reflection of different metals thermally evaporated on glass. Silver has good useful reflection to be used in thin film solar cells. Other metals show absorption in the useful region for photovoltaic conversion.

Even though the total reflection of silver is maximum, in practice silver leads to a poor interface with silicon (amorpholous and microcrystalline). This interface seems to absorb some light so that the high reflection of silver is not usually realized within silver/silicon devices. Also silver and silicon have poor adherence on each other. An intermediate oxide layer is found to form optically as well as mechanically a good interface between silicon and silver. On the other hand, for amorphous silicon solar cells the diffusion of metal atoms from the back contact to the device is supressed when there is an oxide layer used as 'diffusion barrier'. For an 'inverted' configuration, i.e., for the N/I/P device structure, this oxide will be exposed to the hydrogen plasma used for the fabrication of device. For this application, ZnO is preferred as it is more

stable w.r.t. the hydrogen plasma than other TCOs. ZnO has proved to be a successful barrier for the diffusion of metal atoms and generally helps in improving the performance of the cell (w.r.t the problem of 'pin holas'[2]). Hence, there is a necessity for an intermediate ZnO layer. Now one has to find ways to get maximum light back into the device with this intermediate layec configuration. In figure 1 the total reflection of surface textured ZnO with high haze factor as well as low haze factors are shown. The total reflection from surface textured ZnO with high haze/Ag/stainless steel is somewhat lower than that of the system with ZnO having a low haze factor. This reduction can be attributed to the light that is escaping at the edges of the film by the wave guide action as well as ultimate absorption of light in the ZnO by the multiple passage of light inside the film because of the high surface roughness. However, this reduction in total reflectance is not so pronounced at the long wavelength region where the back reflection is really now needed.

However, one must note that the really important requirement is to diffuse the light back into the device so that the light rays have longer optical path lengths. This is seen from the diffuse reflectance. Figure 3 shows the diffuse reflectance of the same samples for which the total reflectance was shown in figure 1. It is seen that the diffuse reflectance of stainless steel, Ag/ stainless steel is very low while comparing with the diffuse reflectance of the system with ZnO of high haze. The diffuse reflectance of the system with ZnO of *low haze factor has a very low diffuse reflectance, even lower than that of Ag/ stainless steel.* This clearly demonstrates the need to have surfece roughness of ZnO. The major portion of diffuse reflectance of the stainless steel or the Ag/ stainless steel combination is due to the irregularities on the stainless steel substrates.

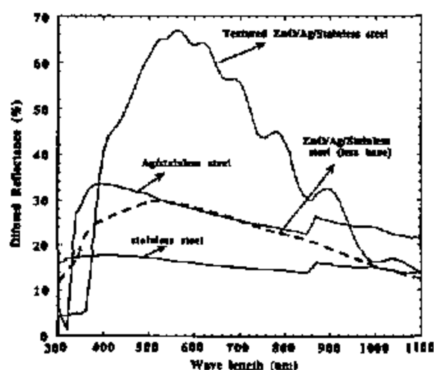


Figure 3. Diffuse reflectance of the samples shown in figure 1. It is seen that the ZnO with high haze factor can diffuse maximum amount of light back into the device.

Figure 4 shows the total and diffuse reflectance of the ZnO/Ag/stainless steel with ZnO grown at different partial pressures of water vapour in the mixture of Ar and water vapour during sputtering. The total working pressure was 5x $10^{-2}$ m bar. The substrate temperature was 200°C. The RF power was 225W. The depositions were done for a number of times with different thickness values to obtain saturated or maximum diffuse reflectance. It is seen that the partial pressure of water vapour during sputtering changes the diffuse transmittance and hence the haze values considerably. It was seen for the growth on glass, the ZnO with columnar surface morphology, that results during growth at low partial pressures of watec vapour, has low haze values when compared with the haze factor of the ZnO with granular surface morphology. The granular surface morphology results during growth at high partial pressures of water vapour. In contrast to the growth on the glass substrates, here the growth on Ag/ stainless steel substrates shows that the low partial pressure water vapou growth (columnar surface morphology) has relatively higher haze values when compared with high partial pressure water vapour growth (granular surface morphology). As the ZnO by sputtering at high RF power, in our experience, is less affected by the interaction of substrate material we assume that there is no influence or negligible influence of silver on the growth of ZnO. The main difference in both growth processes (on glass and on Ag/stainless steel) are the surface irregularities on Ag/stainless steel

substrates. These irregularities limit the size of the surface mountains in the case of granular morphology. This, in turn, affects the diffuse reflectance and haze factor (see section 3.3 on AFM analysis of columnar and granular morphologies). It seems that these irregularities do not reduce the haze factor of columnar surface morphology. In fact, the haze factor in the columnar surface morphology is enhanced due to the irregularities on the Ag/stainless steel substrate.

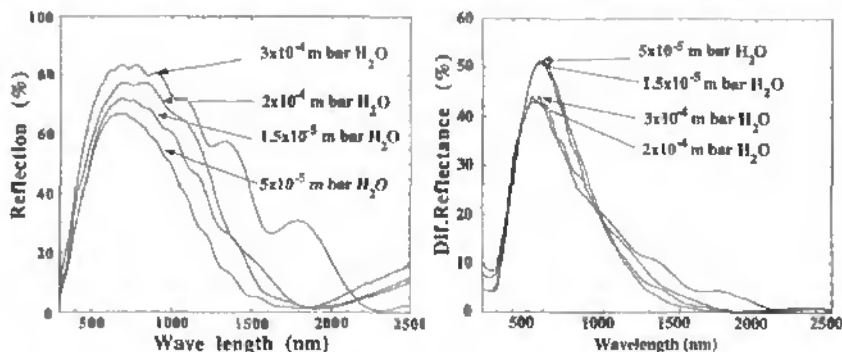


Figures 4(a)(left) and 4(b)(right). The total 4(a) and diffuse 4(b) reflectance of surface textured ZnO/Ag/stainless steel. The ZnO films are grown at different partial pressures of water vapour. The substrate temperature was 200°C. The RF power was 225W. The samples grown at low partial pressures of water vapour show high diffuse reflectance.

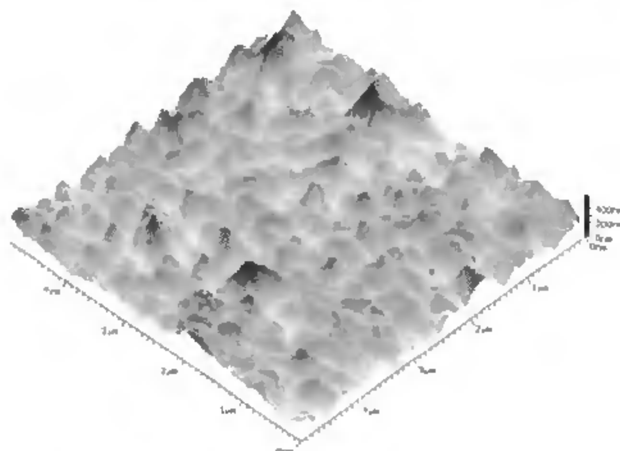

Figure 5. AFM picture of the surface morphology of ZnO film on Ag/stainless steel substrate grown at high partial pressure of water vapour. The partial pressure of water vapour was 2x $10^{-4}$ m bar. The substrate temperature was 200°C. The RF power was 225W. At this experimental conditions, on glass substrate we obtained granular morphology. Similarly we obtain granular morphology here. However the top view of the surface show that there are hexagons present on the surface. The surface peaks in this granular morphology is limited by the irregularities in the Ag/ stainless steel substrate. This can be compared with the granular morphology of ZnO obtained on glass substrates. Due to the reduced size of surface mountains, the diffuse reflectance of granular morphologies is less than that of columnar morphology samples.

In figure 4(a) the total reflectance curves show that as the diffuse reflectance and hence the surface roughness increase, the total reflectance decreases. For this measured reduction, as explained before, both the absorption in the material as well as the escape of light at the edges of the sample should be taken into account.

In figure 5, the AFM picture of the surface morphology of the ZnO grown on Ag/ stainless steel at high partial pressure of water vapour is shown. At this pressure we expect granular surface morphology. The figure shows indeed granular surface morphology. However, the top view shows that there are still hexagons present on the surface (not shown here). The size of the surface peaks are smaller while comparing with the granular morphology on glass substrate (see analysis of AFM picture in section 3.3). It shows that the size of the surface mountains in granular morphology is limited by the irregularities on the Ag/stainless steel substrate.

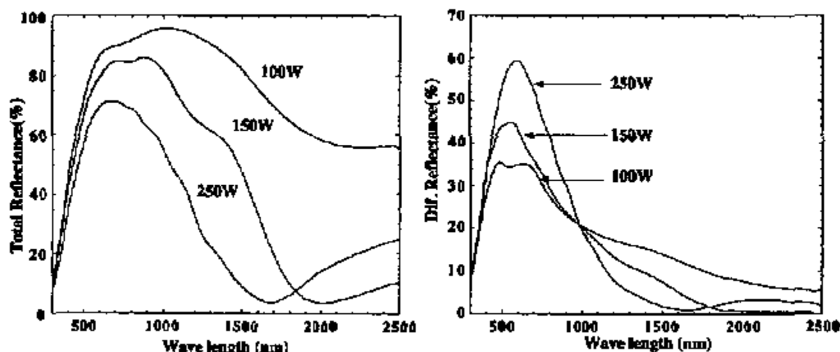


Figures 6(a) (left) and 6(b) (right). The total (6(a)) and diffuse (6(b)) reflectance of the ZnO/Ag/stainless steel system. ZnO was grown at different RF power values. The substrate temperature was 200°C. The partial pressure of water vapour was kept at $1.5x10^{-4}$ mbar.

Figure 6 shows the total and diffuse reflectance of samples grown at different RF power values. The partial pressure of water vapour was kept at $1.5x\ 10^{-4}$ m bar. The substrate temperature was 200°C. A number of ZnO films were grown at different thickness values. In figure 6, the samples with 'maximum' or 'saturated' diffuse reflectance are shown. As is seen, the RF power increases the surface roughness hence the diffuse reflectance. Similar to the water vapour series the total reflectance decreases with an increase in the surface roughness. The trend of variation in surface roughness with RF power is the same as that for surface texture growth on glass substrates. That is; the surface texture increases with an increase in RF power.

Figure 7 shows the total and diffuse reflectance of ZnO on Ag/stainless steel substrates at different substrate temperature values. For the growth of these films shown in figure 7, the RF power was kept at 225W and the partial pressure of water vapour was kept at $1.5x10^{-4}$ mbar. The surface roughness and hence the diffuse reflectance increase, in general, with an increase in substrate temperature. It is seen that even for the growth at room temperature the diffuse reflectance is highly pronounced. The change in the amount of diffuse reflectance of the samples grown at RT and at 75°C shows a different trend when compared with the samples grown at 200°C, 150°C and 100°C as shown in figure 7(b). This series was repeated and deposition was done for different thickness values of ZnO and the diffuse reflectance showed the same trend. Based on the knowledge of the growth of surface textured ZnO on glass substrates we can explain this behaviour. It was seen that the diffuse transmittance of surface textured ZnO on glass showed a maximum when the substrate temperature was reduced. This is due to the presence of granular grains *on the* columns of highly oriented ZnO (mixed morphology). Here it seems that at 75°C there are already granular grains *on the columns* of ZnO. In general, the reason for the growth of granular grains on the columns is the reduction of surface mobility of adatoms during growth due to the reduction of substrate temperature. For the growth on glass this would also

increase the diffuse reflectance of the sample grown at room temperature. In figure 4(b) it is shown that the diffuse reflectance of ZnO with granular morphology grown on Ag/stainless steel substrates has a reduced diffuse reflectance when compared with the ZnO with columnar morphology grown on the same Ag/stainless steel substrates. Hence for the case of ZnO grown at room temperature shown in figure 7(b), it seems that there are *more granular grains* when compared with the ZnO grown at 75°C.

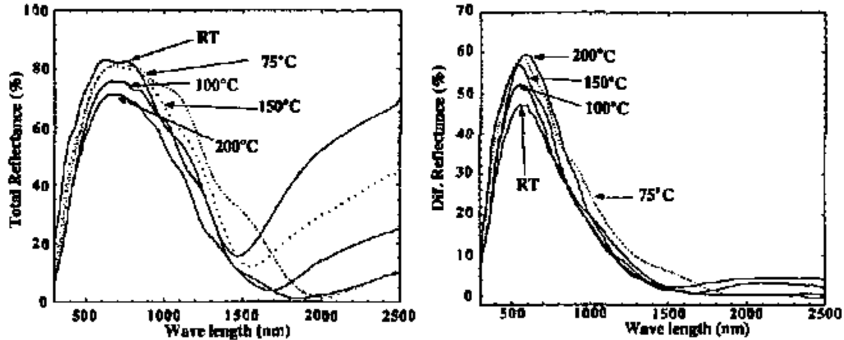


Figure 7. Figure 7(a) (left) and 7(b) (right) The total (7(a)) and diffuse(7(b)) reflectance of the ZnO/Ag/stainless steel system. The ZnO was grown at different at substrate temperature values. The RF power was 225W. The partial pressure of water vapour was kept at $1.5 x 10^{-4}$ mbar.

Figure 8(b) shows the diffuse reflectance of ZnO samples grown at different durations of deposition time with the same experimental conditions. The partial pressure of water vapour was $1.5 \times 10^{-4}$ m bar. The substrate temperature was 200°C. The total working pressure was $2.5 \times 10^{-4}$ mbar. The RF power was 250W. The duration of the deposition was varied as follows: $t_1$=30 $t_2$=90 $t_3$=150 minutes. Further increase in the film thickness does not increase the diffuse reflectance. The total reflectance of the same films are shown in figure 8(a). Depending on the thickness as well as surface roughness the reflectance spectrum shows differences in both the long wavelength as well as in the short wavelength regions. The increase in the total reflectance of samples with reduced thickness at long wavelength regions is due to the reduction in the number of charge carriers. We know that the 'reflectance' which is measured here, in this ZnO/Ag/stainless steel system, is the reflectance from ZnO as well as the transmittance of ZnO combined with the reflectance from silver. This, in addition is influenced by multiple reflections and transmissions in the ZnO/Ag system. This reduction in the reflectance at the long wavelength region may happen also with the change in material property. For example the sample grown at high partial pressure of water vapour may show a low free carrier absorption (see figure 4(a), curve for ZnO grown at $3.5 \times 10^{-4}$ m bar of partial pressure of water vapour) due to an increase in electrical resistivity. Again this can be varied by changing the thickness. For example, a thick low conducting ZnO can give the same long wavelength reflectance as a thin high conducting ZnO.

In the short wavelength region, ZnO is weakly absorbing, in ideal cases it is transparent (after the band to band transition at around 375nm). But we have seen previously that there could be point defects, color centers and other defects that affect the shape of the transmission of ZnO in this region. The absorption in this region is increased when the thickness is increased as well as when the surface roughness is increased. In both cases the effective thickness of the material is increased and hence the absorption is enhanced. This is the reason for the reduction of total reflectance when the diffuse reflectance was increased. Also, there is a definite amount of light that escapes at the edges by waveguide action when the surface is rough. This is also seen as 'absorbed' light. The diffuse reflectance depends on the thickness, on the nature of the surface texture (granular or columnar) and on the size of the surface peaks as well as on the material properties, (conductivity, defects). The variation of total reflectance as well as of diffuse

reflectance is shown in figures 4, 6, 7 and 8 for the different experimental conditions described above.

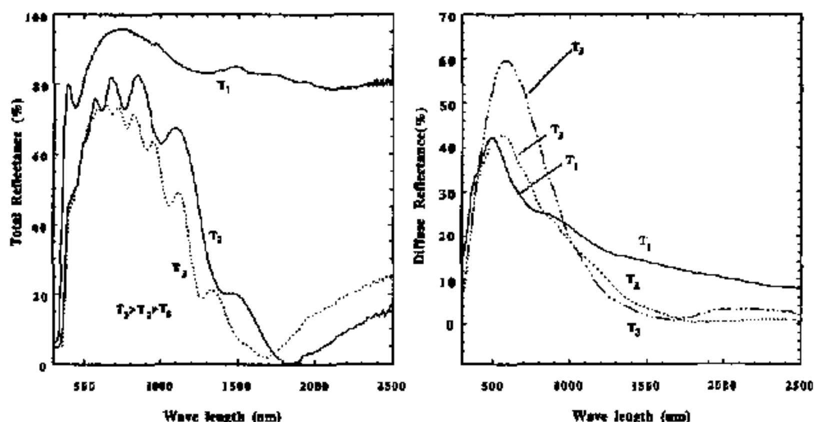


Figure 8(a)(left) and 8 (b)(right). The total and diffuse reflection of ZnO film with different thickness values. The RF power was 225W. The partial pressure of water vapour was 1.5 $\times 10^{-4}$ m bar. The depositions times are $T_1$=30min., $T_2$=90min and $T_3$=150min. As the thickness increases the diffuse reflection increases and it reaches the maximum at the thickness of $T_3$. The total reflectance increases with decrease in thickness as well as increase in surface roughness.

It was shown in the section on structural properties (section 3.6) that surface-textured ZnO films have intrinsic stress in the film. The tensile stress increases with an increase in surface roughness. For the present study on the surface textured ZnO/Ag/stainless steel system, we do not use any film in between Ag and stainless steel substrates. The silver showed poor adherence on stainless steel. When the substrates are not clean silver easily peels off from stainless steel. However, the cleaned stainless steel substrate in general, lead to a relatively better adherence. But ZnO has a good adherence on silver and vice versa. *When the surface roughness of ZnO deposited on Ag/stainless steel increased the intrinsic stress in the films got increased. Hence the films with increased surface roughness lead the ZnO/silver to peel off from stainless steel.* This showed that the ZnO films on silver have similar mechanical behaviour as the ZnO films on glass. It is difficult to make a device on highly textured ZnO/Ag/stainless steel substrates. To overcome this problem a thin ZnO layer is grown in between Ag and stainless steel so that Ag has good adherence in both sides.

### 3.9.3 Conclusions

The surface textured ZnO/Ag/stainless steel system is analysed in this section. It has been shown that without surface texturing of ZnO, the diffuse reflectance from the back contact of a solar cell can be inferior to the diffuse reflectance from silver alone. The total reflectance from the surface textured ZnO/Ag stainless steel can be lower than the same system without surface texturing. To obtain a combination of both maximum total reflectance and maximum diffuse reflectance we must vary those experimental conditions that give rise to changes in material property as well as the thickness and the surface roughness. In this section the variation in surface roughness and in the optical properties for different experimental conditions have been shown.

## References

[1] H. Ehrenreich et al IEEE spectrum 2, 1965, 162
[2] M. Goetz, Ph.D thesis, 1997. Thesis number 1637, EPFL.

# 3.10 ZnO grown by Chemical Vapour Deposition (CVD) and its comparison with ZnO grown by sputtering

## 3.10.1 Introduction

A transparent conducting oxide for thin film solar cell should basically have three important qualities; electrical conductivity, optical transmittance, surface texture. The third property is important in connection with photovoltaic solar cell. ZnO has established as an important TCO for thin film solar cells. Hence the efforts have been made to grow ZnO with surface texture. The successful growth of device quality ZnO with all the three properties have been carried out by chemical vapour deposition (CVD). By sputtering however, there is no work, except the present one, reported about the surface texture growth on the device. All reports [1,2] were about the surface texture growth in thin film stage.

Among the various works done on the growth of ZnO by CVD [3,4,5,6,7,8,9], the main work of surface textured growth of ZnO has been done by Yamada [10], Wenas [11,12,13] and the co workers and Hu and Gorden [14,15,16]. Metal Organic Chemical Vapour Deposition is particularly useful for large scale coatings at high growth rates. The most commonly used organo metallic Zinc precursors are diethylzinc (DEZ) and dimethyl zinc (DMZ). Zinc can be oxidised by using pure oxygen, water [10,11,12,15], alcohol [13,14] nitrous oxide, carbon dioxide or even some oxygen containing cyclic compounds [8].

CVD is an attractive option for the growth of ZnO. The growth rate of ZnO by CVD can be double or more the growth rate of ZnO by sputtering. The common disadvantage of the above mentioned methods is the usage of the toxic gases for the doping of ZnO. To analyse the growth and properties of ZnO by CVD as well as to compare the properties of ZnO by CVD an sputtering, we grow ZnO by CVD [17]. A non toxic gas for the doping will make CVD more useful. For this purpose we selected a non toxic boron doping gas, trimethyl borate[18].

In this section we study the growth and properties of ZnO by the method of CVD and we compare the ZnO grown by sputtering and CVD.

## 3.10.2 Experimental

ZnO thin films doped with boron were grown by using trimethyl borate (TMB) as doping gas. Diethyl Zinc (DEZ) and water vapour were allowed to react with each other by mixing them in a chamber. DEZ can react with water spontaneously at room temperature. The doping gas (trimethyl borate) was added during the reaction and the resulting films formed on the substrate kept at temperatures varying from room temperature up to 360°C. All the depositions described here were done at a pressure of 0.5 mbar. The distance between the nozzle of the reaction gases and the substrate was 5 cm. Three different series were done. In the first series the ratio between water to diethyl zinc (DEZ) was varied. In the second series the amount of doping gas was changed. In the third series, the substrate temperature was changed. The films were characterised for their optical properties, electrical properties, surface properties and the structural properties by the same techniques used for sputtered ZnO.

## 3.10.3 *Results and Discussion:* *1. Growth rate and electrical resistivity*

Figure 1 shows the growth rate of ZnO films grown at different partial pressures of water vapour. The total pressure was kept at 0.5 m bar and the flow rate of DEZ was kept at 35sccm.

The substrate temperature was 200°C. The flow rate of the doping gas TMB is 2 sccm. It is seen that as the ratio of water to DEZ is varied the growth rate increases to high values and then it reaches a steady value. The water and DEZ react spontaneously with each other. The basic reaction that happens with DEZ and water vapour is the oxidation of DEZ that leads to ZnO as product. The oxidation of DEZ is a chain reaction with a slow initiation step [19]. The end of this reaction is exothermic. Hence when there is more oxygen during growth the branching reaction is important. The oxygen during the present growth comes from water. When the amount of water dissociated is more, there is more oxygen during growth hence the oxidation of DEZ.

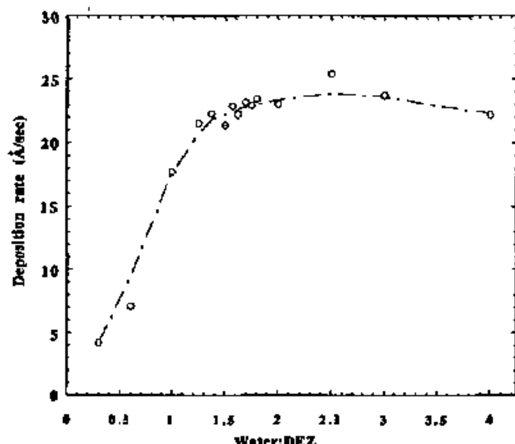


Figure 1 The effect of water to diethyl zinc ratio on the deposition rate of ZnO. The deposition temperature was kept at 200°C. The flow rate of the doping gas was kept at 2 sccm. The total working pressure was 0.5 m bar. At low partial pressure of water vapour the amount of water is not sufficient to make reaction with all available DEZ. As the water content increases the reaction increases and there is more ZnO deposited. After 1:1 ratio of water to DEZ, the growth rate reaches a maximum showing that the water is sufficient to make complete oxidation of DEZ.

The growth rate is given by the following empirical relation [20],

$$R= Kf[O_2]g[DEZ]\ T \exp(-E/RT) \qquad (1)$$

Where K is a rate constant, $f[D_2]$ and g[DEZ] are functions of the reactant gas concentrations and E is the activation energy of the reaction. The equation suggests that at low substrate temperatures the effect of substrate temperature on the growth rate is small and the growth rate is proportional to the concentration of reacting gases. At high substrate temperature, however the substrate temperature has an active part to increase the growth rate. Roth and Williams [19] have analysed the properties of ZnO prepared by the oxidation of DEZ using oxygen. For their experiment, the growth rate was independent of substrate temperature when the substrate temperature values are less than 350°C. In the present case, the substrate temperature is 210°C. Hence we can expect the active role of concentration of reacting gases on the growth rate. At reduced partial pressure of water vapour, the amount of oxygen dissociated from water vapour is less. The concentration of oxygen necessary for the oxidation of DEZ at a fixed partial pressure of DEZ and the total pressure is, thus less at low partial pressures of water vapour. Hence the amount of ZnO deposited is less. By increasing concentrations of water vapour we increase the oxidation of DEZ and hence the growth rate of ZnO. When the ratio of water to DEZ is around 1.25 the deposition rate reaches a maximum showing a complete oxidation of DEZ. Further increase of water does not increase the growth rate showing a saturation value of the concentration oxygen necessary for the complete oxidation. Further addition of water vapour would disturb the growth by the excess water.

Figure 2 shows the resistivity in function of the water to DEZ ratio for the same ZnO films shown in figure 1. The flow rate of doping gas is kept constant. Hence the changes that happen in resistivity is mainly caused by water vapour. Figure shows a minimum value of resistivity at the ratio of water vapour to DMZ at around 1.7. The reduction of water vapour below the ratio 1.2 increases the value of sheet resistance to very high values. Similarly the increase of the ratio after 1.8 lead to films with high resistivity values and they seem to remain

constant. The later values are not as high as the resistivity values obtained at low partial pressures of water vapour.

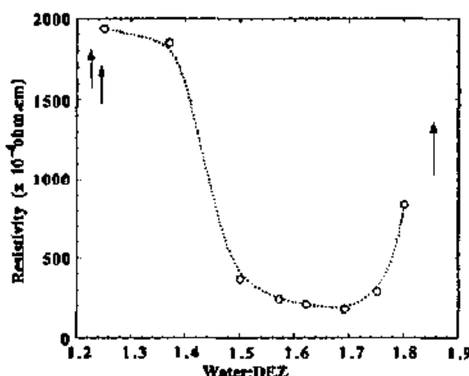


Figure 2. Resistivity of ZnO:B films in function of the ratio of water to DEZ during growth. The resistivity has a minimum value when the ratio is around 1.7. The resistivity starts decreasing rapidly when the ratio is around 1.2. Before that at low partial pressure of water vapour the resistivity is very high. Similarly when the ratio is around 2 the resistivity increases again to high values and it remains constant. However, the magnitude of resistivity is less than the resistivity values obtained at low partial pressures of water vapour.

In figure 1 it is seen that the deposition rate increases with increase in water to DEZ ratio. It was observed that when the ratio is 1.25 the growth rate has a maximum value. The resitivity starts decreasing around the same values of water to DEZ ratio. The values of ratios of water to DEZ of 1.6 to 1.7 correspond to maximum growth rate and minimum resistivity. The conduction of ZnO films can be by defect structure (interstitial Zn and oxygen vacancies) and/or by the external doping. However, very high conductivity is possible only by external doping. Here we assume that the major cause for conductivity is the external doping of boron from TMB. During doping, the B atoms occupy the positions of Zn. At low partial pressure of water vapour the doping is not efficient. The effect of increase in deposition rate and the decrease in resistivity is due to the efficient increase in oxidation of ZnO due to the increase in water vapour. At the ratio of 1.6 to 1.7 the oxidation is highly efficient and all the oxygen in the growth atmosphere is efficiently used for the growth of ZnO. At higher water pressures above the ratio of 1.8, however, there is an excess oxygen for the growth of ZnO at a fixed partial pressure of DEZ. This oxygen is incorporated in the film and thus reduces the conductivity.

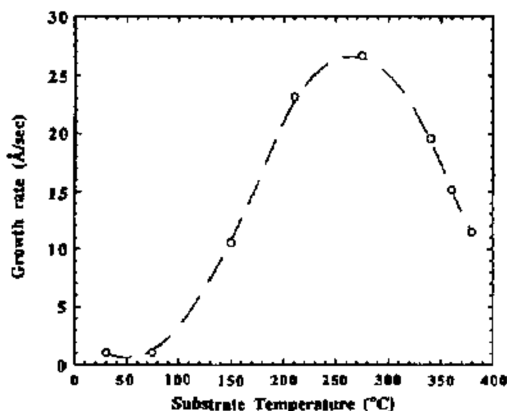


Figure 3. The growth rate of ZnO as function of substrate temperature. The *working pressure was 0.5 m bar.* The ratio water to DEZ is kept constant at 1.7. The flow rate of the TMB was 2sccm. The growth rate has a maximum at around 275°C.

Figure 3 shows the growth rate of ZnO in function of the substrate temperature. All other growth parameters were kept constant. The total working pressure was 0.5 mbar. The flow rate of TMB was 2sccm. The water to DEZ ratio was 1.7. As is seen the growth rate increases with

increase in substrate temperature. It has a maximum at 275°C and further increase in substrate temperature decreases the growth rate. During the oxidation of DEZ using oxygen [19], the growth rate of ZnO was found to be nearly the same at low substrate temperature and at around 300°C it started to increase with increase in substrate temperature. During the growth of ZnO using DEZ and water with diborane as dopant gas [12], the growth rate was reported to vary with substrate temperature in a similar manner but at low substrate temperature region. However, the growth rate is also a function of total pressure as well as the ratio of water to DEZ. As these parameters are not the same we can not make a direct comparison of our results with the above mentioned works.

In the present case the growth rate increases right from 75°C, with an increase in substrate temperature. Furthermore here, as is seen the growth rate decreases after 275°C with further increase in substrate temperature. This is observed only in the present case. (In Ref.[12], it seems thet the similar trend would have been obtained if the authors have increased the substrate temperature more than 300°C). In equation (1), it is seen that the growth rate is proportional to the concentration of the reacting gases *at* low substrate temperature and such a behaviour is observed in figure 1. However, in figure 3 the ratio of water to DEZ ratio is 1.7, and this is already a high growth rate region *for* a substrate temperature of 200°C. Here almost we have optimised partial pressure of water vapour for the reaction with DEZ at 200°C. The increase in substrate temperature from 75°C basically increases the reaction *on the substrate surface*. The branching reactions (multiple chain reactions of DEZ and Oxygen) take place on the substrate surface [19]. Hence an increase in substrate temperature increases the reaction between water and DEZ, hence the formation of ZnO. At the substrate temperature of around 200°C, the water is sufficiently dissociated for the growth of ZnO. An increase of substrate temperature beyond 200°C may increase the dissociation of water vapour. This, in turn, perturbs the growth of ZnO. That means there will be more oxygen during the growth. This reduces the rate of formation of ZnO. In this case, one would expect the resistivity to increase in a similar manner.

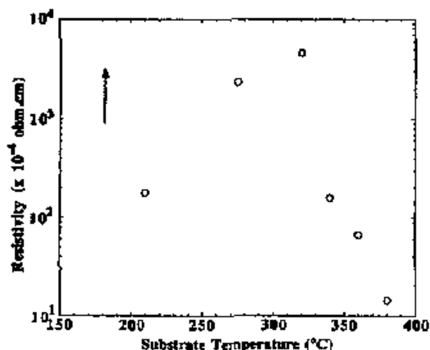


Figure 4. The resitivity of ZnO:B films as a function of substrate temperature for the same samples shown in figure 3. The resitivity increases due to the incorporation of oxygen in the films. Beyond 320°C, the increase in crystallinity and the doping efficiency increases the conductivity.

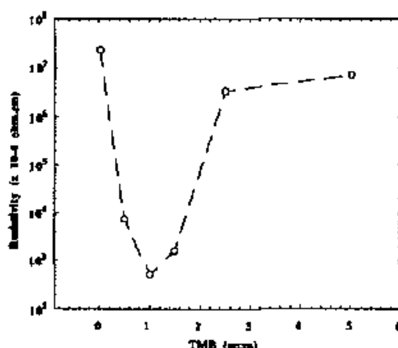


Figure 5 Variation of resistivity of ZnO:B films in function of the flow rate of the doping gas TMB. The substrate temperature was 200°C. The total working pressure was 0.5mbar. The ratio of water to DEZ was 1.7. It shows a minimum around 1sccm. Further increase in flow rate increases the resistivity.

In figure 4 we see the resistivity in function substrate temperature. As expected, from 200 - 320°C, the resistivity increases as the substrate temperature increases. Hence we come to the conclusion that the incorporation of oxygen increases as the substrate temperature is increased. However further increase in substrate temperature, despite the perturbation due to the

high dissociation of water vapour on the substrate surface, increases the surface mobility of adatoms. This in one hand increases the crystallinity by increasing the grain size, on the other hand increases the doping efficiency. Hence at high substrate temperatures the films have low resistivity. This is further discussed during the analysis of optical properties. The resistivity obtained at 380°C is 14.4 x$10^{-4}$Ω. cm. Below 150°C the films show very high resitivities.

In Figure 5 the variation of resistivity in function of the flow rate of the doping gas is shown. The substrate temperature was 200°C. The total working pressure was 0.5mbar. The ratio of water to DEZ was 1.7. As one would expect increase in doping gas should increase the conductivity. But as is seen in the figure, the resistivity shows a minimum value at the flow rate of around 1sccm. Similar effect has been observed for the doping with diborane [11]. The increase in flow rate of diborane increases the amount of boron in ZnO. When the flow rate is increased more than the flow rate that corresponds to the minimum in resistivity, the boron atoms are found (by both hall effect and SIMS measurements) to be electrically neutral in the material[11]. Further increase in flow rate of diborane reduces the free carrier concentration and the mobility leading to low values of conductivity. Here in our films, we found the same trend independent of the doping gas.

Further we would like to see the effect of flow rate of the doping gas *at high substrate temperatures*. Figure 6 shows the resistivity of ZnO:B films deposited at different flow rates of TMB. The substrate temperature was 380°C. All other parameters are kept constant as the series mentioned above. As is seen the resistivity decreases with increase in flow rate of the doping gas. Hence *the boron atoms that could be in electrically neutral situation at low substrate temperature are electrically active when the substrate temperature is increased*. This is due to the increased kinetic energy of adatoms that leads to efficient doping of B atoms. The minimum resistivity achieved at the flow rate of 4 sccm is 2.1 x $10^{-4}$ Ω.cm. This is the lowest value of resistivity achieved by using TMB as the dopant gas.

The growth rate of ZnO films shown in figure 6 are shown in figure 7. The growth rate increases linearly with the increase in the flow rate of TMB. The flow rate of the doping gas TMB can change the growth rate from 10Å/sec to 20Å/sec. The increase in the growth rate can be attributed to the orientation of the growing films and this will be explained later.

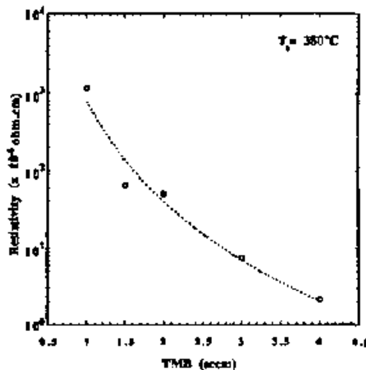


Figure 6. The resistivity in function of TMB at high substrate temperature of 380°C. The resistivity decreases as the flow rate is increased. The substrate temperature was 200°C. The total working pressure was 0.5mbar. The ratio of water to DEZ was 1.7. The B atoms are made electrically active at high substrate temperature. See also figure 5.

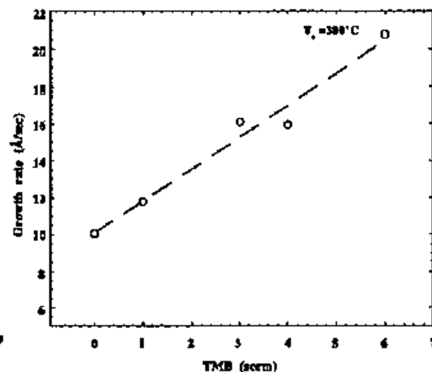


Figure 7 The growth rate of ZnO:B films as a function of the flow rate of the doping gas TMB at 380°C. The deposition conditions are the same for figure 6 and figure 7. The growth rate can vary from 10Å/sec to 20Å/sec by changing the flow rate of doping gas. The growth rate increases linearly with the increase in the flow rate. It is due to the fast non equilibrium growth of ZnO.

### 3.10.3.2 Optical properties

In figure 8 the total transmittance of the ZnO:B samples grown at different substrate temperatures are shown. The total working pressure was 0.5 m bar. The ratio of water to DEZ was 1.7. The flow rate of TMB was 2sccm. The growth rate and the resistivity of the same samples are shown in figure 3 and 4. In figure 8, it is seen that as the substrate temperature increases the free carrier absorption increases for the samples grown at 380°C ,360°C, 340°C and 320°C. The samples grown at 275°C, 210°C and 150°C show the variation in free carrier density in a similar way of variation of resistivity as shown in figure 4. The films grown at the substrate temperatures of 150°C and 210°C have different orientations of growth than the films grown at 320°C and 340°C (see figure 14). At 275°C the transition in the growth orientation takes place.

In figure 9 the total transmittance in the visible region of the same samples (of those shown figure 8) is shown. It is seen that as the substrate temperature increases the absorption in the wavelength region between 400-600nm increases for the samples grown at 380°C, 360°C, 340°C and 320°C. In section 3.4 on optical properties of ZnO grown by sputtering, it is explained that the reason for the absorption in this wavelength region is the presence of color centers. These defects increase as the substrate temperature is increased. In section 3.5 on electrical properties of ZnO grown by sputtering it was seen that the increase in RF power and substrate temperature (transition from granular to columnar morphology) increased the defects in the material. Here a similar trend is followed. However there is another regime at which the increase in substrate temperature does not increase the absorption at 400-600nm wave length region (for samples grown at 150°C and 210°C). The reason for this behaviour could probably be the change in structural properties. As mentioned earlier these two sets of ZnO have different structural properties. The transition from one regime to the other occurs at 275°C.

The CVD process used for thin film solar cells [9-12] generally uses the first regime at low substrate temperatures. In this regime the absorption due to the defects is highly reduced. This makes a considerable change in the visible region of the spectral response of the solar cells that uses ZnO grown by CVD.

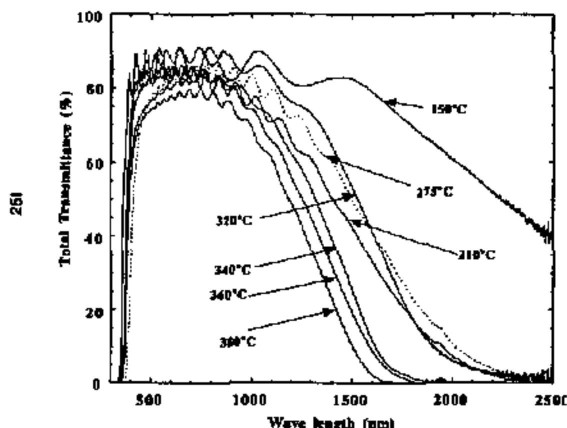


Figure 8. The total transmittance of the ZnO:B films deposited at different substrate temperatures. The total working pressure was 0.5 m bar. The ratio of water to DEZ was 1.7. The flow rate of TMB was 2sccm. The ZnO films grown at 380°C, 360°C, 340°C and 320°C they can be compared with each other. For these samples the increase in substrate temperature increases the conductivity and this mainly increases the free carrier absorption in the near infra red region (see figure 4). The samples grown at 150°C, 275°C and 210°C follow the variation in resistivity as shown in figure 4. The two sets of samples (grown at 320°C, 340°C & 150°C, 210°C ) also differ in their structural orientation during growth.

Figure 10 shows the diffuse transmittance of the same films shown in figure 8 and figure 9. Here also two different behaviours are observed. At low substrate temperature the increase in substrate temperature increases the diffuse transmittance. There is a transition in the structural properties at 275°C. After that the films belong to another regime. The films have a flat surface at around 300°C of substrate temperature. Further increase in substrate temperature

increases the surface roughness and hence the diffuse transmittance. It seems at 360°C the diffuse transmittance reaches the maximum value.

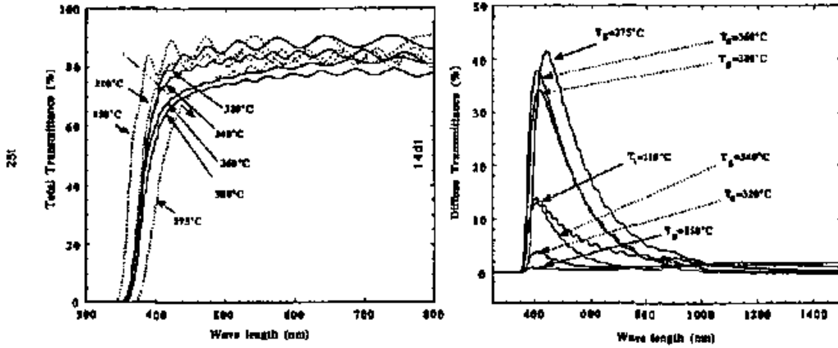


Figure 9 (left). The total transmittance in the visible region of the ZnO:B films deposited at different substrate temperatures (same samples shown in figure 8).It is seen that for the samples grown at 380°C ,360°C, 340°C and 320°C, the increase in substrate temperature increases the absorption in the 400nm-600nm wave length region. It is explained in section 3.4 on optical properties that the reason for absorption in this wavelength regions is the presence of color centres. The samples grown at 150°C, 275°C and 210°C differ in their structural properties with the high temperature grown samples

Figure 10 (right). Diffuse transmittance of the same ZnO:B films shown in figure 8 and 9. Here also two different behaviours are observed. The films have smooth surface at around 300°C of substrate temperature.

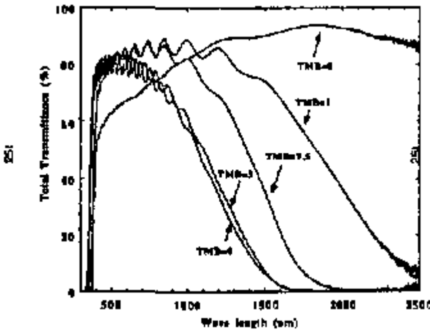


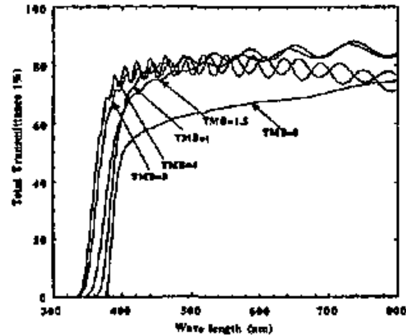


Figure 11. Total transmittance of ZnO films grown at different flow rates of the doping gas TMB. The substrate temperature was 380°C. The water to DEZ ratio was 1.7. The total working pressure was 0.5 m bar. Unlike at low substrate temperatures, the number of free carrier increases with increase in the flow rate of the doping gas. (See figures 5 and 6)

Figure 12. The total transmittance of the same samples shown in figure 11 in the visible spectral region. The change in the amount of B dopants does not make a considerable change in the absorption in the visible region. (Note the shift in the band edge and compare these figures 11 and 12 with figure 11 and 12 in chapter 1)

The total transmittance of ZnO films grown at different flow rates of the boron doping gas is shown in figure 11. The total working pressure is 0.5 m bar. The substrate temperature was kept at 380°C. The water to DEZ ratio was 1.7. It is seen that the increase in boron doping increases the free carrier absorption. The films grown without the doping gas show no absorption

in the near infrared region. This just shows the efficiency of external doping with TMB (see figure 6). In figure 12 the transmittance of the same samples in the visible spectral region is shown. ZnO grown without any external doping shows high absorption that starts from the visible region (400nm) and extends up to 1200nm. The doping of B atoms seems to make no considerable change in the absorption in the wavelength range 400-600nm. The shift in the onset of band to band transition with increase in boron doping towards the short wavelength region is noted in the figure. This effect is mainly due to Burnstein -Moss shift that is explained already in section 3.4 as well as in chapter 1. The doping of B atoms clearly influences the free carrier density. (Figure 11 and 12 can be compared with figure 11 and 12 of chapter 1).

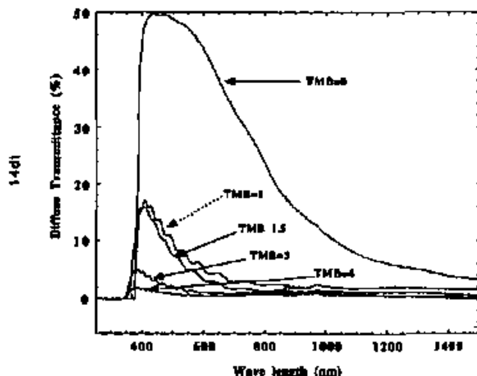


Figure 13 The diffuse transmittance of ZnO films at different flow rates of the doping gas (see figure 11 for experimental conditions).The film without B doping has high surface roughness. The surface roughness decreases with increase in boron doping. The samples grown with the TMB flow rate of 1(sccm) and 1.5(sccm) have different orientations while comparing with the samples grown with the flow rate of 3 (sccm) and 4 (sccm).

The diffuse transmittance of the same ZnO films, shown in figure 11 and 12, are shown in figure 13. The ZnO film grown without doping shows high surface roughness and hence high diffuse transmittance. The addition of B atoms decreases the surface roughness of the films. The samples grown with the TMB flow rates of 1(sccm) and 1.5 (sccm) have different orientation of growth while comparing with the samples grown at the TMB flow rates of 3(sccm) and 4(sccm). This will be explained later. Here it is observed that just the doping can influence the change in surface texture.

### 3.10.3.3 Structural properties

The x-ray diffraction pattern of the ZnO films grown at different substrate temperatures are shown in figure 14. The total working pressure was 0.5mbar. The ratio of water to DEZ was 1.7. The flow rate of the doping gas TMB was 2 sccm. The substrate temperature values are marked in each diffraction pattern. In the first look it is noted that the [0002] orientation which is typical for ZnO grown by sputtering, is not present. There are diffraction peaks due to $(10\bar{1}0)$ and $(10\bar{1}1)$ planes.

In section 3.6 on structural properties of ZnO, it is explained that the (0002), $(11\bar{2}0)$ and $(10\bar{1}0)$ respectively are the three planes with lowest surface energy densities. In equilibrium growth, the film always grow along [0002] direction which corresponds to the closest packed plane. During non equilibrium growth other two orientations of growth may result. Also it is explained that a orientation along $[10\bar{1}1]$ is not expected and it is considered as an abnormal [21]growth direction.

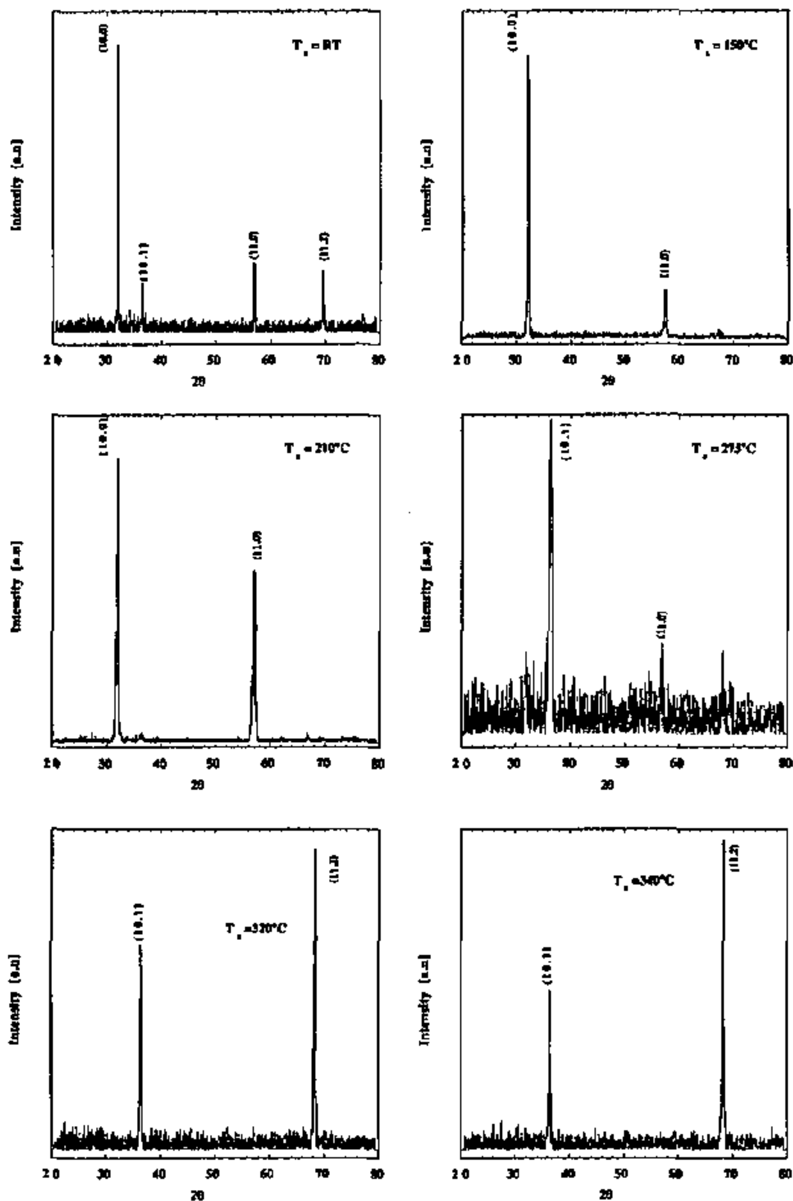
Intensity (a.u)
2θ
$T_s$ = RT
$T_s$ = 150°C
$T_s$ = 210°C
$T_s$ = 275°C
$T_s$ =320°C
$T_s$ =340°C
(10.0)
(10.1)
(11.0)
(11.2)
20
30
40
50
60
70
80

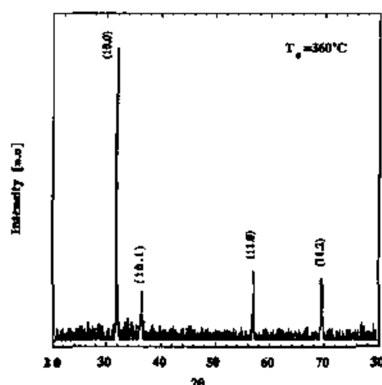

Figure 14. The X-ray diffraction pattern of ZnO:B films grown at different substrate temperature values. The total working pressure was 0.5 mbar. The water to DEZ ratio was 1.7. The flow rate of TMB was 2 sccm. The substrate temperatures are marked in each diffraction pattern. It is seen that as the substrate temperature is increased the preferred orientation of growth changes. At low substrate temperature the films grow along [10 $\bar{1}$ 0] direction. There is a transition in the orientation at 275°C. The sample grown 275°C and there after has a orientation of (10 $\bar{1}$ 1) orientation. This orientation is an abnormal orientation for ZnO films. At 360°C, the films again grow along [10 $\bar{1}$ 0] direction. This corresponds to the plane with third lowest surface energy.

In figure 14, it is seen that at low substrate temperatures the films have orientation corresponding to (10 $\bar{1}$ 0) planes which is the plane with third lowest surface energy. This is a non equilibrium growth of ZnO. At 275°C there is change or transition in the growing direction. The films have [10 $\bar{1}$ 1] direction as the growing direction. As is already explained this is an abnormal orientation of ZnO. The growth along this direction continues up to the substrate temperature of 340°C. At 360°C, it seems that there is transition of the direction of growth again to [10 $\bar{1}$ 0] direction.

The existence of cubic ZnO has been analysed in section 3.6. The 'd' (interplanar distance) values of the ZnO:B films grown at substrate temperature values of 275°C, 320°C and 340°C were compared with the 'd' values of ZnO with hexagonal wurtzite structure and cubic structure. The values are comparable for both the hexagonal and cubic structures.

Figure 15 shows the ZnO films grown at different flow rates of the doping gas TMB. The substrate temperature was 380°C. The water to DEZ ratio was 1.7. The total pressure was 0.5 mbar. It is seen that *the addition of dopants could considerably change the orientation of the growing films*. When there is no external doping the films have [0002] orientations. The growth along [0002] orientation continues at low concentrations of dopants. Up to the doping of 1.5 sccm the dominant orientation of [0002] exists. This is the equilibrium growth obtained by CVD. Further increase in dopants leads to non equilibrium growth of ZnO. The films grow along [11 $\bar{2}$ 0] and [10 $\bar{1}$ 0] directions respectively with the increase in the dopant concentrations. As the [11 $\bar{2}$ 0] and [10 $\bar{1}$ 0] are the second and third planes respectively with the low surface energy, it means that the addition of boron atoms increases the non equilibrium growth of ZnO, while no addition of boron atoms corresponds to equilibrium growth.

Another important point is noticed here. At high temperatures, without any dopant atoms ZnO grows with its minimum energy plane, i.e., (0002) plane parallel to the substrate. The addition of dopant atoms alone can make modification in the orientation of the growth. At substrate temperatures from 275°C to 340°C with TMB flow rate of 2sccm, the ZnO films grow with an abnormal orientation along [10 $\bar{1}$ 1] direction (see figure 14). May be, the B dopant

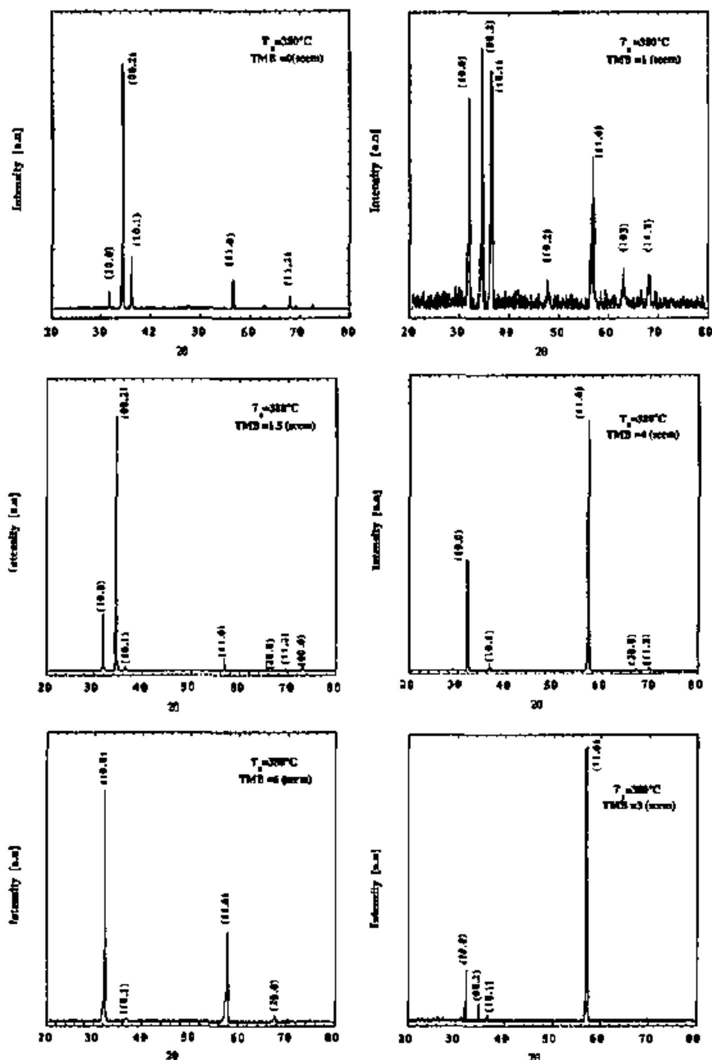


Figure 15. The x-ray diffraction pattern of ZnO films grown with different flow rates of the doping gas TMB. The substrate temperature was 380°C. The water to DEZ ratio was 1.7. The total pressure was 0.5 mbar. The flow rates are marked in each diffraction pattern. It is seen that the dopant atoms can considerably change the orientation of the growing films. Without dopant atoms, ZnO grows along [0002] direction. At 1.5sccm there is dominant [0002] orientation. An equilibrium growth of ZnO by CVD. After this, the addition of more boron atoms leads to non equilibrium growth of ZnO along [11 $\bar{2}$ 0] and [10 $\bar{1}$ 0] directions respectively. The non equilibrium growth corresponds to increase in growth rate.

atoms occupying the Zn site make changes in the preferences of the adatoms for the occupation of minimum energy atomic sites. This leads to the abnormal orientation of ZnO films.

From these studies on the orientation of growth of ZnO we can make another interesting study. Normally, ZnO at equilibrium grows along[0002] direction. According to evolutionary selection theory, this is due to the high growth rate of (0002) planes in equilibrium conditions. If there is another orientation to suppress this growth along [0002] direction, it should have higher growth rate. This would be a non equilibrium growth that would have faster growth rate than the equilibrium one[22]. According to this a $[11\bar{2}0]$ orientational growth should have faster growth rate than [0002] orientation growth and $[10\bar{1}0]$ orientational growth should have faster growth rate than $[11\bar{2}0]$ orientation growth. As the addition of boron atoms in ZnO enhances the non equilibrium growth, we can expect the growth rate also to increase in a similar way. Indeed, that is what we observed in growth rate. It is seen in figure 7, the growth rate of the same samples of ZnO, increases with the addition of Boron atoms. Comparison with figure 15 explains that

growth rate for (0002) $<$ growth rate for $(11\bar{2}0)$ $<$ growth rate for $(10\bar{1}0)$.

This effect may not be observed when there are many changes during growth. For example, the change in the amount of reacting gases or the change in the substrate temperature that changes the nature of reaction or the steps of the chain reaction, may hinder this effect. However in the above case, the substrate temperature and the reacting gases are kept constant. Only the amount of dopants has changed. These dopants could modify the orientation of the growing films and the effect of these modification on the growth rate is clearly displayed. This demonstrates the non equilibrium growth of ZnO.

## 3.10.3.4 SURFACE PROPERTIES AND GROWTH KINETICS

### 3.10.3.4.1 Variation in substrate temperature

Figure 16 shows SEM photographs of surface morphologies of ZnO films grown at different substrate temperatures. The total pressure was 0.5 mbar. The water to DEZ ratio was 1.7. The flow rate of TMB was 2 sccm. As is seen the roughness of the ZnO films easily gets modified depending on the substrate temperature. The variation in the surface roughness can be compared to the variation of diffuse transmittance of the same films shown in figure 10.

The surface roughness, as explained in the section on structural properties of surface textured ZnO, can be explained in terms of the structural properties and the kinetic energy of the adatoms during growth. The surface morphological variations shown in figure 16 can be explained in terms of the growth orientations of the ZnO shown in the X-ray diffraction patterns in figure 14.

The ZnO films grown at room temperature shows surface morphology with rounded grains. This is an example of evolution of surface morphology with low surface mobility. When the substrate is at room temperature the adatoms do not have sufficient surface mobility. The adatoms stick at the sites where they intercept the substrate. This results in the roughness as shown in figure 16(a). When the substrate is at room temperature, where does the energy for the film formation come from? It is mentioned in the beginning that the oxidation of DEZ is an exothermic reaction. This heat energy is used for the growth of the film. However, this energy is not sufficient to make faster growth. The thickness of the ZnO film shown in figure 16(a) is 95nm. The growth rate is 1.05Å /sec. The reduction in growth rate is also due to the fact that at low substrate temperatures the reaction between water and DEZ is highly reduced on the surface of the substrate. It is the same film that would grow on the walls of the reaction chamber. The growth orientation shows that it is non equilibrium growth.

As the substrate temperature increases, the non equilibrium growth along $[10\bar{1}0]$ direction continues. Two main things happen with increase in substrate temperature. One is, as explained in the beginning, increase in the branching reactions of DEZ and water. Second is the increase in surface mobility. The orientation of growth of the films shown in figure 16(b) and 16(c) are the same like the orientation of the film shown in figure 16(a). But the difference is the surface mobility during growth. That means, the film shown in figure 16(a) should have the same

surface morphology like the ones shown in 16(b) or 16(c), if the surface mobility is higher. Figure 16(a), 16(b) and 16 (c) show three important classes of surface morphologies.

• In figure 16(a), the atoms in the growing films *do not have enough* kinetic energy for the movement inside the grain and on the substrate.-example of roughness that results due to so called 'statistical fluctuation of thickness'. We call this 'low surface mobility growth'.

• In figure 16(b), the film has *enough* surface mobility to make the movement in the grains and it leads the growth of film with *smooth surface* so that the surface energy of the film is minimised. We call this 'normal growth'.

• In figure 16(c), the film *has high surface mobility* so that the adatoms can move in the grains and even on the surface of the substrates. This leads to the growth along the minimum energy crystal planes of the growing planes. This makes the film to grow with a regularly faceted rough surface. We call this 'intensified growth'.

All these three films have c-axis parallel to the substrate. Until now, it is believed that for the surface textured growth of ZnO, the film 'should have c-axis parallel to the substrate'[10, 11, 12, 13,23]. However, as is seen, the control over the orientation of the film is just one of the criterion [24] to have surface textured growth.

At 275°C the film has a transition in the growth direction. The film has an abnormal preferred orientation along $[10\bar{1}1]$. The surface morphology is shown in figure 16(d). It has high surface roughness as also seen in the diffuse transmittance shown in figure 10.

Further increase in substrate temperature gives rise to the growth of $(11\bar{2}2)$ plane in addition to the growth of $(10\bar{1}1)$ planes. Here the $(11\bar{2}2)$ have the dominant orientation. These films have reduced surface roughness (see figure 10). It means that the surface mobility for the formation of facets along $(11\bar{2}2)$ and $(10\bar{1}1)$ planes are reduced. The surface morphology of the films with abnormal orientations may be compared with the surface morphology of the centre of the fourlings of the tetrapode-like ZnO crystals [25] whose structure is considered either as cubic [26] or fourfold twin structure with $\{11\bar{2}2\}$ planes [27].

At 360°C, growth orientation of the films again change to $[10\bar{1}0]$ direction. With high surface mobility at substrate temperature of 360°C, the film growth enhances the uniform facets along $[10\bar{1}0]$ direction as shown in figure 16(f). This can be compared with figure 16(c).The common thing between the two films is that both have the c-axis of the hexagonal crystal system parallel to the substrate. But the film shown in figure 16(c) has both $[10\bar{1}1]$ and $[11\bar{2}0]$ orientations with relatively low surface mobility and the film grown at the substrate temperature of 360°C (shown in figure 16(f)) has mainly $[10\bar{1}1]$ orientation with high surface mobility.

It is to be noted that the change in the substrate temperature could make wide variations in the structural properties and the resulting film properties.

3.10.3.4.2 VARIATION IN THE DOPANTS

The SEM photographs of surface morphology of ZnO films grown with different flow rates of the doping gas TMB are shown in figure 17. The substrate temperature was kept constant at 380°C. The total working pressure was 0.5 m bar. The ratio of water to DEZ was 1.7. The roughness of the ZnO films decreases with the increase in doping. The change in roughness shown in figure 17 can be compared with the diffuse transmittance of the same films shown in figure 13. The orientations of these films are shown in figure 15.

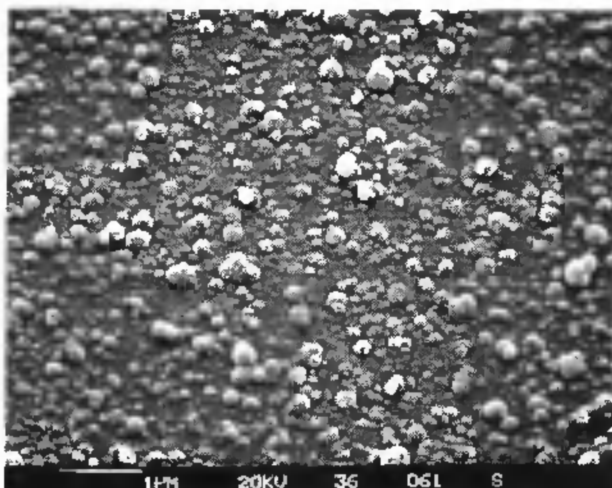


(a) Room temperature

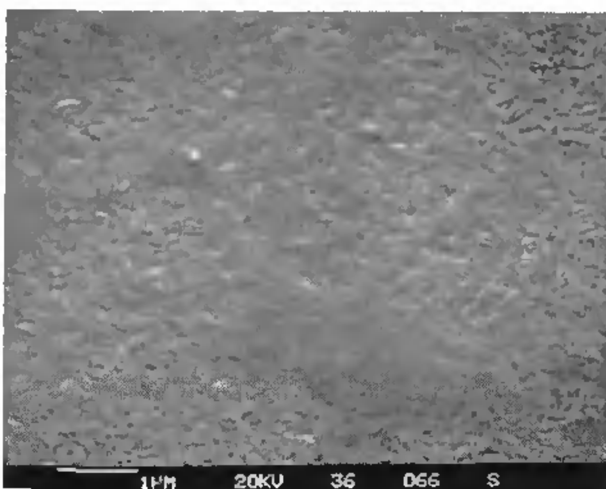


(b) 150°C

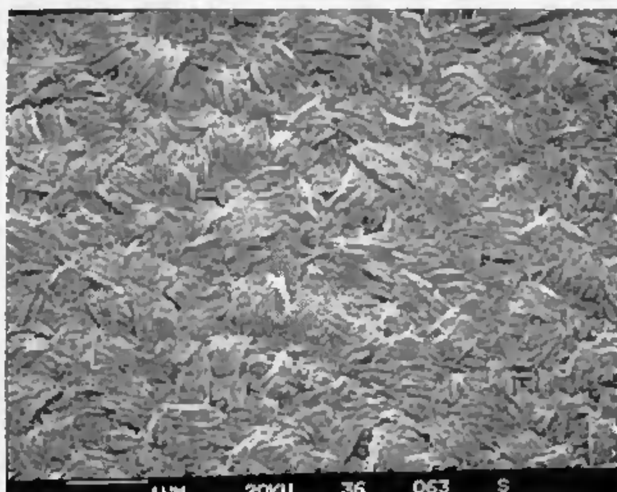


(c) 210°C

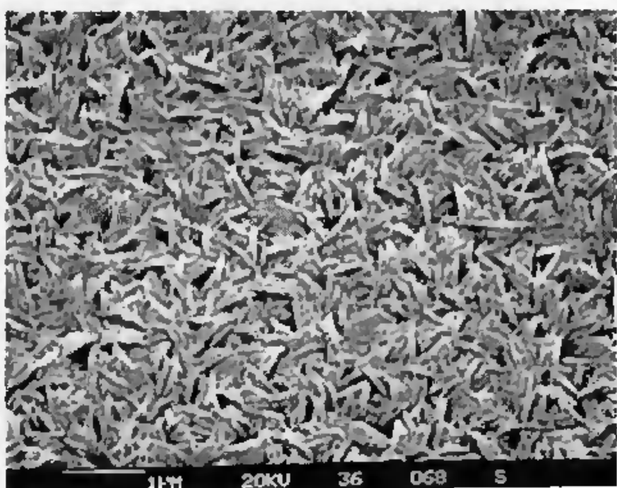


(d) 275°C

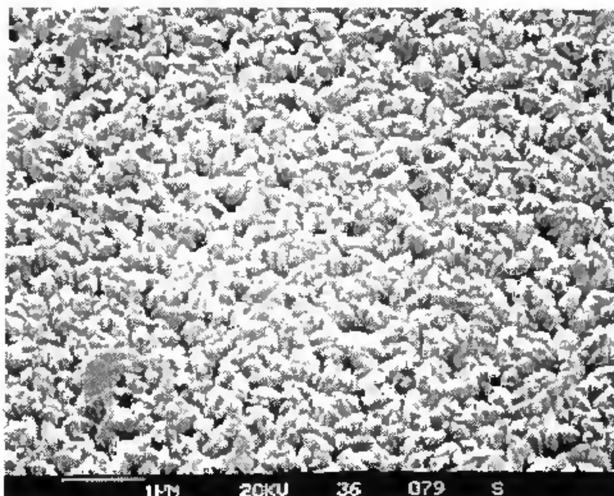


(e) 340°C

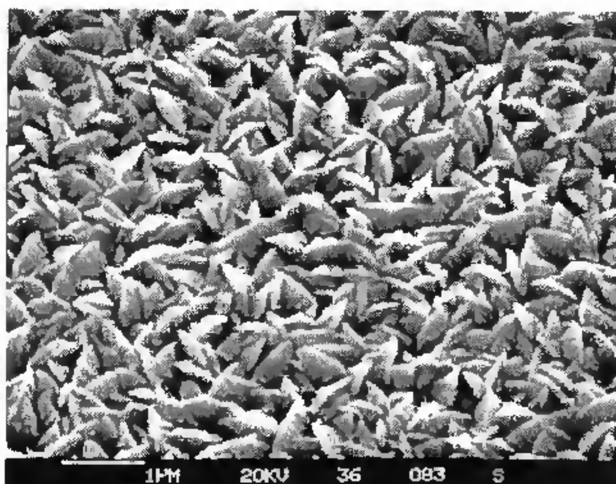


(f) 360°C

Figure 16. SEM photographs of the surface morphologies of ZnO films grown at different substrate temperatures. The water to DEZ ratio was 1.7. The flow rate of the doping gas TMB was 2sccm. The total pressure was 0.5 mbar. At 275°C there is a transition in the growth orientation. Again there is a transition in the growing direction at 360°C. Depending on the surface mobility during growth, the surface morphology reflects the orientation of the growth. (See also figure 14 and figure 10)

At high substrate temperatures of 380°C without doping ZnO grows along [0002] direction. This is the usual growing direction of ZnO by sputtering. The addition of B doping does not affect this equilibrium growth when the concentration of dopants in the film is low. When the predominant orientation is along [0002] direction, the hexagonal unit cells are standing perpendicularly on the substrates. Depending on the surface mobility during growth, these hexagons can be revealed by the surface morphology.

The ZnO film grown with the TMB flow rate of 1.5 (shown in figure 17 (b)) clearly shows the hexagons on the surface. It seems that the addition of B atoms reduces the surface mobility. Still, the surface morphology belongs to the 'high surface mobility' category. A closer look at figure 17(b) shows the hexagonal grains corresponding to [0002] orientation as well as the grains corresponding to [10 $\bar{1}$ 1] (see figure 15) orientation. *The hexagon perpendicular to the substrates does not give a morphology similar to the 'columnar morphology' obtained by sputtering*. This will be discussed later.

When the flow rate of TMB is increased further to 3 or 4 sccm, the equilibrium growth gets modified and the preferred orientation is [11$\bar{2}$0]. The surface morphology of the films correspond to the orientation along [11$\bar{2}$0] direction. *However, as the surface mobility is constantly reduced due to the addition of B atoms, the films have less surface roughness*. At the TMB flow rate of 6 sccm, the film shows almost smooth surface. *It shows clearly that the dopants are perturbing the growth*. Hence at very high concentration of doping one may expect a surface roughness of low surface mobility, similar to the one shown in figure 16(a).

Figure 17(d) can be compared with figure 16(e). The main difference between the growth condition of the two films is that the first one is grown at high substrate temperature and at high dopant concentrations and the second is grown at reduced substrate temperature and reduced dopant concentration. Both the films have *similar orientations* but different grain sizes (due to the difference in the substrate temperature). The surface mobility during growth is modified in both cases. The surface morphology shown in figure 17(d) would have the surface morphology like the one shown in figure 16(c), if the surface mobility during growth is increased.

### 3.10.3.5 The surface texture growth mechanism in CVD process.

#### 3.10.3.5.1 Ambiguities about the surface texture growth

In the ZnO literature, the evolution of surface roughness has been an ambiguous thing. First the roughness of the ZnO films grown by CVD has different morphologies. These morphologies were called 'tetropod like' morphology, 'cigar like' morphology etc. On the other hand, the ZnO growers, by sputtering got a surface morphology which is completely different from the ones got by CVD.

The reason to have surface roughness also has been misunderstood in many cases. H. Iida et al. [28, 29] in some of the first reports about surface textured TCO ($SnO_2$), refers the surface roughness as 'grain size'. T. Minami et al. [2] for the surface texture growth of ZnO by sputtering observed that the milky color of the film may not be related with the 'grain size'. This is well explained in the section on the AFM studies of surface textured ZnO. The connection between surface roughness and the grain size depends on the type of surface morphology. For example, a granular type surface mountain may have more than one grain. And a columnar type surface mountain *may* correspond to one grain ( see section 3.2).

W. Winas [11-13] claimed that 'for the growth of surface textured ZnO, the film should have c-axis parallel to the substrate'. According to H. Sato [30,23] et al the origin of the formation of textured surface is the 'suppression of the c-axis orientation'. Tokio Nakada who grew surface textured ZnO by sputtering could not agree [23] this statement as the textured ZnO by sputtering grew with the c-axis perpendicular to the substrates. By the present systematic and

detailed study on the surface texture growth of ZnO, we understand that these statements do not give the correct picture of the surface texture growth of ZnO.

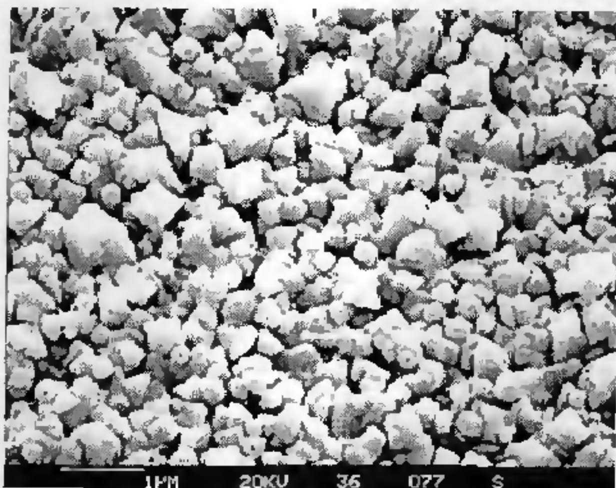


(a) TMB=0 sccm

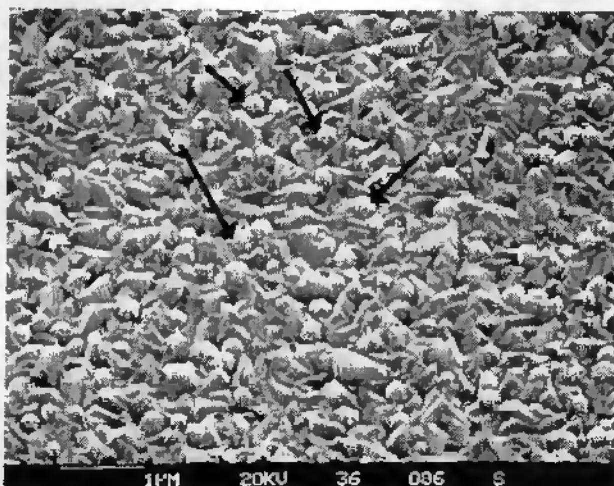


(b) TMB=1.5 sccm

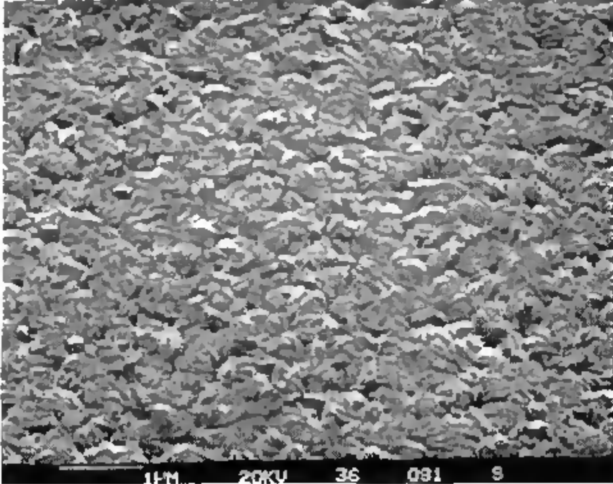


(c) TMB=3

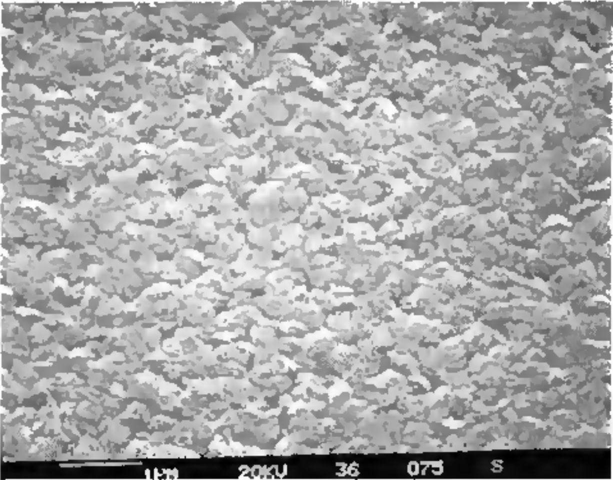


(d) TMB=4sccm

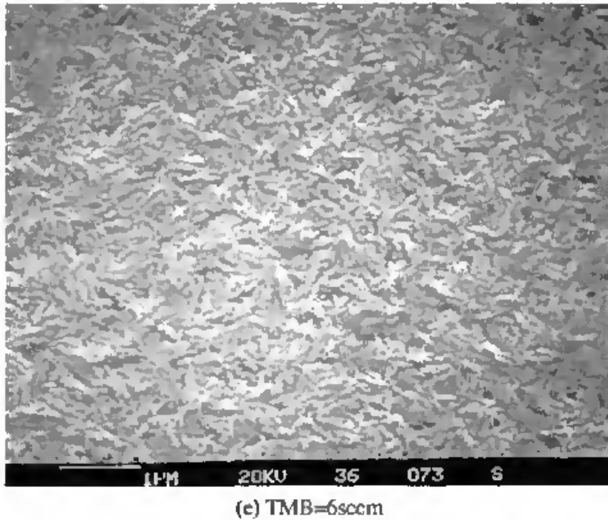


(e) TMB=6sccm

Figure 17. SEM photographs of the surface morphologies of ZnO films grown at different flow rates of the doping gas TMB. The water to DEZ ratio was 1.7. The substrate temperature was 380°C. The total pressure was 0.5 mbar. When the flow rate is low the films grow with c-axis perpendicular to the substrate. At more TMB flow rates, the growth gets modified to non equilibrium growth of ZnO. Depending on the surface mobility during growth, the surface morphology reflects the orientation of the growth. (see also figure 15 and figure 13)

3.10.3.5.2 SURFACE TEXTURE MECHANISM IN CVD

The surface texture growth of ZnO by sputtering has been analysed in detail in the previous chapters. Here it is noted that depending on the method, the surface morphologies are different even if the orientations are the same (for example the orientation of the ZnO films grown at substrate temperatures of 380°C with low doping has [0002] orientation similar to the films grown by sputtering. But they possess different surface morphologies although one could identify hexagons on the surface. To explain this, we select three samples with the three main orientations. Figure 18 shows the surface morphology of ZnO films grown with the three main orientations, namely [0002], $[11\bar{2}0]$ and $[10\bar{1}0]$.

Figure 18(a) shows the surface morphology of a film with c-axis perpendicular to the substrate. Figure 18(d) shows a closer look of the same surface shown in 18(a). The arrow marks show the hexagons on the surface. As is seen *the hexagons are not formed by the action of etching. That is, there are no etch pits, instead there are hexagonal pyramids*. By sputtering, it is seen that the hexagons on the surface of the surface textured ZnO is the action of etching of dissociated water molecules in the plasma. Here by CVD, there is *growth along the minimum energy plane*, that is, (0002) plane. The morphology of unit cells of ZnO with different growth orientations are shown in figure 19.

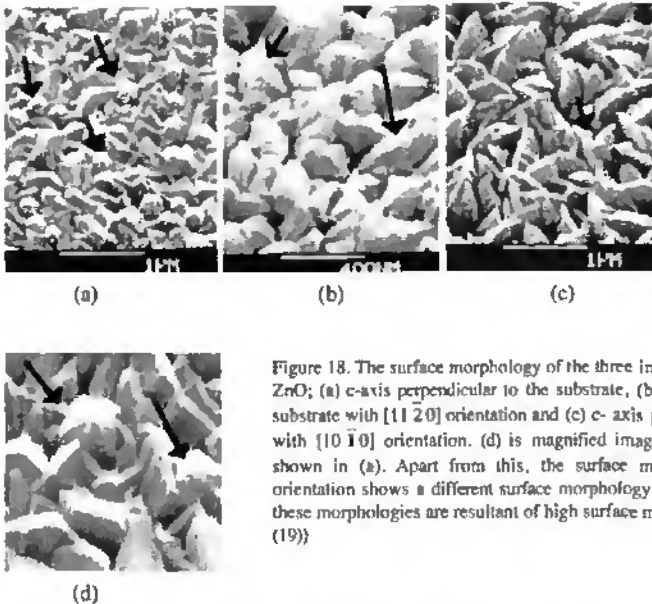

Figure 18. The surface morphology of the three important orientations of ZnO; (a) c-axis perpendicular to the substrate, (b) c-axis parallel to the substrate with [11$\bar{2}$0] orientation and (c) c- axis parallel to the substrate with [10$\bar{1}$0] orientation. (d) is magnified image of the same surface shown in (a). Apart from this, the surface morphology of [10$\bar{1}$1] orientation shows a different surface morphology (see figure 16(d)). All these morphologies are resultant of high surface mobility. (also see figure (19))

In figure 19(a), the growth habit of unit cell of ZnO with its c-axis perpendicular to the substrate is shown. Such a growth is possible when the 'c/a' ratio of the lattice parameters of the hexagonal system is greater than 1 (that is, the lattice parameter 'c' is greater than the lattice parameter 'a'). For ZnO the c/a ratio is 1.60. However, this growth is enhanced when there is very high surface mobility so that the adatoms move inside the grains as well as on the surface of the substrate. Figure 18(a) and 18(d) shows the surface hexagons of ZnO grown which is similar to figure 19(a). Clearly, the growth of surface textured ZnO by CVD is growth of adatoms along the minimum energy directions.

In non equilibrium growth conditions either [10$\bar{1}$0] or [11$\bar{2}$0] orientations will result. The morphology of unit cells of ZnO in these cases are shown in figures 19(b) and 19(c). With those figures, it is easy to figure out the surface 'hexagons' of ZnO in SEM photographs of surface morphology of the corresponding ZnO films shown in figure 18(b) and 18(c). In figure 19(b) the [11$\bar{2}$0] is the orientation of the growth and in figure 19(c) the [10$\bar{1}$0] is the orientation of the growth. In these cases the hexagons are not exposed to the surface but they are being perpendicular to the substrate since the c-axis is parallel to the substrate. The surface morphologies clearly reflects the orientation of the growing films [32].

It is important to note that the orientation of the film alone does not say anything about the surface morphology of the film [24]. But by the growth conditions, in particular, by increasing the surface mobility of adatoms, these orientations can be realised on the surface[31]. Since we do get smooth films as well as rough films in *all* orientations.

By this, the growth mechanism of surface texture growth by CVD is readily understood. It may not be appropoiate to make general rules based on 'c-axis parallel to the substrate'. One should, thus have the knowledge of the growth conditions. This may differ from system to system.

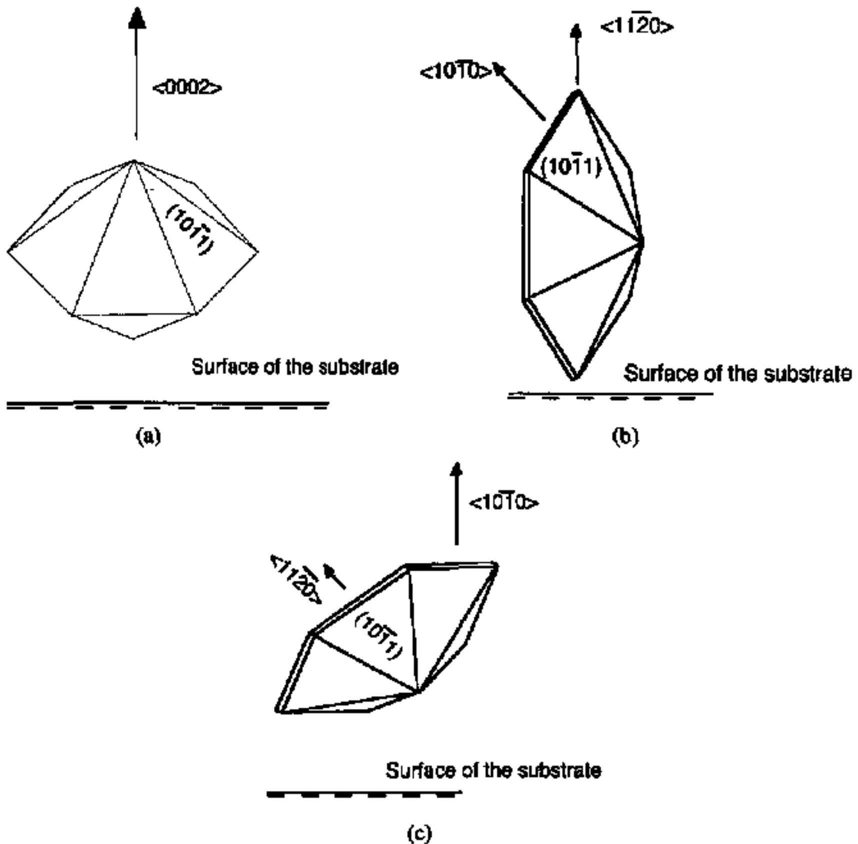


Figure 19. The morphology of unit cell of ZnO with different orientations during growth by CVD. When the surface mobility of adatoms is very high, these orientations are exhibited on the surface (see figure 18). This can be compared to the columnar morphology obtained by sputtering (figure 8 of section 3.6).

## 3.10.3.6 COMPARISON BETWEEN ZnO GROWN BY SPUTTERING AND BY CVD

The main reasons to analyse the growth of ZnO by CVD is to analyse the surface texture growth of ZnO in general as well as to compare the properties of ZnO grown by sputtering and by CVD. Since CVD and sputtering are the two major processes for the fabrication of thin films for large scale purposes, it is important to know the differences in the properties of the same film grown by different methods. In this chapter, we have analysed the growth of ZnO by CVD and in previous chapters the growth of ZnO by sputtering has been analysed in detail. Now we can compare the properties of ZnO grown by these two processes.

### 1. THE MECHANISMS OF SURFACE TEXTURE GROWTH

The surface texture growth of ZnO by CVD and sputtering follow different mechanisms and this has been explained above.

During sputtering using only Ar, we have the knocking of atoms and molecules from the target material. Without using water vapour, it is a physical vapour deposition. When the water is introduced in the plasma the oxygen and OH-group molecules from the dissociated water vapour makes the deposition process a reactive one.

During Ar sputtering, in normal growth conditions the adatoms have sufficient surface mobility. In normal growth conditions all the films have smooth (or flat) surface. When the growth takes place with very high surface mobility during sputtering, the growing film is constantly exposed to high energy bombardment of species from the plasma. This leads to etching of the surface of the growing films. The surface texture growth by sputtering is basically a combined action of *etching plus growth.* The action of etching is also possible with only Ar gas when the RF power is high.

On the other hand the surface texture growth by CVD is, as seen in this section, a growth of the film along the minimum energy crystallographic directions. We classify the surface textured growth by CVD into three categories

1. *Intensified Growth*; At high surface mobility the growth leads to a film with regularly faceted grains. As the growth is more than the normal growth by which a flat or smooth surface is obtained, it is called 'intensified growth'.

2. *Normal Growth:* Here *normal growth* means a growth with sufficient surface mobility so that the growing film has smooth surface in order to minimise the surface free energy of the film.

3. *Low surface mobility Growth* ; A low surface mobility growth that leads to the growth of rounded or granular grains: The adatoms grow just at the sites where they intercept the substrate.

The basic difference in surface texture growth of ZnO by sputtering while comparing with CVD is as follows. By sputtering even when the surface mobility of adatoms during growth are very high, an intensified growth along the minimum energy planes are not possible. That is *a surface texture of 'intensified growth' type can not be achieved by sputtering*. The main reason for the surface texture growth in the high surface mobility region is etching. On the other hand a low surface mobility growth is possible with granular grains (similar to the surface morphology of the films grown at room temperature by CVD).

Results on the devices using surface textured ZnO as well as on the mechanical properties of the films show that a surface texture ZnO with surface texture of high surface mobility category (a columnar growth in sputtering, a intensified growth in CVD) is highly suitable for devices. When the film with surface texture is to be grown on a device (for example, a back reflector for pin solar cell), by sputtering method, one depends on growth plus *etching*. The initial growth of such a layer definitely affects the exposed material of the device (n layer in the present example) and hence the interface between the device and ZnO. However, this can not be considered as a disadvantage of surface texturing by sputtering as this can be easily solved by making a 'soft growth' in between. This will be explained in the next section. By CVD a problem of etching at the interface is not present.

II. FOLLOWING THE SURFACE MORPHOLOGY OF THE SUBSTRATE OR DEVICE

As the surface texture growth suitable for device requires a surface texture of high surface mobility (intensified growth), in both sputtering and CVD processes the adatoms move on the grains as well as on the surface during the growth at high surface mobility. This makes the growing thin film (ZnO) to follow the surface morphology of substrate or the device. However, during sputtering, the bombardment of high energy atoms and molecules on the device should be considered. On the other hand, for growth of flat films, both methods offer high quality 'surface covering' of the substrate. A surface texture growth of low surface mobility in both cases (granular morphology in sputtering) may not cover the surface morphology of the substrate and devices.

III. EQUILIBRIUM GROWTH AND NON EQUILIBRIUM GROWTH

By sputtering with only Ar, almost all ways one gets [0002] orientation. It is explained in section 2 that many changes in the growth conditions do not make any change in this 'c- axis perpendicular orientation'. This is the equilibrium growth of ZnO. By sputtering we get only c-axis perpendicular orientation. There is no other orientation present in the films.

Hence it is nature of sputtering that gives rise to fiber texture orientation of ZnO. *To have a non equilibrium growth by sputtering one has to make external efforts* like adding water vapour or oxygen during growth. However, the device quality surface textured ZnO can be obtained only with the c-axis perpendicular orientation.

By CVD one has wide choice of deposition conditions to change the orientations of growing films. It is always easy to obtain a non equilibrium growth along $[10\bar{1}0]$ or $[11\bar{2}0]$ directions. In fact, for the equilibrium growth one has to take special efforts (for example, high substrate temperature and reduced concentration of dopants). However, this never gives only c-axis orientation. Always there are other orientations present in the film. *This shows that the films do not have complete columnar structure*. By CVD one has *a variety of surface morphologies and ability to get different orientations*.

Hence basically, sputtering leads to equilibrium growth and CVD leads to non equilibrium growth

IV. GROWTH RATE

The maximum deposition rate of a surface textured ZnO is 4.5Å/sec. The maximum deposition rate of surface textured ZnO by CVD, in the present case is 26Å/sec. This is certainly a great advantage of the growth of ZnO by CVD.

V. ADVANTAGES OF CVD

By CVD one has variety of orientations. It posses a variety of surface morphologies. It has a high growth rate. The ease to the change deposition conditions (example-doping of ZnO) gives a good freedom to obtain required properties. The growth is relatively soft while comparing with sputtering. This makes the growth that leads to high quality interface during device fabrication.

All the above mentioned advantages of CVD may not be obtained by sputtering. The growth during sputtering(with Ar) is always in equilibrium.

VI. MECHANICAL PROPERTIES

As the growth mechanism of sputtering and CVD are different they have their consequences in the film properties. For example a sputtered material has high mechanical strength while comparing with a CVD grown ZnO. By sputtering the film growth is at equilibrium. By CVD, the film growth is mostly at non equilibrium. A non equilibrium growth is a meta stable one. When there is a perturbation, the material tends to come to the equilibrium condition. A non equilibrium grown material (c-axis parallel), on annealing, however, did not show deterioration of the non equilibrium growth but it improved the orientation [22]. Anyhow such a orientation is not mechanically stable. Hence most of the time ZnO grown by CVD is not mechanically stable. The ZnO films grown by sputtering and CVD were kept in the same atmosphere for 36 months. The ZnO grown by sputtering has an excellent mechanical strength and the film properties have not changed. On the other hand ZnO grown by CVD showed deterioration of the surface morphology and the film properties.

The excellent mechanical properties of sputtered ZnO is used for the surface texture of the flat films. However, the post treatments in order to get surface texture can not be done for films grown by CVD, in general. A ZnO grown by CVD can even be etched away by simply using water with ultrasonic agitation.

A closer observation of the growth mechanism reveals a basic difference in the film formaion. By sputtering one has a complete columnar growth. That is, there is no other grain

oriented in direction other than [0002]. By CVD, however one do not have such a growth. The *SEM pictures of the surface morphology and X-ray diffraction patterns of ZnO grown by CVD* suggest that the film by CVD growth can have several grains along the thickness. These grains are easy to be deteriorated.

As it is a general case, a mechanically stable material can still be obtained by CVD. As the orientation and the non equilibrium growth are seems to be the reasons for the poor mechanical strength of ZnO grown by CVD, the mechanical strength can be improved by modifying the orientation (to equilibrium growth).

VII. OPTICAL PROPERTIES

By sputtering and by CVD the optical absorption of ZnO films in the region of 400-600nm can be changed depending on the growth conditions. During the analysis of sputtered ZnO it was seen that when the surface texture growth is 'soft' (reduced RF power, substrate temperature), the absorption in the 400-600 wavelength region is reduced. During CVD the growth in general, is 'soft'. There is no impinging of high energetic atoms and molecules on the growing films. This reduces the defects in the material, which in turn, leads to less absorption in the 400-600nm wavelength region (see figure 9). For this reason, care should be taken to reduce this absorption when ZnO is grown by sputtering.

## 3.10.4 Conclusions

In this chapter, growth of ZnO by CVD process is analysed and it is compared with growth by sputtering. A non toxic target was used for the first time for the doping of ZnO by CVD. High electrical conductivity, transmittance and surface texture are obtained at a substrate temperature of 380°C. This is highly useful method to produce ZnO window layers for pin solar cells. The substrate temperature can be reduced below 200°C when a highly reacting gas source is used for doping.

Table I Comparison between the growth of ZnO by sputtering and CVD process(general case)

| Property | CVD | *Sputtering* |
|---|---|---|
| Usual growth | non equilibrium | equilibrium |
| Orientation | c-axis parallel, inclined and perpendicular | c-axis perpendicular |
| Surface texture growth | Intensified growth | growth plus etching |
| Growth rate | high | low |
| Fiber texture growth | mixed orientations | fiber texture growth |
| Surface Morphologies | variety of morphologies depending on the orientation | columnar and granular |
| Mechanical property and resistance against environmental conditions | moderate | very good |
| Ability for post treatments of the grown films | poor | excellent |
| Growth of surface textured ZnO on device | good | etching the device is possible |

The surface texture growth of CVD has been understood in terms of the structural properties. The methods of sputtering and CVD were compared with each other. The main results

are given in table 1. The table lists the properties observed in general cases of growth by CVD and sputtering. However, the detailed study of both the methods (in previous sections as well as the current section) shows that by understanding the growth process, it is always possible to achieve many of the important properties by both methods.

## References


[1] Tokio Nakada, Y. Ohkubo and A. Kunioka, J. J. App. Phys 30, 12A, 1991, 3344-3348.
[2] T. Mianmi, H. Sonohara, S. Takata and I. Fuckuda J. Vac. Sci. Tech. A 13(3), 1995 1053.
[3] C. K. Lau, S. K. Tiku and K. M. Lakin, J. Electrochem. Soc. 127, 1980,1843.
[4] M. Shimizu, T. Horii, T. Shiosaki, and A. Kawabata, thin solid films 96, 1982, 149
[5] F. T. J. Smith, Appl. Phys. Lett. 43, 1983, 1108.
[6] P. J. Wright, R. J. M. Griffiths and B. Cockayne, J. Crys. Growth 66, 1984, 26.
[7] S. Oda, H. Tokunaga, N. Kitajima, J. Hanna, I. Shimizu and H. Kokado, Jpn. J. Appl.Phys. 24, 1985, 1607.
[8] P. Souletie, S. Bethke, B. W. Wessels and H. Pan, J. Cryst. Growth 86, 1988, 248.
[9] T. Maruyama and A. Nakai, Jpn. J. Appl. Phys. 28, 1989, L346.
[10] A. Yamada, W. W. Wenas, M. Yoshino, M. Konagai and K. Takahashi J. J. App. Phy. V.30, 7A, 1991, L1152-1154.
[11] W. W. Winas, A. YaMada, M. Konagai and K. Takahashi, Proceedings of 12th European Photovolataic conference 11-15 1994, p385.
[12] W. W. Winas, A. Yamada, K. Takahashi, M. Yoshino and M. Konagai J. Appl. Phy 70(11),1991, 7119.
[13] W. W. Winas, A.Yamada, M. Konagai and K. Takahashi, J.J. App.Phys 1991 L441-443.
[14] J.Hu and R. G. Gordon.Solar cells, 30 (1991) 437-450.
[15] J.Hu and R. G. Gordon.J.App. Phys. 71(2), 15, 1992.
[16] J.Hu and R. G. Gordon. J.App. Phys. 72 (11) 1992, 5381.
[17] J.Cuperus and U.Kroll 'User manual of ZnO deposition sytem' IMT Progress Report, December 1996.
[18] U. Kroll, IMT Progress Report, October 1996.
[19] A. P. Roth and G. F. Williams J. Appl. Phys. 52 (11) 1981.
[20] B. J. Balinga and S. K. Ghandhi, J. Appl. Phys. 44, 990 (1973).
[21] Morito Matsuoka and Ken'ichi Ono Appl. Phy. Lett. 53 (15) 1988.
[22] N. Fujimura, T. Nishihara, S. Goto, J. Xu, T. Ito, J. Cryst. Growth 130 (1993) p.269-279
[23] T. Nakada, N. Murakami and A. Kunioka in Thin films for Photovoltaics and Related Device Applications Edited by David Ginley, Anthony Catalona, Hans W. Schock, Chris Eberspacher, Terry M. Pereson, Takahiro Wada MRS proceedings, volume 426(1996), p411.
[24] J. A. Anna Selvan, H. Keppner, U. Kroll, J. Cuperus and A. Shah, T. Adatte, N. Randall in Polycrystalline Thin Films: Structure, Texture and Applications, Material Research Socity, spring 1997, (in press).
[25] M. Kitano, T. Hamabe and S. Maeda J. Crystal. Growth 102 (1990) 965-973.
[26] M. Shiojiri and C. Kaito, J. Crystal Growth 52 (1981) 173.
[27] G. W. Sears, R. Powell and B. Donn, J. Chem. Phys. 39 (1963) 2248.
[28] H. Ida, N. Shiba, T. Mishuka, H. Karasawa, A. Ito, M. Yamanaka and Y. Hayashi, IEEE electron device letters, Vol. 4, No.5,1983 153.
[29] H. Ida ,T. Mishuku, A. Ito, Y. Hayashi IEEE trans. on Elec. Devices Vol. 34, 1987.
[30] H. Sato, T. Minami, T. Maya, S. Tacit and M. ICI, Thin solid films 246 (1994) 65.
[31] *Symmetry Scapes Award, Material ResearchSociety, 1997, San Francisco (J. A. Anna Selvan and coworkers)*
[32] J. A. Anna Selvan, H. Keppner, U. Kroll, J. Cuperus, T. Adatte, C. Ketterer and A. Shah. Helvetica Physica Acta 70 S9-S10.

# 4

# Incorporation of ZnO film into solar cells

The present work is the study of ZnO as a Transparent Conducting Oxide (TCO) so that the films can be applied to the devices, efficiently. The application of ZnO to thin film solar cells was the major aim of the analysis of the growth and properties of ZnO. In this section the application of ZnO films in the thin film solar cells will be analysed. Flat films, surface textured thin films of ZnO were applied to thin film solar cells and the results will be shown in this section. The consideration one has to make for the deposition of ZnO on the device will also be presented.

## 4.1 Experimental

Doped ZnO films were applied to two sorts of solar cells. One has P/I/N and the other has N/IP configuration. In P/I/N configuration the substrate is glass and the light for solar cell action enters through the P side of the device (see figure 1 in section 3.1). For N/I/P solar cells the substrate is usually a metallic or flexible polymer one. For the present study the metal substrates made up of stainless steel were used. The active photovoltaic material is either hydrogenated amorphous silicon (a-Si:H) or hydrogenated microcrystalline silicon (μc-Si:H). The cells were produced by PECVD using Very High Frequency-Glow Discharge Plasma (VHF-GD) method. The solar cells were analysed for their spectral response and current-voltage characteristics. ZnO can be applied to the solar cells as a top window layer or as a bottom back reflector. In the present study the application of ZnO as back reflector as well as diffusion barrier is given the main emphasis.

## 4.2 Results and Discussion

### 4.2.1 Back reflectors for Microcrystalline silicon solar cells (NIP structure).

Microcrystalline cells were deposited on stainless steel/Ag/ZnO substrates. For this, surface textured ZnO films were grown by sputtering using water vapour and Ar mixtures on silver deposited stainless steel substrates. The details of surface texture growth of ZnO under different deposition conditions were presented in section 3.9. The ZnO films on Ag/stainless steel had differed in their properties, mainly, in the surface roughness and in the resulting optical properties. The cells deposited were of around 3.6μm thickness. The structure of the cell is stainless steel/Ag/tex.ZnO/N/I/P/ITO. The cells were deposited in a single chamber parallel-plate reactor by the VHF-GD technique [1,2,3,4]. The i-layer was deposited with 5% of silane diluted in hydrogen at substrate temperature of 200° C at a high frequency power of 22W and an excitation frequency of 130MHz. More details about the active part of solar cell are given else where [1]. Here our aim is to see if the variation in the properties of ZnO can make any change in the performance of the cell.

It is appropriate here to mention the meaning of spectral response. The electron hole pair creation of a semiconductor caused by a monochromatic light is given by

$$G= (1-R)\alpha N\exp(-\alpha x) \qquad (1)$$

where N is the incident photon flux. Other symbols have the usual meanings. For a short wavelength region the absorption coefficient is very high so that the light is immediately absorbed upon entering the semiconductor. Normally the solar cells are not very efficient at collecting light generated near the surface. At intermediate wavelength, $\alpha$ is smaller and the large proportion of the carriers are generated in regions where the collection probability is high. The quantum collection efficiency (number of electrons flowing in the external short circuiting lead per incident photon in the monochromatic light) therefore increases. *At long wavelength region, light is absorbed very weakly and only a small proportion is absorbed in the active region of the cell.* The quantum collection efficiency therefore decreases. When the photon energy is insufficient to make electron hole pair, the quantum energy becomes zero. The purpose of back reflector is to give the longer wavelength light more chances to be absorbed. A rough back contact is more efficient than the flat one.

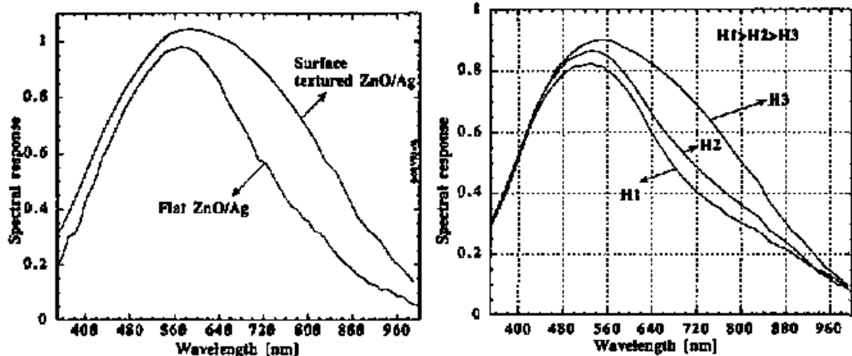


Figure 1 (left). Spectral response of microcrystalline solar cell using flat and surface textured ZnO. The substantial increase in the response of the 650nm to 1000nm wave length region is due to the surface texture of ZnO film.

Figure 2 (right). The spectral response of microcrystalline solar with surface textured ZnO/Ag back reflectors of *different haze values. The ZnO was grown at different substrate temperature values. H1= 75°C, H2=100°C,* H3=room temperature. Partial pressure of water vapour during the growth of ZnO was 1.5 x $10^{-3}$ m bar. The RF power was 225W. The figure shows how the surface morphology of ZnO can affect the performance of solar cell. The haze value of H3> the haze value of H2> the haze value of H3. This shows just by haze factor it is difficult to predict the performance of the cell. The reasons for this behaviour is explained in the text.

Figure 1 shows the spectral response of the solar cell with flat ZnO and surface textured ZnO as back contacts. The aim of using a back reflector was explained in sections 3.1 and 3.9. To mention here, the aim is to reflect back *efficiently* the light that is weakly absorbed by the solar cell so that one increases the amount of light going inside the cell hence the performance of the solar cell. It is also explained that the main aim of having surface texture is to increase the optical path length of the light that is reflected back in to the device. The effect of a back reflector is seen in the wavelength region of 650nm to 1000nm. In figure 1 it is clearly seen thet the surface textured ZnO increases the spectral response in the wavelength region between 650nm-1000nm.

Surface textured ZnO was deposited with different surface temperatures and the properties of these films were explained in section 3.9. The ZnO/Ag/stainless steel substrates were used for the deposition of above mentioned N/I/P solar cell. The spectral response of the same cells deposited on different ZnO films are shown in figure 2. First, clearly it is observed *that the change in the surface morphology of the ZnO affects the performance of the solar cell.* When the

haze factor of ZnO films vary, the spectral response of the solar cell in the wavelength region of 650nm-1000nm also varies.

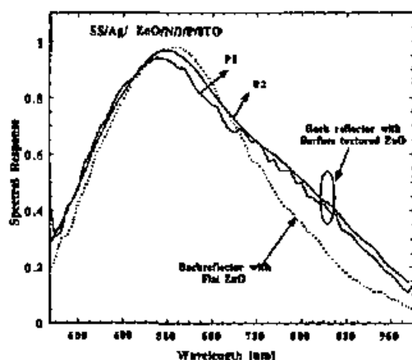


Figure 3. Spectral response of Microcrystalline solar cell using flat and surface textured ZnO as back reflectors. The ZnO films in cells p1 and p2 were grown at 250W and 150W respectively. When the surface texture in general makes a distinct enhancement in the spectral response, the variation in the surface roughness of P1 and P2 is not strongly pronounced in the device performance.

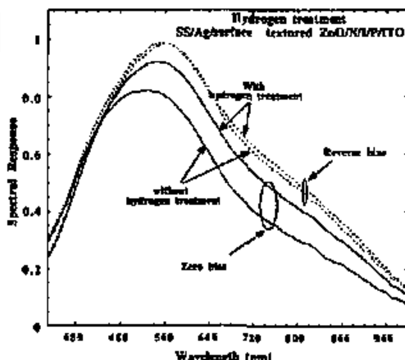


Figure 4. Effect of hydrogen treatment on the surface textured ZnO before depositing Si. The figure shows the spectral response of similar cell with and without hydrogen treatment. At a reverse bias voltage of -4v, both the cells have almost same spectral response. However, at zero bias there is a considerable difference in the cell performance.

The ZnO film corresponding to curve H1 was grown at 75°C, the ZnO corresponding to curve H2 was grown at 100°C and the ZnO corresponding to curve H3 was grown at room temperature. The diffuse reflectance and hence the haze factor of the films (see section 3.9) shows the following trend. Haze factor of sample H1> the haze factor of sample H2> haze factor of the sample H3. The increase in haze factor corresponds to a reduction in the cell performance in the 'back reflection region'. Certainly we do not expect this trend.

The reason for no improvement or reduced improvement for cell performance with increase in diffuse reflectance may be the one of the followings.

1. The measurement of diffuse reflectance or diffuse transmittance and hence the haze factor. There is always a cone of light which is escaping with the direct beam. This is never seen as a diffuse light. This makes a change in the measured haze factor of the film. Also a surface roughness with such a 'diffuse light' may be advantageous.

2. The surface morphology. Clearly this factor plays an important role. The angular distribution of diffuse reflectance depends on the surface morphology. As the substrate temperature during sputtering is reduced, the surface morphology of ZnO changes from mixed columnar and granular morphology to granular morphology. This changes the way how the light is reflected back in the cell. Furthermore, this changes the way how the device is deposited on the surface textured substrates. Also when the deposition conditions changes, the size of the surface mountains of ZnO changes. At low substrate temperature there may be surface peaks with a size corresponding to the resonance scattering of light of wavelength from 650 to 900nm.

In any case, it is not meaningful to predict the performance [5] of solar cell based on the haze factor measurement.

In figure 3 the spectral response of the micro crystalline silicon solar cells with back reflectors of flat ZnO and surface textured ZnO are shown. Clearly, the increase in current in the

long wave length region is due to the surface texture of ZnO. The ZnO films for the curves P1 and P2 were grown by sputtering with water vapour at different RF power values of 250W and 150W respectively. The haze factor or the surface roughness of ZnO sample corresponding to P1 is more than the haze factor of ZnO sample corresponding to P2. Both films have columnar morphology with reduced sizes of hexagons on the surface due to the reduction in the RF power during sputtering. With the variation in the spectral response as shown in figure 3, it is not possible to say which one is advantageous. However, the interference pattern in the spectral response due to smooth surface is reduced with increase in the haze factor.

The growth of a solar cell on a surface textured ZnO substrate may not yield a proper junction between the cell and the ohmic contact material (ZnO) in the substrate. To check this we made two sets of same microcrystalline silicon solar cells on substrates with same (a part of a same sample) surface textured ZnO. During deposition of first cell the surface of the ZnO was exposed to hydrogen plasma at 10W at substrate temperature of 200°C at a pressure of 0.8mbar for 7 minutes. Like this, the very top layer of the ZnO is etched away for few nano metres. This, does not affect the surface morphology but it reveals a new surface for the deposition of the device on it.

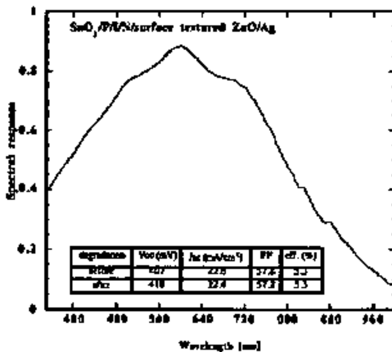

Figure 5. The spectral response of a microcrystalline silicon solar cell with surface textured ZnO grown on it. The structure of the cell is $SnO_2$/P/I/N/Ag/surface textured ZnO. The surface textured growth of ZnO on the cell by sputtering is demonstrated for the first time.

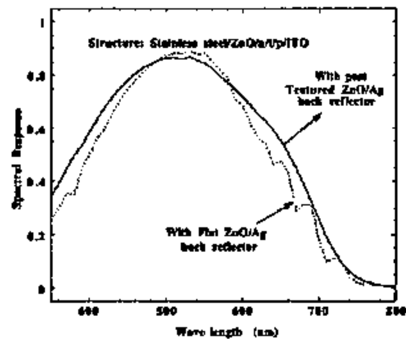


Figure 6. The spectral response of a-Si:H solar cells with structure of SS/Ag/etched ZnO/N/I/P/ITO. The surface roughness enhances the current in the 580-800 nm region. The etched ZnO can be applied to the device.

The second cell was fabricated with out this hydrogen treatment. The spectral response of both the cells with and without hydrogen treatment is shown in figure 4. As is seen the hydrogen treatment on the surface of the surface textured ZnO lead to a high quality interface. The spectral response at zero bias voltage of the cell fabricated without hydrogen treatment is inferior to the response of the cell fabricated with hydrogen treatment. At increased reverse bias voltage of -4 V, both the solar cells have similar spectral response.

### 4.2.2 SURFACE TEXTURE GROWTH OF ZnO ON P/I/N MICROCRYSTALLINE SILICON SOLAR CELLS FOR THE PURPOSE OF FABRICATING BACK REFLECTORS.

The advantage of surface texture growth is realised when one has to grow such a layer on a cell. Application of a post-treatment to obtain surface texturing is not practical for this purpose. The surface textured growth of ZnO by using water vapour and Ar mixtures during sputtering was done on microcrystalline solar cells. The spectral response of the solar cell is shown in figure 5. For the fabrication of the cells, the i layers were deposited at a dilution level of 2.5% silane into a total gas flow of hydrogen and silane at an effective substrate temperature of 220°C at a high frequency power of 110 MHz. More details of the active part of the devices are given else

where [1]. The surface textured growth of ZnO was done at a substrate temperature of 150°C. The RF power was 200W. The partial pressure of water vapour during sputtering was $1.5x\ 10^{-4}$ mbar. The surface morphology of such a ZnO is mainly columnar. The spectral response of the cell has an enhanced response in the region between 650 to 1000 nm due to the surface texture of ZnO. The cells have a 22.6 $mA/cm^2$ of short circuit current density. The stabilised efficiency of the cell is 5.3%. By this, it is seen that the surface textured growth of ZnO by sputtering using water vapour can be successfully done on the cell. With this, for the first time, by sputtering the surface textured growth of ZnO on the cell is demonstrated. Similar depositions were done for the back reflection of 'micromorph' tandem solar cells [6,7,8,9,10,11] (a-Si:H/μc-Si;H stacked solar cells).

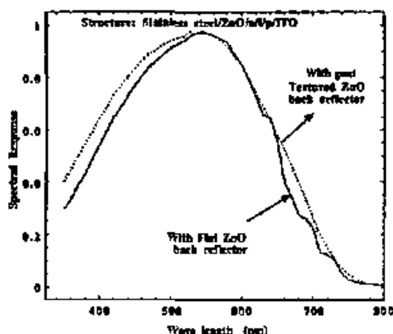


Figure 7. The spectral response of a-Si solar cells with structure of SS/etched ZnO/N/I/P/ITO. The cells are the same like the previous one but without silver layer. The effect of surface roughness is reduced without silver.

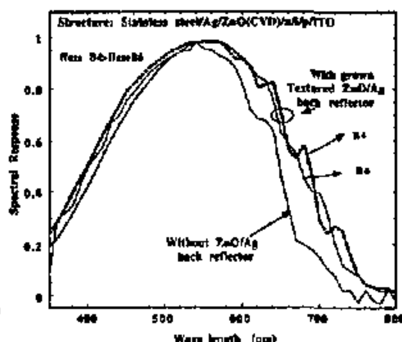


Figure 8. Spectral response of a-Si:H solar cells with SS/Ag/surface textured ZnO/N/I/P/ITO configuration. The ZnO was grown by CVD using TMB as doping gas. The small difference in the surface roughness of ZnO has very small variation in spectral response.

### 4.2.3 USE OF THE POST TEXTURED ZnO BY CHEMICAL TEXTURING METHOD AS BACK REFLECTOR IN NIP AMORPHOUS SILICON SOLAR CELLS

The making of surface texture of ZnO from flat film is explained in section on 'surface texturing of flat ZnO' (section 3.8). The ZnO, with fiber texture growth, on chemical etching reveals the hexagons on the surface. This increases the surface roughness of the ZnO films substantially. To study the use of such layers in solar cells, we fabricated amorphous silicon solar cells on the stainless steel/Ag/surface textured ZnO (by etching) substrates. For this, amorphous silicon solar cells were fabricated with i-layers of two different thickness (250nm and 500nm) values. The i-layer is deposited at around 200°C at the excitation frequency of 70MHz. The working pressure was 0.3 m bar. The <p> layer was microcrystalline SiC:H and <n> layer was microcrystalline Silicon. $PH_3$ and $B_2H_6$ diluted in hydrogen were used as the dopant sources for the doping of <p> and <n> layers respectively. More details of the active part of the devices were presented elsewhere [12].

For all the devices Argon plasma with 10W was exposed on the surface of ZnO for 5 minutes to clean the surface. Figure 6 shows the spectral response of the cells fabricated on the surface textured (etch textured) ZnO/Ag/stainless steel substrates. First of all, it shows that the surface texturing by chemical etching is compatible for the making up of the interface between the ZnO coated substrate and the device. This makes the post etching of ZnO a useful technique. In figure 6 the difference in the spectral response in the wavelength region of 550nm to 800nm (note that the wave length region for back reflectors was 650 to 1100 nm for micrcrystalline silicon solar cells) due to the surface roughness of ZnO is clearly observed. However, the increase in the

current does not correspond to the increase in the surface roughness. It is noted that when the thickness of the cell is increased (from 250nm to 500nm) the surface roughness effect in the long wave length region is reduced.

As mentioned before the response of the solar cell in the long wavelength region depends also on the shape and the size of the surface roughness or surface mountain. For the surface roughness made by anisotropically etching the crystal planes of c-axis oriented ZnO, it is always possible to change the size of the surface hexagons depending on the experimental conditions. This, however, should be investigated further. Now it is demonstrated that the chemical etching technique of highly oriented ZnO can be an efficient method to produce back reflectors for solar cells.

In figure 7 the spectral response of the same device configuration without Ag layer is shown. As is seen the effect of surface roughness is reduced without silver. This is basically due to the reduction of total and diffuse reflection of light due to the absence of silver.

### 4.2.4 ZnO grown by CVD

To see the effect of ZnO grown by CVD using TMB as doping gas, solar cells were made on the surface textured ZnO(CVD)/ Ag/stainless steel substrates. ZnO films with different surface properties were grown for this study on Ag (sputtered) coated stainless steel substrates. Different surface properties of ZnO were obtained by changing the flow rate of the doping gas TMB with a substrate temperature of 380°C. The electrical properties of ZnO also evidently vary with this variation of doping gas. The properties of the films were explained in previous section on growth of ZnO by CVD (section 3.10). An identical cell was deposited on all the substrates with surface textured ZnO. The thickness of the cell was 500nm. Figure 8 shows the spectral response of the cells mentioned above. It shows that the ZnO films grown by CVD using TMB as doping gas can be efficiently used in the solar cells. The films for the curves B4 and B6 have flow rates of TMB of 4 and 6 sccm respectively and they have small difference in the surface roughness. Samples with high surface roughness and low electrical conductivity yielded very bad solar cell performance. Table I shows the change in the cell parameters due to the change in the deposition condition of ZnO during growth. It is seen that as the resistivty of ZnO (on highly conducting Ag/SS substrates) is increased it affects the series resistance of the cell. Also differences in the roughness (low values) of the films have an impact on short circuit current density.

*Table I. The variation in the doping of ZnO and the related properties of solar cell.*

| No. | TMB flow rate | Series resistance of the cell [$\Omega$*cm$^2$] | Surface roughness - Haze factor of ZnO values(%) | Short circuit current density mA/cm$^2$ |
|---|---|---|---|---|
| 1 | 6 | 6.4 | flat | 15.426 |
| 2 | 4 | 7.6 | 1.7 | 16.044 |
| 3 | 2 | 12.1 | 5.8 | 16.81 |
| 4 | no ZnO | 7.1 | flat | 13.759 |

### 4.2.5 ZnO as top window layer in amorphous silicon solar cells

ZnO can also be used as a top window layer for thin film solar cells. Either this can be used as an anti reflection coating or as a thick ohmic contact film. When used as an anti reflection coating the thickness of ZnO can be adjusted to give minimum reflection in the wavelength region where one has maximum quantum collection efficiency of a particular device. For example, for an amorphous silicon solar cell the maximum in quantum collection efficiency can be at 525 nm. Hence the thickness of the ZnO can be adjusted to give minimum reflection at 525nm. The refractive index of ZnO is 2 and this makes it suitable for silicon as an anti reflection coating. Figure 9 shows the reflectance of ZnO/a-Si:H/window glass system. The ZnO is deposited by sputtering using Ar. The thickness of ZnO is 65nm. The minimum in reflectance at 525 nm

makes more light available for photovoltaic action at 520nm. Similarly the thickness of the ZnO can be optimised for a 'mirror layer' in between an a-Si and μC-Si solar cells [13,14]. Due to the difference in their work functions, ohmic contact of ZnO with p-type a-Si:H is normally a problem. With μc-Si:H, ZnO yields a good ohmic contact. The work function of ZnO (4.2eV) is less than the work function of ITO and $SnO_2$:F (4.8eV). For this reason, ITO was used in cases where we used a-Si:H as a p-layer[19].

Here we want to see the difference in the process of deposition of ZnO film on the performance of the solar cell. Amorphous silicon solar cells (with microcrystalline P-layer) were deposited on stainless steel substrates. Details of theses devices are presented else where [15]. For the top contact (or the window layer), thick, about 1 μm, ZnO (not AR) was deposited. For this, two sets of depositions of ZnO were made. For the first set, the ZnO films were deposited by sputtering. And for the second set ZnO films were deposited by CVD . For sputtering, the RF power was 75W. The working pressure was 5 x$10^{-3}$ mbar. The electrode separation of the sputtering system was 4.5 cm. The deposition was done at room temperature. The spectral response of the same cell with ZnO window layer deposited by two different methods is shown in figure 10. The cells with ZnO deposited by CVD shows good performance in the low wavelength region. As the only difference between the two cells is the deposition process of ZnO, there could be two reasons for this behaviour. Either there is an absorption in the material or the absorption due to the bad interface between the cell and ZnO.

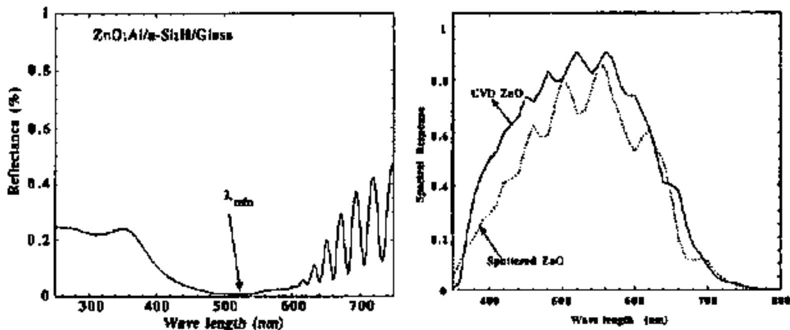


Figure 9 (left). The transmittance of thin ZnO/a-Si:H/glass. The sputtered ZnO has thickness of 65nm and this acts as an anti reflection coating.

Figure 10 (right). Effect of the deposition process on the solar cell performance. The figure shows spectral response of the same amorphous silicon solar cells with different top contacts. ZnO films were deposited by sputtering as well as by CVD. Both of the films were thick and not performing the anti reflection for the optimum wavelength. The transmittance of the same ZnO layers grown on glass do not show a considerable difference. The reason for the difference in spectral response of the cells is explained to be due to the difference in process. The process of sputtering 'spoils' the interface between the device and the ZnO. This can be overcome by a proper interface making (soft start). ZnO by CVD makes relatively smooth interface.

The transmittance of the ZnO deposited by sputtering was very high. At RF power of 75W at room temperature the material has a good electrical and optical properties. Hence, the main reason for such behaviour is the process of deposition. As explained in the previous chapter (section 3.10), CVD is a relatively soft process and the interface with the underlying layers can be of good quality. By sputtering, even though the material (ZnO) has good optical and electrical properties, the process damages the underlying device. Especially in the present example the electrode separation for sputtering is 4.5 cm. It seems that the bombardment of energetic ions and molecules damages the top layer (<p>) of the device. The poor quality interface, thus lead to an enhanced absorption in the low wavelength region, absorption that is located near the boundary between the ZnO and the <p> layer of the solar cells. This absorption does not lead to photo-

generation of carriers and is simply lost. Hence making interface by sputtering needs more care than CVD.

The problem of low quality interface or interface damage observed in sputtering can be overcome by a soft start. By this, the very first layer of ZnO is grown with low RF power. That is, the device interface is exposed to the low energetic bombardment of atoms and ions during sputtering.

#### 4.2.6 Heat mirrors with ZnO

It was seen in section 3.4 on optical properties of ZnO as well as in chapter 2 that the absorption in the near infra red wavelength region can be controlled by the deposition conditions. Generally, higher the density of free carriers in the films is, the higher will be the absorption in the lower wavelength side (of near infra red region). For an amorphous silicon solar cell the useful wavelength region is 350 to 700nm. Hence for the wavelengths not absorbed in the a-Si:H the ZnO film becomes absorbing, converting the near-IR part of the light in to heat. This can be collected by a hybrid module (thermal/photovoltaic). With this, we have used ZnO to optimise the thermal efficiency of a a-Si:H based hybrid collector [16].

#### 4.2.7 Comments on making devices with ZnO

As is seen above making interface of ZnO (or TCO) with the device in general is a crucial process. It is important to understand the growth mechanism of the ZnO on the substrate or on the device. As far as ZnO is used as a substrate material one has more freedom to get required properties. For example, the substrate with ZnO can be annealed in high substrate temperatures to increase the quality of ZnO. On the other hand, when ZnO is deposited on top of a device, the importance is given to the immediate layer deposited on the device.

By sputtering, when one makes an interface by using high RF power and low electrode separations, it may lead to poor interfaces as explained above. One may not blame the process of sputtering for such an interface. Because high quality ZnO films with unique features can be obtained by sputtering (for ex. high mechanical strength, fiber texture growth). Growing first few nano meters of ZnO with low RF power prevents the device from interface damage. However, this has not been shown in this work.

*During the surface textured growth of ZnO, independent of the process, most of the time water vapour is used.* Such a growth *on* a device needs more attention. For a normal surface texture growth the substrate is kept at a temperature of 150°C. When the water vapour is allowed in the chamber, before the reaction it has a good chance to make oxidation on the device. A thin or thick oxide layer will probably grow on the device depending on the time it is exposed to the water vapour or any source of oxide. If this would be the case, it is always possible to make a flat ZnO thin layer, which do not require water vapour during growth by sputtering, on the device and to make the surface textured growth on the flat ZnO.

During the surface textured growth it is always preferred to have *a surface roughness of high surface mobility*. The surface roughness of low surface mobility may lead to the presence of porous particles and voids at the interface.

## 4.3 Conclusions

The incorporation of surface textured ZnO and flat ZnO in to devices is demonstrated successfully. The effect of surface roughness is clearly realised in the solar cells. The connections between the shape and size of surface morphology on the cell performance is actually not straight forward. The surface morphology. (the size, the shape and the type) of the ZnO films should correspond to the structure of a device. In any case, in the present work the ways to obtain several shapes and sizes of different types of surface morphologies are well explained. With that, one can control the angle with which the light should be diffused into the cell and one can select

the wavelength of maximum diffuse light. And this, in addition to the high quality interface, lead to a 'best ZnO' for a particular cell.

## References


[1] P. Torres, J. Meier, R. Flückiger, U. Kroll, J. A. Anna Selvan, H. Keppner and A. Shah, S. D. Littlwood and I. E. Kelly and P. Giannoulès Appl. Phys. Lett. 69(10) 1996, 1373.

[2] R. Flükiger, Ph.D thesis, Institute of Microtechnology, University of Neuchâtel, 1995, ISBN 3-89191-965-4.

[3] H. Keppner, U.Kroll, J. Meier and A.Shah, Solid State Phenomena 44-46, 97 (1995).

[4] K. Prasad, Ph.D. thesis. Institute of Microtechnology, University of Neuchâtel, 1991.

[5] Hegadus, W. Buchanan, X.Liu and R. Gordon, 25th IEEE photovoltaic specialist conference, Washinton D.C 1996, pp1129.

[6] J. Meier, S. Dubail, D. Fischer, J. A. Anna Selvan, N. Pellaton Vaucher, R. Platz, C. Hof, R. Flückiger, U. Kroll, N. Wyrsch, P. Torres, H. Keppner, A. Shah, K.-D. Ufert, Proceedings of the 13th EC Photovoltaic Solar Energy Conference, Nice, October 1995, pp. 1445-1450.

[7] J. Meier, P. Torres, R. Platz, S. Dubail, U. Kroll, J.A. Anna Selvan, N. Pellaton-Vaucher, Ch. Hof, D. Fischer, H. Keppner, A. Shah, K.-D. Ufert, P. Giannoulès, J. Köhler, Proceedings of the MRS Symp., Spring Meeting, San Francisco, April 1996, Vol. 420, pp. 3-14.

[8] J. Meier, P. Torres, R. Platz, S. Dubail, U. Kroll, J.A. Anna Selvan, N. Pellaton Vaucher, Ch. Hof, D. Fischer, H. Keppner, A. Shah, K.-D. Ufert, Technical Digest of the 9th PVSEC, Miyazaki, November 1996, pp. 653-654.

[9] J. Meier, P. Torres, R. Platz, S. Dubail, U. Kroll, J.A. Anna Selvan, N. Pellaton Vaucher, Ch. Hof, D. Fischer, H. Keppner, A. Shah, Technical Digest of the 10th "Sunshine" Workshop on Thin Film Solar Cells, Tokyo, November 1996, pp. 9-17.

[10] H. Keppner, U. Kroll, P. Torres, J. Meier, R. Platz, D. Fischer, N. Beck, S. Dubail, J. A. Anna Selvan, N. Pellaton Vaucher, M. Goerlitzer, Y. Ziegler, R. Tscharner, Ch. Hof, M. Goetz, P. Pernet, N. Wyrsch, J. Vuille, J. Cuperus, A. Shah, J. Pohl, AIP Proceedings , NREL/SNL PV Program Review Meeting, Denver, November 1996.

[11] H. Keppner, P. Torres, J. Meier, R. Platz, D. Fischer, U. Kroll, N. Beck, S. Dubail, J. A. Anna Selvan, N. Pellaton Vaucher, M. Goerlitzer, Y. Ziegler, R. Tscharner, Ch. Hof, M. Goetz, P. Pernet, N. Wyrsch, J. Vuille, J. Cuperus, A. Shah, J. Pohl, Proceedings of t he MRS Symp., Fall Meeting, December 1996, Boston, 1997, Vol. 452, pp. 865-874.

[12] P. Pernet, M. Goetz and R. Felder, 'A-si solar cells on metal and plastic substrate' in proceedings of 4th euregional workshop on Amorphous silicon solar cells 1996.

[13] D. Fischer, S. Dubail, J. A. Anna Selvan, N. Pellaton Vaucher, R. Platz, Ch. Hof, U. Kroll, J. Meier, P. Torres, H. Keppner, N. Wyrsch, M. Goetz, A. Shah, K.-D.Ufert, Proceedings of the 25th IEEE Photovoltaic Specialists Conference, Washington D.C., May 1996, pp. 1053-1056.

[14] D. Fischer, H. Keppner, U. Kroll, P. Torres, J. Meier, R. Platz, S. Dubail, J. A. Anna Selvan, N. Pellaton Vaucher, Y. Ziegler, R. Tscharner, Ch. Hof, N. Beck, M. Goetz, P. Pernet, M. Goerlitzer, N. Wyrsch, J. Vuille, J. Cuperus, A. Shah, Proceedings of the 14th EC Photovoltaic Solar Energy Conference, Barcelona, July 1997.

[15] M.Goetz, Ph.D thesis University of Neuchâtel.

[16] R. Platz, D. Fischer, M.A. Zufferey, J. A. Anna Selvan, A. Haller and A.Shah, 26th IEEE phtovoltaic specialist conference, 1997, Anaheim, to be published.

[17] T. Nakada Y. Okubo and A.Kunioka IEEE photovoltaic specialists conferenc, 1991.

[18] T.Mianmi, H. Sonohara, S. Takata and I. Fuckuda J.Vac.Sci. Tech. A 13(3), 1995 1053.

[19] The work function of ZnO (4.2eV) is less than the work function of ITO and $SnO_2$:F (4.8eV). For a p type semiconductor, the metal should have higher work function than the semiconductor to form a ohmic contact. Hence ITO or $SnO_2$:F is more suitable for ohmic contact with p-type a-Si. For n-type a-Si, ZnO is more suitable as an ohmic contact.

# Summary and Conclusions

Thin film solar cells require a transparent conducting oxide with three important properties; electrical conductivity, optical transmission and surface texture. They can play crucial role for both top window layers as well as near infra red reflecting back contact. In this context ZnO has many advantages over other available TCOs. Although its potential to contribute to further cost reduction is not fully exploited, it can be considered a mandatory required for thin film solar cells. So far most of the work on ZnO was carried out looking at flat (non surface textured) films; we therefore first summarise the most striking properties of such layers.

### Flat films

ZnO films with flat surfaces can be obtained by sputtering using an oxide target of ZnO and carrying out thin film deposition with low RF power. The growth rate of such a smooth surface ZnO can be highly modified by varying RF power. The sputtering pressure of Ar has a stronger influence on the resistivity of such ZnO films. A high electrical conductivity ($4.5 \times 10^{-4}$ Ω.cm), and high optical transmittance (more than 85%) can be obtained by optimising these two parameters. Independently measured structural properties (grain size, crystallinity) have been correlated with the electro-optical properties.

An increase in RF power during sputtering can change the transmittance of ZnO in the 400-500 nm wave length region. This is explained due to the formation of colour centers that arise from intrinsic defects like ionised oxygen vacancies ($F^+$-centre) of ZnO. These intrinsic defects result from the use of high RF power. Such colour centers increase the optical absorption of a ZnO front contact in the solar cell in the short wavelength regime that lead to the loss in the blue response for the solar cell. Thus, high optical transmittance of ZnO for solar cell application requires the use of a low energetic ion impingement during sputtering.

During sputtering with Ar alone the resulting ZnO films always show fiber texture orientation along the c-axis of the hexagonal wurtzite structure of ZnO independent of the sputtering pressure, RF power and thickness. Therefore to obtain fiber texture orientation of ZnO, which is highly required for other applications of ZnO to utilise its piezoelectric properties, sputtering with Ar using an oxide target is highly preferred.

Material properties like band gap, absorption coefficient, crystallinity, doping efficiency and orientation during growth can be strongly influenced and, hence can also be controlled by understanding the growth mechanisms and, as a consequence thereof by tailoring the growth parameters.

ZnO with fiber texture orientation yields a columnar structure. Hence an optimised flat film with fiber texture growth can be post etched to obtain superior surface properties combined with high electro-optical properties. By such a post etching, the polycrystalline ZnO with fiber texture growth reveals surface morphology like a single crystalline wafer. By that using a two step process the highly wanted surface texturing of originally flat ZnO can be achieved.

### Surface textured ZnO films

Surface texturing of ZnO by sputtering can be achieved by sputtering ZnO target with a mixture of Ar and water vapour. In this work, for the first time, extremely high haze factors (>50%) could be achieved by RF magnetron sputtering. Two different surface morphologies of ZnO can be identified when employing this method; columnar and granular morphologies. The fiber texture orientation of ZnO is modified due to the addition of water vapour. This is classified as equilibrium and non equilibrium growth. With the increase in addition of water vapour the film growth which is originally in equilibrium will be changed into non equilibrium one. The equilibrium growth is associated with an appearance of columnar surface morphology and non equilibrium growth is associated with appearance of granular surface morphology. ZnO with columnar morphology has superior structural and mechanical properties when compared with

ZnO with granular morphology. The surface morphological evolution during growth has been studied in detail.

The key parameter that affects surface texture growth is the variation of surface mobility. The surface mobility can be modified by changing the partial pressure of water vapour, the RF power and the substrate temperature. High quality films are obtained with high surface mobility of adatoms during growth.

The degree of dissociation of water vapour during sputtering partially decides the surface morphology. A columnar morphology is associated with an etching action of dissociated water vapour on the growing film and with high surface mobility. A granular morphology results due to the reduction of surface mobility of adatoms during growth.

The surface roughness evolution in the atmosphere of mixture of water and Ar does not follow the classical microstuctural evolution models. The difference between the present case and the standard models is that in the present case a medium that reacts on the growing film is used as sputtering gas and in standard models sputtering with Ar is considered.

The optical properties can be substantially modified due to the surface texture. The diffuse transmittance and reflectance, the haze factor, the onset of band to band transitions, free carrier absorption and the absorption coefficient of ZnO can all be strongly influenced by the growth conditions. This has been described in detail.

Based on experimental evidences a microstuctural evolution model for ZnO is presented.

More insights on the surface morphological evolution of ZnO is obtained by looking at the CVD deposition process. Three classes of surface morphologies can be identified here. They are named as *intensified growth, normal growth and low surface mobility growth*. In normal growth the films have a smooth surface so as to reduce the surface free energy. In intensified growth, growth along the minimum energy crystallographic planes of ZnO takes place. Such a surface has uniform facets of ZnO. In the low surface mobility growth, a morphology similar to granular morphology that is obtained with sputtering results, due to the large reduction in the surface mobility of adatoms. Such a surface has a non uniform roughness.

The orientation of ZnO can be modified by changes during growth. The substrate temperature, the ratio of reacting gases, and even the doping gas play an important role in deciding the surface mobility and orientation of ZnO. The three minimum energy planes of ZnO are (0002), $(11\bar{2}0)$ and $(10\bar{1}0)$ respectively. All the three orientations can be obtained by changing the growth parameters. An abnormal growth along $[10\bar{1}0]$ can also be obtained. The reason for this orientation is explained to be either due to the effect of the dopant or to the presence of cubic structure of ZnO.

Surface morphology typical of intensified growth can be obtained for all these orientations by increasing the surface mobility during growth.

The comparison between the growth of ZnO by sputtering and CVD shows that the surface roughness of columnar morphology obtained by sputtering is always related to etching plus growth and never to an intensified growth. This is a basic difference between CVD and sputtering. On the other hand the granular morphology obtained by sputtering can be similar to that of low surface mobility growth obtained by CVD.

Understanding the growth mechanisms of surface texture growth is of great importance in order to incorporate surface-textured ZnO in devices.

With this knowledge of the growth mechanisms and of the microstructural evolution of ZnO, high quality ZnO with good electrical, optical and surface properties are obtained. Surface texture growth on Ag/Stainless steel system as well as on thin film solar cells have been demonstrated successfully.

The smooth and surface textured ZnO film were successfully incorporated into thin film solar cells. It is found that based on the haze factor alone one can *not* predict the observed

changes in the short circuit current of a solar cell. The textured surfaces of ZnO obtained by all the above mentioned methods, showed clear advantages in terms of spectral response over a flat surface ZnO when incorporated in thin film solar cells.

For the first time, one has obtained here a complete picture of growth of ZnO with smooth and rough surfaces, the analysis of the properties and their incorporation in thin film solar cells. The ways to obtain different surface morphologies with different shapes of surface peaks of ZnO (or other thin film to some extends) furthermore a certain procedure to control the structural properties, the opto-electronic properties, and the surface properties of ZnO can indeed be obtained by following the present studies.

## சுருக்கம்


மெல்லிய படிமங்களைக் கொண்டு உண்டாக்கப் படும் சூரிய செல்கள் (Thin film solar cells) மனிதனின் எதிர்கால சக்தி தேவைகளுக்கு மிகுந்த நம்பிக்கையை ஏற்படுத்தி வருகின்றன. மெல்லிய படிமங்கனளக் கொண்டு உண்டாக்கப் படும் சூரிய செல்களின் பல்வேறு வகைகளில், சிலிக்கன் நுண்ணிய படிக மெல்லிய படிமங்கள் (microcrystalline silicon thin films) பல சிறப்புகளைப் பெற்று இருக்கின்றன. அதிக பரப்பு உற்பத்தி, குறைந்த தயாரிப்பு செலவு மற்றும் தொடர்ச்சியான உற்பத்தி திறன் இவற்றுடன் மிகக் குறைந்த இயக்கு திறன் இழப்பு, இந்த வகையான சூரிய செல்களை கவர்ச்சிகுரியவைகளாக்குகின்றன. இந்த ஆய்வு இத்தனகய செல்களின் பல்வேறு தயாரிப்பு நிலைகளை ஆராய்கின்றது. மேலும், சிலிக்கன் நுண்ணிய படிக மெல்லிய படிமங்கள் மற்றும் ஒழுங்கற்ற கட்டமைப்பு கொண்ட மெல்லிய படிமங்கள் கொண்டு உருவாக்கப்பட்ட இந்த ஆய்வகத்தின் கண்டு பிடிப்பான 'மைக்ரோமார்ஃப்' செல்களில் செயல்படுதிறனை மேம்படுத்துவது குறித்தும் விளக்குகிறது. இந்த வகை 'மைக்ரோமார்ஃப்' செல்கள் உலகசாதனை இயக்குதிறனைப் பெற்றிருக்கின்றன.

ஒளி தம்முள் ஊடுறுவும் தன்மையினையும் மின் கடத்தும் திறனையும் ஒருங்கே பெற்ற ஆக்ஸைடுகள் (Transparent Conducting Oxides) தமது மெல்லியப் படிம நிலையில்,பல்வேறு தொழில் நுட்பப் பயன்களைக் கொண்டிருக்கின்றன. இத்தகைய வியப்புக்குரிய ஆக்ஸைடுகளில் ஒன்றான துத்தநாக ஆக்ஸைடு, அதன் மெல்லிய படிம நிலையில் மிக முக்கியதுவம் வாய்ந்ததாக விளங்குகிறது. மென்படிம சூரிய செல் அமைப்பில் துத்தநாக ஆக்ஸைடுகளின் மெல்லியப் படிமங்களின் பங்கு மிக முக்கியதுவம் வாய்ந்தது. ஒரு சூரிய செல்லினுள் நுழையும் சூரிய ஒளி ஆற்றவாதை,எந்த அளவுக்கு பயன்படுத்தப் படுகிறதோ, அனதப் பொருத்து அதன் இயக்குதிறன் (solar cell efficiency) அமைகிறது. எனவே, சூரிய செல் ஆராய்ச்சியாளர்கள் அதிக அளவு சூரிய ஒளினய செல்லினுள் செலுத்துவதில் மிகுந்த கவனத்தை செலுத்துவதால், தற்கால சூரிய செல் ஆராய்ச்சியில் இது முக்கியப்பங்கு வகிக்கிறது. மென்படிமங்களின் கட்டுப்பாடான மேற்பரப்பு வளர்ச்சி அனதக்கொண்டு உண்டாக்கப்படும் மின்னனு கருவிகளின் (Electronic Devices) செயல்பாடுகளில் தெளிவான விளைவுகளை ஏற்படுத்துகின்றது. குறிப்பாக,சமமில்லா மேற்பரப்பு வழியே செல்லும் ஒளிக்கற்றையின் பாதை நீளம், சமமான மேற்பரப்பு வழியே செல்லும் ஒளிக்கற்றையின் பானத நீளத்தைவிட அதிகம். அதாவது, சமமில்லா மேற்பரப்பினுள் செல்லும் ஒளி, அதைக் கொண்டு உண்டாக்கப்படும் சூரிய செல்களினுள் நீண்ட தூரம் செல்கிறது. இது, ஒளி மின் தன்மை பெற்ற திண் படிமங்களில் உட்கொள்ளப் படும் ஒளியின் அளவை அதிகரிப்பதால், சூரிய ஒளியின் மூலம் உண்டாக்கப்படும் மின்னோட்டத்தை (short circuit current)அதிகரிக்க செய்கின்றது. இதன் காரணமாக, சூரிய செல்களின் இயக்குதிறன் அதிகரிக்கிறது. இதனை 'ஒளிப்பொறி' (Light Trapping) என அழைக்கலாம். இந்த ஆராய்ச்சி மென்படிம நிலையில் ஒளிப்பொறி உண்டாக்குவதற்கான முறைகளை விளக்குகிறது. மேலும் ஒரு திண்படிம கருவிக்கு தேவையான பல்வேறு சிறப்புப் பண்புகளை ஒருங்கே பெற தேவையான முறைகள் ஆராயப் பட்டுள்ளன.

ஒரு திண்படிமத்தின் படிக வளர்ச்சியினை முறைப்படுத்தும் வகைகள் தெளிவாக ஆராயப்பட்டுள்ளன. இதன் மூலம் அவற்றின் பரப்பின் வளர்ச்சியினை தேவைக்கேற்ப கட்டுப் படுத்தலாம். திண் படிம மேற்பரப்பின் தோற்றம் மற்றும் அளவு ஆகியவற்றைக் கட்டுப்படுத்துவதன் மூலம் ஒரு சூரிய செல்லுக்கு தேவையான முக்கிய ஒளி அலை நீளம் மற்றும், 'ஒளிப்பொறி'க்குத் தேவையான கோணம் ஆகியவற்றைத் தேர்வு செய்யலாம். மற்றும் திண்படிமங்களின் மின் கடத்தும் பண்புகள் மற்றும் ஒளி பண்புகள் (electronic properties), கட்டமைப்பு பண்புகள் ஆகியவற்றை கட்டுப்படுதும் முறைகளும் தெளிவாக ஆராயப்பட்டுள்ளன. தற்காலத் தொழில் நுட்பத்தில் பெரும் பங்கு வகிக்கும் முக்கிய இரண்டு திண்படிம வளர்ச்சி முறைகள் ஆராயப்பட்டுள்ளன. பொதுவான ஆராய்ச்சி முடிவுகள், துத்தநாக மெல்லிய படிமங்களுக்கு மட்டுமின்றி அனைத்து திண்படிம வளர்ச்சிக்கும் பயன்பயப்பன. அனைத்து முடிவுகளையும் கொண்டு தயாரிக்கப்பட்ட மெல்லிய படிம கட்டமைப்புகளைக்கொண்டு உருவாக்கப்பட்ட சூரிய செல்கள் தமது இயக்குதிறனில் சிறந்து விளங்குகின்றன.

## *Acknowledgements*

I would like to acknowledge:

Prof. A. Shah for integrating me in to his research group, for allowing me to begin a new research domain in the group, and for offering me the possibility to develop new ideas. I was always impressed by his supervision as well as the way he brought about to progress in the work of the group members.

Dr. H. Keppner, my immediate supervisor, as a source of unlimited energy and inspiration to me. Apart from his encouragement, I received a lot of moral support from him. Personally, I felt that the combination of Prof. Shah and Dr. H. Keppner was a great asset in the pursuit of research.

'Commission Fédérale des Bourses pour des étudiants étrangers' for the financial support by which this work was realised. I think a program like this should continue in order to have scientific collaboration with other countries.

all the members and friends in the 'Amorphous silicon and microcrystalline thin film solar cell group'at Institute of Microtechnology (IMT) for their help as well as their friendship during the period of this work. Christian Hof, Dr. Michael Goetz, Peter Torres, Dr. Johannes Meier, Dr. Diego Fischer, Pascal Pernet, Natalie Beck, Yvan Ziegler and Rainer Platz had an active role in different stages of the work. Further, they continuously appreciated the work, and the ZnO fabricated under many critical experimental conditions was incorporated into thin film solar cells with great patience. I must say that, due to this interest, ZnO became a success in our lab.

Dr. U. Kroll and J. Cuperus for the fabrication and calibration of the CVD system for ZnO development. I greatly appreciate the in house development of CVD system.

Prof. L. Zuppiroli, Dr. C. Beneking, Prof. F. Stoeckli and Dr. H. Keppner for accepting to be the members of my examination board. Moreover, I had active collaboration with them during the research period of the present work.

Dr. T. Adatte, Institute of Geology, Mr. N. Randall, CSEM and Dr. D. Hugi, Institute of Chemistry, Neuchâtel for their assistance during the characterisation studies.

Dr. C. Beneking for the invitation to spend some time on the ZnO activities at Forschungszentrum Jülich, Germany. I thank my friend O. Kluth and the colleagues in Julich for their hospitality, and I wish all the best for the TCO groups at Julich and at Institute of Microtechnology, Neuchâtel.

Dr. K. Ufert, Siemens Solar GmbH, Germany, for his technical collaborations.

S. Dubail, J. Vuille, R. Tcharner, H. Laaroussi for their technical help during many of the stages of my work.

Ingrid Mantle, secretary, for taking care of me so that I do not get lost on the highway with my bike. I equally appreciate Jöelle Banjac and all the secretaries at IMT for their aid during the period of my stay at IMT.

Pascal Duport for his introduction to Swiss life both in the lab as well as outside the lab. Nanda Duport, Oliver von Allmen and Martial Renaud from conseiller des étudiants, were of great support in my social life.

Dr. A. Subrahmanyam, Indian Institute of Technology, Madras for his support during this work. I would also like to thank all my project guides, teachers and friends in India for their support and love.

my mother, my brothers and my sister who were of great moral support to me in carrying out my work far from my home.

Dobrinka Chiekova for helping me in many important moments of my thesis.

Finally, I would like to remember my father and thank him for all his efforts, his love and his perseverance.

John Appa Durai Anna Selvan